Title	Hydrogen peroxide and hydrohalic acid mediated synthesis of halogenated benzimidazolequinones and anti-cancer evaluation of benzotriazinones
Author(s)	Sweeney, Martin
Publication Date	2019-11-29
Publisher	NUI Galway
Item record	http://hdl.handle.net/10379/15607

Hydrogen Peroxide and Hydrohalic Acid Mediated Synthesis of Halogenated Benzimidazolequinones and Anti-Cancer Evaluation of Benzotriazinones

Martin Sweeney, BSc (Hons)

Thesis presented for the PhD degree

of the

National University of Ireland, Galway

School of Chemistry

National University of Ireland, Galway

November 2019

Head of School: Dr. Patrick O'Leary

Supervisors: Prof. Paul V. Murphy and Prof. Fawaz Aldabbagh

Chapter 3: One-Pot Synthesis of Dihalogenated Ring-Fused Benzimidazoles & Benzimidazolequinones using H_2O_2/HX

Chapter 4: Evaluation of Benzo[1,2,4]triazin-7-ones as Thioredoxin Reductase (TrxR) Inhibitors and their Anti-cancer Activity

Declaration

I declare that the work included in this thesis is my own work, except where stated otherwise, and has not been previously submitted for a degree to this or any other academic institution.

_____

Martin Sweeney

Abstract

Chapter 1 provides a literature review of metal and metal-free oxidative annulations employed to access ring-fused benzimidazoles while highlighting their significance and application towards anti-tumour benzimidazolequinones. The aims and objectives of the thesis are included at the end of this Chapter.

Chapter 2 starts with a review detailing the green credentials of H_2O_2, EtOAc, and methanesulfonic acid (MSA) with an emphasis on the sustainability of their production. Pyrrolo[1,2-*a*]benzimidazoles were prepared from *o*-pyrrolo substituted anilines using H_2O_2 in EtOAc, avoiding the traditional use of carboxylic acid solvents. The protocol circumvented aqueous extraction and chromatography, and could be applied to six, seven, and eight-membered cyclizations. Pyrido[1,2-*a*]benzimidazole formation and the cyclization of 3,6-dimethoxy-2-(cycloamino)anilines required one equivalent of MSA in order to achieve high yields.

Chapter 3 starts with a review discussing the impact of carbon-halogen bonds in medicinal chemistry, H_2O_2/HX as a benign method for the synthesis of halogenated heterocycles, and current methods to form *p*-quinones. The one-pot tunable protocol of H_2O_2/HX can be used to either perform 4-electron or 6-electron oxidation to access dimethoxy ring-fused benzimidazoles, as well as chlorinated and brominated ring-fused benzimidazolequinones in high yields. HPLC reaction profiling indicated that halogenation occured prior to oxidative cyclization. Cl_2 and Br_2 were determined as active species in the one-pot reactions. $H_2{}^{18}O$ labeling experiments on dimethoxy benzimidazoles provided insight into the mechanism of ether cleavage. The nitration of 2-fluoro-1,4-dimethoxybenzene formed exclusively 1-fluoro-2,5-dimethoxy-4-nitrobenzene.

Chapter 4 starts with a brief description of subject heterocycle synthesis, the National Cancer Institute Development Therapeutic Program (NCI-DTP), thioredoxin reductase (TrxR), and defines the different types of reversible enzyme inhibition. The in-house cytotoxicity evaluation of a series of benzo[1,2,4]triazin-7-ones is described. COMPARE analysis at the NCI showed a very strong correlation between 1,3-diphenylbenzo[1,2,4]triazin-7-ones and pleurotin. The latter natural antibiotic is an irreversible TrxR inhibitor. Enzyme assay data were analysed using the Lineweaver-Burk plot, which confirmed that 1,3-diphenylbenzo[1,2,4]triazin-7-one and the 3-CF$_3$ substituted analogue are reversible TrxR inhibitors. The latter is more potent displaying uncompetitive inhibition, rather than the mixed inhibition of the parent compound.

Acknowledgements

Abbreviations

δ	chemical shift in ppm downfield from TMS
°C	degrees Celsius
μM	micromolar
Å	angstrom
Ac	acetyl
ACCN	1,1′-azobis(cyclohexanecarbonitrile)
AChE	acetylcholinesterase
ACS	American Chemical Society
AIBN	2,2′-azobis(isobutyronitrile)
AP-1	activating protein 1
APBI	acetamido pyrrolo[1,2-*a*]benzimidazolequinone
API	active pharmaceutical ingredient
Aq	aqueous
ASK1	apoptosis signal-regulating kinase 1
AT	adenine-thymine base pair
ATCC	American Type Culture Collection
ATR	universal attenuated total reflectance
Aβ	beta-amyloid
BChE	butyrylcholinesterase
bs	broad singlet
BSS	balanced salt solution
Bu	butyl
C	cysteine
Ca.	circa
Calcd.	calculated
CAN	cerium(iv) ammonium nitrate
CCDC	Cambridge Crystallographic Data Centre
CDC	cross dehydrogenative coupling
CDK	cyclin dependent kinase
CED	cumulative energy demand
CHEM21	Chemical Manufacturing Methods for 21$^{\text{st}}$ Century

CNS	central nervous system
Cod	1,5-cyclooctadiene
Cp*	pentamethylcyclopentadienyl
CRF$_1$	corticotropin releasing factor 1
CSA	camphorsulfonic acid
CV	cyclic voltammetry
CYP450	cytochrome c P450 reductase
Cys	cysteine
d	doublet
DABCO	1,4-diazabicyclo[2.2.2]octane
DBU	1,8-diazabicyclo[5.4.0]undec-7-ene
DCBA	2,4-dichlorobenzoic acid
DCE	1,2-dichloroethane
DCM	dichloromethane
DDQ	2,3-dichloro-5,6-dicyano-1,4-benzoquinone
Dec.	decomposition
DEPT	Distortionless Enhancement by Polarization Transfer
Dil	dilution
DIPEA	*N*,*N*-diisopropylethylamine
DMA	*N*,*N*-dimethylacetamide
DMAP	4-*N*,*N*-dimethylaminopyridine
DMEM	Dulbecco's modified Eagle medium
DMF	*N*,*N*-dimethylformamide
DMSO	dimethyl sulfoxide
DNA	deoxyribonucleic acid
DPIQ	dipyridoiminoquinone
DTNB	5,5'-disulfanediylbis(2-nitrobenzoic acid)
DTP	Development Therapeutics Program
E°'	formal potential
EAS	electrophilic aromatic substitution
EDG	electron donating group
EDTA	ethylenediaminetetraacetic acid
EI	electron impact
Enzvol	enzyme volume

Equiv.	equivalents
ESI	electrospray ionization
Et	ethyl
EU	European Union
EWG	electron withdrawing group
F-106	phenylalanine-106
FA	fanconi anaemia
FAD	flavin adenine dinucleotide
FBS	fetal bovine serum
Fc	ferrocene
GC-EIMS	gas chromatography-electron impact mass spectrometry
GCI-PR	Green Chemistry Institute- Pharmaceutical Roundtable
GC-MS	gas chromatography-mass spectrometry
GC-TCD	gas chromatography-thermal conductivity detector
GI	growth inhibition
GSK	GlaxoSmithKline
h	hours
HAS	homolytic aromatic substitution
HIF-1α	hypoxia inducible factor-1α
HOTT	S-(1-oxido-2-pyridinyl)-1,1,3,3-tetramethylthiouronium hexafluorophosphate
HPLC	high performance liquid chromatography
HRMS	high resolution mass spectrometry
Hz	hertz
I	inhibitor
i-	iso
IC	inhibition concentration
IR	infrared
J	coupling constant
JNK	c-Jun N-terminal kinase
JoSPOphos	(R, S (p), R (SPO)-(1-t-butylphosphinoyl)-2-[1-(diphenylphosphino)ethyl]ferrocene
K	Kelvin
Ki	inhibitory constant

*K*m	Michaelis constant
LC	lethal concentration
LDA	lithium diisopropylamide
Lit.	literature
m-	*meta*-
m	multiplet
m/z	mass-to-charge ratio
M$^+$	mass of molecular ion
MAPK	mitogen-activated protein kinase
*m*CPBA	*m*-chloroperoxybenzoic acid
Me	methyl
MEK	methyl ethyl ketone
MEM	minimum essential media
MG-MID	mean graph-midpoint
MHz	megahertz
MIBK	methyl isobutyl ketone
min	minutes
mM	millimolar
MMC	mitomycin C
mp	melting point
MS	mass spectrometry
MSA	methanesulfonic acid
Msr	methionine sulfoxide reductase
MTBE	methyl *t*-butyl ether
MTT	3-(4,5-dimethylthiazol-2-yl)-2,5-diphenyltetrazolium bromide
NADPH	nicotinamide adenine dinucleotide phosphate
NBS	*N*-bromosuccinimide
NCI	National Cancer Institute
NF-kB	nuclear factor-kB
NHC	*N*-heterocyclic carbene
NHE	normal hydrogen electrode
NIGMS	National Institute for General Medical Sciences
NIH	National Institutes of Health
NMP	*N*-methylpyrrolidinone

NMR	nuclear magnetic resonance
NQO1	NAD(P)H:quinone oxidoreductase 1
Nrf-2	nuclear factor erythroid 2-related factor 2
NSC	National Service Centre
o-	*ortho-*
p-	*para-*
p53	tumour protein p53
PBI	pyrrolo[1,2-*a*]benzimidazolequinone
PCC	Pearson Correlation Coefficient
Pet. ether	petroleum ether
Ph	phenyl
pH	power/potential of hydrogen
PIDA	phenyliodine(III) diacetate
PIFA	phenyliodine(III) bis(trifluoroacetate)
Piv	pivaloyl
ppm	parts per million
Pr	propyl
PTEN	protein tyrosine phosphatase and tensin homolog
PTOC	pyridine-2-thione-*N*-oxycarbonyl
q	quartet
quint	quintet
REACH	Registration, Evaluation, Authorisation and Restriction of Chemicals
R_f	retention factor
RNR	ribonucleotide reductase
ROS	reactive oxygen species
RPMI	Roswell Park Memorial Institute
rt	room temperature
s	singlet
SAS	Statistical Analysis System
Sat.	saturated
SD	standard deviation
Sec	selenocysteine
SET	single electron transfer

S$_N$Ar	nucleophilic aromatic substitution
S$_N$ArH	nucleophilic aromatic hydrogen substitution
SV40	simian virus 40
SVHC	substance of very high concern
t-	*tertiary-*
t	triplet
TBAP	tetrabutylammonium perchlorate
TCCA	trichloroisocyanuric acid
TCI	Tokyo Chemical Industry
TEMPO	2,2,6,6-tetramethylpiperidin-1-yl)oxidanyl
TGI	total growth inhibition
THF	tetrahydrofuran
THIQ	tetrahydroisoquinoline
TLC	thin layer chromatography
TMEDA	tetramethylethylenediamine
TNB	5-thio-2-nitro-benzoic acid
TNF	tumour necrosis factor
TOF-MS	time-of-flight mass spectrometry
Trx	thioredoxin
TrxR	thioredoxin reductase
U	selenocysteine
UV	ultraviolet
V	Volt
V_0	initial velocity
vdW	van der Waals
V_{max}	maximum velocity
Vol	volume
W-105	tryptophan-105

Chapter 1

General Introduction

The Formation of Ring-Fused Benzimidazoles via Oxidative Cyclization
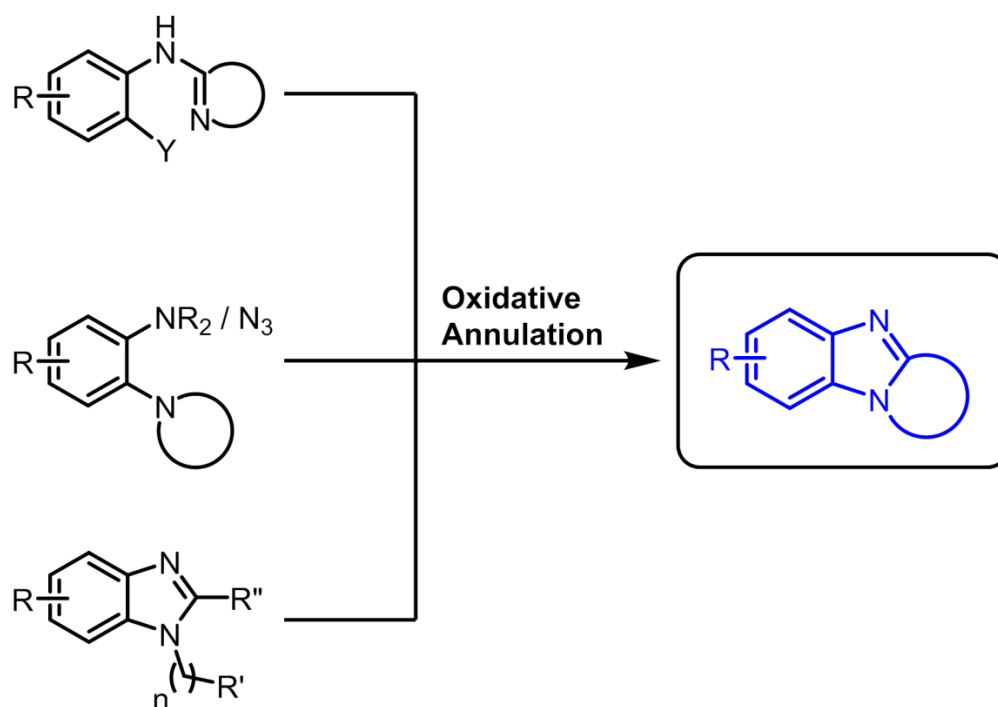
1.1. Introduction

1.1.1. Significance

Benzimidazoles are important heterocycle pharmacophores, with therapeutic interest increasing from the mid-20th century when 5,6-dimethylbenzimidazole was discovered as a degradation product of Vitamin-B$_{12}$ (Figure 1.1).[1]
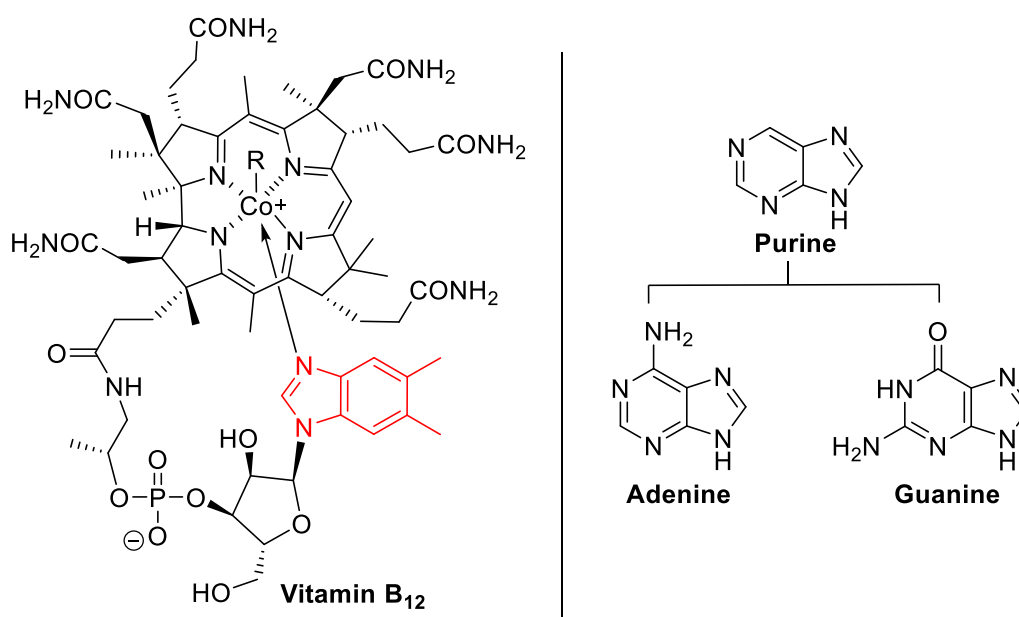
Figure 1.1. Benzimidazole as a key motif in Vitamin-B$_{12}$ and bioisostere of purine nucleobases.[1]

As bioisosteres of the purine nucleobases adenine and guanine, benzimidazoles possess a wide range of biological activities. Specifically, ring-fused benzimidazoles have displayed properties as pain-relievers,[2] therapeutic agents in the treatment of acute coronary syndrome,[3] applications in subcutaneous fat reduction,[4] cyclin dependent kinase (CDK) inhibitors,[5, 6] corticotropin releasing factor 1 (CRF$_1$) antagonists,[7] as histamine H$_3$ receptor ligands,[8] and modulators of the tumour necrosis factor (TNF) (Figure 1.2).[9] In addition, ring-fused benzimidazoles have displayed activity as anti-cancer agents (Figure 1.2).[10, 11]
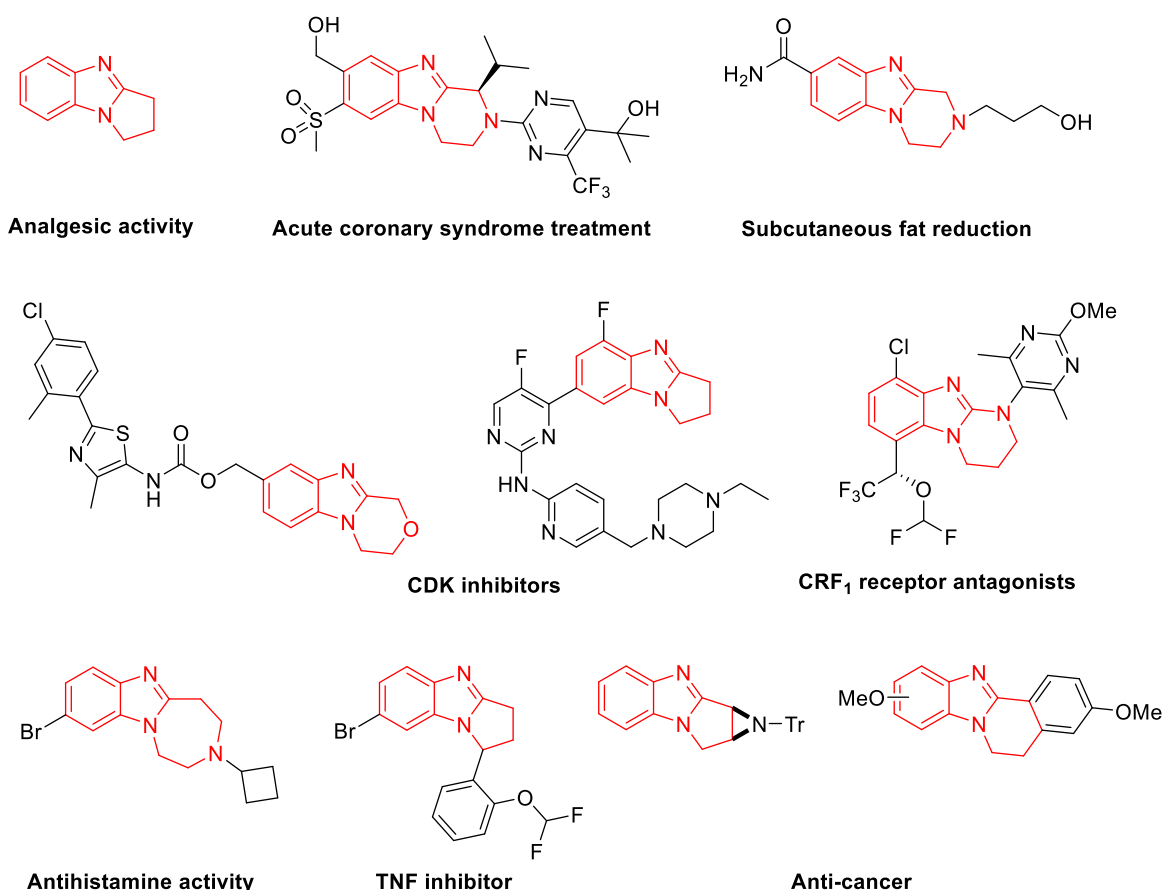
Figure 1.2. The various biological activities of ring-fused benzimidazoles.[2-11]

1.1.2. Benzimidazolequinones

Benzimidazoles serve as valuable synthetic precursors to benzimidazolequinones that are activated upon bioreduction to produce a chemotherapeutic effect. Quinones can be easily reduced by enzymes to hydroquinones due to their tendency to form full aromatic systems.[12] The bioreduction of quinones can occur via one-electron or two-electron pathways.[12-18] The single-electron transfer (SET) produces a semiquinone radical through activation by the enzymes NAD(P)H cytochrome c P450 reductase (CYP450), cytochrome b5 reductase, and ubiquinone oxidoreductase. SET is reversible, oxygen-dependent and is prevalent under hypoxic conditions (Scheme 1.1). Under continued hypoxic conditions the semiquinone radical will be reduced to the hydroquinone. The Aldabbagh group has reported alicyclic ring-fused benzimidazolequinones with nanomolar toxicity in hypoxic tumour cells (Figure 1.4).[19] The two-electron irreversible reduction is carried out by NAD(P)H:quinone oxidoreductase 1 (NQO1),[16] which is expressed at high levels in many solid tumour breast,[20, 21] cervical,[22] prostate,[23] lung [24] and colon cancers.[25]
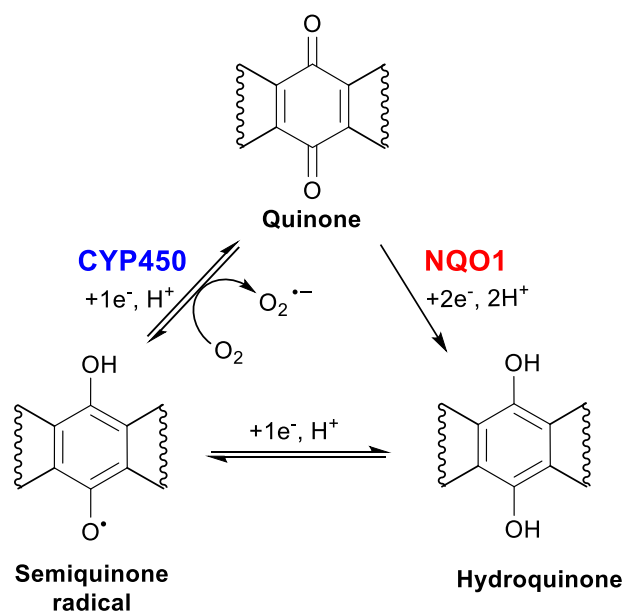
Scheme 1.1. One and two-electron bioreduction of quinones.[12]

Compared to established anti-cancer indolequinones such as mitomycin C (MMC), benzimidazolequinones contain an extra electronegative nitrogen on the imidazole ring to enhance bioreduction of the quinone moiety.[26] Skibo first took advantage of the electronegative nitrogen to synthesize a series of anti-cancer pyrrolo[1,2-*a*]benzimidazoles (PBIs) which were active against breast, non-small cell lung, colon, CNS, melanoma, ovarian, and renal cancer cell lines (Figure 1.3).[27-37]
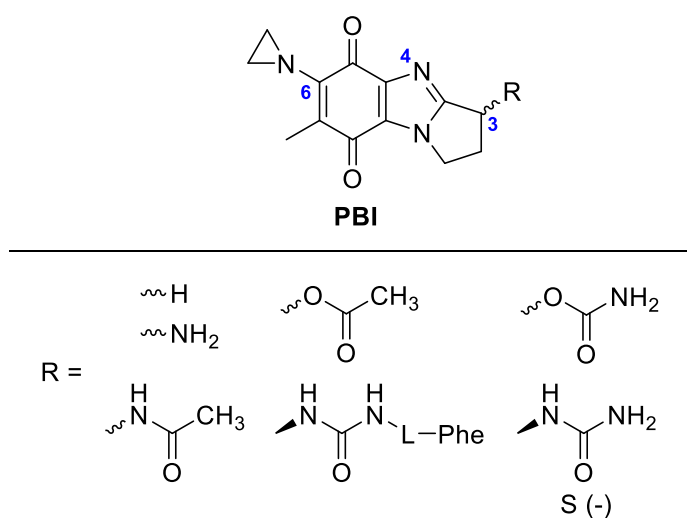
Figure 1.3. Skibo's anti-cancer PBIs.[27-37]

The PBIs are reduced by NQO1 to generate the active hydroquinone species that hydrogen bond to the AT base pairs in the major groove of DNA. The hydrogen bonding orientates the protonated aziridine ring of the hydroquinone to enable DNA addition and cleavage via a labile phosphotriester.[29, 38, 39]

Alterations to substituents at the 3-position significantly changes the cytotoxicity profile of PBIs. The 3-amino substituents such as amide and urea (R = NHCOCH$_3$, NHCONH$_2$) greatly enhanced cytotoxicity, since hydrogen bonding to thymine in the major groove of DNA is promoted (Figure 1.3).[33, 35] The presence of lipophilic L-phenylalanine linked substituents at the 3-position improves cellular uptake giving higher cytotoxicity against melanoma cell lines (Figure 1.3).[37, 40] Enantioselective cytotoxicity was achieved with the *S*-enantiomer of the 3-substituted urea (R = NHCONH$_2$) being 100 times more selective towards ovarian cancer cell lines than the *R*-enantiomer (Figure 1.3).[36]
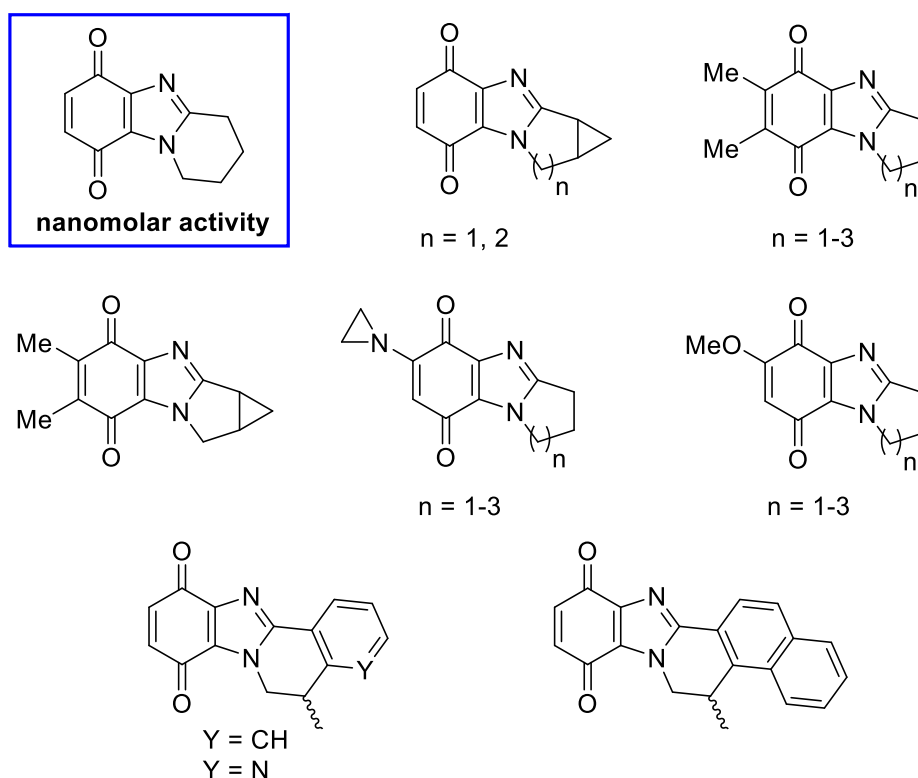
Figure 1.4. Aldabbagh's reported anti-cancer benzimidazolequinones.[19, 41-46]

Aldabbagh et al designed a series of anti-cancer ring-fused benzimidazolequinones with enhanced cytotoxicity compared to indolequinones such as MMC (Figure 1.4).[19, 41-46] The pyrido[1,2-*a*]benzimidazolequinone proved the most potent with cytotoxicity in the

5

nanomolar range under hypoxic conditions despite the absence of a DNA damaging functionality.[19] The additional ring-fused cyclopropane did not alter the cytotoxicity response despite its DNA damaging capabilities.[19, 41, 42] The presence of methyl substituents with or without ring-fused cyclopropane on benzimidazolequinones reduced overall cytotoxicity. This was due to the donating effect of the methyl substituents slowing the rate of bioreduction.[19, 43]

Fahey and Aldabbagh assembled methoxy and aziridinyl substituted benzimidazolequinones (Figure 1.4). Their cytotoxicity was evaluated against the Fanconi anaemia (FA) cell line (PD20i) and a normal human skin fibroblast cell line (GM00367).[44, 45] The aziridine moiety was necessary to induce hypersensitivity of FA cells lacking FANCD2 protein with cytotoxicity in the nanomolar range, whereas the methoxy substitutent gave negligible cytotoxicity.[45] Potency towards normal human skin fibroblast cell line decreased with increasing alicyclic ring size, but the aziridinyl substituted compounds were more cytotoxic in comparison to the methoxy analogues. Importantly, this work showed that the quinone functionality is not essential for hypersensitivity via the the FANC-pathway.[45] Moriarty and Aldabbagh synthesized highly conjugated benzimidazolequinones containing fused aryl, pyridinyl and naphthyl rings (Figure 1.4).[46] The aromatic resonance stabilisation of the chemically reduced quinone intermediates led to greater specificity and cytotoxicity towards both cervical (HeLa) and prostate cancer (DU-145) cells that over-express NQO1.[15, 46] The highly conjugated benzimidazolequinone (naphthyl-fused) displayed the best selectivity towards HeLa and DU-145 cell lines with negligible cytotoxicity towards the normal human skin fibroblast cell line (GM00367).[46]

In further studies, Skibo reported a series of 6-acetamidopyrrolo[1,2-a]benzimidazolequinones (APBIs) (Figure 1.5), which are structurally related to PBIs (strong NQO1 substrates) (Figure 1.3). National Cancer Institute (NCI) COMPARE analysis established an inverse correlation between APBIs and NQO1. The APBIs are reduced to the inactive hydroquinone species by NQO1.[30] APBIs only intercalate DNA in the oxidised quinone form acting as potent topoisomerase II inhibitors. Skibo designed imidazo[4,5-f]benzimidazolequinones to add steric bulk around the quinone core to lessen the deactivation by NQO1.[47] Unexpectedly, dipyrrolo-, mono acetylated dipyrrolo- and dipyridoimidazo[4,5-f]benzimidazolequinones proved excellent substrates for NQO1 stabilised by W-105 and F-106 residues of NQO1 (Figure 1.5).[48] The presence of two

acetylated groups on dipyrroloimidazo[4,5-*f*]benzimidazolequinone prevented reduction by NQO1 due to steric bulk. Both dipyrroloimidazo[4,5-*f*]benzimidazolequinone and its diacetylated analogue were found to inhibit topoisomerase II.[47]
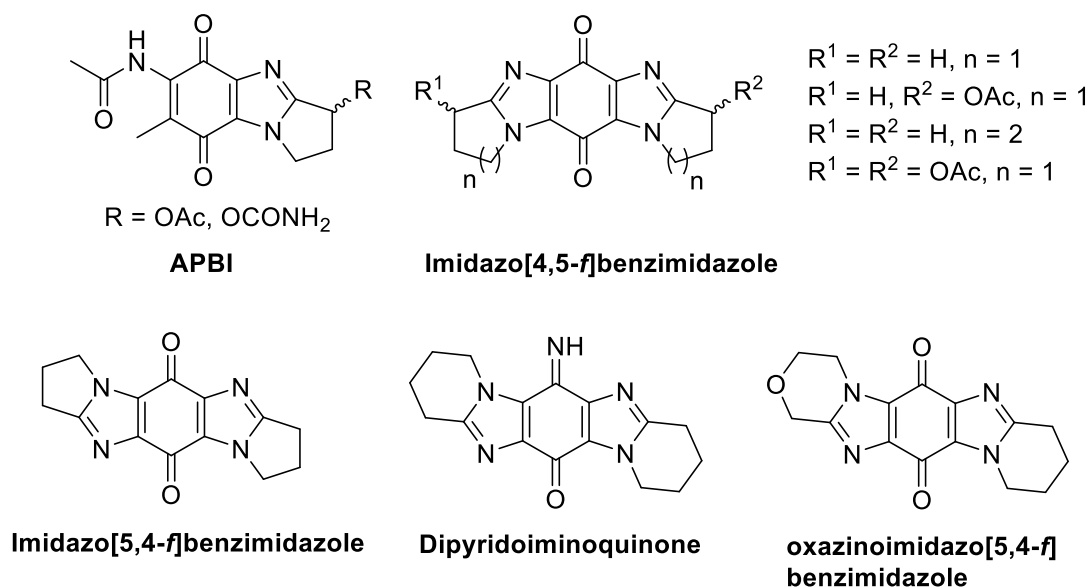
Figure 1.5. Imidazobenzimidazole based anti-cancer agents.[30, 47-51]

Fagan and Aldabbagh reported the symmetrical and unsymmetrical imidazo[5,4-*f*]benzimidazolequinone isomers (Figure 1.5) with specificity towards NQO1. The [5,4-*f*] isomer displayed greater cytotoxicity than the imidazo[4,5-*f*]benzimidazolequinones towards HeLa and DU-145 cell lines.[49, 50] NCI COMPARE analysis of the dipyridoiminoquinone (DPIQ) cytotoxicity profile and computational docking into the NQO1 active site has shown the iminoquinone motif to have a particularly high affinity towards NQO1.[51] DPIQ has high specificity towards the prostate cancer cell line (DU-145), as the toxicity was twelve times greater than that of a normal human skin fibroblast cell line.[49] The presence of an oxygen atom in the 1,4-oxazino ring of the unsymmetrical imidazo[5,4-*f*]benzimidazolequinone provides enhanced toxicity against the tested cancer cell lines.[50]

1.2. Synthetic overview

Access to privileged ring-fused benzimidazoles continues to be of interest, and is detailed in several recent reviews.[52-57] The focus of this thesis is on oxidative cyclizations and therefore this Introduction will primarily review the oxidative transformations of *o*-cyclic amine substituted anilines and their derivatives (Route A) alongside other oxidative examples in Route C and E (Scheme 1.2).
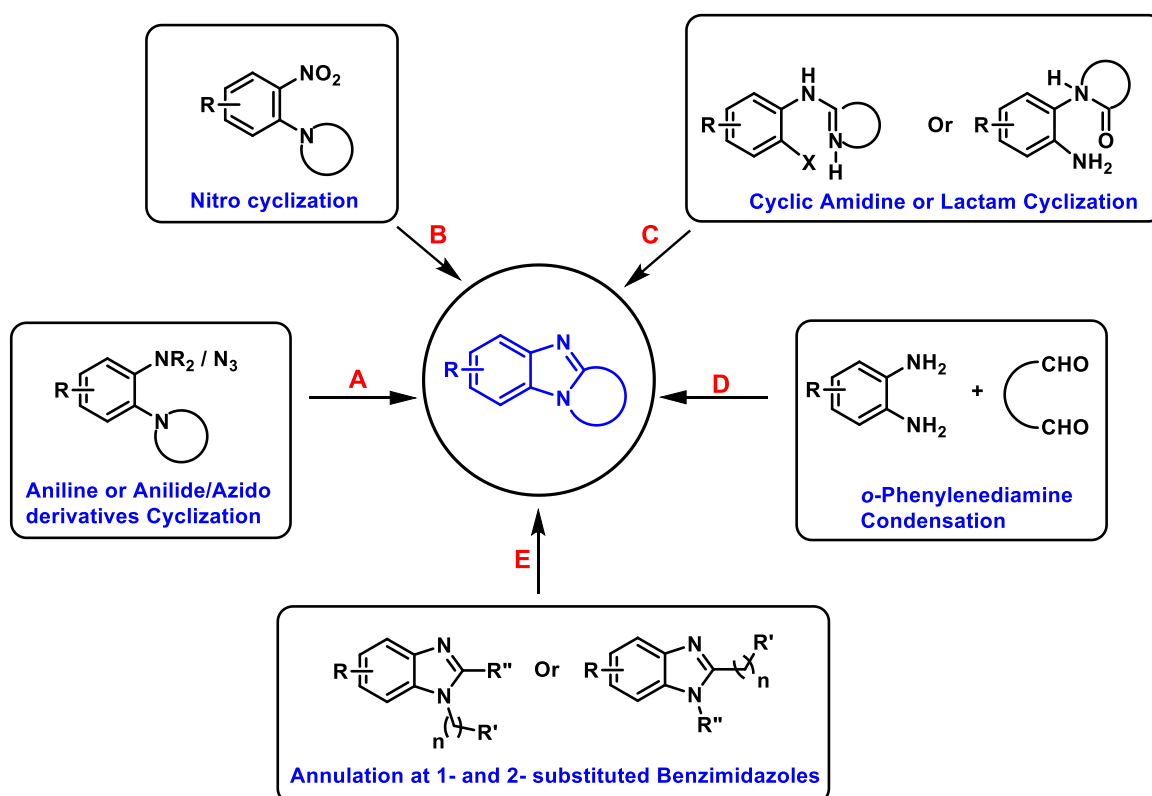
Scheme 1.2. Classifying the different synthetic routes to ring-fused benzimidazoles.

The reductive cyclization of nitrobenzenes (Route B) commonly employs metal reductants in acid such as $Ac_2O/ZnCl_2$,[27, 31-33, 58] $HCl/TiCl_3$,[59, 60] and $AcOH/Fe$.[61] Molecular iodine catalytically reduced nitrobenzenes with formic acid, which is used as the source of hydrogen.[62] Palladium catalysis was utilized for reduction with reagents of CO/Pd (high pressure)[63] and H_2/Pd.[64] The reductions can be carried out thermally under solvent free conditions[65, 66] or in mineral acid.[67] Photolytic cyclization of nitroarenes in mineral acid has been employed previously,[67] but more recently visible light and a thiourea catalyst have carried out the reductive cyclization of nitoarenes via biradical combination (Scheme 1.3).[68]
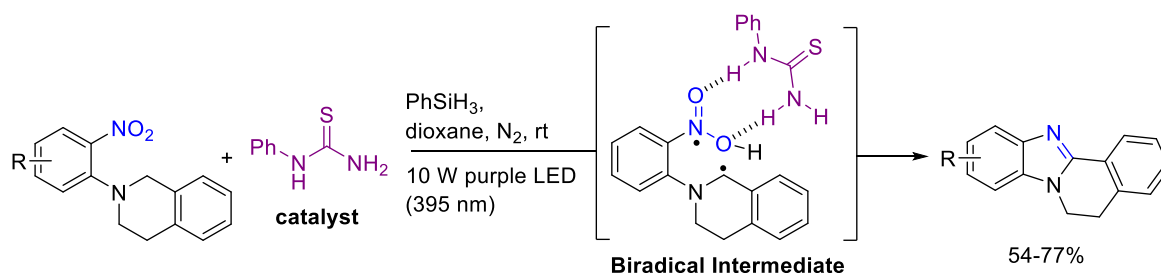
Scheme 1.3. Reductive cyclization of nitroarenes via biradical recombination mediated by visible light, thiourea, and silane reductant.[68]

o-Haloarylamidines (Route C) undergo non-redox transition metal-catalyzed coupling reactions with ligand/CuI,[69-71] or transition metal-free methods of DMSO/KOH,[72] and Cs$_2$CO$_3$/DMA.[5] The lactam substituted anilines cyclize using di-*t*-butyl sulfoxide/NBS via an aza-Wittig reaction.[73] *t*-BuLi directs the *o*-lithiation of cyclic arylamidines followed by intramolecular trapping of an aryne intermediate to form ring-fused benzimidazoles regioselectively.[74] A traditional synthesis of benzimidazoles involves the condensation of 1,2-phenylenediamines with aldehydes,[75-77] and acid anhydrides[78] (Route D). The cyclization of *N*-alkenyl-1,2-diaminobenzenes via hydroformylation intermediates with syngas (CO/H$_2$) and catalysed by rhodium gave mixtures of alicyclic ring-fused benzimidazoles.[79, 80]

Route E differs from the other routes in that annulations occur onto the 1- and 2- positions of pre-prepared benzimidazoles to provide a diverse range of ring-fused benzimidazoles. These include annulations of alkenyl[81-84] and alkynyl[85] substituted benzimidazoles under transition metal-catalysis by Rh, Ni, Ni-Al, Ir, and Ag respectively. The use of chiral ligands has allowed for *endo-* and *exo-* enantioselective annulations.[83, 84] More recently, a nickel catalyzed enantioselective *endo*-cyclization between an imidazole and alkene alongside the chiral secondary phosphine oxide preligand (JoSPOphos) was achieved to produce tricyclic benzimidazoles (Scheme 1.4). [86]
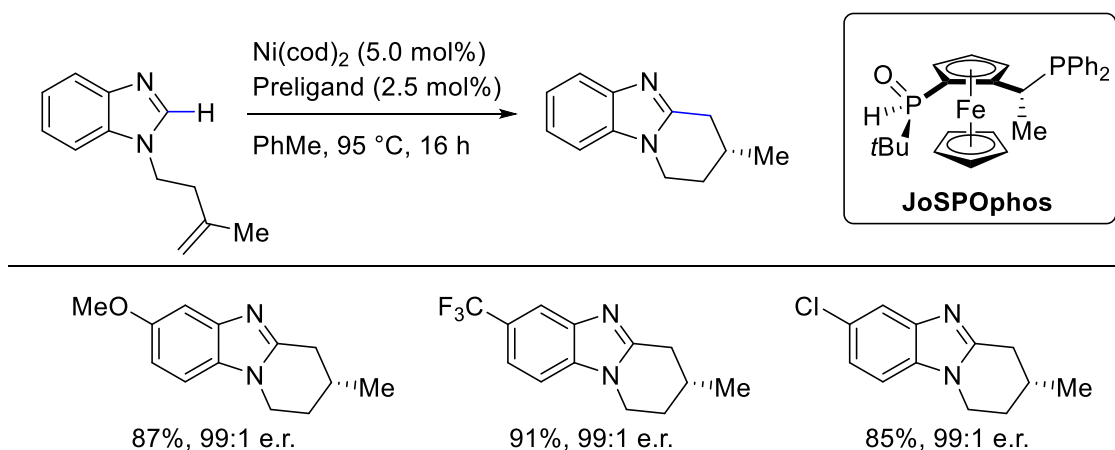
Scheme 1.4. Nickel catalysed enantioselective synthesis of alicyclic ring-fused benzimidazoles.[86]

The cyclization of alkyl substituted benzimidazoles is achieved using bases of NaH,[87, 88] KOH,[89] and LDA.[90] The [4+2] annulations of 2-substituted benzimidazoles occurred with styrene/Ru[91] or under metal-free conditions using a bromoethylsulfonium salt.[92] The formation of pyrrolo-, pyrido-, azepino- and azocino[1,2-a]benzimidazoles with a fused cyclopropane ring involves N-aziridinyl imines (Eschenmoser hydrazones) undergoing thermolysis at reflux in m-xylene with a loss of nitrogen and trans-stilbene (Scheme 1.5).[41-43]
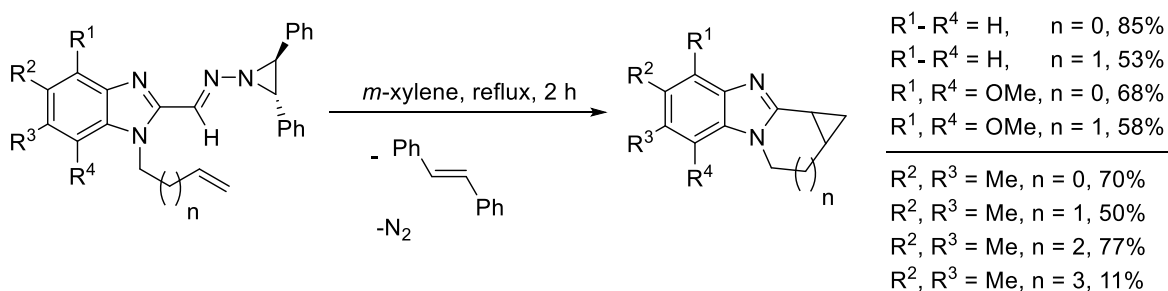
Scheme 1.5. Synthesis of cyclopropane fused benzimidazoles via Eschenmoser hydrazones.[41-43]

Metal-free methodologies including initiator-free radical photochemical annulations of benzimidazol-2-yl radicals,[93] benzimidazole cyclization with aryne using CsF and K₂CO₃,[94] and N-Heterocyclic Carbene (NHC) catalyzed intramolecular hydroacylation of N-allylbenzimidazole-2-carboxaldehydes[95] are additional pathways to ring-fused benzimidazoles.

1.2.1. Oxidative cyclization of aniline, anilide and azide derivatives (Route A)

In 1908, Spiegel and Kaufmann showed that Caro's acid (peroxymonosulfuric acid) oxidized *o*-cyclic amine substituted aniline **1** to a tricyclic ring-fused [1,2-*a*]benzimidazole **2** (Scheme 1.6).[96] The absence of the electron withdrawing nitro group on **1** resulted in no oxidative cyclization. Caro's acid was already known to oxidise anilines to nitrosobenzenes[97] supporting the idea of a nitroso-intermediate.
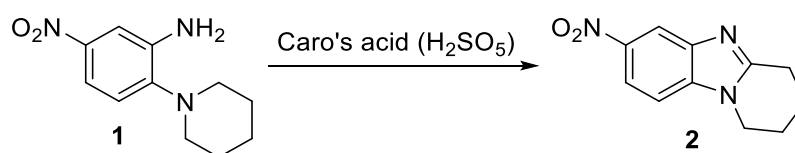
Scheme 1.6. Caro's acid oxidative cyclization of *o*-cyclic amine substituted aniline.[96]

Prominent 20th century chemist and creator of Adam's catalyst, Roger Adams with Nair refined the methodology to access a wider range of ring-fused [1,2-*a*]benzimidazoles in good to high yields of 58-91% using peroxytrifluoroacetic acid generated in situ (Scheme 1.7).[98]
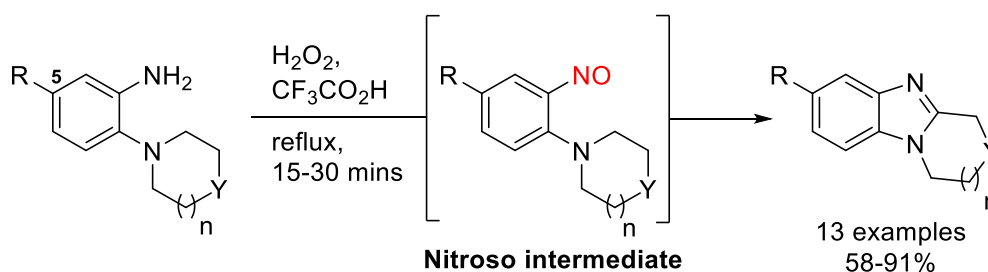
n	Y	R, Yield (%)			
		H	Cl	CH$_3$	NO$_2$
0	CH$_2$	81	75	86	72
1	CH$_2$	58	66	60	95
1	O	73	62	61	76
2	CH$_2$	91	—	—	—

Scheme 1.7. Oxidative cyclization of *o*-cyclic amine substituted anilines.[98]

The presence of an electron-withdrawing group at the 5-position of *o*-cyclic amine substituted anilines allowed more facile oxidation to give the highest yielding benzimidazoles (Scheme 1.7), consistent with previous studies on the oxidation of anilines to nitro aromatic compounds.[99]

Due to the ability of peroxy-acids to oxidise anilines to nitrosobenzenes,[100] Nair and Adams believed the oxidative cyclization proceeded via oxidation of the primary amine to a nitroso-intermediate, which subsequently cyclized onto the α-methylene carbon of the tertiary cyclic amine.[98] Further support for the nitroso intermediate came when the involvement of an alternative tertiary amine *N*-oxide intermediate was investigated (Scheme 1.8). The attempt to oxidize the *o*-cyclic amine substituted anilide didn't yield the desired ring-fused benzimidazole under the same reaction conditions presented in Scheme 1.7.[98]
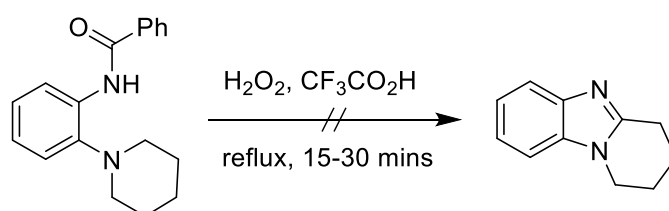
Scheme 1.8. Failed oxidative cyclization of *o*-cyclic amine substituted anilide.[98]

Meth-Cohn and Suschitzky have rationalized these reactions through the "*tertiary amino effect*", whereby tertiary anilines with an *o*-substituent leads to cyclization.[101] The paradigm has allowed oxidative cyclizations to be performed with a variety of *o*-substituents such as amino, acylamino and azido groups to give ring-fused benzimidazoles.
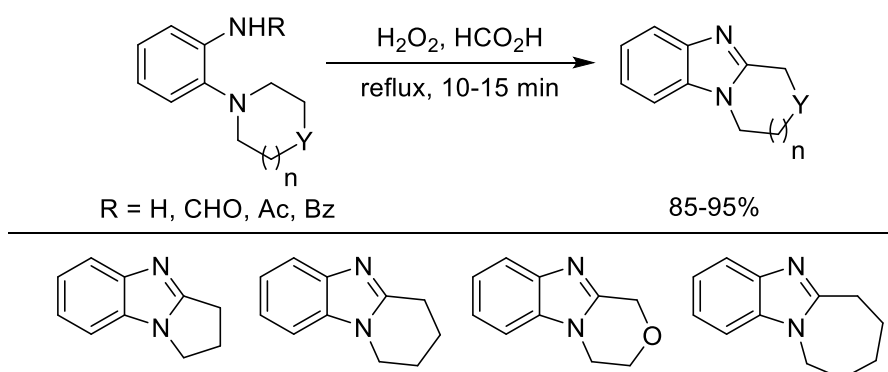
Scheme 1.9. Oxidative cyclization of *o*-cyclic amine substituted anilines & anilides.[102]

Meth-Cohn and Suschitzky further explored the use of in situ generated peroxy-acids, combining H_2O_2 and formic acid to generate performic acid.[102] This furnished a series of alicyclic ring-fused [1,2-*a*]benzimidazoles in excellent yields starting from either *o*-cyclic amine substituted aniline or anilide derivatives (Scheme 1.9). Meth-Cohn contradicted the observation of Nair (Scheme 1.8), showing that the acyl derivatives in Scheme 1.9 (R = formyl, acetyl and benzoyl) were oxidatively cyclized using either peroxytrifluoroacetic acid or performic acid.[102] Meth-Cohn preferred the use of *o*-cyclic amine substituted anilides as substrates for making ring-fused benzimidazoles.[102] The reactions proceeded more cleanly and Meth-Cohn believed Nair and Adams[98] had possibly formed the *o*-cyclic amine substituted anilides in situ as trifluoroacetic acid was first added to the *o*-cyclic amine substituted anilines followed by hydrogen peroxide.[103]
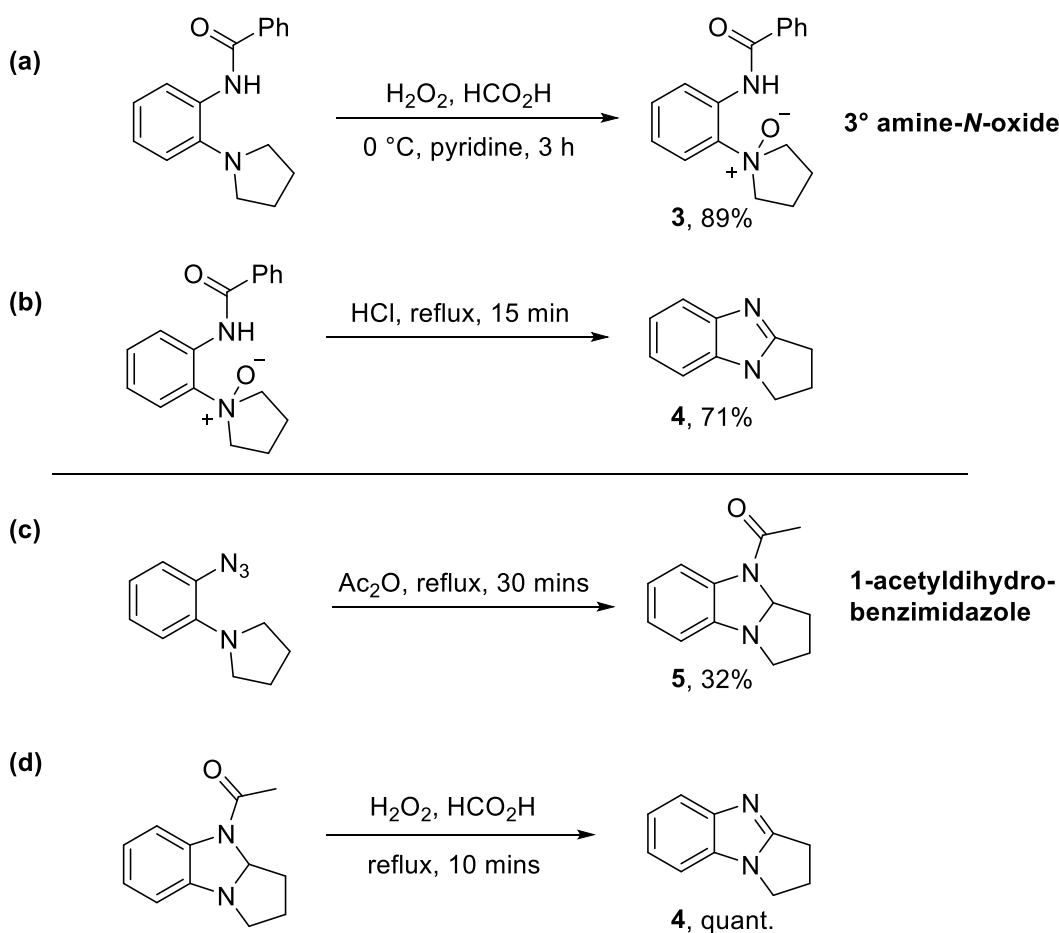
Scheme 1.10. Isolated intermediates provide mechanistic insight into cyclization of anilides.[103, 104]

The *o*-cyclic amine substituted anilides are not susceptible to acid hydrolysis circumventing the possibility of cyclization via a nitroso intermediate,[102] directing research towards a mechanistic route involving tertiary amine-*N*-oxides (Scheme 1.10). Performic acid was added dropwise for 10 min. at 0 °C to the anilide (Scheme 1.10a) in pyridine and the reaction was then brought to room temperature over 3 h. The reaction contents were concentrated down with addition of water in vacuo and then the product was extracted with choloroform followed by recrystallization from benzene. This was the first ever reported isolation of any benzimidazole tertiary amine-*N*-oxide and gave **3** in excellent yield of 89%.[103] The subsequent treatment of **3** with hydrochloric acid (2*N*) at reflux led to the corresponding pyrrolo[1,2-*a*]benzimidazole **4** in 71% yield (Scheme 1.10b). Meth-Cohn prepared 1-acetyldihydrobenzimidazole (Scheme 1.10c) **5** in 32% yield by refluxing an aryl azide in acetic anhydride as part of an investigation into the mechanism for the thermal cyclization of aryl azides (Scheme 1.27).[104] The isolated dihydrobenzimidazole **5** was then oxidized using performic acid to give pyrrolo[1,2-*a*]benzimidazole **4** in almost quantitative yield (Scheme 1.10d).[104]
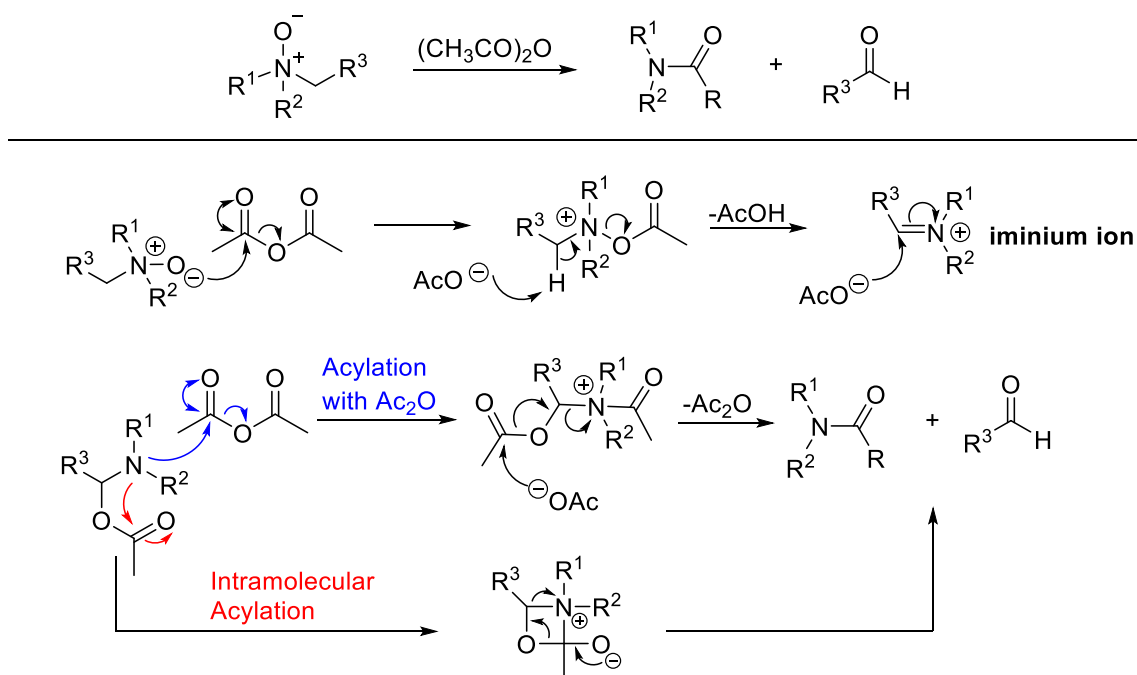
Scheme 1.11. Acylation and fragmentation of tertiary amine-*N*-oxide in the Polonovski reaction.[105, 106]

The isolation of the amine *N*-oxide and acylated hydrobenzimidazole intermediates, followed by treatment with acids to form benzimidazoles (Scheme 1.10) led Meth-Cohn to propose a Polonovski-type reaction[105-107] (Scheme 1.11). The Polonovski reaction involves

the acylation of a tertiary amine-*N*-oxide with acetic anhydride or acyl chloride that fragments to form an acetamide and aldehyde (Scheme 1.11). Meth-Cohn's mechanism states that the tertiary amine-*N*-oxide **3** reacts intramolecularly with the acyl group (Scheme 1.12), rearranging to a hemiaminal. The hemiaminal undergoes dealkylation via an elimination reaction with loss of water to produce an iminium ion. The resultant iminium ion undergoes nucleophilic addition from the adjacent amide group to give 1-acyldihydrobenzimidazole, which is further oxidized to yield the desired ring-fused [1,2-*a*]benzimidazole **4** with loss of carboxylic acid (Scheme 1.12).
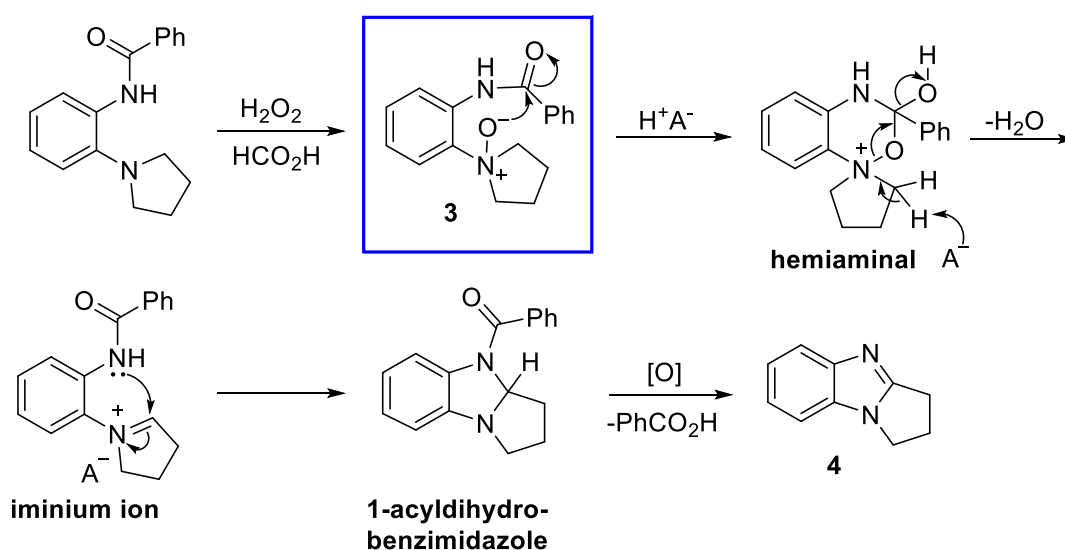
Scheme 1.12. Meth-Cohn proposed oxidative cyclization of *o*-substituted *N*-oxides.[103]

However, experimental NMR studies by Meth-Cohn showed strong hydrogen bonding between the oxygen of the *N*-oxide and the NH of the amide in the intermediate tertiary amine-*N*-oxide **3** (Scheme 1.13, blue box).[103] This meant that the carbonyl of the amide was oriented away from the *N*-oxide and is at odds with the mechanism (Scheme 1.12, blue box) showing the nucleophilic addition of the amine *N*-oxide onto the carbonyl of the anilide.

Fagan and Aldabbagh's research provided insight by obtaining an X-ray crystal structure of the dimorpholine *N*-oxide **6** (Scheme 1.13, red box). The data showed the carbonyl of the amide was indeed orientated away from the amine *N*-oxide due to hydrogen bonding (Scheme 1.13).[50] Based on this, a new mechanism incorporating the hydrogen bonded amine *N*-oxide intermediate was proposed, serving as an alternative to the Polonovski-type reaction (Scheme 1.12). The *o*-cyclic amine substituted anilide is oxidized to the amine *N*-

oxide **7**. The *N*-oxide is then protonated in acidic media resulting in the α-hydrogen beside the quaternized nitrogen becoming acidic, which leads to iminium ion and imidol formation with loss of water. The imidol adds on to the iminum ion in a nucleophilic addition leading to the brominated morpholino[1,2-*a*]benzimidazole **8**.
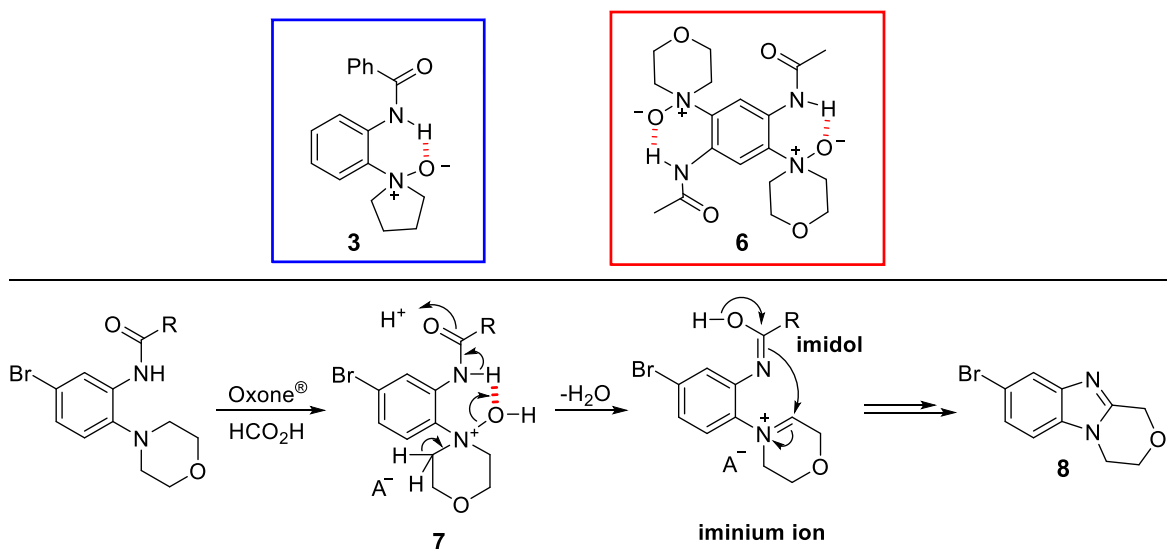
Scheme 1.13. Fagan and Aldabbagh proposed mechanism of H-bonded amine *N*-oxide intermediate.[50, 103]

The versatility of performic acid was extended to perform double annulations of the *o*-cyclic amine substituted anilides **9** giving pentacyclic ring-fused imidazo[4,5-*f*]benzimidazole **10b** in 74% yield (Scheme 1.14b).[102] Skibo and co-workers later synthesized the dipyrido ring-fused derivative **10b** with performic acid as a precursor to the anti-cancer imidazobenzimidazolequinones (Figure 1.5).[47, 48] However, the yield of 31% is significantly lower than that reported by Meth-Cohn (Scheme 1.14b) and the dipyrrolo analogue **10a** was obtained in an even poorer yield of 10%.[47] The variance in yield may be attributed to the isolation of **10b** which was obtained via sublimation in vacuo by Meth-Cohn and recrystallization by Skibo.

Fagan and Aldabbagh obtained the imidazo[5,4-*f*]benzimidazole isomer series of pentacyclic ring-fused compounds (**12a-12c**) using the solid peroxide Oxone® (potassium salt of peroxymonosulfuric acid) in 90% formic acid (Scheme 1.14c).[50] A diverse range of symmetrical and unsymmetrical ring-fused imidazo[5,4-*f*]benzimidazoles containing oxygen heteroatoms and alicyclic rings of varying size were prepared (Scheme 1.14c). The

ring-fused imidazo[5,4-*f*]benzimidazoles were converted to their iminoquinone and quinone derivatives (Figure 1.5) with enhanced cytotoxicity towards cancer cell lines over-expressing NQO1.[49-51] Oxone® was also shown to work well for the mono cyclization of the brominated *o*-cyclic amine substituted anilide giving the corresponding benzimidazole **8** in a high yield of 80% (Scheme 1.14a).

(a)

Oxone®, HCO$_2$H
40 °C, 6 h

8
80%

(b)

H$_2$O$_2$, HCO$_2$H
reflux, 10-15 min*
or
70 °C, 2 h†

9

imidazo[4,5-*f*]benzimidazoles
10a: n = 1, 10%†
10b: n = 2 (74%; ref. 102)*, (31%; ref. 48)†

(c)

Oxone®, HCO$_2$H
40 °C, 6 h

11

imidazo[5,4-*f*]benzimidazoles
12a: X, Y = OCH$_2$, 58%
12b: X = OCH$_2$, Y = (CH$_2$)$_2$, 47%
12c: X = (CH$_2$)$_2$, Y = CH$_2$, 52%
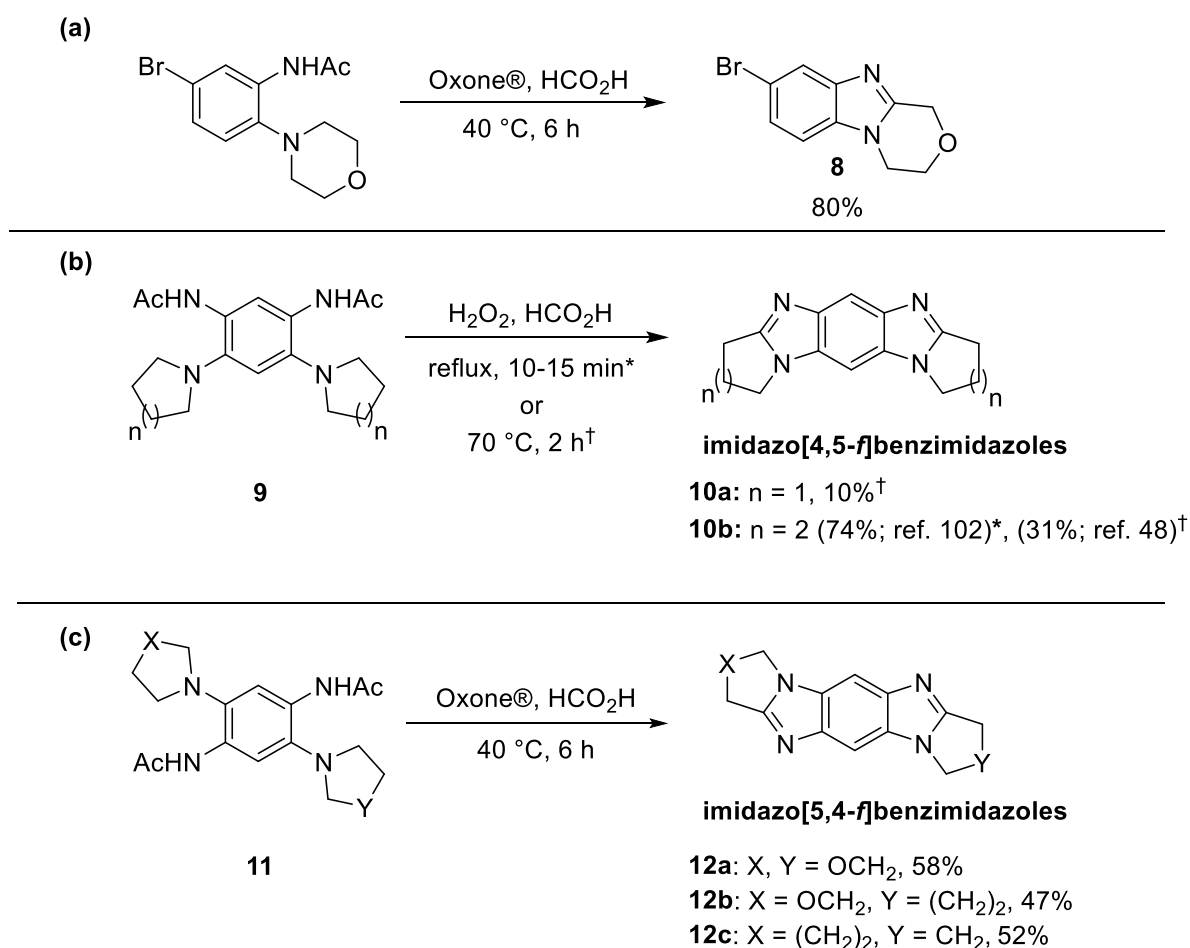
Scheme 1.14. The oxidative annulation and double annulation of *o*-cyclic amine substituted acetanilides.[47, 48, 50, 102]

Oxone® is advantageous over H$_2$O$_2$/organic acid methods, because it facilitates the precipitation of the benzimidazoles from acidic solution with solid sodium carbonate (without the requirement for further purification) to give good yields of 47-58% for the double annulated adducts. This overcomes the low yields (<30%),[47, 48] associated with the extraction of imidazo[4,5-*f*]benzimidazoles from aqueous acidic mixtures that Skibo experienced.

Performic acid continues to be of synthetic utility since Meth-Cohn's seminal work more than five decades ago (Scheme 1.15). Many of the benzimidazoles synthesized with this methodology serve as valuable precursors to biologically active compounds.
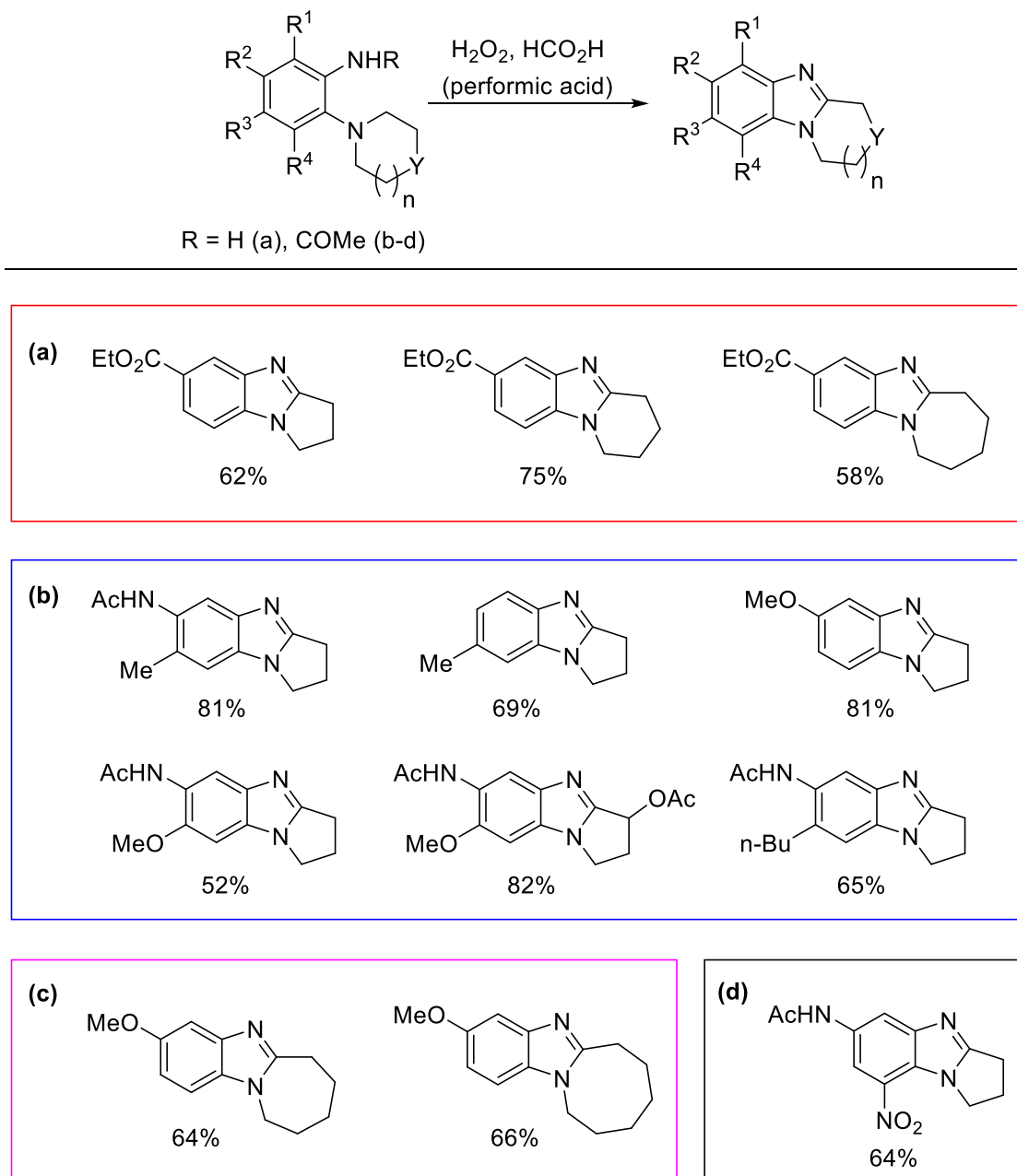
Scheme 1.15. The continued use of performic acid in literature to carry out oxidative cyclizations.[27, 28, 31-33, 44, 108, 109]

Alkhader obtained ester substituted benzimidazoles (Scheme 1.15a) of varying alicyclic ring size in good yields, and used them as precursors to access more complicated heterocycles such as [4,5-*g*]imidazoquinazolinones.[108] From the beginning of the 1990s,

Skibo and co-workers have ubiquitously used performic acid to synthesise pyrrolo[1,2-a]benzimidazoles (Scheme 1.15b) as synthetic precursors to benzimidazolequinone reductive alkylating agents, and topoisomerase II inhibitors (Figure 1.3).[27, 28, 31-33] Aldabbagh et al. focused on the synthesis of ring-expanded azepino- and azocino[1,2-a]benzimidazoles (Scheme 1.15c) obtaining them in good yields (64-66%) with performic acid.[44] Similarly these compounds would serve as precursors to the anti-cancer aziridinyl substituted benzimidazolequinones (Figure 1.4).[44, 45] Finally, Groves furnished 7-acetamido-2,3-dihydro-8-nitro-1*H*-pyrrolo[1,2-a]benzimidazole (Scheme 1.15d) in 64% yield as a precursor to novel pyrazines and quinoxalines.[109]

Martínez showed that the picolinamide group directs copper catalysed *o*-C–H amination of anilines with morpholine using a stoichiometric amount of the oxidant phenyliodine(III) diacetate (PIDA) (Scheme 1.16a).[110] The picolinamide group is well tolerated in the presence of performic acid, and undergoes oxidative cyclization to yield the morpholino[1,2-a]benzimidazole **13** in an good yield of 80% with loss of picolinic acid (Scheme 1.16b).[110]
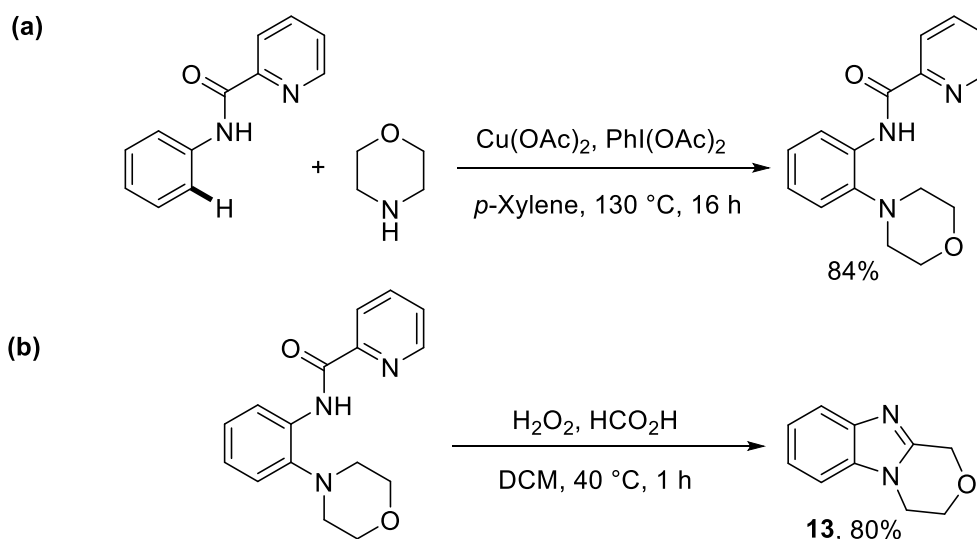
Scheme 1.16. Picolinamide group directed *o*-C–H amination and oxidative cyclization of *o*-cyclic amine substituted anilides.[110]

Alternatives to peroxide-based oxidizing systems have been explored since the late 1960s. MnO$_2$ oxidized tertiary amines in cold chloroform and the resultant cyclization gave the ring-fused [1,2-a]benzimidazoles (Scheme 1.17) in 15-20% yield. The poor yields were due to formation of red by-products, thought to be azo-compounds due to oxidation of

anilines.[111] In addition, Gerloff et al. used a mercury(II) EDTA complex to deliver the ring-fused [1,2-*a*]benzimidazoles (Scheme 1.17) in quantitative yield, apart from the morpholino analogue which was synthesised in 47% yield and had a slower reaction time of 90 minutes.[112]
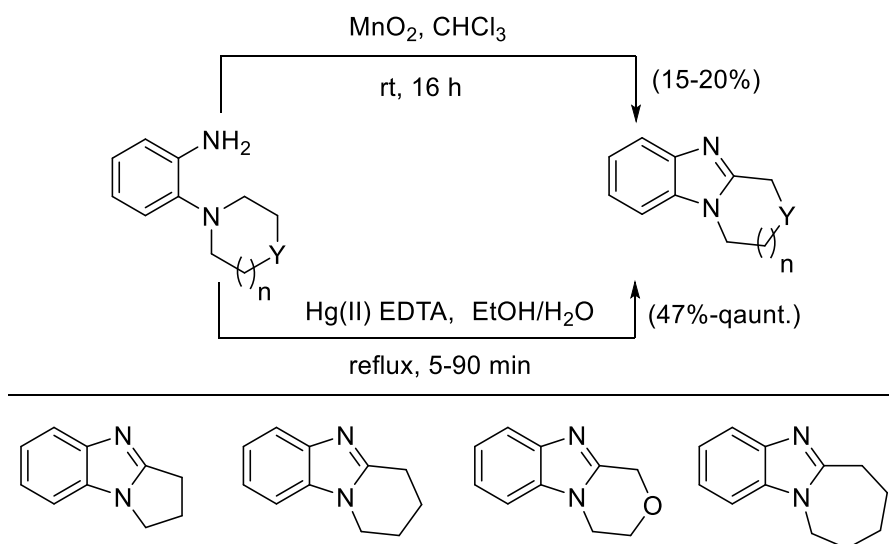
Scheme 1.17: MnO₂ and Hg(II) mediated oxidative cyclizations of *o*-cyclic amine substituted anilines.[111, 112]

The bench stable radical TEMPO (2,2,6,6-tetramethylpiperidin-1-yl)oxidanyl) was used in stoichiometric amounts aerobically under metal-free conditions to achieve the synthesis of the hydroisoindole ring-fused benzimidazole after 5 h in a good yield of 81% (Scheme 1.18).[113] The dihydroisoquinoline ring-fused benzimidazole took twice as long at 10 h, but still was isolated in a good yield of 83%. TEMPO was regenerated during the oxidative process with water as the only by-product (Scheme 1.19), boosting atom economy and environmental aspects of the reaction.
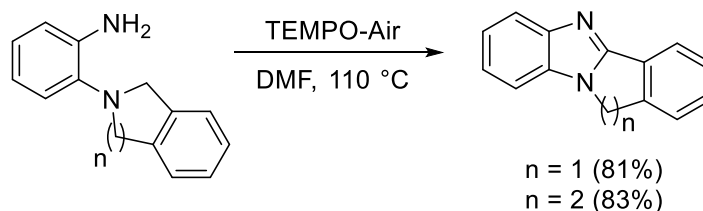
Scheme 1.18: TEMPO mediated oxidative cyclization to give tetracyclic ring-fused benzimidazoles.[113]

The TEMPO mediated reaction (Scheme 1.19) proceeds initially via a SET to generate an aminium radical cation, which undergoes a hydrogen atom transfer with another TEMPO molecule to generate an iminium ion with loss of water. The iminium ion undergoes nucleophilic attack forming a dihydrobenzimidazole intermediate, which undergoes further oxidation to obtain the desired tetracyclic ring-fused benzimidazole.[113]
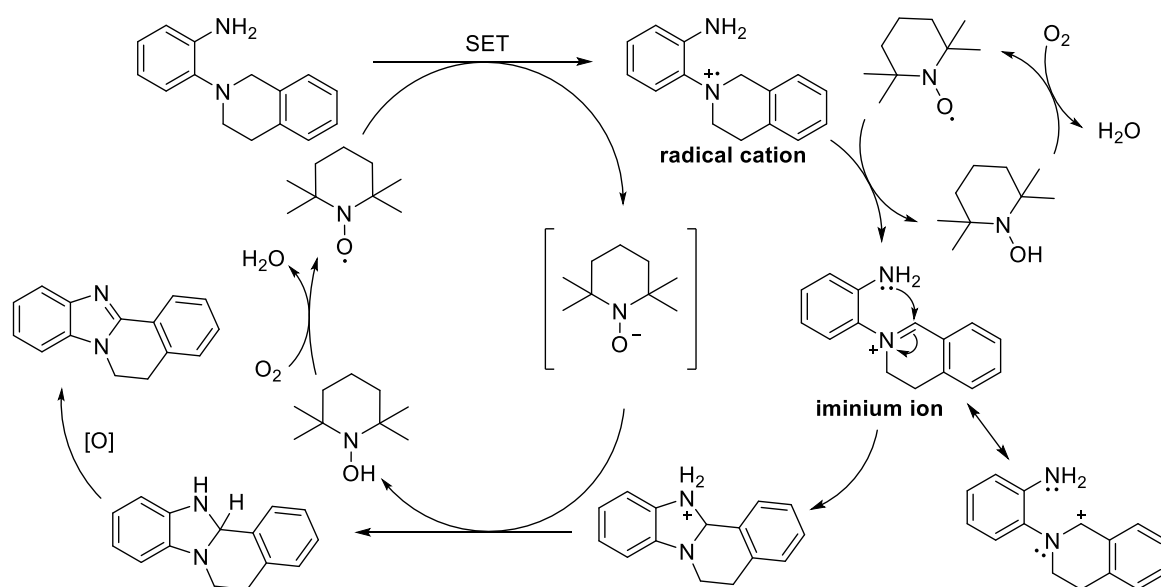
Scheme 1.19. TEMPO-mediated annulation mechanism to give tetracyclic ring-fused benzimidazoles.[113]

Recent literature is littered with examples of ring-fused benzimidazole formation via cross dehydrogenative coupling (CDC). CDC is a process where a C-N bond is formed directly from C-H and N-H bonds under oxidative conditions with a formal loss of H_2, often catalysed by metals.[114] The main advantage of CDC is that it avoids prefunctionalisation of substrates. Pentamethylcyclopentadienyl iridium(III) dichloride ($[Cp^*IrCl_2]_2$) and a 2-hydroxypyridine complex in trifluoroethanol catalyzed the CDC oxidative cyclization of *o*-tetrahydroisoquinoline substituted aniline derivatives in high yield albeit with the requirement for long reaction times (96-120 h) (Scheme 1.20).[115] Interestingly, regioselective control is dictated by the bulk around the primary amine. The *o*-cyclic amine substituted aniline cyclization proceeds via C(1)H_2 of tetrahydroisoquinoline due to stabilisation of the benzylic carbocation, giving the thermodynamic product **14** in 94% yield. The presence of the acetamide derivative hinders cyclization at the preferred position due to steric bulk and the cyclization occurs via C(3)H_2, forming the other isomer **15**, which is the kinetic product in a yield of 82%. The formamide derivative has less bulk

than the acetamide and therefore forms a mixture of the thermodynamic and kinetic products with a higher yield of 44% for the thermodynamic product **14** (Scheme 1.20).
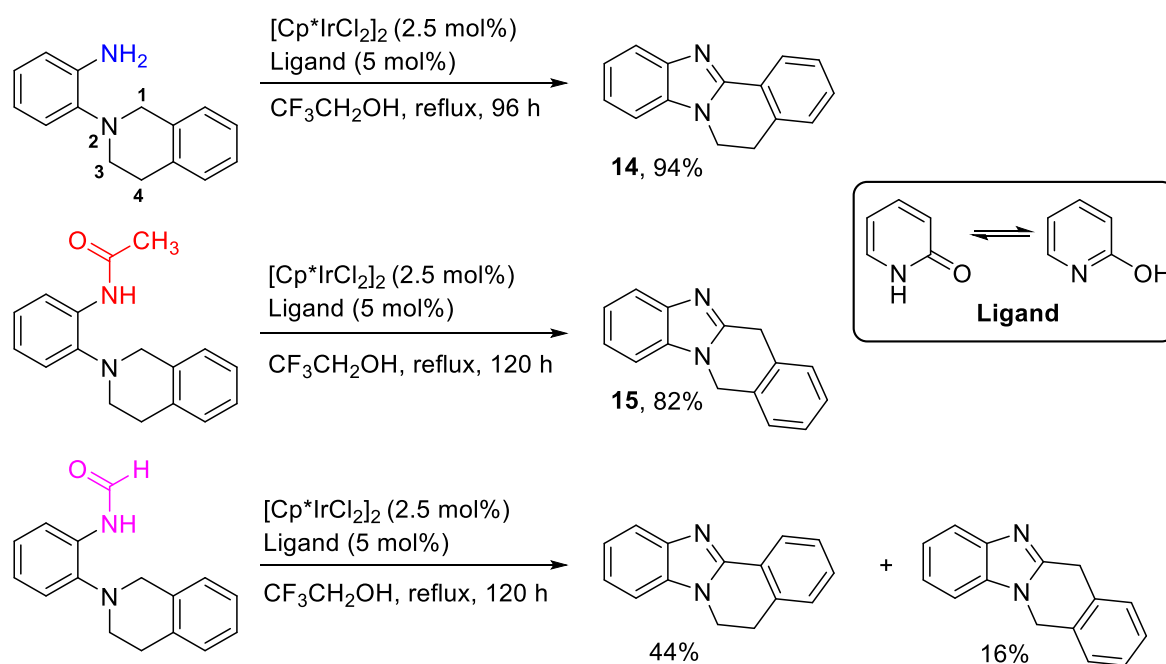
Scheme 1.20. Dihydroisoquinoline ring-fused benzimidazole isomer formation.[115]

Sun and co-workers delivered a series of ring-fused benzimidazoles via oxidative cyclization catalyzed by bis(1,5-cyclooctadiene)diiridium(I) dichloride ([Ir(cod)Cl]$_2$) in trifluoroethanol without the requirement of a ligand (Scheme 1.21).[116] The reaction was classified as acceptorless CDC due to the release of H$_2$ gas, which was detected by GC-TCD analysis. The pyrrolo-, azepino- and azocino[1,2-*a*]benzimidazoles were synthesized in very good yields with the iridium catalyst, but the morpholino and piperazino analogues were only found in trace amounts. The reduced electronic density on the α-carbon of the tertiary amine was attributed for the lack of reactivity in those analogues. The dihydroisoquinoline and hydroisoindole ring-fused benzimidazoles were also afforded via cyclization onto benzylic methylene groups in 92 and 77% yield respectively (Scheme 1.21). The yields are similar to those achieved with TEMPO (Scheme 1.18) and Ir(III) catalysts (Scheme 1.20).
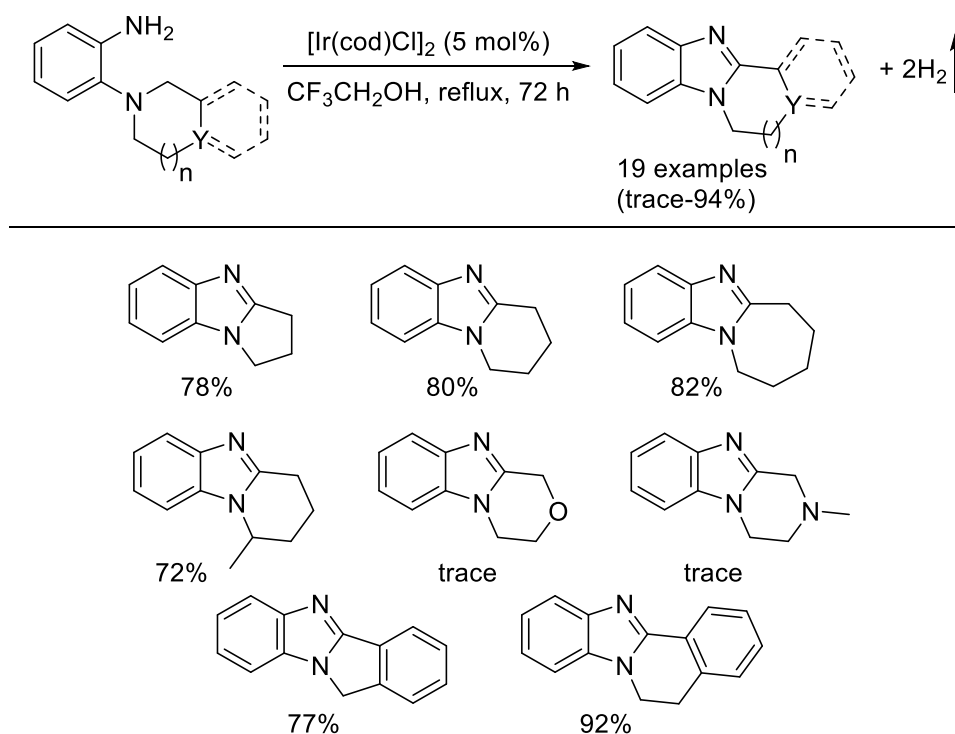
Scheme 1.21. Oxidative cyclization via [Ir(cod)Cl]$_2$ transition metal-catalysis.[116]

The proposed mechanistic route (Scheme 1.22) involves coordination of the amino group with Ir(I) catalyst allowing CH insertion to take place to give intermediate **16**. The oxidative addition intermediate **17** is formed by the release of H$_2$ and then undergoes reductive elimination to form the dihydrobenzimidazole. The abstraction of a hydride generates Ir-H and an iminium ion. The release of another molecule of H$_2$ allows rearomatization to give the desired alicyclic ring-fused [1,2-*a*]benzimidazole.
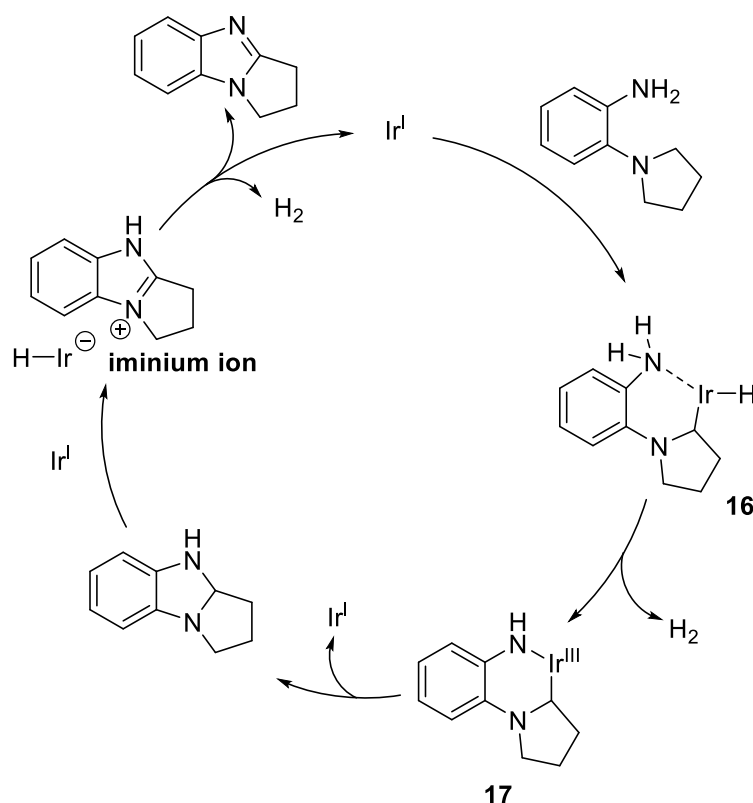
Scheme 1.22. [Ir(cod)Cl]$_2$ mediated mechanistic route to synthesize benzimidazoles.[116]

Mal and co-workers have isolated the dihydroisoquinoline ring-fused benzimidazole **14** in good yield of 78% via an organocatalysis using PhI-*m*CPBA in hexafluoroisopropanol and CH$_2$Cl$_2$ (Scheme 1.23a).[117] A large stoichiometric amount of *m*CPBA is required to oxidize a catalytic amount of iodobenzene (PhI) to generate iodine(III) species that perform the oxidative cyclization.
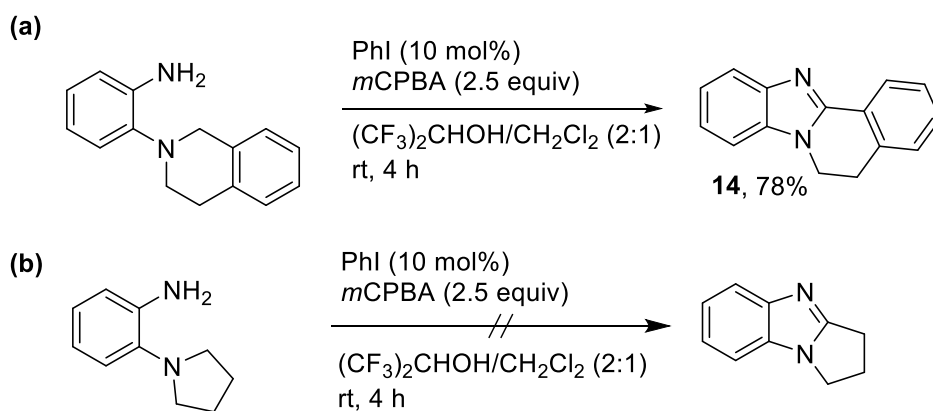
Scheme 1.23. *m*CPBA-mediated oxidative cyclization of *o*-tetrahydroisoquinoline substituted aniline.[117]

The limited substrate scope using the PhI-*m*CPBA methodology was illustrated by the failed attempt to cyclize *o*-pyrrolo substituted aniline (Scheme 1.23b), showing the stabilising effect of a benzylic carbocation was necessary for cyclization.[117]

Purkait et al. have accomplished a 2 in 1 pot oxidative annulation of nitrosobenzenes (Scheme 1.24).[118] The process facilitates selective nucleophilic aromatic hydrogen substitution (S_NArH) of nitrosobenzenes with alicyclic secondary amines, followed by oxidative annulation in toluene at reflux with the additive of 2,4-dichlorobenzoic acid (DCBA) to produce ring-fused benzimidazoles (Scheme 1.24).[118]
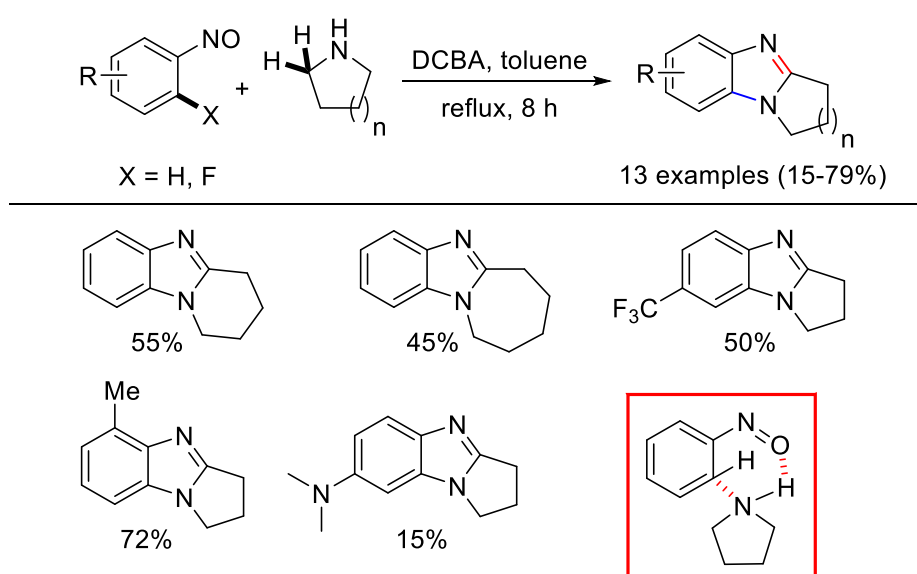
Scheme 1.24. S_NArH of nitrosobenzene followed by annulation to form ring-fused [1,2-*a*]benzimidazoles.[118]

Purkait et al. had to prepare nitrosobenzenes for every reaction by oxidizing commercially available anilines with Oxone®. The strongly donating dimethylamino substituent reduced the electrophilicity of the nitroso moiety, and led to a low yield of 15%, but in general both electron withdrawing and donating substituents were well tolerated (Scheme 1.24). S_NArH of nitrosobenzene with ring-expanded piperido- and azepino- analogues, followed by subsequent annulation to form ring-fused [1,2-*a*]benzimidazoles gave poor yields. The piperido- and azepino- analogues required nucleophilic aromatic substitution (S_NAr) of 2-fluoronitrosobenzene to achieve reasonable yields of 55 and 45% respectively (Scheme 1.24).

The versatility of the substrate scope of this methodology was illustrated by the *ipso*-nucleophilic substitutions of nitrosonaphthols with secondary cyclic amines and subsequent oxidative cyclization to deliver a diverse range of ring-fused naphthoimidazoles (Scheme 1.25). The *R*-prolinol ring-fused imidazole was isolated in high enantiomeric purity (>99% ee) but with a low yield of 30%.[118]
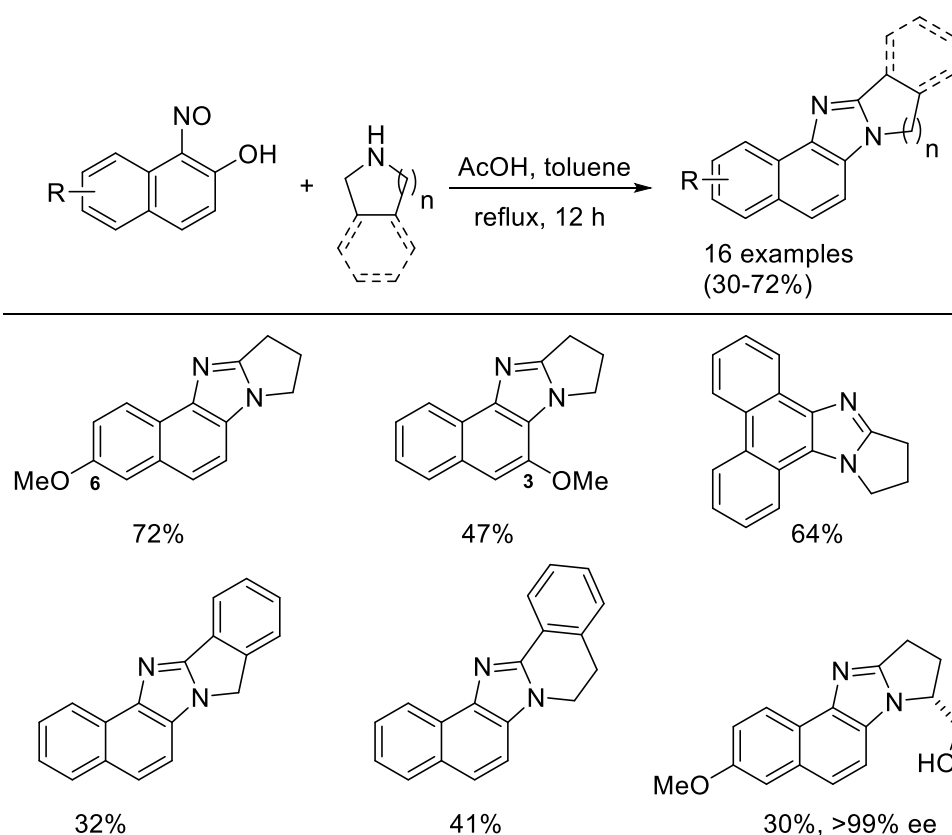
Scheme 1.25. *ipso*-Substitution of nitrosonaphtol followed by annulation to form ring-fused naphthoimidazoles.[118]

The amination of nitrosobenzene with pyrrolidine occurred by S$_N$ArH (blue arrows) and substitution was directed *o*-selective by the hydrogen bonding of the nitroso group, which was supported by DFT studies (Scheme 1.24). The substitution went through mass spectrometry detected *o*-cyclic amine substituted phenyl hydroxylamine **18**, which was then oxidized to the *o*-cyclic amine substituted nitrosoarene intermediate **19** (Scheme 1.26). Compound **19** undergoes a 1,5-hydrogen shift to generate an iminium ion **21** which annulates and further acid mediated dehydration forms pyrrolo[1,2-*a*]benzimidazole. The nitrosonaphthol (red arrows) tautomerises to the keto-oxime derivative and undergoes *ipso*-nucleophilic substitution to form the pyrrolidine substituted oxime intermediate **20**,

which upon loss of water forms the pyrrolo substituted nitrosoarene **19**. Alternatively, the iminium ion **21** can be formed by dehydration of intermediate **20**, which is followed by deprotonation and mesomerization of the resultant isomeric iminium ion (Scheme 1.26).
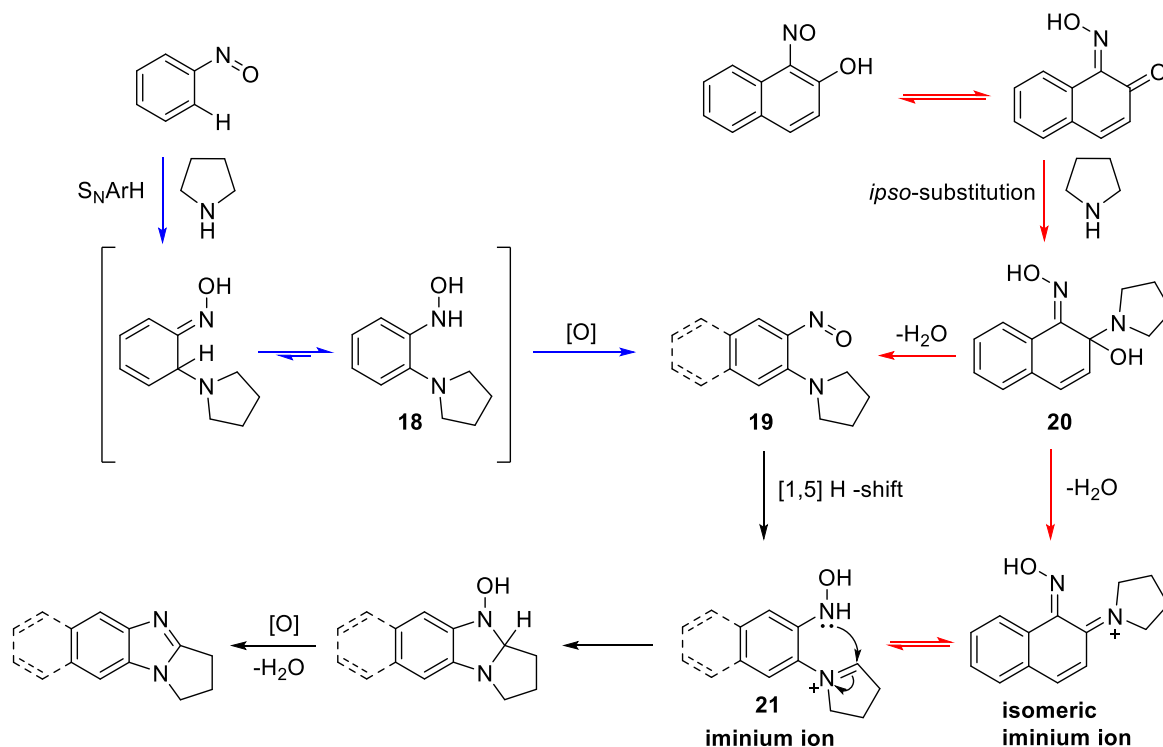
Scheme 1.26. Mechanistic pathway detailing S_NArH and *ipso-* nucleophilic substitution followed by annulation to form ring-fused benzimidazoles.[118]

Following Saunders initial work on aryl azides,[119] Meth-Cohn also showed that aryl azides as *o*-substituents decompose under thermal conditions in nitrobenzene at high temperatures and cyclize onto the tertiary amine to yield ring-fused imidazo[4,5-*c*]pyridines (Scheme 1.27).[104] The reaction yields increase as the tertiary amine ring size becomes larger, with the azepino analogue having the highest yield at 72%. A downside to this synthetic approach is that the majority of oxidative cyclizations can be carried out successfully on *o*-cyclic amine substituted anilines, without further need for functionalisation to the aryl azide via diazotization and subsequent substitution with sodium azide (Scheme 1.27).
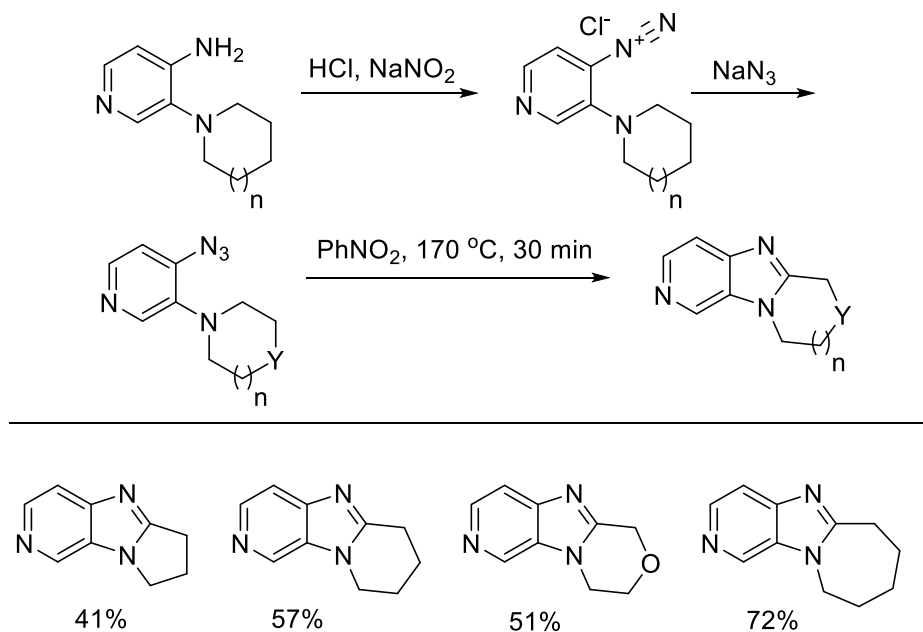
Scheme 1.27. Aryl azide thermal decomposition to give ring-fused imidazo[4,5-c]pyridines.[104]

A new route to ring-fused [1,2-a]benzimidazoles has been achieved by reacting o-cyclic tertiary amine substituted phenyl iodide **22** with sodium azide under copper catalysis (Scheme 1.28).[120] The CuI-catalyzed coupling reaction of **22** with sodium azide alongside Cu promoted SET oxidation leads to the aryl azide intermediate **23**. The iminium ion undergoes nucleophilic attack from the azide group forming a hydrobenzimidazole, which is further oxidized to give the pyrido[1,2-a]benzimidazole in a poor yield of 25%. The other pathway proposed involved a concerted intramolecular cyclization.[120] The yield is considerably reduced when compared to that achieved using the metal-free performic acid or Ir(I) metal catalysis methodologies.[102, 116]
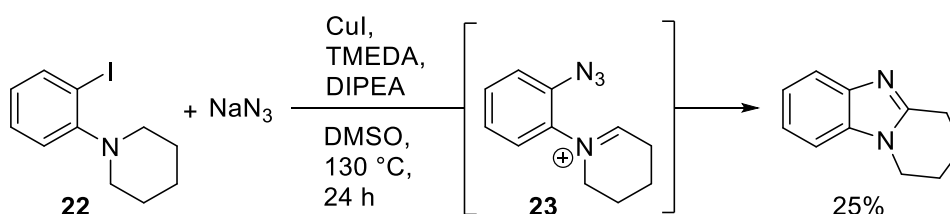
Scheme 1.28. Aryl azide annulation catalysed by CuI.[120]

In addition to oxidative C-N bond forming reactions, halogenation can occur in parallel under specified reaction conditions. Meth-Cohn showed that o-cyclic amine substituted

anilines in neat sulfuryl chloride react in an endothermic fashion to undergo oxidative cyclization with concomitant tetrachlorination of the highly activated aromatic nucleus in good yield (Scheme 1.29).[121] The attempt to tetrachlorinate the *o*-pyrrolo substituted aniline analogue led to an inseparable mixture of mono-, di- and trichloro ring-fused benzimidazoles. The aromatic halogenation is believed to occur first followed by cyclization of the sulphonylamine either through a nitrene or by intramolecular hydrogen abstraction and cyclization.
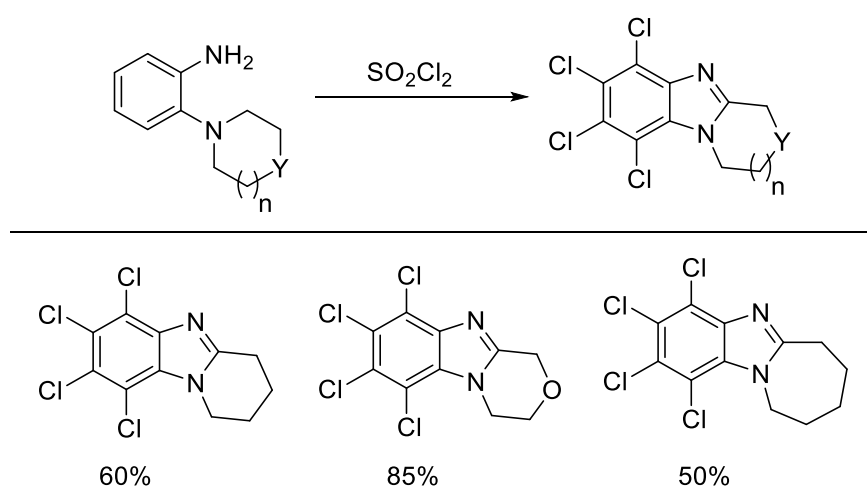
Scheme 1.29. Sulfuryl chloride facilitated oxidative cyclization and aromatic chlorination.[121]

1.2.2. Oxidative cyclization of amidine derivatives (Route C)
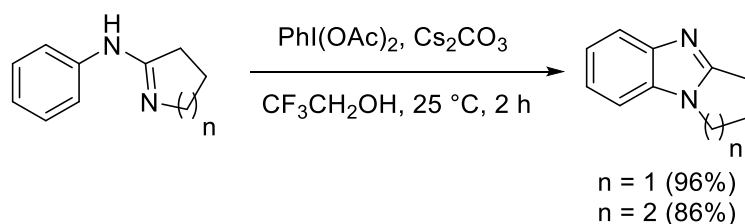
Scheme 1.30. PIDA oxidative annulation of cyclic *N*-alkylbenzamidines.[122]

Zhu and Huang obtained the pyrrolo- and pyrido[1,2-*a*]benzimidazoles in excellent yields under metal-free conditions of PIDA with the inorganic base Cs_2CO_3 in trifluroethanol at room temperature (Scheme 1.30).[122] The reaction mechanism is believed to go through an imidyl radical that adds onto the aromatic ring which is oxidized to a cyclohexadienyl cation by SET and finally hydrogen abstraction gives the required ring-fused benzimidazole. However, synthesis of the cyclic arylamidines is usually multi-step, requiring the use of air sensitive reagents ($POCl_3$, PCl_5) and harsh reaction conditions, which ultimately limits the substrate range.

Saito and Kutsumura employed metal-free hypervalent iodine reagents to effect the dehydrogenative oxidative transformation of cyclic *N*-alkylbenzamidines to yield the desired thiazolo, thiazino and oxazino ring-fused benzimidazoles (Scheme 1.31).[123] Kosher's reagent (PhI(OH)OTs) in acetonitrile was shown to be the most effective reagent producing the highest yielding benzimidazoles. The substituted thiazolo and thiazino ring-fused benzimidazoles were isolated in good yields except for when there was a substituent at the R^2 position (Scheme 1.31). The methoxy analogue at the R^3 position was realised in a yield more than two times greater when compared to the equivalent methoxy analogue at the R^2 position (Scheme 1.31). The fluoro analogue at the R^2 position was only detected in trace amounts after 20 h. The oxazino ring-fused benzimidazole was isolated in a good yield of 76% but required the use of 4Å molecular sieves due to acid sensitivity and had a long reaction time of 27 h (Scheme 1.31). The reaction scope was extended out to the additional aromatic ring-fused oxazino-benzimidazole, which was synthesized in a good yield of 79%.
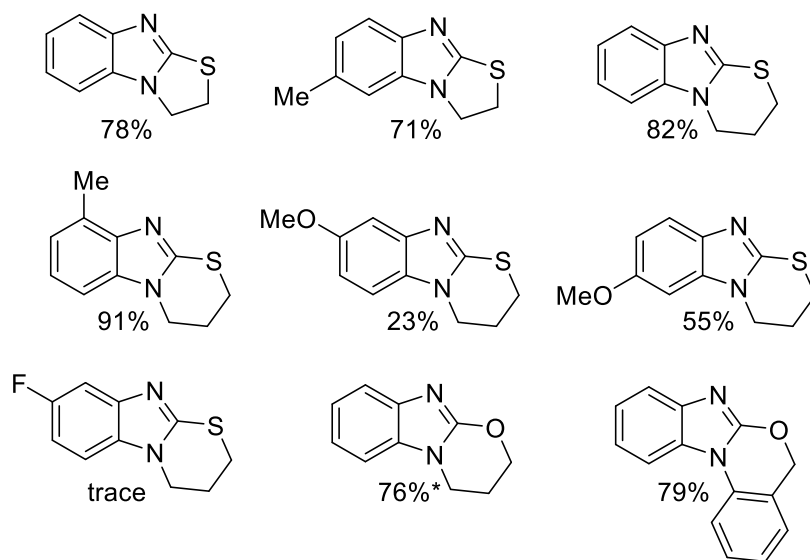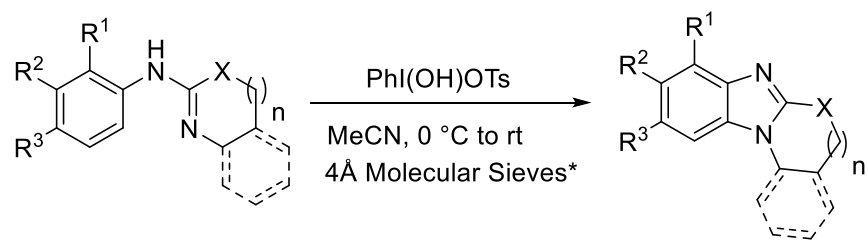
Scheme 1.31. Hypervalent iodine reagent oxidative annulation of cyclic *N*-alkylbenzamidines.[123]

1.2.3. Oxidative cyclizations of 1- and 2- substituted benzimidazoles (Route E)

Intramolecular homolytic aromatic substitutions (HAS) are achieved with trialkylmetal hydrides (Bu_3SnH) and azo-initiators (2,2-azobisisobutyronitrile (AIBN)). HAS is termed oxidative overall as it involves the formal loss of a hydrogen atom (rearomatization) despite being in the presence of a reductant (Bu_3SnH).
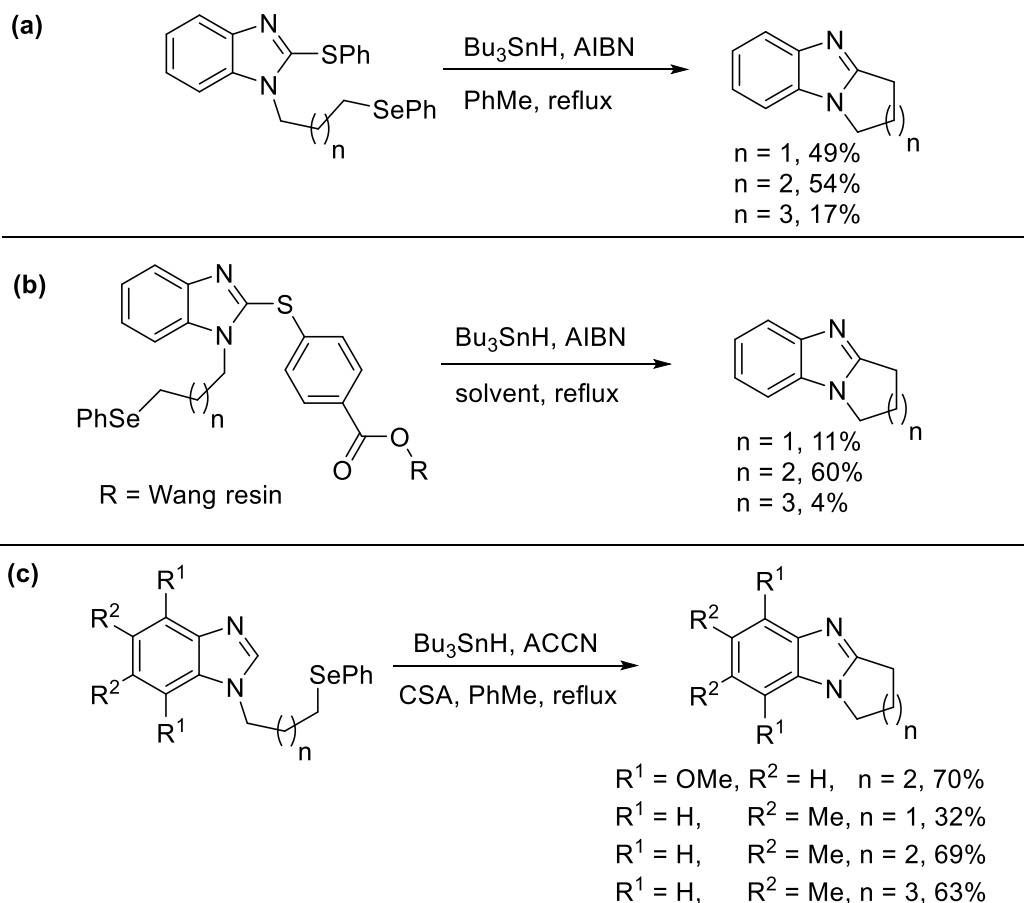
Scheme 1.32. Trialkymetal hydrides and azo-initiator mediated homolytic aromatic substitution.[19, 124, 125]

Bowman and Aldabbagh carried out intramolecular alkyl radical *ipso*-substitutions using phenylselenide radical precursors, displacing the phenylsulfanyl radical leaving group at the 2-position of the benzimidazole (Scheme 1.32a).[124] The pyrido[1,2-*a*]benzimidazole was isolated in the highest yield of 54%. Bowman and Allin reported the immobilisation of the phenylselenide radical precursor on a Wang resin that facilitated solid state oxidative HAS (Scheme 1.32b).[125] The reaction is advantageous as only the ring-fused benzimidazole is released from the resin upon cyclization and the product is separated

from the radical reagents with a dilute HCl extraction. The yields are comparable to solution-phase reactions, with the less strained six-membered ring cyclization occurring in higher yields to that of the more strained five and seven-membered cyclizations.[125]

Aldabbagh and Lynch used Bu$_3$SnH/1,1'-azobis(cyclohexanecarbonitrile) (ACCN) HAS to obtain alicyclic ring-fused benzimidazoles without the requirement for radical leaving groups at the imidazole-2-position by activating 3-*N* of imidazole with camphorsulfonic acid (CSA) (Scheme 1.32c).[19] The pyrido- and azepino[1,2-*a*]benzimidazoles were obtained in a good yield but a poor yield of 32% was obtained for the more strained five-membered cyclization.

Aldabbagh and Fagan utilised Bu$_3$SnH/ACCN to carry out a one-pot double intramolecular oxidative cyclization of primary alkyl radicals onto imidazo[5,4-*f*]benzimidazoles and imidazo[4,5-*f*]benzimidazoles in air (Scheme 1.33).[49] The pyrido- imidazobenzimidazoles were reported in excellent yields of 81% (**10b**) and 90% (**12e**) for the respective [4,5-*f*] and [5,4-*f*] isomers.

imidazo[4,5-*f*]benzimidazoles
10a: n = 1, 48%
10b: n = 2, 81%*
10c: n = 3, 48%

imidazo[5,4-*f*]benzimidazoles
12d: n = 1, 47%
12e: n = 2, 90%*
12f: n = 3, 54%
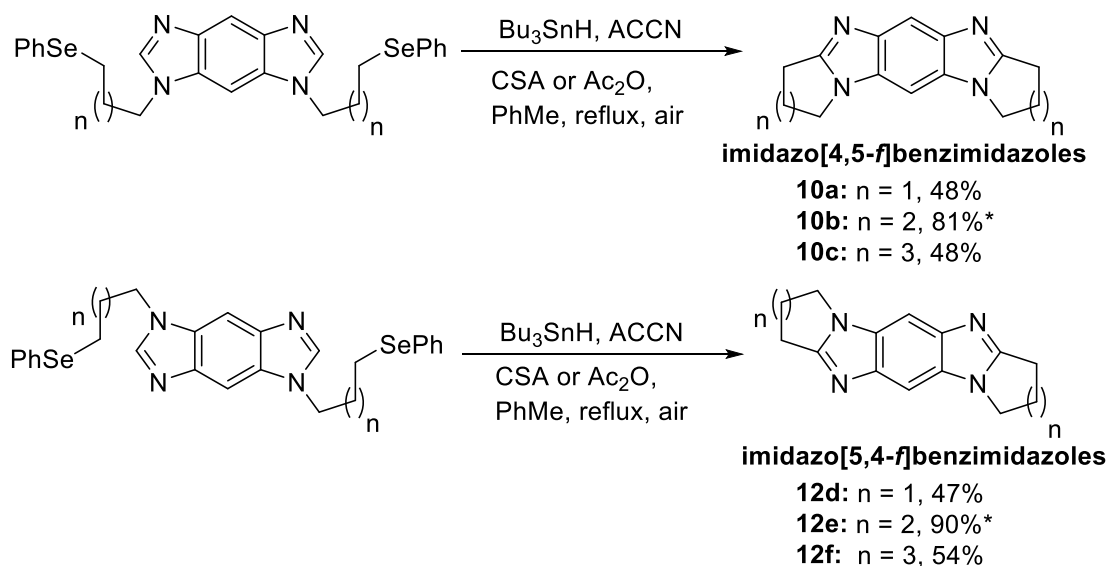
Scheme 1.33. Bu$_3$SnH/ACCN mediated double intramolecular homolytic aromatic substitution onto imidazobenzimidazoles.[49] *No CSA or Ac$_2$O required.

The reactions negated the need for quaternisation of the basic nitrogen atoms and provided imidazobenzimidazoles of superior yield in the comparison to the performic acid methodology (Scheme 1.14). The quarternization of the basic nitrogen atoms was required

to obtain the pyrrolo- and azepino- imidazobenzimidazoles in moderate yields with CSA and Ac$_2$O used for the analogues respectively.

However, the concentration of reductant Bu$_3$SnH must be kept low via syringe pump addition in order to avoid reduction of the cyclizing radicals, and to promote the aromatic substitution reaction. The non-chain reaction produces significant amount of organotin waste, which is difficult to dispose of. The hydrogen abstraction required for oxidative rearomatization is performed by azo-initiators and as a result, stoichiometric amounts of the hazardous and toxic initiators are required.

Aldabbagh and Coyle achieved a more benign intramolecular HAS route towards ring-fused [1,2-*a*]benzimidazoles via Barton ester intermediates (pyridine-2-thione-*N*-oxycarbonyl (PTOC) or *O*-acyl thiohydroxamate ester) formed using *S*-(1-oxido-2-pyridinyl)-1,1,3,3-tetramethylthiouronium hexafluorophosphate (HOTT) under tin and initiator-free conditions (Scheme 1.34).[126]
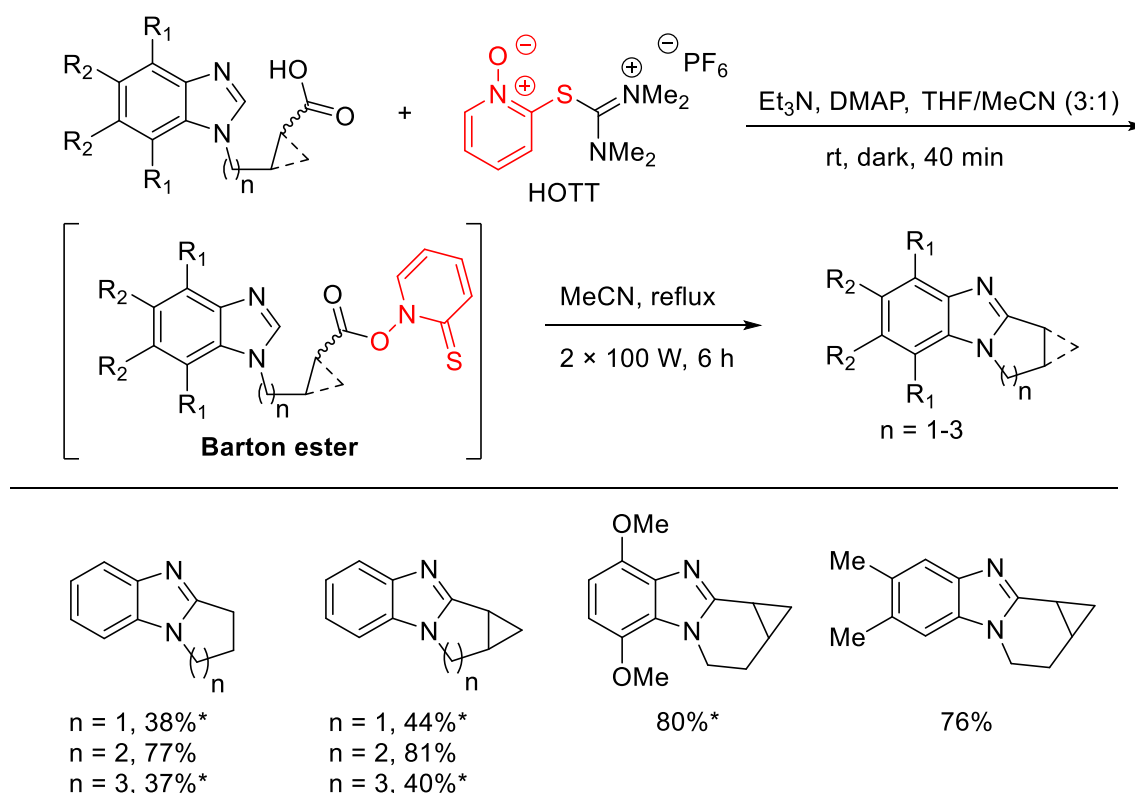
Scheme 1.34. Intramolecular oxidative homolytic aromatic substitution via Barton ester intermediates.[126] *CSA required.

HOTT reacts with the carboxylic acid in the dark to form a Barton ester intermediate that upon exposure to light decomposes to cyclopropyl and alkyl radicals that add onto the 2-position of the benzimidazoles (Scheme 1.34). Yet again, the formation of pyrido[1,2-*a*]benzimidazoles with or without ring-fused cyclopropane were more favoured than their pyrrolo- and azepino[1,2-*a*]benzimidazole analogues and were isolated in excellent yields of 76-81% (Scheme 1.34). The methoxy groups on the 4,7-dimethoxybenzimidazole deactivate radical cyclization at the imidazole-2-position and CSA was required to quaternize 3-*N* of imidazole for HAS to proceed.

DeBoef and Pereira employed Pd(II)/Cu(I) catalysis with the oxidant of Cu(II) acetate to effect oxidative dehydrogenative coupling of 1-benzyl substituted benzimidazoles in 1,4-dioxane using microwave heating (Scheme 1.35).[127] The addition of CsOPiv eliminated any acetoxylated oxidation by-products. The presence of electron donating groups (EDG) on the aromatic rings promoted coupling and gave the desired ring-fused benzimidazoles in higher yields when compared to the lower yielding benzimidazoles that beared electron withdrawing groups (EWG). A combination of EDGs and EWGs on aromatic rings of 1-benzyl substituted benzimidazoles decreased the yields relative to those obtained with just EDGs.
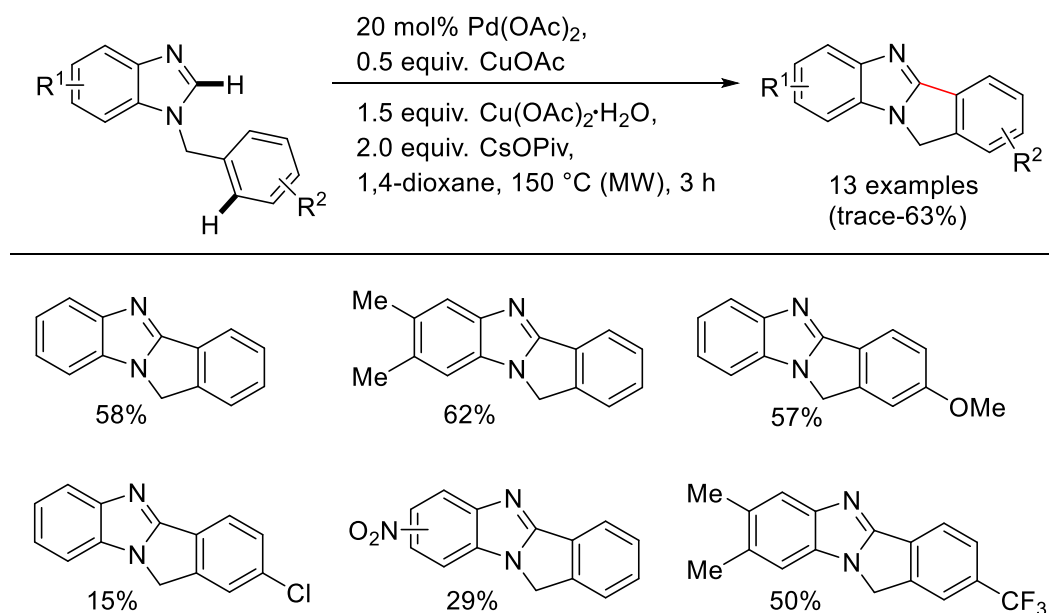
Scheme 1.35. Pd/Cu catalysed coupling of 1-aryl substituted benzimidazoles.[127]

The mechanism follows two metalation steps, firstly the insertion of Cu(I) onto the 2-position of the benzimidazole to form a Cu(I)-benzimidazole complex. Subsequently, there is palladation on the arene of the benzyl substituent followed by transmetalation to form a Pd(II) complex with loss of Cu(OAc). Finally, reductive elimination generates the desired aryl coupled benzimidazole.[127]

Wang and Guo reported a double one-pot palladium catalysed oxidative coupling between 2-aryl substituted benzimidazoles and 1H-benzimidazoles in DMF using Cu(OAc)$_2$ as an oxidant to furnish hexacylic ring-fused benzimidazoles (Scheme 1.36).[128] In line with DeBoef and Pereira's observation, EDGs allowed the coupling reactions to proceed in good yield but with increasing strength of the EWGs, reactions occurred in reduced yields.
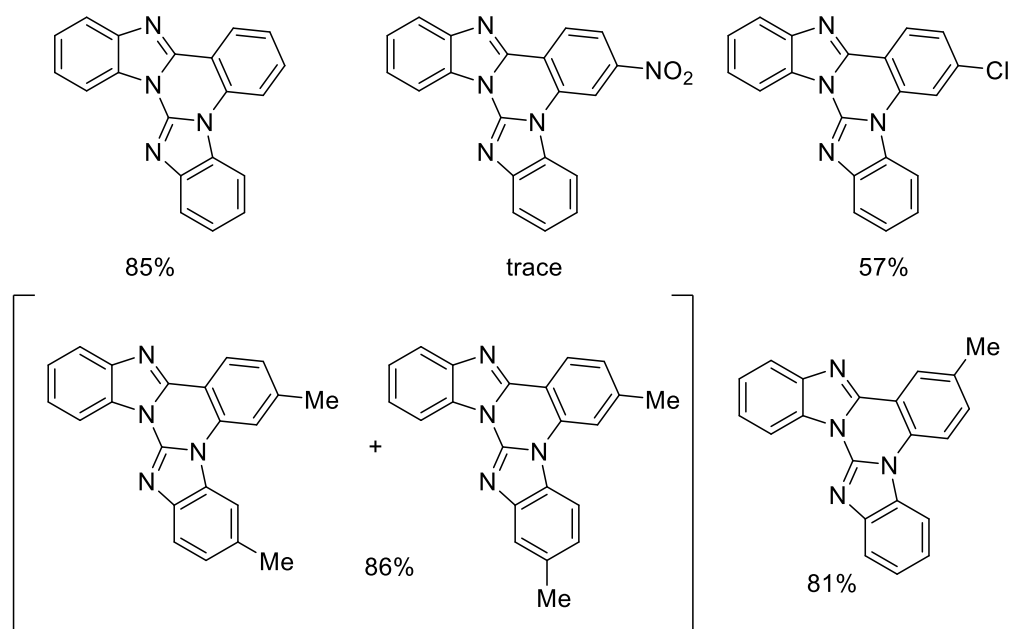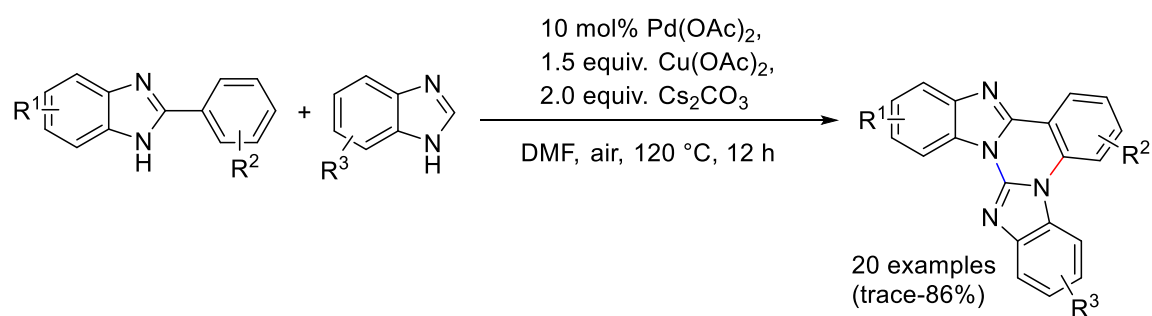
Scheme 1.36. Pd catalysed CDCs between aryl substituted benzimidazoles and unsubstituted benzimidazoles.[128]

Wang and Guo believe the reduced electron density on the aryl ring from EWGs disfavours palladium chelation and hence the reduced yields. The placement of EDGs on R^2 and R^3 positions of the aryl rings results in a mixture of isomers in a high yield of 86%. The mechanism proceeds by the arylbenzimidazole undergoing palladation at 3-*N* of the imidazole. Then, Cu(OAc)$_2$ mediated oxidative addition of 1*H*-benzimidazole at the 3-*N* position occurs to produce an oxidized Pd(IV) species that is reductively eliminated to form the aminated arylbenzimidazole. The aminated arylbenzimidazole then undergoes further palladation at 1-*N* of the imidazole followed by CS$_2$CO$_3$ deprotonation with loss of acetic acid to form a Pd(II) palladacycle. The final step of reductive elimination forms the desired hexacyclic benzimidazole.[128] The downside to the CDC reactions of Pereira and Guo is that to achieve good yields, the substrate scopes are limited to those with EDGs. The CDCs also employ expensive palladium catalysts.

Yu and Sun have achieved the first known decarboxylative tandem radical addition/cyclization of functionalised 2-arylbenzimidazoles and carboxylic acids using Ag catalysis under inert conditions (Scheme 1.37).[129] A diverse range of ring-fused benzimidazoles were formed in excellent yield due to the wide substrate scope of carboxylic acids available. Many tertiary α-substituted aliphatic carboxylic acids including pivalic acid reacted with the functionalised 2-arylbenzimidazoles to form the tetracyclic ring-fused benzimidazoles and in particular, the pharmaceutically relevant adamantane analogue was isolated in 73% yield (Scheme 1.37). In addition, secondary and surprisingly primary α-substituted aliphatic carboxylic acids have been incorporated onto the benzimidazole scaffold e.g. 2-ethylbutanoic acid, four-membered ring carboxylic acids and propionic acid (Scheme 1.37). The placement of EDGs and EWGs on the aryl rings had no electronic effect on the decarboxylative tandem radical cyclization with pivalic acid. 2-oxocarboxylic acids were also suitable precursor alkyl radicals to initiate the tandem radical cyclization giving the corresponding benzimidazoles in high yields of 76 and 79% (Scheme 1.37).
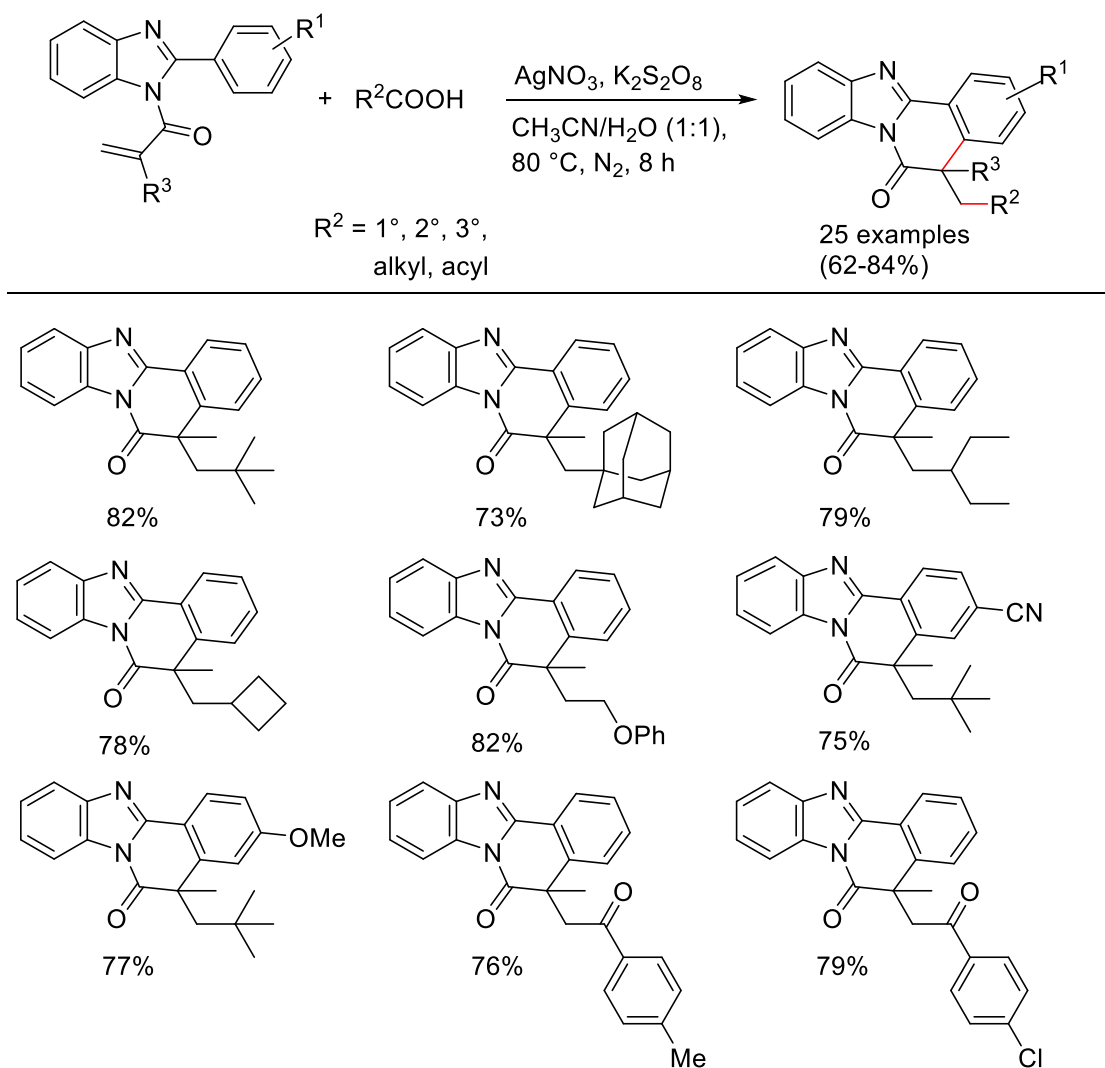
Scheme 1.37. AgNO$_3$/K$_2$S$_2$O$_8$ mediated decarboxylative tandem radical cylizations.[129]

The mechanism involves the oxidation of Ag(I) by persulfate (S$_2$O$_8^{2-}$) to generate Ag(II) species that interacts with tertiary α-substituted aliphatic pivalic acid **24** yielding a silver carboxylate complex **25** (Scheme 1.38). Carboxylate **25** undergoes homolytic cleavage generating a *t*-butyl radical **26** with the release of CO$_2$ and regeneration of the Ag catalyst. The tertiary radical **26** adds onto the alkene of the 2-aryl substituted benzimidazole to deliver the intermediate radical **27** which undergoes a 6-*endo*-trig cyclization to yield the annulated intermediate **28**. Cyclohexadienyl radical **28** is oxidized by Ag^{2+} via SET to give the cyclohexadienyl cation intermediate that is rearomatized by deprotonation to deliver the desired ring-fused benzimidazole.
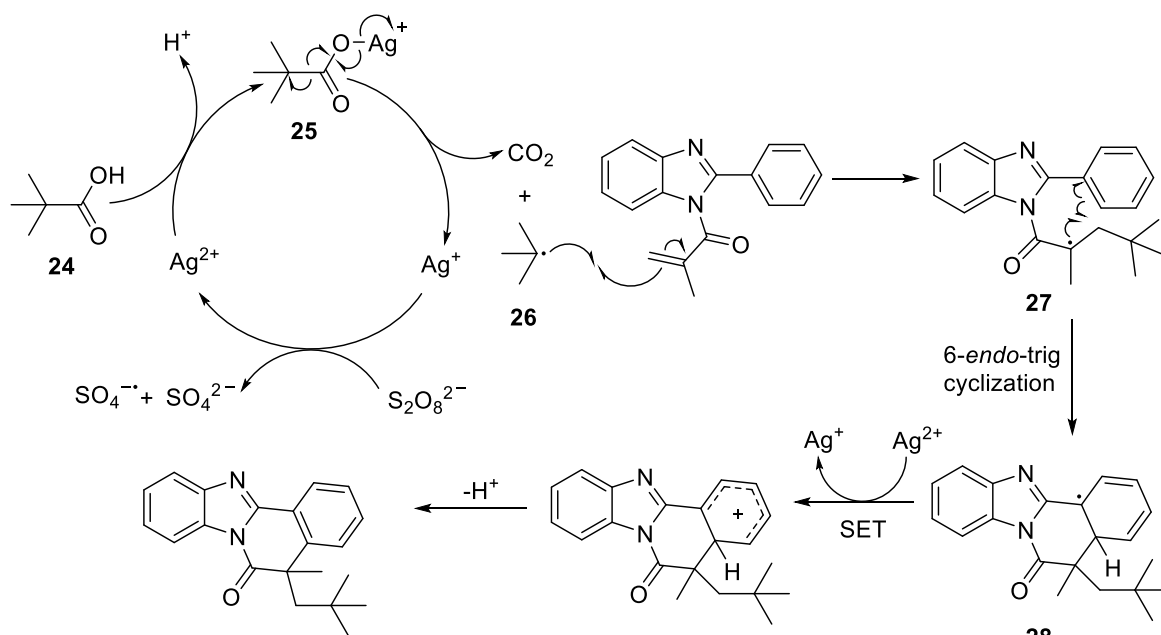
Scheme 1.38. Proposed mechanism of decarboxylative tandem radical cyclization.[129]

1.3. In Summary

The combination of formic acid and hydrogen peroxide, despite use in stoichiometric amounts, offers broad substrate scope and functional group tolerance to maintain a critical role in mono- and double oxidative annulations. The advent of cross dehydrogenative coupling (CDC) with stoichiometric oxidants[113, 117] and metal catalysts[115] requires more activated benzylic methylene groups for cyclization. [Ir(cod)Cl]$_2$[116] showed the best substrate scope, reacting with both benzyl and alkyl methylene groups but when heteroatoms were placed on alkyl tertiary amines, negligible amounts of benzimidazole were formed. The palladium catalysed CDCs only proceeded well in the presence of electron rich substrates.[127, 128] However, the CDCs display high atom economy as no prefunctionalization of substrates is required and often H$_2$ gas is the only by-product. The synthesis of cyclic amidine precursors involves harsh, multi-step conditions and there is a limited substrate scope for oxidative annulation.[122, 123] Homolytic aromatic substitution (HAS) employs toxic organotin reagents and hazardous azo-initiators[19, 124] with more benign HAS achieved with the recently developed Barton's esters.[126] The one-pot S$_N$ArH and oxidative annulations involving nitrosobenzenes and nitrosonaphthols are advantageous as the need for a multi-step synthesis is avoided.[118] However, the alicyclic tertiary amine substituted nitrosobenzenes are very unstable and have never been isolated.[101]

1.4. PhD Thesis Aims and Objectives

- To develop a greener synthesis of ring-fused benzimidazoles, including appropriate substitution to allow the synthesis of bioreductive ring-fused benzimidazolequinone anti-cancer agents. This will involve modification to the well-established H_2O_2 in carboxylic acid solvent mediated ring-closure of o-cyclic amine substituted anilines. (Work to be described in Chapter 2)
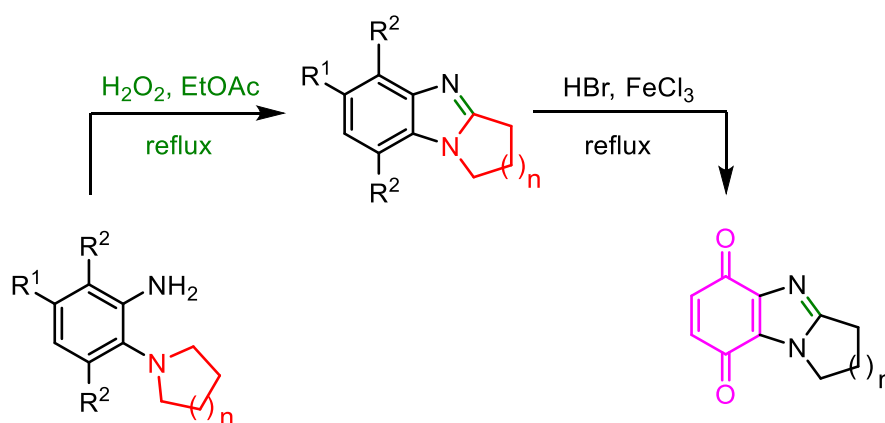
- To establish scope and reactivity patterns for the one-pot synthesis of halogenated ring-fused benzimidazolequinones from 3,6-dimethoxy-2-(cycloamino)anilines using H_2O_2 with HCl and HBr. This follows on from preliminary findings made in the PhD thesis of Michael Gurry (former Aldabbagh group member). This thesis will also establish the use of elemental halogens for this transformation. (Work to be described in Chapter 3).
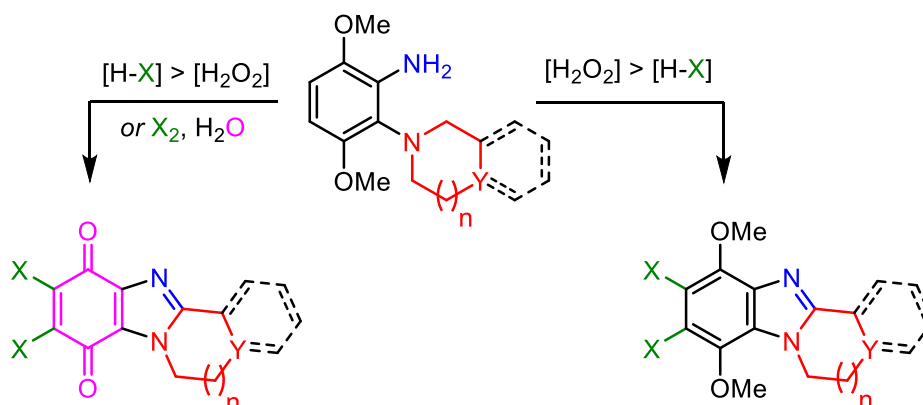
- To evaluate anti-cancer activity and mechanism of action for a library of benzo[1,2,4]triazin-7-ones supplied by the Koutentis group (University of Cyprus). (Work to be described in Chapter 4).

Pleurotin   Benzo[1,2,4]triazin-7-ones
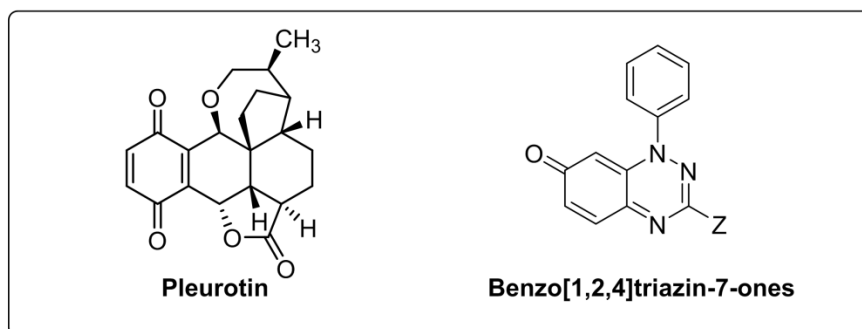
1.5. References

1. Brink, N. G.; Folkers, K. *J. Am. Chem. Soc.* **1950**, *72*, 4442-4443.

2. Charlson, A. J.; Harington, J. S. *Carbohydr. Res.* **1975**, *43*, 383-387.

3. Gregg, R. E. Compounds for Use in Treating Acute Coronary Syndrome and Related Conditions. U.S. Patent 20170231992A1, August 17, 2017.

4. Kamerzell, T. Fused Heterocyclic Organic Compounds, Pharmaceutical Compositions, and Medical Uses Thereof. WO Patent 2015061280A1, 30 April, 2015.

5. Wang, Y.; Liu, W.-J.; Yin, L.; Li, H.; Chen, Z.-H.; Zhu, D.-X.; Song, X.-Q.; Cheng, Z.-Z.; Song, P.; Wang, Z.; Li, Z.-G. *Bioorg. Med. Chem. Lett.* **2018**, *28*, 974-978.

6. Wenjian, L.; Yin, L.; Li, H. Kinase Inhibitor, And Preparing Method And Pharmaceutical Use Thereof. U.S. Patent 20180305363A1, October 25, 2018.

7. Kojima, T.; Mochizuki, M.; Takai, T.; Hoashi, Y.; Morimoto, S.; Seto, M.; Nakamura, M.; Kobayashi, K.; Sako, Y.; Tanaka, M.; Kanzaki, N.; Kosugi, Y.; Yano, T.; Aso, K. *Bioorg. Med. Chem.* **2018**, *26*, 2229-2250.

8. Chytil, M.; Engel, S. R.; Fang, Q. K.; Spear, K. L. Histamine H3 Inverse Agonists and Antagonists and Methods Of Use Thereof. U.S. Patent 20100204214A1, August 12, 2010.

9. Alexander, R. P.; Calmiano, M. D.; Defays, S.; Durieu, V.; Deligny, M.; Heer, J. P.; Jackson, V. E.; Keyaerts, J.; Kroplien, B.; Mac Coss, M.; Sabnis, Y. A.; Selby, M. D.; Swinnen, D. L. L.; Van Houtvin, N.; Zhu, Z.; Heinelt, U.; Wehner, V. Fused Tricyclic Benzimidazole Derivatives as Modulators of TNF Activity. U.S. Patent 9932343B2, April 3, 2018.

10. Bonham, S.; O'Donovan, L.; Carty, M. P.; Aldabbagh, F. *Org. Biomol. Chem.* **2011**, *9*, 6700-6706.

11. Deady, L. W.; Rodemann, T. *Aust. J. Chem.* **2002**, *54*, 529-534.

12. Chen, Y.; Hu, L. *Med. Res. Rev.* **2009**, *29*, 29-64.

13. Asche, C. *Mini-Rev. Med. Chem.* **2005**, *5*, 449-467.

14. Garuti, L.; Roberti, M.; Pizzirani, D. *Mini-Rev. Med. Chem.* **2007**, *7*, 481-489.

15. Fahey, K.; Aldabbagh, F. *Irish Chemical News* **2009**, *25*, 24-27.

16. Zhang, K.; Chen, D.; Ma, K.; Wu, X.; Hao, H.; Jiang, S. *J. Med. Chem.* **2018**, *61*, 6983-7003.

17. Sharma, A.; Arambula, J. F.; Koo, S.; Kumar, R.; Singh, H.; Sessler, J. L.; Kim, J. S. *Chem. Soc. Rev.* **2019**, *48*, 771-813.

18. Colucci, M. A.; Couch, G. D.; Moody, C. J. *Org. Biomol. Chem.* **2008**, *6*, 637-656.

19. Lynch, M.; Hehir, S.; Kavanagh, P.; Leech, D.; O'Shaughnessy, J.; Carty, M. P.; Aldabbagh, F. *Chem. Eur. J.* **2007**, *13*, 3218-3226.

20. Yang, Y.; Zhang, Y.; Wu, Q.; Cui, X.; Lin, Z.; Liu, S.; Chen, L. *J. Exp. Clin. Cancer Res.* **2014**, *33*, 14.

21. Bentle, M. S.; Reinicke, K. E.; Dong, Y.; Bey, E. A.; Boothman, D. A. *Cancer Res.* **2007**, *67*, 6936-6945.

22. Ma, Y.; Kong, J.; Yan, G.; Ren, X.; Jin, D.; Jin, T.; Lin, L.; Lin, Z. *BMC Cancer* **2014**, *14*, 414.

23. Dong, Y.; Bey, E. A.; Li, L.-S.; Kabbani, W.; Yan, J.; Xie, X.-J.; Hsieh, J.-T.; Gao, J.; Boothman, D. A. *Cancer Res.* **2010**, *70*, 8088-8096.

24. Li, Z.; Zhang, Y.; Jin, T.; Men, J.; Lin, Z.; Qi, P.; Piao, Y.; Yan, G. *BMC Cancer* **2015**, *15*, 207.

25. Ji, L.; Wei, Y.; Jiang, T.; Wang, S. *Int. J. Clin. Exp. Pathol.* **2014**, *7*, 1124-1131.

26. Boruah, R. C.; Skibo, E. B. *J. Med. Chem.* **1994**, *37*, 1625-1631.

27. Islam, I.; Skibo, E. B. *J. Org. Chem.* **1990**, *55*, 3195-3205.

28. Islam, I.; Skibo, E. B.; Dorr, R. T.; Alberts, D. S. *J. Med. Chem.* **1991**, *34*, 2954-2961.

29. Skibo, E. B.; Schulz, W. G. *J. Med. Chem.* **1993**, *36*, 3050-3055.

30. Schulz, W. G.; Islam, I.; Skibo, E. B. *J. Med. Chem.* **1995**, *38*, 109-118.

31. Skibo, E. B.; Islam, I.; Schulz, W. G.; Zhou, R.; Bess, L.; Boruah, R. *Synlett* **1996**, 297-309.

32. Zhou, R.; Skibo, E. B. *J. Med. Chem.* **1996**, *39*, 4321-4331.

33. Skibo, E. B.; Gordon, S.; Bess, L.; Boruah, R.; Heileman, M. J. *J. Med. Chem.* **1997**, *40*, 1327-1339.

34. Skibo, E. B. *Expert Opin. Ther. Pat.* **1998**, *8*, 673-701.

35. Craigo, W. A.; LeSueur, B. W.; Skibo, E. B. *J. Med. Chem.* **1999**, *42*, 3324-3333.

36. Huang, X.; Suleman, A.; Skibo, E. B. *Bioorg. Chem.* **2000**, *28*, 324-337.

37. Ghodousi, A.; Huang, X.; Cheng, Z.; Skibo, E. B. *J. Med. Chem.* **2004**, *47*, 90-100.

38. Schulz, W. G.; Nieman, R. A.; Skibo, E. B. *Proc. Natl. Acad. Sci. U. S. A.* **1995**, *92*, 11854-11858.

39. Skibo, E. B.; Xing, C. *Biochemistry* **1998**, *37*, 15199-15213.

40. Skibo, E. B.; Jamil, A.; Austin, B.; Hansen, D.; Ghodousi, A. *Org. Biomol. Chem.* **2010**, *8*, 1577-1587.

41. O'Shaughnessy, J.; Cunningham, D.; Kavanagh, P.; Leech, D.; McArdle, P.; Aldabbagh, F. *Synlett* **2004**, 2382-2384.

42. O'Shaughnessy, J.; Aldabbagh, F. *Synthesis* **2005**, 1069-1076.

43. Hehir, S.; O'Donovan, L.; Carty, M. P.; Aldabbagh, F. *Tetrahedron* **2008**, *64*, 4196-4203.

44. Fahey, K.; Aldabbagh, F. *Tetrahedron Lett.* **2008**, *49*, 5235-5237.

45. Fahey, K.; O'Donovan, L.; Carr, M.; Carty, M. P.; Aldabbagh, F. *Eur. J. Med. Chem.* **2010**, *45*, 1873-1879.

46. Moriarty, E.; Carr, M.; Bonham, S.; Carty, M. P.; Aldabbagh, F. *Eur. J. Med. Chem.* **2010**, *45*, 3762-3769.

47. Schulz, W. G.; Skibo, E. B. *J. Med. Chem.* **2000**, *43*, 629-638.

48. Suleman, A.; Skibo, E. B. *J. Med. Chem.* **2002**, *45*, 1211-1220.

49. Fagan, V.; Bonham, S.; Carty, M. P.; Aldabbagh, F. *Org. Biomol. Chem.* **2010**, *8*, 3149-3156.

50. Fagan, V.; Bonham, S.; McArdle, P.; Carty, M. P.; Aldabbagh, F. *Eur. J. Org. Chem.* **2012**, *2012*, 1967-1975.

51. Fagan, V.; Bonham, S.; Carty, M. P.; Saenz-Méndez, P.; Eriksson, L. A.; Aldabbagh, F. *Bioorg. Med. Chem.* **2012**, *20*, 3223-3232.

52. Khajuria, R.; Rasheed, S.; Khajuria, C.; Kapoor, K. K.; Das, P. *Synthesis* **2018**, *50*, 2131-2149.

53. Dawood, K. M.; Abdel-Wahab, B. F. *Arkivoc* **2010**, *2010*, 333-389.

54. Horton, D. A.; Bourne, G. T.; Smythe, M. L. *Chem. Rev.* **2003**, *103*, 893-930.

55. Singh, P. K.; Silakari, O., Chapter 2 - Benzimidazole: Journey From Single Targeting to Multitargeting Molecule. In *Key Heterocycle Cores for Designing Multitargeting Molecules*, Silakari, O., Ed. Elsevier 2018; pp 31-52.

56. Dawood, K. M.; Elwan, N. M.; Abdel-Wahab, B. F. *Arkivoc* **2011**, *2011*, 111-195.

57. Manna, S. K.; Das, T.; Samanta, S. *ChemistrySelect* **2019**, *4*, 8781-8790.

58. Grantham, R. K.; Meth-Cohn, O. *J. Chem. Soc. C* **1969**, *0*, 70-74.

59. Suschitzky, H.; Sutton, M. E. *Tetrahedron* **1968**, *24*, 4581-4587.

60. Shawcross, A. P.; Stanforth, S. P. *J. Heterocycl. Chem.* **1990**, *27*, 367-369.

61. Alonso, J.; Halland, N.; Nazaré, M.; R'kyek, O.; Urmann, M.; Lindenschmidt, A. *Eur. J. Org. Chem.* **2011**, *2011*, 234-237.

62. Nguyen, T. B.; Ermolenko, L.; Al-Mourabit, A. *Green Chem.* **2016**, *18*, 2966-2970.

63. Hubbard, J. W.; Piegols, A. M.; Söderberg, B. C. G. *Tetrahedron* **2007**, *63*, 7077-7085.

64. Joardar, S.; Bhattacharyya, A.; Das, S. *Synthesis* **2014**, *46*, 3121-3132.

65. Suschitzky, H.; Sutton, M. E. *Tetrahedron Lett.* **1967**, *8*, 3933-3938.

66. Nguyen, T. B.; Ermolenko, L.; Al-Mourabit, A. *Chem. Commun.* **2016**, *52*, 4914-4917.

67. Fielden, R.; Meth-Cohn, O.; Suschitzky, H. *Tetrahedron Lett.* **1970**, *11*, 1229-1234.

68. Lu, C.; Su, Z.; Jing, D.; Jin, S.; Xie, L.; Li, L.; Zheng, K. *Org. Lett.* **2019**, *21*, 1438-1443.

69. Deng, X.; McAllister, H.; Mani, N. S. *J. Org. Chem.* **2009**, *74*, 5742-5745.

70. Deng, X.; Mani, N. S. *Eur. J. Org. Chem.* **2010**, *2010*, 680-686.

71. Liubchak, K.; Nazarenko, K.; Tolmachev, A. *Tetrahedron* **2012**, *68*, 2993-3000.

72. Baars, H.; Beyer, A.; Kohlhepp, S. V.; Bolm, C. *Org. Lett.* **2014**, *16*, 536-539.

73. Chen, Y.; Xu, F.; Sun, Z. *RSC Adv.* **2017**, *7*, 44421-44425.

74. Caroon, J. M.; Fisher, L. E. *Heterocycles* **1991**, *32*, 459-467.

75. Chen, J.; Qu, J.; Zhang, Y.; Chen, Y.; Liu, N.; Chen, B. *Tetrahedron* **2013**, *69*, 316-319.

76. Elder, M. S.; Melson, G. A.; Busch, D. I. *Inorg. Chem.* **1966**, *5*, 74-77.

77. Bahrami, K.; Khodaei, M. M.; Kavianinia, I. *Synthesis* **2007**, *2007*, 547-550.

78. Kumar, A.; Banerjee, S.; Roy, P.; Sondhi, S. M.; Sharma, A. *Mol. Diversity* **2018**, *22*, 113-127.

79. Anastasiou, D.; Chaouk, H.; Jackson, W. R. *Tetrahedron Lett.* **1991**, *32*, 2499-2500.

80. Anastasiou, D.; Campi, E. M.; Chaouk, H.; Jackson, W. R. *Tetrahedron* **1992**, *48*, 7467-7478.

81. Tan, K. L.; Bergman, R. G.; Ellman, J. A. *J. Am. Chem. Soc.* **2001**, *123*, 2685-2686.

82. Tan, K. L.; Vasudevan, A.; Bergman, R. G.; Ellman, J. A.; Souers, A. J. *Org. Lett.* **2003**, *5*, 2131-2134.

83. Wang, Y.-X.; Qi, S.-L.; Luan, Y.-X.; Han, X.-W.; Wang, S.; Chen, H.; Ye, M. *J. Am. Chem. Soc.* **2018**, *140*, 5360-5364.

84. Jiang, X.; Chen, X.; Li, Y.; Liang, H.; Zhang, Y.; He, X.; Chen, B.; Chan, W. T. K.; Chan, A. S. C.; Qiu, L. *Org. Lett.* **2019**, *21*, 608-613.

85. Zhang, X.; Zhou, Y.; Wang, H.; Guo, D.; Ye, D.; Xu, Y.; Jiang, H.; Liu, H. *Green Chem.* **2011**, *13*, 397-405.

86. Loup, J.; Müller, V.; Ghorai, D.; Ackermann, L. *Angew. Chem., Int. Ed.* **2019,** *58*, 1749-1753.

87. Haque, M. R.; Rasmussen, M. *Tetrahedron* **1997**, *53*, 6937-6958.

88. Bastug, G.; Eviolitte, C.; Markó, I. E. *Org. Lett.* **2012**, *14*, 3502-3505.

89. De Selms, R. C. *J. Org. Chem.* **1962**, *27*, 2165-2167.

90. McClure, J. R.; Custer, J. H.; Schwarz, H. D.; Lill, D. A. *Synlett* **2000**, *2000*, 710-712.

91. Dhole, S.; Sun, C.-M. *Adv. Synth. Catal.* **2019**, *361*, 535-541.

92. Qin, H.; Miao, Y.; Xu, J.; Bi, Q.; Qu, W.; Liu, W.; Feng, F.; Sun, H. *Org. Chem. Front.* **2019**, *6*, 205-208.

93. O'Connell, J. M.; Moriarty, E.; Aldabbagh, F. *Synthesis* **2012**, *44*, 3371-3377.

94. Li, B.; Mai, S.; Song, Q. *Org. Chem. Front.* **2018**, *5*, 1639-1642.

95. Walker, J. A.; Stanley, L. M. *Org. Biomol. Chem.* **2016**, *14*, 9981-9984.

96. Spiegel, L.; Kaufmann, H. *Ber. Dtsch. Chem. Ges.* **1908**, *41*, 679-685.

97. Bamberger, E.; Tschirner, F. *Ber. Dtsch. Chem. Ges.* **1899**, *32*, 1675-1678.

98. Nair, M. D.; Adams, R. *J. Am. Chem. Soc.* **1961**, *83*, 3518-3521.

99. Emmons, W. D. *J. Am. Chem. Soc.* **1954**, *76*, 3470-3472.

100. Holmes, R. R.; Bayer, R. P. *J. Am. Chem. Soc.* **1960**, *82*, 3454-3456.

101. Meth-Cohn, O.; Suschitzky, H., Heterocycles by Ring Closure of *Ortho*-Substituted *t*-Anilines (The *t*-Amino Effect). In *Adv. Heterocycl. Chem.*, Katritzky, A. R.; Boulton, A. J., Eds. Academic Press 1972; Vol. 14, pp 211-278.

102. Meth-Cohn, O.; Suschitzky, H. *J. Chem. Soc.* **1963**, *0*, 4666-4669.

103. Meth-Cohn, O. *J. Chem. Soc. C* **1971**, *0*, 1356-1357.

104. Meth-Cohn, O.; Smalley, R. K.; Suschitzky, H. *J. Chem. Soc.* **1963**, *0*, 1666-1669.

105. Wang, Z., Polonovski Reaction. In *Comprehensive Organic Name Reactions and Reagents*, Wiley-Interscience: Hoboken, 2010; pp 2251-2255.

106. Li, J. J., Polonovski reaction. In *Name Reactions: A Collection of Detailed Mechanisms and Synthetic Applications Fifth Edition*, Springer International Publishing: Cham, 2014; pp 486-487.

107. Polonovski, M. *Bull. Soc. Chim. Fra.* **1927**, *41*, 1186-1190.

108. Alkhader, M. A.; Perera, R. C.; Sinha, R. P.; Smalley, R. K. *J. Chem. Soc., Perkin Trans. 1* **1979**, *0*, 1056-1062.

109. Groves, C. L.; Ralph, J. T.; Temple, A. F. *J. Heterocycl. Chem.* **1987**, *24*, 27-29.

110. Martínez, Á. M.; Rodríguez, N.; Arrayás, R. G.; Carretero, J. C. *Chem. Commun.* **2014**, *50*, 2801-2803.

111. Meth-Cohn, O.; Suschitzky, H.; Sutton, M. E. *J. Chem. Soc. C* **1968**, *0*, 1722-1726.

112. Möhrle, H.; Gerloff, J. *Arch. Pharm. (Weinheim, Ger.)* **1978**, *311*, 381-393.

113. Xue, D.; Long, Y.-Q. *J. Org. Chem.* **2014**, *79*, 4727-4734.

114. Li, C.-J. *Acc. Chem. Res.* **2009**, *42*, 335-344.

115. Sun, X.; Hu, Y.; Nie, S.-Z.; Yan, Y.-Y.; Zhang, X.-J.; Yan, M. *Adv. Synth. Catal.* **2013**, *355*, 2179-2184.

116. Sun, X.; Lv, X.-H.; Ye, L.-M.; Hu, Y.; Chen, Y.-Y.; Zhang, X.-J.; Yan, M. *Org. Biomol. Chem.* **2015**, *13*, 7381-7383.

117. Bose, A.; Maiti, S.; Sau, S.; Mal, P. *Chem. Commun.* **2019**, *55*, 2066-2069.

118. Purkait, A.; Roy, S. K.; Srivastava, H. K.; Jana, C. K. *Org. Lett.* **2017**, *19*, 2540-2543.

119. Saunders, K. H. *J. Chem. Soc.* **1955**, 3275-3287.

120. Chen, Z.; Li, H.; Cao, G.; Xu, J.; Miao, M.; Ren, H. *Synlett* **2017**, *13*, 504-508.

121. Martin, J.; Meth-Cohn, O.; Suschitzky, H. *Tetrahedron Lett.* **1973**, *14*, 4495-4498.

122. Huang, J.; He, Y.; Wang, Y.; Zhu, Q. *Chem. Eur. J.* **2012**, *18*, 13964-13967.

123. Kutsumura, N.; Kunimatsu, S.; Kagawa, K.; Otani, T.; Saito, T. *Synthesis* **2011**, *2011*, 3235-3240.

124. Aldabbagh, F.; Bowman, W. R. *Tetrahedron* **1999**, *55*, 4109-4122.

125. Allin, S. M.; Bowman, W. R.; Karim, R.; Rahman, S. S. *Tetrahedron* **2006**, *62*, 4306-4316.

126. Coyle, R.; Fahey, K.; Aldabbagh, F. *Org. Biomol. Chem.* **2013**, *11*, 1672-1682.

127. Pereira, K. C.; Porter, A. L.; DeBoef, B. *Tetrahedron Lett.* **2014**, *55*, 1729-1732.

128. Guo, X.; Hu, J.; Zhang, M.; Wang, L. *Asian J. Org. Chem.* **2019**, *8*, 417-421.

129. Sun, K.; Li, S.-J.; Chen, X.-L.; Liu, Y.; Huang, X.-Q.; Wei, D.-H.; Qu, L.-B.; Zhao, Y.-F.; Yu, B. *Chem. Commun.* **2019**, *55*, 2861-2864.

Chapter 2

Hydrogen Peroxide in Ethyl Acetate Mediated Oxidative Annulations
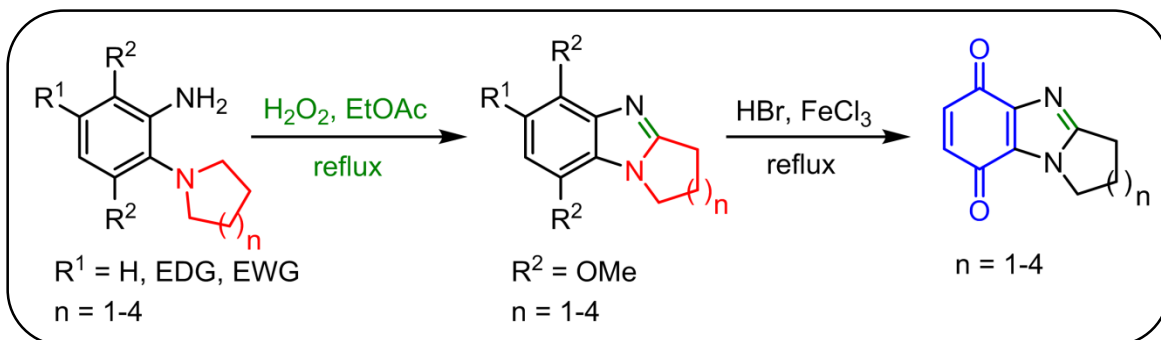
The material in this Chapter has been published as part of:

Greener synthesis using hydrogen peroxide in ethyl acetate of alicyclic ring-fused benzimidazoles and anti-tumour benzimidazolequinones

Martin Sweeney, Michael Gurry, Lee-Ann J. Keane, Fawaz Aldabbagh *

School of Chemistry, National University of Ireland Galway, University Road, Galway, Ireland

A B S T R A C T

Environmentally-friendly and cost effective hydrogen peroxide in ethyl acetate was used to prepare in high yields pyrrolo[1,2-a]benzimidazoles from commercial o-(pyrrolidin-1-yl)anilines without the requirement for organic-aqueous extraction and chromatography. Six, seven and eight membered ring-fused analogues were similarly obtained in high yields with methanesulfonic acid required for the pyrido[1,2-a]benzimidazole. Anti-tumour benzimidazolequinone derivatives were obtained in high yield via the cyclization of 3,6-dimethoxy-2-(cycloamino)anilines.

The majority of compounds described in this Chapter were made by the author of this thesis, however compounds first prepared as part of the thesis of Michael Gurry (PhD, NUI Galway 2016) are denoted by the symbol: # and compounds prepared as part of the PhD thesis of Lee-Ann Keane are denoted by the symbol: †

2.1. Introduction

As previously described in the oxidative cyclization review (Chapter 1), the many methodologies to prepare ring-fused benzimidazoles employ toxic & corrosive acids,[1, 2] expensive transition metal catalysts,[3-5] high molecular weight reagents[6, 7] and toxic tin hydrides.[8-11] This Chapter attempts to negate some of these drawbacks.

From a green chemistry perspective, there are significant advantages to using the low molecular weight and strong oxidant of hydrogen peroxide (H_2O_2). H_2O_2 is very atom efficient due to its high oxygen content (47.1% w/w),[12] environmentally benign since degradation products are only water and oxygen, and is cheaper than alternative peroxy-acids. The most acidic aqueous solution of H_2O_2 is 50% (w/v) with pH dependent upon the concentration of H_2O_2 (Table 2.1).[13] The weak acidic property of H_2O_2 could remove the requirement for organic and mineral acids presently used in oxidative cyclizations.[1, 2, 14-18]

Table 2.1. pH at different aqueous concentrations of H_2O_2.[13]

H_2O_2 conc., wt%	Equivalence point	True pH	Correction factor
35	3.9	4.6	+0.7
50	2.8	4.3	+1.5
70	1.6	4.4	+2.8
90	0.2	5.1	+4.9

The global demand for H_2O_2 is approximately 4 million tonnes per year[19] and over 40% of all H_2O_2 manufactured is employed in the pulp and paper bleaching industries.[12] H_2O_2 has replaced chlorinated-based bleaching agents to avoid the environmental issue of dioxins and chlorinated products in the waste streams.[20] Other applications involve the oxidation of hydrogen sulfide in wastewater treatment[21] and as an oxidant in the synthesis of propene oxide.[22] The major industrial process for H_2O_2 production is the indirect oxidation of anthraquinones (Scheme 2.1).[12, 21, 23, 24] The process was developed in 1939 by Riedl and Pfleiderer and involves the hydrogenation of a 2-alkyl-9,10-anthraquinone using a nickel or palladium catalyst to form the corresponding hydroquinone (Scheme 2.1). The catalyst is removed and the hydroquinone is then oxidized in air to regenerate the 2-alkyl-9,10-

anthraquinone and produce H_2O_2 (Scheme 2.1). The H_2O_2 is extracted with water and the anthraquinone is returned back to the hydrogenator. The anthraquinone process is very efficient but is only economically viable on an industrial scale so requires the transport of high concentrations of H_2O_2, which is hazardous and expensive. There is also an issue of anthraquinone loss due to degradation in the hydrogenation step.[21] A greener approach involves the direct synthesis of H_2O_2 using a combination of H_2 and O_2 with a catalyst.[12, 20, 21, 25] This approach offers the opportunity of on-site generation of H_2O_2 at a concentration of choice but suffers selectivity issues as water is the thermodynamically favoured product. Thus, the anthraquinone process will remain the preferred process of H_2O_2 production in the foreseeable future.
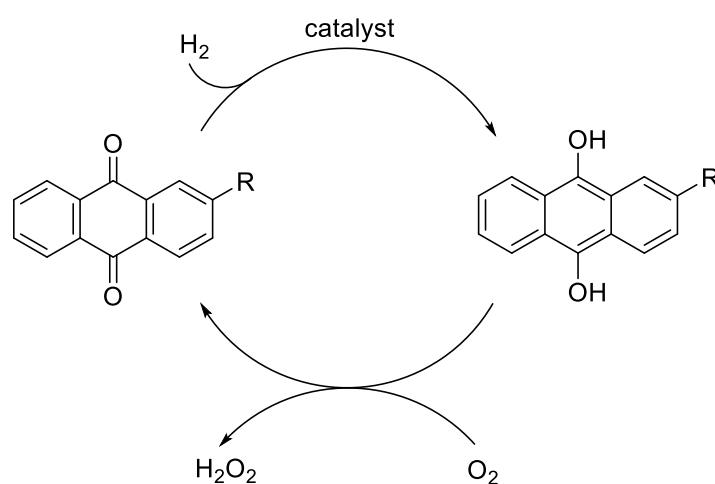
Scheme 2.1. Riedl and Pfleiderer anthraquinone oxidation to produce H_2O_2.[24]

Solvents are by far the biggest mass contributor to waste, accounting for 56% of materials required in the manufacture of APIs.[26] Ethyl acetate is one of the most prevalently used solvents worldwide with an annual usage of 2.5 million tons[27] and sales worth 3 billion US dollars in 2017.[28] Ethyl acetate is primarily used in paints, varnishes, perfumes, printing inks, nail polish removers and as a solvent for decaffeinating coffee beans.[29] Ethyl acetate is also readily biodegradable breaking down to carbon dioxide and water.[30, 31] The fossil fuel derived ethanol and acetic acid are used in the traditional acid catalysed Fischer esterification to produce ethyl acetate (Scheme 2.2a)[32] A new greener route to furnish ethyl acetate involves the dehydrogenation of ethanol derived from biomass (Scheme 2.2b) that produces no net carbon dioxide and has a valuable by-product of hydrogen gas.[30] The synthesis was developed by Davy Process Technology and put into commercial production

by Sasol in South Africa with a high atom economy of 96%.[30, 31] The cumulative energy demand (CED) for the green process is comparable to that of the fossil based Fischer esterification, making it a viable alternative.[33, 34]
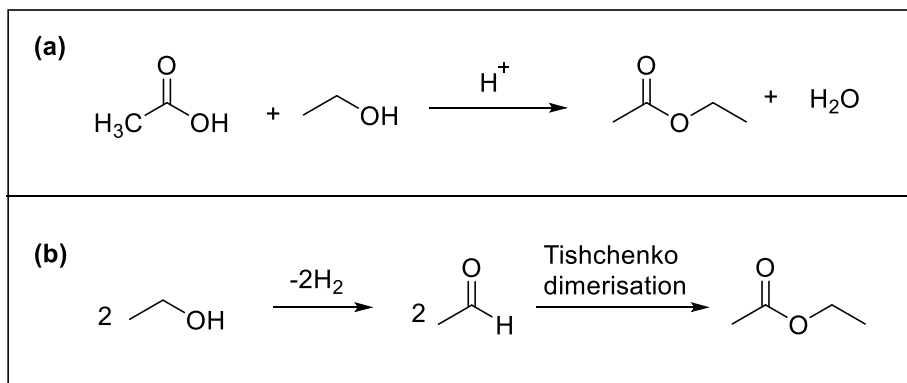
Scheme 2.2. Traditional esterification to form ethyl acetate from non-renewable fossils versus synthesis via renewable bioethanol.[30-32]

Aside from environmental concerns, increased regulation is another driving force behind the push for more sustainable solvents. Registration, Evaluation, Authorisation and Restriction of Chemicals (REACH) is an EU regulation that serves to protect humans and the environment from harmful chemicals.[35] At this moment, REACH has common dipolar aprotic solvents of *N,N*-dimethylformamide (DMF) and *N*-methylpyrrolidinone (NMP) alongside chlorinated solvents such as 1,2-dichloroethane (DCE) classified as substances of very high concern (SVHC).[36] In addition, chloroform and dichloromethane are restricted substances under REACH which limits or bans their use within the EU.[37]

Pfizer assessed the green credentials of classical solvents on aspects of process safety, occupational health, and environmental considerations.[38] Pfizer classified the solvents into categories of preferred, usable and undesirable with ethyl acetate categorized as "preferred" and recommended as a substitute for dichloromethane in extractions and chromatography (Table 2.2). This resulted in an overall 50% reduction of chlorinated solvent usage across the Pfizer research division.[38] A GSK solvent guideline give ethyl acetate high ratings for environmental impact, health, and reactivity/stability.[39] Sanofi guidelines also categorized ethyl acetate as "recommended" based on safety, health, environment, quality, and industrial considerations.[40]

Table 2.2. Pfizer guidelines for solvent selection following green chemistry principles.[38]

Preferred	Usable	Undesirable
Water	Cyclohexane	Pentane
Acetone	Heptane	Hexane(s)
Ethanol	Toluene	Di-isopropyl ether
2-Propanol	Methylcyclohexane	Dichloromethane
Ethyl Acetate	Methyl *t*-butyl ether	Dichloroethane
Isopropyl Acetate	Isooctane	Chloroform
Methanol	Acetonitrile	Dimethyl formamide
1-Butanol	2-MethylTHF	*N*-Methylpyrrolidinone
t-Butanol	Tetrahydrofuran	Pyridine

Chemical Manufacturing Methods for 21st Century (CHEM21) was an EU funded public-private partnership with the aim of manufacturing sustainable pharmaceuticals.[41] The consortium consisted of six pharmaceutical companies, 13 universities and four small or medium enterprises from across Europe.[41]

Table 2.3. CHEM21 solvent guideline based on all publically available solvent guidelines.[41]

Recommended	Water, EtOH, *i*-PrOH, **EtOAc**, *i*-PrOAc, anisole, sulfolane.
Recommended or problematic?	MeOH, benzyl alcohol, acetone, ethylene glycol, acetic acid, MEK, MIBK.
Problematic	Heptane, toluene, xylenes, chlorobenzene, acetonitrile, DMSO.
Problematic or hazardous?	MTBE, THF, cyclohexane, DCM, formic acid, pyridine.
Hazardous	1,4-dioxane, pentane, hexane, DMF, NMP, methoxy-ethanol, Et$_3$N.
Highly Hazardous	Diethyl ether, benzene, chloroform, CCl$_4$, DCE, nitromethane.

As part of their mandate, CHEM21 unified all publically available solvent guidelines from Astra Zeneca, GSK, Pfizer, Sanofi and ACS Green Chemistry Institute Pharmaceutical Roundtable (GCI-PR) into a comprehensive solvent guide (Table 2.3) aimed at the academic setting.[41, 42] CHEM21 grouped the solvents into four categories: recommended, problematic, hazardous and highly hazardous. Ethyl acetate was a recommended solvent and should be one of the first used solvents in screening reactions. On the other end of the scale, highly hazardous solvents should not be used in laboratories.[41]

Methanesulfonic acid (MSA) is marketed as a benign replacement for conventional acids[43] such as trifluoroacetic acid that is employed in oxidative cyclizations (Scheme 1.7, Chapter 1).[1, 2] MSA has many desirable properties (Figure 2.1) including acid strength (pK_a of -1.9), non-oxidising nature, absence of colour or odour that allows beneficial practical applications in pharmaceutical and electronics industry.[44] As part of the natural sulfur cycle, MSA undergoes biodegradation resulting in the release of CO_2 and sulfate,[45] and is considered a green acid due to its less toxic and corrosive nature.[46] BASF produces MSA on an industrial scale by reacting methanol, elemental sulfur and hydrogen to form the intermediate dimethylsulfide.[47] The dimethylsulfide is then catalytically oxidized to the final product. Recently, Ott and Díaz-Urrutia have developed a greener and more cost-effective selective synthesis of MSA (83% yield) via the sulfonation of methane with sulfur trioxide in sulfuric acid (oleum) at 50 °C.[48]
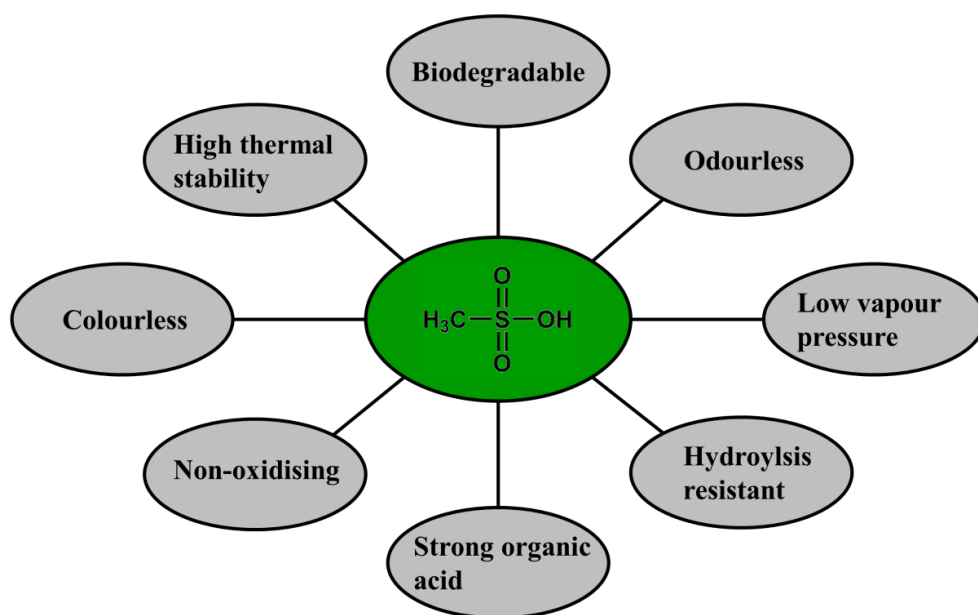
Figure 2.1. Advantageous properties of methanesulfonic acid.

2.2. Aims and Objectives

- To carry out the oxidative cyclization of o-cyclic tertiary amine substituted anilines to produce ring-fused benzimidazoles using H_2O_2 in ethyl acetate.

- To employ a more environmentally friendly acid if necessitated for the oxidative cyclization of o-cyclic tertiary amine substituted anilines.

- To make reactions compliant with green chemistry principles,[49] include use of safer solvents to minimize waste/effluent generation and to avoid aqueous extraction or chromatography as much as possible.

- To investigate if the ring-expanded analogues, azepino- and azocino[1,2-a]benzimidazoles can be prepared using H_2O_2 in ethyl acetate.

- To establish if 3,6-dimethoxy-2-(cycloamino)anilines undergo oxidative cyclization using H_2O_2 in ethyl acetate and to further functionalize the ring-fused benzimidazoles to give novel anti-cancer benzimidazolequinones.

2.3. Results and Discussion

The oxidative cyclization of 5-methoxy-2-(pyrrolidin-1-yl)aniline **1a** to the corresponding 6-methoxy-2,3-dihydro-1*H*-pyrrolo[1,2-*a*]benzimidazole **2a** was the model reaction on which optimization was carried out (Table 2.4). As a control reaction, H_2O_2 (20 equiv.) was refluxed in ethyl acetate (EtOAc) over 12 h without the presence of substrate **1a**. A ^{1}H NMR was obtained of the neat reaction mixture and only H_2O_2 and EtOAc characteristic chemical shifts were observed. Interestingly, our hypothesis was realized when benzimidazole formation proceeded with H_2O_2 in EtOAc without the presence of additional acid. The optimized conditions of H_2O_2 (20 equiv.) in distilled EtOAc (Table 2.4, Entry 2) at reflux for 20 min gave the best yield of **2a** in 79% without acid. At lower equivalents of H_2O_2 (Table 2.4, Entry 3), the cyclization proceeded at a slower rate and had a 52% NMR conversion after 20 mins.

Table 2.4. Optimization of H_2O_2 in EtOAc Reaction Conditions.[a,b]
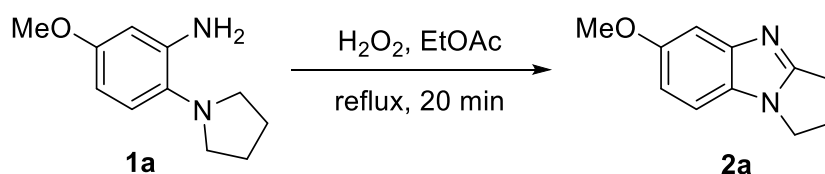
entry	H_2O_2 (equiv.)	acid (equiv.)	2a (%)[c]
1	20	none	36[d]
2	20	none	**79**
3	10	none	40
4	20	MSA (3)	55[e]
5	20	MSA (0.3)	77
6	20	Amberlite (100 mg)	55

[a]Reaction conditions: Aniline (1.0 equiv.), EtOAc (5 mL). [b]Work-up involves addition of solid Na_2CO_3 and additional EtOAc with no aqueous extraction necessary. [c]Aniline **1a** was fully converted to benzimidazole **2a**, apart from entries 1 and 3 which had NMR conversions of 50 & 52% respectively. [d]rt for 2 h. [e]Na_2CO_3 (aq) neutralisation followed by EtOAc extraction was necessary.

The procedure avoided aqueous extractions and flash column chromatography, as the addition of solid sodium carbonate to the reaction and subsequent stirring for 20 mins formed sodium percarbonate, allowing a simple filtration. The EtOAc filtrate was evaporated and the solvent was recovered and reused for further reactions. This procedure circumvents the requirement for auxiliary substances, allows solvent recycling and there is no aqueous effluent.

The scope of alternative environmentally friendly acids was investigated for oxidative cyclization. The use of less than stoichiometric amounts of MSA in combination with H_2O_2 (Table 2.4, Entry 5) avoided an aqueous work-up and led to comparable yields to that of the optimized conditions. Oxidative cyclization with H_2O_2 and a reusable sulfonic acid immobilised on an ion-exchange resin (Amberlite IR120 H-form) led to a moderate yield of 55% for **2a** (Table 2.4, Entry 6).

Optimized reaction conditions were extended to *o*-cyclic tertiary amine substituted anilines containing both electron withdrawing and donating groups (Table 2.5). Longer reaction times were required for full conversion of anilines containing an electron-withdrawing substituent at the 5-position, with the CF_3 substituent taking the longest at 8 h. Despite 100% conversion of **1g** with just H_2O_2 in EtOAc, the yield of 2,3-dihydro-1*H*-pyrrolo[1,2-*a*]benzimidazole-6-carbonitrile **2g** was raised to 85% from 59% by addition of 0.5 equivalents of MSA. Similiarly, the yield of 6-nitro-2,3-dihydro-1*H*-pyrrolo[1,2-*a*]benzimidazole **2i** was raised to 71% from 29% with 0.5 equivalents of MSA (Table 2.5).

Table 2.5. Synthesis of 2,3-dihydro-1*H*-pyrrolo[1,2-*a*]benzimidazoles.[a]
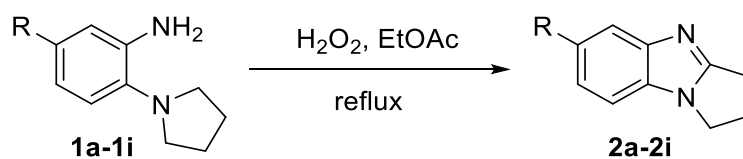
aniline	R	time	yield (%)
1a	OMe	20 min	**2a**, 79
1b	H	20 min	**2b**, 80
1c	Me	40 min	**2c**, 81
1d	NHAc	20 min	**2d**, 64
1e	Br	2 h	**2e**, 88
1f	F	50 min	**2f**, 84
1g	CN	4 h	**2g**, 85[b]
1h	CF$_3$	8 h	**2h**, 93
1i	NO$_2$	4 h	**2i**, 71[b]

[a]Reaction conditions: Aniline **1a-1i** (1.0 mmol), H$_2$O$_2$ (50% w/v, 20 mmol) and EtOAc (5 mL). When GC-MS indicated all the aniline was consumed, the reaction was quenched by addition of solid Na$_2$CO$_3$ (~3 g) and additional EtOAc (20 mL). The mixture was filtered and evaporated to give the ring-fused [1,2-*a*]benzimidazole. [b]Included MSA (0.5 mmol).

The formation of ring-expanded analogues using the reaction conditions successfully applied to prepare pyrrolo[1,2-*a*]benzimidazoles **1a-1i** was investigated (Scheme 2.3). The six-membered cyclization of 5-methoxy-2-(piperidiny-1-yl)aniline was slow without the addition of acid and one equivalent of MSA was deployed to give 7-methoxy-1,2,3,4-tetrahydropyrido[1,2-*a*]benzimidazole **3a** in a faster time of 1 h with a yield of 75% (Scheme 2.3). Unfortunately, the use of full equivalents of MSA necessitated the use of saturated sodium carbonate solution in an organic-aqueous extraction. No acid was required for the seven and eight-membered cyclizations, which occurred in 65% and 73% yield respectively using H$_2$O$_2$ in EtOAc (Scheme 2.3). However, 3-methoxy-7,8,9,10-tetrahydro-6*H*-azepino[1,2-*a*]benzimidazole **4a** required purification using flash chromatography in order to remove unidentified impurities.
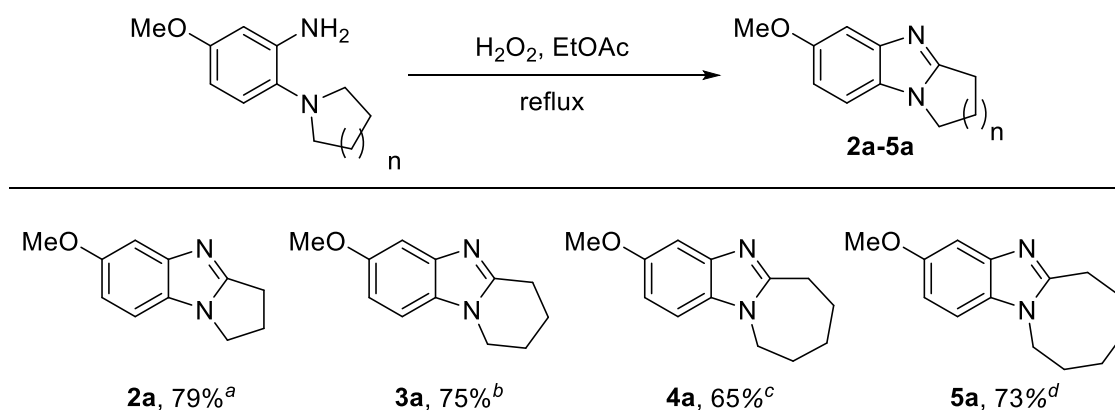
Reaction conditions and work-up is the same as Table 2.5. [a]20 min. [b]Included MeSO$_3$H (1 mmol). Extraction with EtOAc (20 mL) and saturated Na$_2$CO$_3$ (aq.) was deemed necessary, 1 h. [c]Flash column chromatography required, 80min. [d]2 h

Scheme 2.3. Synthesis of five to eight-membered ring-fused [1,2-*a*]benzimidazoles.

In line with previous observations (Table 2.5), the oxidative cyclization of 3,6-dimethoxy-2-(cycloamino)anilines proceeded most efficiently with the five-membered analogue. Despite this, the cyclization occured slowly using H$_2$O$_2$ in EtOAc to give 5,8-dimethoxy-2,3-dihydro-1*H*-pyrrolo[1,2-*a*]benzimidazole **8a** in a yield of 81% over 18 h (Table 2.6). The analogous six-membered cyclization proved difficult using H$_2$O$_2$ alone. The addition of a full equivalent of MSA allowed the clean isolation of **8b** in 80% yield after 12 h of reflux in EtOAc without the requirement for chromatography. It may be that the intermediate tertiary amine *N*-oxide of the six-membered ring is more stable through hydrogen bonding or a possible nitroso-intermediate is more difficult to form for the six-membered ring,[50] requiring acidic conditions for oxidative cyclization. The seven and eight-membered cyclizations of 3,6-dimethoxy-2-(cycloamino)anilines **7c** and **7d** proceeded in good yields of 60 and 72% respectively after 6 h in the presence of 1 equivalent of MSA. The absence of MSA led to lower yields and long reaction times as shown in Table 2.6.

Table 2.6. Synthesis of five to eight-membered ring-fused dimethoxy substituted [1,2-*a*] benzimidazoles.[a]
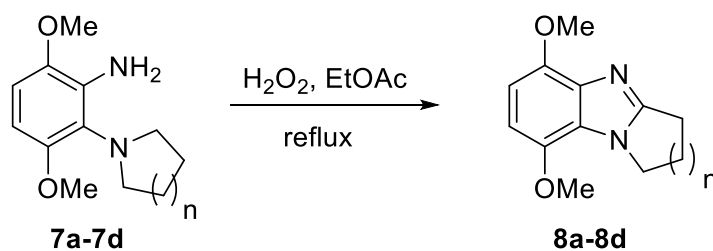
aniline	n	time (h)	MSA (equiv.)	yield (%)
7a	1	18	0	**8a**, 81[#]
7b	2	12	1	**8b**, 80[b]
7c	3	24	0	**8c**, 34[b,c]
7c	3	6	1	**8c**, 72[b]
7d	4	36	0	**8d**, 35[b,c†]
7d	4	6	1	**8d**, 60[b,c†]

[a]Reaction conditions and work-up is the same as Table 2.5. [b]Extraction with EtOAc (20 mL) and saturated Na_2CO_3 (aq.) was deemed necessary. [c]Flash column chromatography required.

The Aldabbagh group has previously reported the conversion of 6,9-dimethoxy-1,2,3,4-tetrahydropyrido[1,2-*a*]benzimidazole **8b** into the pyrido[1,2-*a*]benzimidazolequinone **9b** via hydrobromic acid-induced demethylation to generate the hydroquinone intermediate in situ, followed by room temperature oxidation with ferric chloride (Scheme 2.4).[10] Pyrido[1,2-*a*]benzimidazole **8b** was however obtained using expensive and environmentally damaging Bu_3SnH-mediated radical cyclization of a phenylselenide precursor (Scheme 1.32, Chapter 1). Furthermore, the scope of radical cyclizations is limited due to difficulties in forming constrained ring-fused systems such as pyrrolo[1,2-*a*]benzimidazole **8a.**

A more benign approach towards the synthetic target of anti-tumour agents **9a** to **9d** was realised, starting with nucleophilic aromatic substitution (S_NAr) (Scheme 2.4). The S_NAr of 1,4-dimethoxy-2,3-dinitrobenzene with the secondary amines of pyrrolidine or piperidine were carried out neat at reflux for 6 h according to the literature procedure of

Mustroph.[51] The S_NAr of azepane or azocane onto 1,4-dimethoxy-2,3-dinitrobenzene involved the base potassium carbonate in the solvent of acetonitrile at reflux for a longer reaction time of 24 h (Scheme 2.4). The *o*-cyclic tertiary amine substituted nitrobenzenes are then reduced by iron[52] to give the cyclization precursors **7a**-**7d** in a two-step (S_NAr & reduction) yield of 26-68% (Scheme 2.4). The dimethoxy substituted benzimidazoles **8a-8d** were readily converted using the $HBr/FeCl_3$ protocol into potential benzimidazolequinone anti-tumour agents **9a-9d** in 52-87% yields (Scheme 2.4). The cytotoxicity evaluation of novel quinones **9c** and **9d** are presented as part of the thesis of Lee-Ann Keane (Aldabbagh group member).
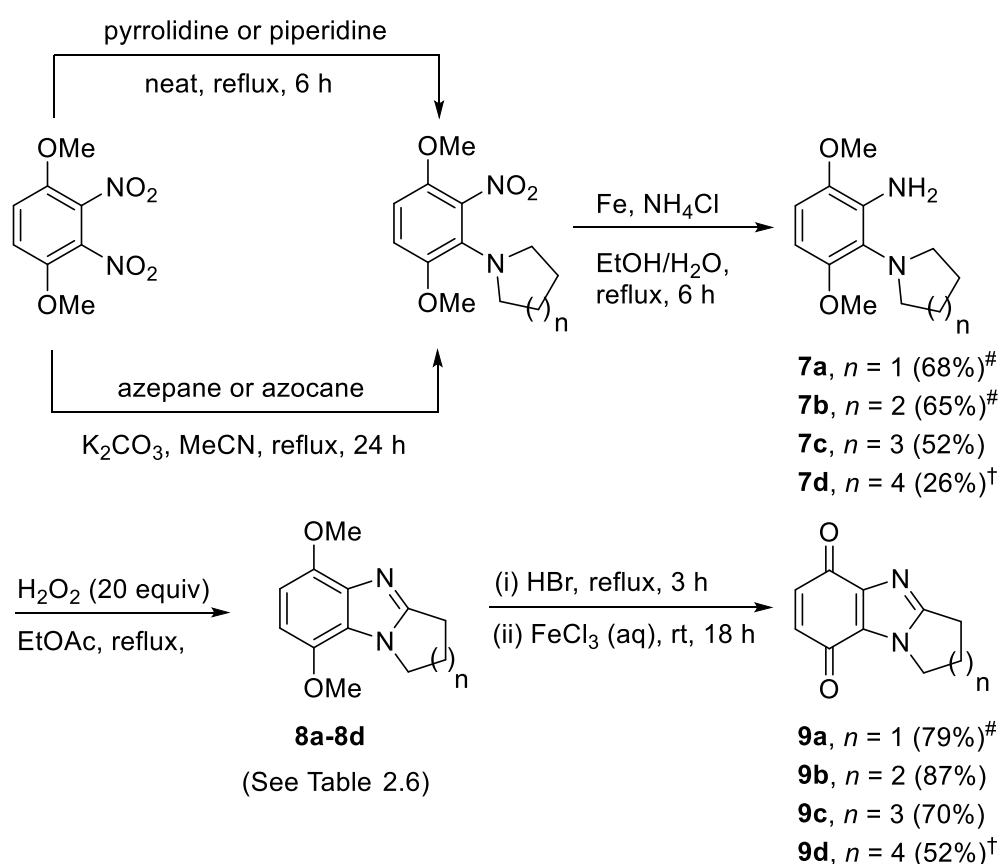
Scheme 2.4. Synthesis of five to eight-membered ring-fused benzimidazolequinones.

Many examples exist of the oxidation of tertiary amines using non-catalyzed H_2O_2. Sheeran[53] and Cope[54] showed that aqueous H_2O_2 oxidized acyclic tertiary amines such as *N,N*-dimethyldodecylamine and *N,N*-dimethylcyclooctanamine to their respective amine *N*-oxides. The dropwise addition of 30% aqueous H_2O_2 allowed VanRheenen to oxidize the cyclic tertiary amine of *N*-methylmorpholine to *N*-methylmorpholine *N*-oxide in 86%

yield after 20 h at 75 °C.[55] However, to the best of our knowledge, no example exists of the oxidation of aniline to nitrosobenzene using non-catalyzed H_2O_2. There are numerous catalysed examples[56-61] and in particular Sudalai[57] and Lykakis[61] state that in the absence of the catalyst, no oxidation occurs. Despite no previous precedent, the involvement of a nitroso-intermediate cannot be ruled out. Oswald and Guertin studied the interaction between tertiary amines and hydrogen peroxide. Using the model substrate of 1,4-diazabicyclo[2.2.2]octane (DABCO), the H_2O_2-DABCO adduct was isolated at low temperatures and infrared studies showed that the adduct was a hydrogen bonded polar complex, that decomposes upon heating to produce the DABCO *N*-oxide.[62]

Based on the literature observations, the tentative mechanism proceeds through an intermediate H_2O_2-tertiary amine adduct that produces an amine *N*-oxide (Scheme 2.5). A loss of water from the amine *N*-oxide occurs to form an iminium ion, which annulates to deliver the hydrobenzimidazole due to nucleophilic attack from the aromatic primary amine. The hydrobenzimidazole then undergoes another cycle of H_2O_2 oxidation to yield the desired ring-fused benzimidazole (Scheme 2.5).
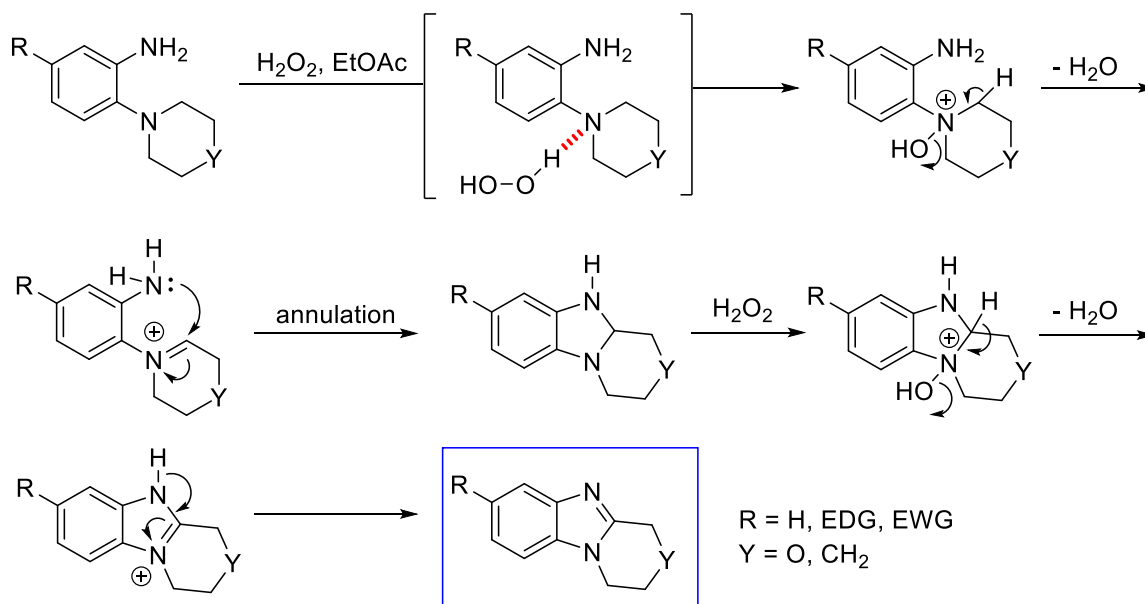
Scheme 2.5. Proposed route of oxidative cyclization using H_2O_2.

Regarding the combination of H_2O_2 and MSA, the formation of a nitroso-intermediate is a possibility. Initial studies of this work showed that oxidative cyclization of 5-methoxy-2-(pyrrolidin-1-yl)aniline **1a**, using H_2O_2 (10 equiv.) and MSA (12 equiv.) produced 1-(4-

methoxy-2-nitrophenyl)pyrrolidine in 5% yield as a minor product (Scheme 2.6). In addition, Fagan et al used H_2O_2 and MSA to deprotect and oxidize *N*-(2,5-difluoro-4-nitrophenyl)acetamide to give 1,4-difluoro-2,5-dinitrobenzene.[50]
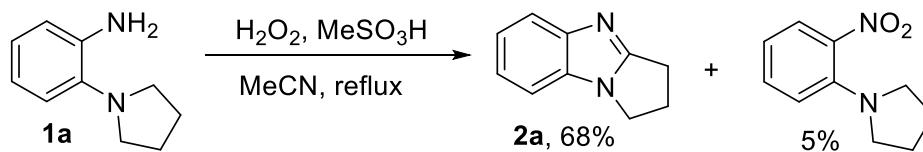
Scheme 2.6. Partial oxidation of aniline to nitrobenzene.

2.4. Experimental

2.4.1 Materials

All chemicals were obtained from commercial sources and used without purification, except for ethyl acetate (Honeywell ACS reagent, reagent, ≥99.5% (GC)), which was purified by distillation. 1,4-Dimethoxy-2,3-dinitrobenzene was prepared according to a literature procedure using 1,4-dimethoxybenzene (Sigma Aldrich 99% (GC)) and nitric acid (Honeywell Fluka, 64-66%).[63, 64] Methanesulfonic acid (TCI, >99% (T)) should be stored under an inert atmosphere due to its hygroscopic nature. H_2O_2 (Honeywell Fluka, 50% w/v in water, stabilized) and HBr (Honeywell Fluka, ≥48% w/v in water) were used as received. Thin layer chromatography (TLC) was performed on Merck TLC silica gel 60 F_{254} plates using a UV lamp (λ = 254 nm) for visualization. Flash chromatography was carried out using Sigma Aldrich technical grade silica gel (particle size 40–63 microns) with the specified eluent.

2.4.2. Measurements

Melting point and Infrared spectroscopy: Melting points were measured on a Stuart Scientific melting point apparatus SMP1. Infrared spectra were recorded using a Perkin-Elmer Spec 1 with ATR attached.

High Resolution Mass Spectrometry (HRMS): HRMS was carried out using ESI time-of-flight mass spectrometer (TOF-MS) using a Waters LCT Mass Spectrometry instrument. The precision of all accurate mass measurements were better than 5 ppm.

Gas chromatography: GC-MS was used to monitor the formation of ring-fused benzimidazoles from their respective anilines. GC-MS analysis was performed on an Agilent 6890 Series GC System equipped with an Agilent 5975 Inert Mass Selective Detector (EI) and a DB-1, 30 m, ID 0.25 mm, FD 0.25 μm column. Helium was used as the carrier gas at a flow rate of 2.4 mL/min. The injector was heated to 160 °C and the oven temperature was increased from 75 to 180 °C at a rate of 22 °C/min and was then further increased to 280 °C at 40 °C/min.

Nuclear Magnetic Resonance (NMR spectroscopy): ^{1}H-NMR spectra were recorded using a Joel ECX 400 MHz instrument equipped with a Dell Precision 360 computer workstation. In the case of **9d**, the ^{1}H-NMR was recorded on a Varian VNMRS 500 MHz instrument equipped with a Dell Precision T3400 computer workstation. The chemical shifts were recorded in ppm relative to tetramethylsilane. ^{13}C NMR data were collected at 100 MHz with complete proton decoupling.

2.4.3. Compound data

2.4.3.1 General procedure for synthesis of ring-fused [1,2-*a*]benzimidazoles

Anilines (1.0 mmol), H_2O_2 (50% w/v, 20 mmol) were stirred in EtOAc (5 mL) at reflux for 20 min-8 h. When GC-MS indicated all the aniline was consumed, the reaction was quenched by addition of solid Na_2CO_3 (~3 g) and additional EtOAc (20 mL). The mixture was filtered and evaporated to give the desired ring-fused [1,2-*a*]benzimidazole.
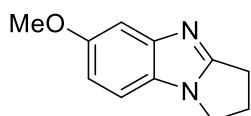
6-Methoxy-2,3-dihydro-1*H*-pyrrolo[1,2-*a*]benzimidazole (2a): 0.148 g, 79%; brown solid; mp 130-134 °C (lit.[14] mp 128-129 °C); ν_{max} (neat, cm^{-1}) 3045, 2958, 2840, 1518, 1480, 1444, 1298, 1197, 1149, 1032; δ_H (400 MHz, CDCl$_3$) 2.60-2.67 (m, 2H), 2.98 (t, *J* 7.6 Hz, 2H), 3.81 (s, 3H), 4.00 (t, *J* 7.1 Hz, 2H), 6.80 (dd, *J* 2.6, 8.7 Hz, 1H), 7.11 (d, *J* 8.7 Hz, 1H), 7.16 (d, *J* 2.6 Hz, 1H); δ_C (100 MHz, CDCl$_3$) 23.7, 26.1, 43.0 (all CH$_2$), 55.9 (Me), 102.4, 109.8, 111.3 (all CH), 127.0, 149.5, 155.9, 161.5 (all C).
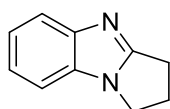
2,3-Dihydro-1*H*-pyrrolo[1,2-*a*]benzimidazole (2b): 0.126 g, 80%; dark brown solid; mp 90-92 °C (lit.[1] mp 114-115 °C); ν_{max} (neat, cm^{-1}) 3052, 2964, 1679, 1625, 1522, 1487, 1446, 1414, 1281, 1217; δ_H (400 MHz, CDCl$_3$) 2.57-2.65 (m, 2H), 2.96 (t, *J* 7.8 Hz, 2H), 3.97 (t, *J* 7.1 Hz, 2H), 7.14-7.23 (m, 3H), 7.64-7.66 (m, 1H); δ_C (100 MHz, CDCl$_3$) 23.5, 26.1, 42.8 (all CH$_2$), 109.6, 119.5, 121.7, 121.8 (all CH), 132.4, 148.8, 161.2 (all C).
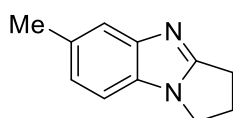
6-Methyl-2,3-dihydro-1*H*-pyrrolo[1,2-*a*]benzimidazole (2c): 0.139 g, 81%; brown solid; mp 126-128 °C (lit.[1] mp 144 °C); ν_{max} (neat, cm^{-1}) 3036, 2955, 2905, 1679, 1619, 1519, 1404, 1296, 1146, 1130; δ_H (400 MHz, CDCl$_3$) 2.43 (s, 3H), 2.60-2.67 (m, 2H), 2.98 (t, *J* 7.6 Hz, 2H), 4.00 (t, *J* 7.1 Hz, 2H), 6.98 (d, *J* 7.9 Hz, 1H), 7.12 (d, *J* 7.9 Hz, 1H), 7.44 (s,

1H); δ_C (100 MHz, CDCl$_3$) 21.7 (Me), 23.6, 26.1, 42.8 (all CH$_2$), 109.1, 119.4, 123.2 (all CH), 130.5, 131.3, 149.2, 161.2 (all C).
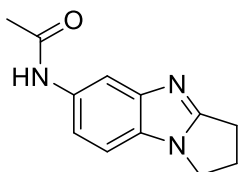
N-(2,3-Dihydro-1H-pyrrolo[1,2-a]benzimidazol-6-yl)acetamide (2d): 0.138 g, 64%; brown solid; mp 258-260 °C (lit.[65] mp 256 °C); ν_{max} (neat, cm^{-1}) 2924, 2319, 1667 (C=O), 1516, 1480, 1372, 1300, 1239, 1148, 1037; δ_H (400 MHz, DMSO-d_6) 2.00 (s, 3H), 2.53-2.61 (m, 2H), 2.88 (t, J 7.6 Hz, 2H), 4.03 (t, J 7.1 Hz, 2H), 7.24 (dd, J 1.8, 8.7 Hz, 1H), 7.28 (d, J 8.7 Hz, 1H), 7.84 (s, 1H), 9.81 (s, 1H, NH); δ_C (100 MHz, DMSO-d_6) 23.5 (CH$_2$), 24.5 (Me), 26.2, 43.0 (both CH$_2$), 110.0, 110.1, 114.5 (all CH), 129.2, 134.0, 149.0, 162.3, 168.3 (all C).
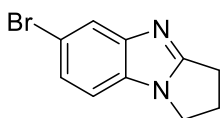
6-Bromo-2,3-dihydro-1H-pyrrolo[1,2-a]benzimidazole (2e): 0.208 g, 88%; brown solid; mp 140-142 °C (lit.[66] mp 150 °C); ν_{max} (neat, cm^{-1}) 2941, 1525, 1456, 1402, 1292, 1211, 1048; δ_H (400 MHz, CDCl$_3$) 2.61-2.68 (m, 2H), 2.97 (t, J 7.6 Hz, 2H), 3.99 (t, J 7.1 Hz, 2H), 7.04 (d, J 8.3 Hz, 1H), 7.21 (dd, J 1.8, 8.3 Hz, 1H), 7.74 (d, J 1.8 Hz, 1H); δ_C (100 MHz, CDCl$_3$) 23.6, 26.0, 43.0 (all CH$_2$), 110.8 (CH), 114.6 (C), 122.2, 124.7 (both CH), 131.3, 150.0, 162.5 (all C).
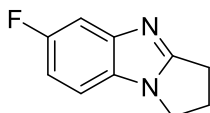
6-Fluoro-2,3-dihydro-1H-pyrrolo[1,2-a]benzimidazole (2f): 0.147 g, 84%; brown solid; mp 111-114 °C (lit.[66] mp 128 °C); ν_{max} (neat, cm^{-1}) 2964, 2911, 1876, 1632, 1888, 1517, 1477, 1415, 1295, 1123; δ_H (400 MHz, CDCl$_3$) 2.64-2.71 (m, 2H), 3.01 (t, J 7.6 Hz, 2H), 4.04 (t, J 7.1 Hz, 2H), 6.91 (td, J 2.5, 9.2 Hz, 1H), 7.14 (dd, J 4.6, 8.7 Hz, 1H), 7.33 (dd, J 2.5, 9.6 Hz, 1H); δ_C (100 MHz, CDCl$_3$) 23.8, 26.1, 43.1 (all CH$_2$), 105.5 (d, J 24.0 Hz,

$^2J_{CF}$, CH), 109.7 (d, J 7.7 Hz, $^3J_{CF}$, CH), 109.9 (d, J 23.2 Hz, $^2J_{CF}$, CH), 129.0 (8a-C), 149.2 (d, J 12.3 Hz, $^3J_{CF}$, 4a-C), 159.1 (d, J 235.2 Hz, $^1J_{CF}$, 6-C), 162.8 (3a-C).
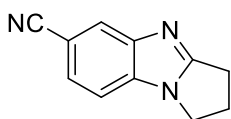
2,3-Dihydro-1*H*-pyrrolo[1,2-*a*]benzimidazole-6-carbonitrile (2g): 0.155 g, 85%; purple solid; mp 191-193 °C (lit.[67] mp 190 °C); v_{max} (neat, cm^{-1}) 3042, 2962, 2907, 2216 (CN stretch), 1619, 1467, 1402, 1294, 1230, 1155; δ_H (400 MHz, CDCl$_3$) 2.68-2.75 (m, 2H), 3.04 (t, J 7.8 Hz, 2H), 4.11 (t, J 7.1 Hz, 2H), 7.27 (d, J 8.5 Hz, 1H), 7.35 (dd, J 1.4, 8.5 Hz, 1H), 7.88 (s, 1H); δ_C (100 MHz, CDCl$_3$) 23.5, 26.1, 43.1 (all CH$_2$), 104.6 (C), 110.7 (CH), 120.2 (C), 124.1, 125.4 (both CH), 135.1, 148.3, 164.1 (all C).
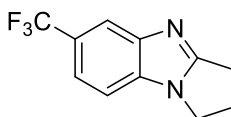
6-(Trifluoromethyl)-2,3-dihydro-1*H*-pyrrolo[1,2-*a*]benzimidazole (2h): 0.211 g, 93%; light brown solid; mp 126-128 °C (lit.[68] mp 148 °C); v_{max} (neat, cm^{-1}) 3082, 2963, 2907, 1621, 1590, 1515, 1403, 1322, 1251, 1099; δ_H (400 MHz, CDCl$_3$) 2.62-2.70 (m, 2H), 3.00 (t, J 7.8 Hz, 2H), 4.03 (t, J 7.1 Hz, 2H), 7.24 (d, J 8.5 Hz, 1H), 7.35 (d, J 8.5 Hz, 1H), 7.88 (s, 1H); δ_C (100 MHz, CDCl$_3$) 23.4, 26.0, 43.1 (all CH$_2$), 110.0 (CH), 116.7 (q, J 3.5 Hz, $^3J_{CF}$, CH), 118.9 (q, J 3.2 Hz, $^3J_{CF}$, CH), 124.2 (q, J 31.9 Hz, $^2J_{CF}$, 6-C), 125.0 (q, J 270.4 Hz, $^1J_{CF}$, CF$_3$), 134.0, 147.5, 163.5 (all C).
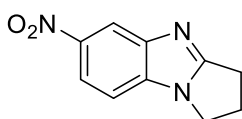
6-Nitro-2,3-dihydro-1*H*-pyrrolo[1,2-*a*]benzimidazole (2i): 0.145 g, 71%; dark orange solid; mp 193-195 °C (lit.[1] mp 209-210 °C); v_{max} (neat, cm^{-1}) 2965, 1685, 1619, 1515 (NO$_2$), 1457, 1309 (NO$_2$), 1287, 1141, 1103, 1058; δ_H (400 MHz, CDCl$_3$) 2.74-2.81 (m, 2H), 3.11 (t, J 7.8 Hz, 2H), 4.17 (t, J 7.3 Hz, 2H), 7.30 (d, J 8.7 Hz, 1H), 8.10 (dd, J 2.3, 8.7 Hz, 1H), 8.52 (d, J 2.3 Hz, 1H); δ_C (100 MHz, CDCl$_3$) 23.7, 26.2, 43.2 (all CH$_2$), 109.4, 116.1, 118.0 (all CH), 136.6, 143.3, 148.2, 165.1 (all C).
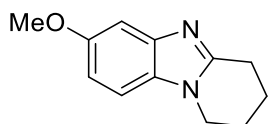
7-Methoxy-1,2,3,4-tetrahydropyrido[1,2-*a*]benzimidazole (3a): 0.152 g, 75%; light brown solid; mp 112-114 °C (lit.[69] mp 300 °C); v_{max} (neat, cm^{-1}) 2952, 1620, 1511, 1489, 1445, 1320, 1199, 1148, 1112, 1030; δ_H (400 MHz, CDCl$_3$) 1.93-1.99 (m, 2H), 2.04-2.10 (m, 2H), 3.03 (t, *J* 6.4 Hz, 2H), 3.83 (s, 3H), 3.99 (t, *J* 6.0 Hz, 2H), 6.84 (dd, *J* 2.1, 8.7 Hz, 1H), 7.13 (d, *J* 8.7 Hz, 1H), 7.16 (d, *J* 2.1 Hz, 1H); δ_C (100 MHz, CDCl$_3$) 20.7, 22.7, 25.4, 42.5 (all CH$_2$), 55.9 (Me), 101.6, 109.1, 111.2 (all CH), 129.3, 143.5, 152.0, 156.2 (all C).
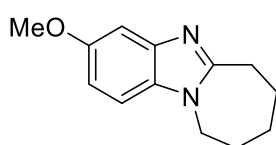
3-Methoxy-7,8,9,10-tetrahydro-6*H*-azepino[1,2-*a*]benzimidazole (4a): 0.141 g, 65%; off white solid; mp 118-120 °C; R_f 0.40 (95:5 CHCl$_3$ / MeOH); v_{max} (neat, cm^{-1}) 2921, 1729, 1538, 1438, 1398, 1366, 1337, 1268, 1194, 1147; δ_H (400 MHz, CDCl$_3$) 1.68-1.75 (m, 4H), 1.82-1.87 (m, 2H), 2.99 (t, *J* 5.7 Hz, 2H), 3.78 (s, 3H), 4.01 (t, *J* 5.0 Hz, 2H), 6.81 (dd, *J* 2.3, 8.7 Hz, 1H), 7.05 (d, *J* 8.7 Hz, 1H), 7.13 (d, *J* 2.3 Hz, 1H); δ_C (100 MHz, CDCl$_3$) 25.6, 28.7, 30.1, 30.9, 44.6 (all CH$_2$), 55.9 (Me), 101.8, 109.1, 111.5 (all CH), 130.4, 142.9, 155.8, 157.7 (all C). HRMS (ESI) *m/z* (M + H)$^+$, C$_{13}$H$_{17}$N$_2$O calcd. 217.1341, observed 217.1347.
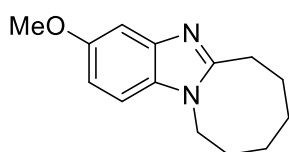
3-Methoxy-6,7,8,9,10,11-hexahydroazocino[1,2-*a*]benzimidazole (5a): 0.168 g, 73%; off-white solid; mp 92-93 °C (lit.[15] mp 102-103 °C); v_{max} (neat, cm^{-1}) 2915, 1729, 1538, 1489, 1439, 1398, 1338, 1201, 1150, 1095; δ_H (400 MHz, CDCl$_3$) 1.10-1.16 (m, 2H), 1.36-1.42 (m, 2H), 1.68-1.74 (m, 2H), 1.77-1.83 (m, 2H), 2.88 (t, *J* 6.2 Hz, 2H), 3.76 (s, 3H), 4.08 (t, *J* 6.0 Hz, 2H), 6.79 (dd, *J* 2.3, 8.7 Hz, 1H), 7.05 (d, *J* 8.7 Hz, 1H), 7.13 (d, *J* 2.3 Hz, 1H); δ_C (100 MHz, CDCl$_3$) 24.0, 25.5, 27.1, 29.8, 31.2, 41.4 (all CH$_2$), 55.8 (Me), 101.8, 109.4, 111.5 (all CH), 129.1, 143.7, 155.9, 156.8 (all C).

2.4.3.2. Preparation of (3,6-dimethoxy-2-nitrophenyl) cyclic amine 6c
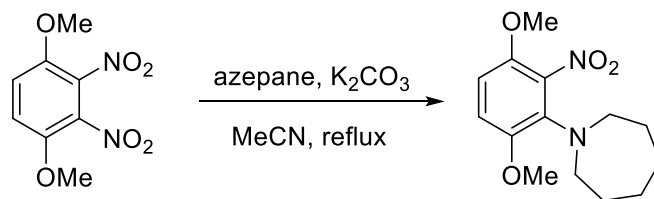
1,4-Dimethoxy-2,3-dinitrobenzene (0.800 g, 3.50 mmol), azepane (1.389 g, 14.00 mmol) and potassium carbonate (2.42 g, 17.54 mmol) were stirred in acetonitrile (10 mL) at reflux for 24 h. EtOAc (20 mL) was added and the organic layer washed with brine (40 mL). The organic extract was dried (MgSO$_4$), evaporated to dryness, and purified by column chromatography using silica as adsorbent with gradient elution of petroleum ether and EtOAc to give 1-(3,6-dimethoxy-2-nitrophenyl)azepane **6c** (0.756 g, 77%) as an orange solid; mp 96-100 °C; R_f 0.57 (10:90 EtOAc / pet. ether); v_{max} (neat, cm^{-1}) 2924, 2850, 1614, 1529 (NO$_2$), 1491, 1382 (NO$_2$), 1256, 1156, 1104, 1057; δ_H (400 MHz, CDCl$_3$) 1.50-1.67 (bs, 8H), 3.05 (t, J 5.5 Hz, 4H), 3.80 (s, 3H), 3.81 (s, 3H), 6.73 (d, J 9.2 Hz, 1H), 6.84 (d, J 9.2 Hz, 1H); δ_C (100 MHz, CDCl$_3$) 27.5, 30.2, 54.5 (all CH$_2$), 56.1, 56.7 (both Me), 109.0, 112.8 (both CH), 136.5, 142.3, 144.2, 152.6 (all C); HRMS (ESI) m/z (M + H)$^+$, C$_{14}$H$_{21}$N$_2$O$_4$ calcd. 281.1501, observed 281.1498.

2.4.3.3. Preparation of 3,6-dimethoxy-2-(cycloamino)aniline 7c
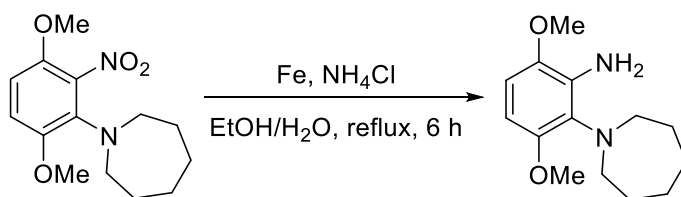
The nitrobenzene **6c** (3.96 mmol) with iron powder (0.709 g, 12.69 mmol) and NH$_4$Cl (0.106 g, 1.98 mmol) was stirred at reflux in ethanol (10 mL) and water (3 mL) for 8 h. EtOAc (30 mL) was added to the cooled mixture. The organic layer was washed with brine (40 mL), dried (MgSO$_4$), evaporated to dryness and purified by column chromatography using silica as adsorbent with gradient elution of petroleum ether and CH$_2$Cl$_2$ to give 2-(azepan-1-yl)-3,6-dimethoxyaniline **7c** (0.673 g, 68%) as a light brown solid; mp 58-60 °C; R_f 0.25 (70:30 CH$_2$Cl$_2$ / pet. ether); ν_{max} (neat, cm^{-1}) 3490, 3381, 2917, 2842, 1605, 1488, 1454, 1256, 1170, 1138; δ_H (400 MHz, CDCl$_3$) 1.56-1.83 (m, 8H), 2.86-2.89 (m, 2H), 3.23-3.26 (m, 2H), 3.75 (s, 3H), 3.79 (s, 3H), 4.31-4.54 (bs, 2H, NH$_2$), 6.16 (d, J 9.0 Hz, 1H), 6.53 (d, J 9.0 Hz, 1H); δ_C (100 MHz, CDCl$_3$) 27.9, 31.4, 54.1 (all CH$_2$), 55.5, 56.0 (both Me), 99.1, 107.0 (both CH), 129.8, 135.3, 142.1, 153.0 (all C); HRMS (ESI) m/z (M + H)$^+$, C$_{14}$H$_{23}$N$_2$O$_2$ calcd. 251.1760, observed 251.1749.
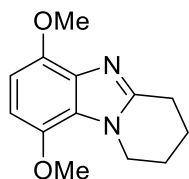
6,9-Dimethoxy-1,2,3,4-tetrahydropyrido[1,2-*a*]benzimidazole   (8b): Preparation from aniline **7b** as described in Table 2.6 to give **8b** (0.186 g, 80%); brown solid; mp 82-84 °C; v_{max} (neat, cm^{-1}) 2942, 1648, 1523, 1256, 1224, 1158, 1110, 1086, 1009; δ_H (400 MHz, CDCl$_3$) 1.90-1.92 (m, 2H), 1.99-2.01 (m, 2H), 3.02 (t, *J* 6.0 Hz, 2H), 3.82 (s, 3H), 3.91 (s, 3H), 4.39 (t, *J* 6.2 Hz, 2H), 6.45 (s, 2H); δ_C (100 MHz, CDCl$_3$) 20.6, 23.3, 25.6, 45.5 (all CH$_2$), 56.0 (2 × Me), 101.6, 102.4 (both CH), 125.5, 134.6, 141.9, 145.6, 150.3 (all C); HRMS (ESI) *m/z* (M + H)$^+$, C$_{13}$H$_{17}$N$_2$O$_2$ calcd. 233.1290, observed 233.1298.
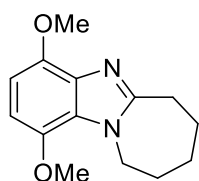
1,4-Dimethoxy-7,8,9,10-tetrahydro-6*H*-azepino[1,2-*a*]benzimidazole (8c): Preparation from aniline **7c** as described in Table 2.6 to give **8c** (0.177 g, 72%); brown oil; v_{max} (neat, cm^{-1}) 2933, 1615, 1525, 1527, 1471, 1405, 1259, 1203, 1108; δ_H (400 MHz, CDCl$_3$) 1.70-1.82 (m, 4H), 1.83-1.90 (m, 2H), 3.07 (t, *J* 5.3 Hz, 2H), 3.86 (s, 3H), 3.92 (s, 3H), 4.55-4.75 (bs, 2H), 6.49 (ABq, *J* 8.7 Hz, 2H); δ_C (100 MHz, CDCl$_3$) 25.6, 29.0, 29.7, 31.1, 46.2 (all CH$_2$), 55.9, 56.0 (both Me), 101.0, 103.1 (both CH), 126.0, 133.8, 141.3, 145.7, 156.7 (all C); HRMS (ESI) *m/z* (M + H)$^+$, C$_{14}$H$_{19}$N$_2$O$_2$ calcd. 247.1447, observed 247.1441.

2.4.3.5. Preparation of benzimidazolequinone anti-tumour agents 9b & 9c

The dimethoxy substituted benzimidazoles **8b** and **8c** (1 mmol) and HBr (10 mL, 90 mmol) were heated at reflux for 3 h. The solution was cooled and evaporated to dryness. Ferric chloride solution (20 mL, 0.7 M) was added and stirred at room temperature for 18 h. The solution was extracted with CH_2Cl_2 (5 × 20 mL). The combined organic extracts were dried ($MgSO_4$), evaporated to dryness, and purified by column chromatography using silica as adsorbent with gradient elution of petroleum ether and EtOAc to give the desired compounds.
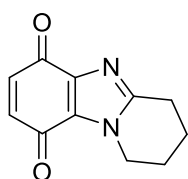
1,2,3,4-Tetrahydropyrido[1,2-*a*]benzimidazole-6,9-dione (9b): (0.176 g, 87%); yellow solid; mp 168-170 °C, (lit.[12] mp 153-155 °C); R_f 0.43 (EtOAc); v_{max} (neat, cm^{-1}) 1647 (C=O), 1511, 1481, 1430, 1409, 1302, 1244, 1206, 1074, 1059, 1035; δ_H (400 MHz, CDCl$_3$) 1.95-2.03 (m, 4H), 2.98 (t, *J* 6.2 Hz, 2H), 4.29 (t, *J* 5.7 Hz, 2H), 6.56 (AB$_q$, *J* 10.3 Hz, 2H); δ_C (100 MHz, CDCl$_3$) 19.8, 22.2, 25.0, 45.5 (all CH$_2$), 130.1 (C), 136.0, 136.2 (both CH), 141.4, 151.9 (both C), 178.2, 181.3 (both C=O). HRMS (ESI) *m/z* (M + H)$^+$, $C_{11}H_{11}N_2O_2$ calcd. 203.0821, observed 203.0819.
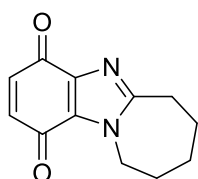
7,8,9,10-Tetrahydro-4*H*-azepino[1,2-*a*]benzimidazole-1,4(6*H*)-dione (9c): (0.151 g, 70%); yellow solid; mp (dec. >150 °C); R_f 0.30 (70:30 EtOAc / pet. ether); v_{max} (neat, cm^{-1}) 2931, 1648 (C=O), 1590, 1515, 1476, 1440, 1330, 1270, 1196, 1063; δ_H (400 MHz, CDCl$_3$) 1.64-1.71 (m, 2H), 1.72-1.79 (m, 2H), 1.82-1.91 (m, 2H), 2.98 (t, *J* 5.5 Hz, 2H), 4.52-4.54 (m, 2H), 6.52 (ABq, *J* 10.5 Hz, 2H); δ_C (100 MHz, CDCl$_3$) 24.8, 28.1, 29.3, 30.8, 45.9 (all CH$_2$), 130.3 (C), 135.9, 136.3 (both CH), 140.7, 158.4 (C), 178.7, 181.2 (both C=O); HRMS (ESI) *m/z* (M + H)$^+$, $C_{12}H_{13}N_2O_2$ calcd. 217.0977, observed 217.0983.

2.5   Conclusions

In summary, nine pyrrolo[1,2-*a*]benzimidazoles have been prepared from *o*-pyrrolo substituted anilines using "acid-free" H_2O_2 in EtOAc protocol, where no aqueous extraction or chromatography is required. Where reactions are slow in the case of **1g** and **1i**, environmentally acceptable MSA can be added. Six to eight-membered ring-fused benzimidazoles can be prepared using H_2O_2 in EtOAc methodology with pyrido[1,2-*a*]benzimidazole **3a** requiring one equivalent of MSA to achieve cyclization in a timely manner.

The cyclization of 3,6-dimethoxy-2-(cycloamino)anilines mostly required one equivalent of MSA in order to achieve high yields in a reasonable time. Nevertheless, the H_2O_2 in EtOAc protocol has considerable merit over reported routes to ring-fused benzimidazoles and benzimidazolequinones, which are more costly, environmentally-damaging, and often ineffective in preparing constrained and ring-expanded systems.

2.6   References

1.   Nair, M. D.; Adams, R. *J. Am. Chem. Soc.* **1961**, *83*, 3518-3521.

2.   Meth-Cohn, O.; Suschitzky, H. *J. Chem. Soc.* **1963**, *0*, 4666-4669.

3.   Sun, X.; Lv, X.-H.; Ye, L.-M.; Hu, Y.; Chen, Y.-Y.; Zhang, X.-J.; Yan, M. *Org. Biomol. Chem.* **2015**, *13*, 7381-7383.

4.   Sun, X.; Hu, Y.; Nie, S.-Z.; Yan, Y.-Y.; Zhang, X.-J.; Yan, M. *Adv. Synth. Catal.* **2013**, *355*, 2179-2184.

5.   Pereira, K. C.; Porter, A. L.; DeBoef, B. *Tetrahedron Lett.* **2014**, *55*, 1729-1732.

6.   Kutsumura, N.; Kunimatsu, S.; Kagawa, K.; Otani, T.; Saito, T. *Synthesis* **2011**, *2011*, 3235-3240.

7.   Huang, J.; He, Y.; Wang, Y.; Zhu, Q. *Chem. Eur. J.* **2012**, *18*, 13964-13967.

8.   Allin, S. M.; Bowman, W. R.; Karim, R.; Rahman, S. S. *Tetrahedron* **2006**, *62*, 4306-4316.

9.   Fagan, V.; Bonham, S.; Carty, M. P.; Aldabbagh, F. *Org. Biomol. Chem.* **2010**, *8*, 3149-3156.

10.   Lynch, M.; Hehir, S.; Kavanagh, P.; Leech, D.; O'Shaughnessy, J.; Carty, M. P.; Aldabbagh, F. *Chem. Eur. J.* **2007**, *13*, 3218-3226.

11.   Aldabbagh, F.; Bowman, W. R. *Tetrahedron* **1999**, *55*, 4109-4122.

12.   Campos-Martin, J. M.; Blanco-Brieva, G.; Fierro, J. L. G. *Angew. Chem., Int. Ed.* **2006**, *45*, 6962-6984.

13.   Eul, W.; Moeller, A.; Steiner, N., Hydrogen Peroxide. In *Kirk‑Othmer Encyclopedia of Chemical Technology*, John Wiley & Sons, Inc. 2001; Vol. 13, pp 1-58.

14.   Zhou, R.; Skibo, E. B. *J. Med. Chem.* **1996**, *39*, 4321-4331.

15.   Fahey, K.; Aldabbagh, F. *Tetrahedron Lett.* **2008**, *49*, 5235-5237.

16.   Fagan, V.; Bonham, S.; Carty, M. P.; Saenz-Méndez, P.; Eriksson, L. A.; Aldabbagh, F. *Bioorg. Med. Chem.* **2012**, *20*, 3223-3232.

17.   Gurry, M.; Sweeney, M.; McArdle, P.; Aldabbagh, F. *Org. Lett.* **2015**, *17*, 2856-2859.

18.   Nguyen, T. B.; Ermolenko, L.; Al-Mourabit, A. *Green Chem.* **2016**, *18*, 2966-2970.

19.   Kim, H. W.; Ross, M. B.; Kornienko, N.; Zhang, L.; Guo, J.; Yang, P.; McCloskey, B. D. *Nat. Catal.* **2018**, *1*, 282-290.

20. Ciriminna, R.; Albanese, L.; Meneguzzo, F.; Pagliaro, M. *ChemSusChem* **2016**, *9*, 3374-3381.

21. Edwards, J. K.; Hutchings, G. J. *Angew. Chem., Int. Ed.* **2008**, *47*, 9192-9198.

22. Blanco-Brieva, G.; Capel-Sanchez, M. C.; Pilar de Frutos, M.; Padilla-Polo, A.; Campos-Martin, J. M.; Fierro, J. L. G. *Ind. Eng. Chem. Res.* **2008**, *47*, 8011-8015.

23. Goor, G.; Glenneberg, J.; Jacobi, S., Hydrogen Peroxide. In *Ullmann's Encyclopedia of Industrial Chemistry*, Wiley-VCH: Weinheim, 2007; pp 393-427.

24. Gustaaf, G., Hydrogen Peroxide: Manufacture and Industrial Use for Production of Organic Chemicals. In *Catalytic Oxidations with Hydrogen Peroxide as Oxidant*, Strukul, G., Ed. Springer Netherlands: Dordrecht, 1992; pp 13-43.

25. Crole, D. A.; Freakley, S. J.; Edwards, J. K.; Hutchings, G. J. *Proc. R. Soc. A* **2016**, *472*, 20160156.

26. Jimenez-Gonzalez, C.; Ponder, C. S.; Broxterman, Q. B.; Manley, J. B. *Org. Process Res. Dev.* **2011**, *15*, 912-917.

27. Nielsen, M.; Junge, H.; Kammer, A.; Beller, M. *Angew. Chem., Int. Ed.* **2012**, *51*, 5711-5713.

28. Ethyl Acetate Market (Application - Printing Inks, Adhesives, Cosmetics, Paints and Coatings, Pharmaceuticals, Food and Beverage, Herbicides) - Global Industry Analysis, Size, Share, Growth, Trends, and Forecast 2018-2026. https://www.transparencymarketresearch.com/ethyl-acetate-market.html (accessed Jul 5, 2019).

29. Molecule of the Week Archive: Ethyl acetate. https://www.acs.org/content/acs/en/molecule-of-the-week/archive/e/ethyl-acetate.html (accessed Jul 5, 2019).

30. Clark, J. H.; Hunt, A. J.; Topi, C.; Paggiola, G.; Sherwood, J., An Appendix of Solvent Data Sheets. In *Sustainable Solvents: Perspectives from Research, Business and International Policy*, The Royal Society of Chemistry 2017; pp 235-347.

31. Ashley, M., Using Bio-Ethanol To Manufacture An Industrial Solvent. *Ingenia* December 2006, pp 46-50.

32. Fischer, E.; Speier, A. *Ber. Dtsch. Chem. Ges.* **1895**, *28*, 3252-3258.

33. Capello, C.; Fischer, U.; Hungerbühler, K. *Green Chem.* **2007**, *9*, 927-934.

34. Nguyen, T. T. H.; Kikuchi, Y.; Noda, M.; Hirao, M. *Ind. Eng. Chem. Res.* **2015**, *54*, 5494-5504.

35.   REACH. http://ec.europa.eu/environment/chemicals/reach/reach_en.htm (accessed Jul 6, 2019).

36.   Candidate List of substances of very high concern for Authorisation. https://echa.europa.eu/candidate-list-table (accesssed Jul 6, 2019).

37.   Substances restricted under REACH. https://echa.europa.eu/substances-restricted-under-reach (accessed Jul 6, 2019).

38.   Alfonsi, K.; Colberg, J.; Dunn, P. J.; Fevig, T.; Jennings, S.; Johnson, T. A.; Kleine, H. P.; Knight, C.; Nagy, M. A.; Perry, D. A.; Stefaniak, M. *Green Chem.* **2008**, *10*, 31-36.

39.   Henderson, R. K.; Jiménez-González, C.; Constable, D. J. C.; Alston, S. R.; Inglis, G. G. A.; Fisher, G.; Sherwood, J.; Binks, S. P.; Curzons, A. D. *Green Chem.* **2011**, *13*, 854-862.

40.   Prat, D.; Pardigon, O.; Flemming, H.-W.; Letestu, S.; Ducandas, V.; Isnard, P.; Guntrum, E.; Senac, T.; Ruisseau, S.; Cruciani, P.; Hosek, P. *Org. Process Res. Dev.* **2013**, *17*, 1517-1525.

41.   Prat, D.; Wells, A.; Hayler, J.; Sneddon, H.; McElroy, C. R.; Abou-Shehada, S.; Dunn, P. J. *Green Chem.* **2016**, *18*, 288-296.

42.   Prat, D.; Hayler, J.; Wells, A. *Green Chem.* **2014**, *16*, 4546-4551.

43.   *Chem. Eng. News Archive* **2012**, *90*, ibc.

44.   Lutropur® –the friendly acid. https://www.google.ie/webhp?sourceid=chrome-instant&ion=1&espv=2&ie=UTF-8#q=lutropur+msa+100 (accessed 6 Jul, 2019).

45.   Baker, S. C.; Kelly, D. P.; Murrell, J. C. *Nature* **1991**, *350*, 627-628.

46.   Gernon, M. D.; Wu, M.; Buszta, T.; Janney, P. *Green Chem.* **1999**, *1*, 127-140.

47.   Molecule of the Week Archive: Methanesulfonic acid. https://www.acs.org/content/acs/en/molecule-of-the-week/archive/m/methanesulfonic-acid.html (accessed Jul 6, 2019).

48.   Díaz-Urrutia, C.; Ott, T. *Science* **2019**, *363*, 1326-1329.

49.   Anastas, P. T.; Warner, J. C., *Green chemistry : theory and practice*. Oxford University Press: New York, 1998; p 30.

50.   Fagan, V.; Bonham, S.; McArdle, P.; Carty, M. P.; Aldabbagh, F. *Eur. J. Org. Chem.* **2012**, *2012*, 1967-1975.

51.   Mustroph, H.; Haessner, R. *J. prakt. Chem.* **1989**, *331*, 319-323.

52.   Zhang, M.-R.; Kumata, K.; Maeda, J.; Haradahira, T.; Noguchi, J.; Suhara, T.; Halldin, C.; Suzuki, K. *J. Med. Chem.* **2007**, *50*, 848-855.

53. Hoh, G. L. K.; Barlow, D. O.; Chadwick, A. F.; Lake, D. B.; Sheeran, S. R. *J. Am. Oil Chem. Soc.* **1963**, *40*, 268-271.

54. Cope, A. C.; Trumbull, E. R., Olefins from Amines: The Hofmann Elimination Reaction and Amine Oxide Pyrolysis. In *Organic Reactions*, 1960; pp 317-493.

55. VanRheenen, V.; Cha, D. Y.; Hartley, W. M. *Org. Synth.* **1978**, *58*, 43.

56. Sakaue, S.; Tsubakino, T.; Nishiyama, Y.; Ishii, Y. *J. Org. Chem.* **1993**, *58*, 3633-3638.

57. Dewkar, G. K.; Nikalje, M. D.; Sayyed Ali, I.; Paraskar, A. S.; Jagtap, H. S.; Sudalai, A. *Angew. Chem., Int. Ed.* **2001**, *40*, 405-408.

58. Zhao, D.; Johansson, M.; Bäckvall, J.-E. *Eur. J. Org. Chem.* **2007**, *2007*, 4431-4436.

59. Ishimoto, R.; Kamata, K.; Mizuno, N. *Angew. Chem., Int. Ed.* **2012**, *51*, 4662-4665.

60. Shiraishi, Y.; Sakamoto, H.; Fujiwara, K.; Ichikawa, S.; Hirai, T. *ACS Catal.* **2014**, *4*, 2418-2425.

61. Fountoulaki, S.; Gkizis, P. L.; Symeonidis, T. S.; Kaminioti, E.; Karina, A.; Tamiolakis, I.; Armatas, G. S.; Lykakis, I. N. *Adv. Synth. Catal.* **2016**, *358*, 1500-1508.

62. Oswald, A. A.; Guertin, D. L. *J. Org. Chem.* **1963**, *28*, 651-657.

63. Hammershøj, P.; Reenberg, T. K.; Pittelkow, M.; Nielsen, C. B.; Hammerich, O.; Christensen, J. B. *Eur. J. Org. Chem.* **2006**, *2006*, 2786-2794.

64. Sweeney, M.; McArdle, P.; Aldabbagh, F. *Molbank* **2018**, *2018*, M984.

65. Garner, R.; Suschitzky, H. *J. Chem. Soc. C* **1967**, 74-76.

66. Libeer, M. J.; Depoorter, H.; Van Mierlo, G. G.; Lemahieu, R. G. Improvements in or Relating to Sensitized Photographic Silver Halide Emulsions and to New Sensitizing Dyes. G.B. Patent 1001061A, August 20, 1965.

67. Libeer, M. J.; Depoorter, H.; Van Mierlo, G. G.; Lemahieu, R. G. Methine Dyes. U.S. Patent 3931156A, January 6, 1976.

68. Suschitzky, H.; Sutton, M. E. *Tetrahedron* **1968**, *24*, 4581-4587.

69. Chen, J.; Qu, J.; Zhang, Y.; Chen, Y.; Liu, N.; Chen, B. *Tetrahedron* **2013**, *69*, 316-319.

Chapter 3

One-Pot Synthesis of Dihalogenated Ring-fused Benzimidazoles & Benzimidazolequinones using H$_2$O$_2$/HX
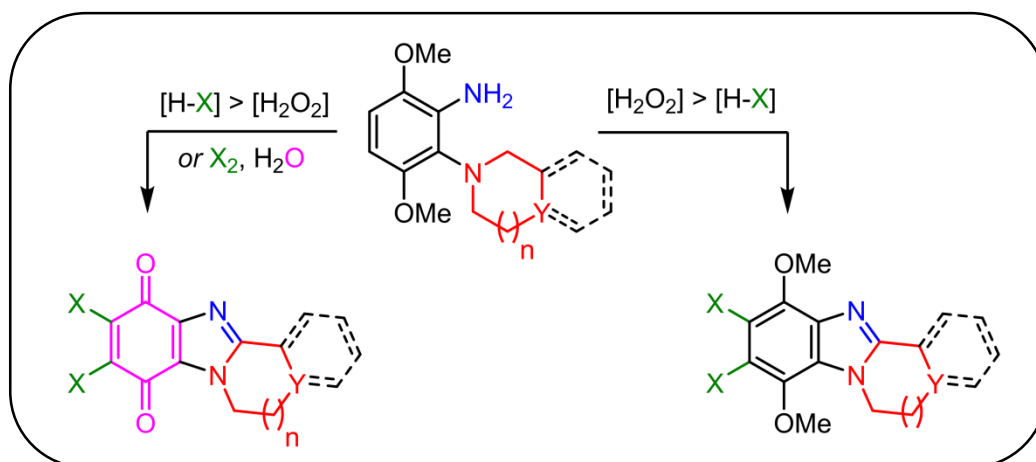
The material in this Chapter has been published as part of:

Organic LETTERS

One-Pot Hydrogen Peroxide and Hydrohalic Acid Induced Ring Closure and Selective Aromatic Halogenation To Give New Ring-Fused Benzimidazoles

Michael Gurry, Martin Sweeney, Patrick McArdle, and Fawaz Aldabbagh*

School of Chemistry, National University of Ireland Galway, University Road, Galway, Ireland

Ⓢ Supporting Information

ABSTRACT: A new series of selectively dichlorinated and dibrominated five- to eight-membered-ring [1,2-*a*]-fused benzimidazoles and [1,4]oxazino[4,3-*a*]benzimidazoles are synthesized in mostly high yields of >80% using the reaction of hydrogen peroxide and hydrohalic acid with commercially available *o*-cyclic amine substituted anilines. Domestic bleach with HCl can also be used for a one-pot ring closure and chlorination.

The novel dihalogenated ring-expanded and ring-contracted benzimidazoles prepared by author of this thesis as part of the above publication are presented in Section 3.3.1.

One-Pot Synthesis of Dihalogenated Ring-Fused Benzimidazolequinones from 3,6-Dimethoxy-2-(cycloamino)anilines Using Hydrogen Peroxide and Hydrohalic Acid

Martin Sweeney,[†] Lee-Ann J. Keane,[†] Michael Gurry,[†] Patrick McArdle,[†] and Fawaz Aldabbagh*[†,‡]

[†]School of Chemistry, National University of Ireland Galway, University Road, Galway, H91 TK33, Ireland

[‡]Department of Pharmacy, School of Life Sciences, Pharmacy & Chemistry, Kingston University, Penrhyn Road, Kingston upon Thames, KT1 2EE, United Kingdom

Ⓢ Supporting Information

ABSTRACT: 3,6-Dimethoxy-2-(cycloamino)anilines undergo 4- or 6-electron oxidations to afford novel ring-fused halogenated benzimidazoles or benzimidazole-quinones using H_2O_2/HCl or H_2O_2/HBr. Cl_2 and Br_2 are capable of the same oxidative transformation to the benzimidazolequinones. Labeling experiments indicate that water is necessary for oxidation of the *para*-dimethoxybenzenes to the corresponding quinones.
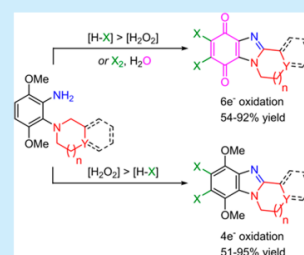
Martin Sweeney [1], Patrick McArdle [1] and Fawaz Aldabbagh [1,2,*]

[1] School of Chemistry, National University of Ireland Galway, University Road, Galway, H91 TK33, Ireland; m.sweeney5@nuigalway.ie (M.S.); patrick.mcardle@nuigalway.ie (P.M.)

[2] Department of Pharmacy, School of Life Sciences, Pharmacy and Chemistry, Kingston University, Penrhyn Road, Kingston upon Thames KT1 2EE, UK

* Correspondence: f.aldabbagh@kingston.ac.uk; Tel.: +44-20-8417-2528

Abstract: 1-Fluoro-2,5-dimethoxy-4-nitrobenzene was synthesized in 90% yield by the reaction of commercial 2-fluoro-1,4-dimethoxybenzene with nitric acid. The structure was confirmed by X-ray crystallography. The new title compound was characterized by ^{1}H and ^{13}C-NMR, elemental analysis, EI-MS and FT-IR.

The majority of compounds described in this Chapter were made by the author of this thesis, however compounds first prepared as part of the thesis of Michael Gurry (PhD, NUI Galway 2016) are denoted by the symbol: # and compounds prepared as part of the PhD thesis of Lee-Ann Keane are denoted by the symbol: †

3.1. Introduction

The carbon-halogen bond (C-X) continues to be of high interest in medicinal chemistry due to its high prevalence in the pharmaceutical and agrochemical industry. Currently, 25% of the "Top 200 prescribed pharmaceuticals"[1] and approximately 66% of all agrochemicals contain halogen substituted aryl moieties (Figure 3.1).[2]

Hydrochlorothiazide (diuretic)   **Imidacloprid (insecticide)**   **Epoxiconazole (fungicide)**
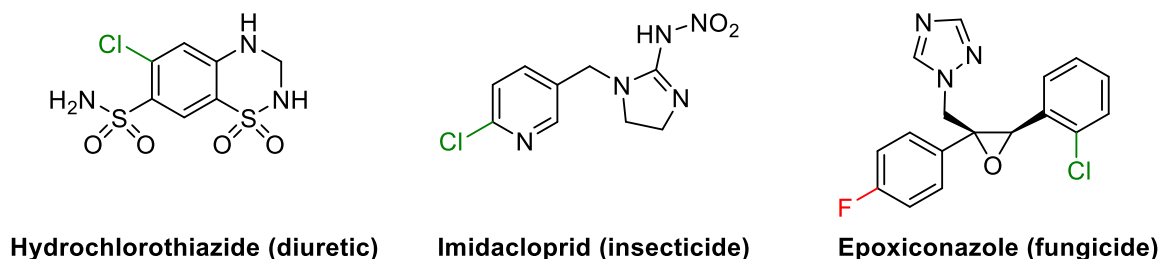
Figure 3.1. Examples of top-selling halogenated compounds in the pharmaceutical and agrochemical industries.

In drug development, the majority of drug candidates (46%) don't reach the launch phase due to lack of efficacy.[3, 4] The addition of a C-X bond to an organic compound primarily improves metabolic stability (less susceptible to oxidation), oral permeability, and blood-brain barrier permeability.[3, 4] Thereby, halogenation improves efficacy and is deployed to increase success rates in drug development.
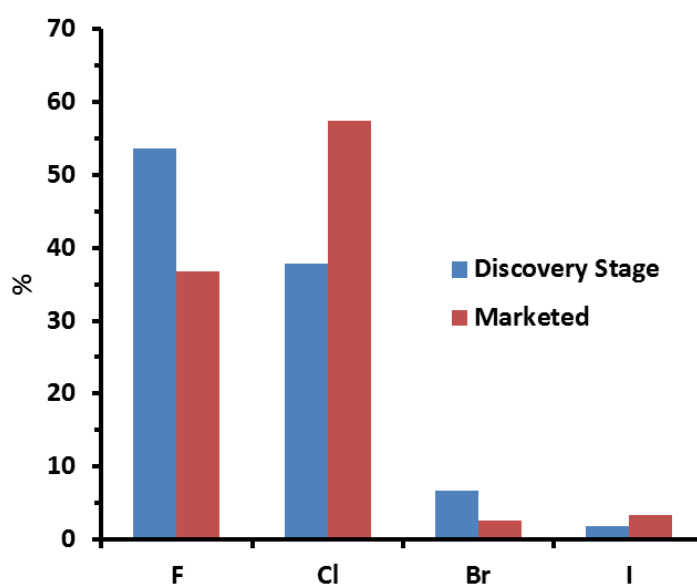
Figure 3.2. Organochlorines represent the most marketed pharmaceutical halogens.[5]

Bromine and iodine are the least marketed organohalogen drugs, contributing approximately 6% to the total amount. Chlorine as a substituent is the most common in marketed drugs whereas there is a lot of focus on fluorine in early stage research but ultimately the marketed output is a smaller percentage (Figure 3.2).[5]

Perhaps this anomaly can be attributed to the occurrence of halogen bonding. Halogen bonding is an intermolecular interaction of the type C−X···Y−R', where X is chlorine, bromine or iodine that acts as a Lewis acid and Y can be any kind of Lewis base such as nitrogen or oxygen (Figure 3.3).[1, 4-7] Halogen bonds are of comparable strength to that of hydrogen bonds (10 to 150 KJ/mol)[8] as they range from 5 to 180 KJ/mol.[9, 10] The bond angle is typically linear and distances are shorter than the sum of vdW radii with the interaction increasing from chlorine to iodine.[5, 11] The other type of halogen bond involves C-X---π interactions where the angle of α is < 60° and θ is > 120° with d(Cl···π) < 4.2 Å, d(Br···π) < 4.3 Å and d(I···π) < 4.5 Å (Figure 3.3).[12] Traditionally, halogens have been considered to have isotropic negative electron density around them but in fact the charge distribution of halogen atoms is anisotropic consisting of a positively charged electrostatic region on the extension of C−X bonds.[7] Politzer and co-workers have named this phenomenon a sigma-hole.[11] For the sigma-hole to have a large electrostatic region of positive charge, the halogen atom should be highly polarizable and bear a strong electron-withdrawing moiety C as part of C-X.[9]
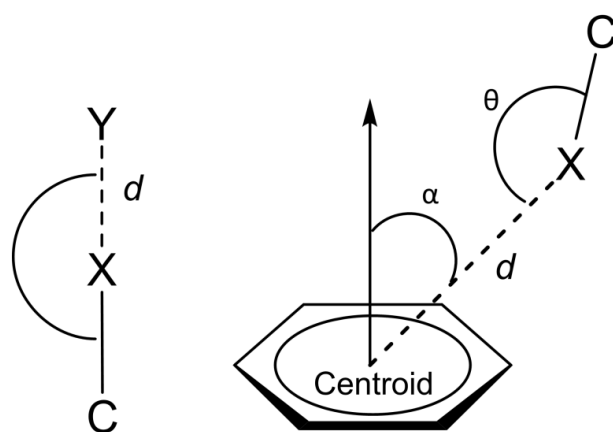
Figure 3.3. The different types of halogen bonding.[5]

As a result of the sigma-hole, halogen atoms exhibit both electrophilic character along the axes of the C–X bonds and nucleophilic character along the vectors that are perpendicular

to these bonds.[13] In modern drug discovery, halogen bonding is becoming an essential tool for lead identification and optimization due to its favourable protein-ligand interactions.[1, 5-7, 14]

The placement of electron withdrawing chlorine groups on the 1,4-benzoquinone motif results in a more electron deficient quinone core, thus allowing a more facile 2 e$^-$/2 H$^+$ reduction to the corresponding hydroquinone species (Figure 3.4.).[15] As the number of chloro- substituents increased from monochloro-1,4-benzoquinone to tetrachloro-1,4-benzoquinone (chloroanil), reduction potentials increased relative to the parent 1,4-benzoquinone, making for easier reduction (Figure 3.4). 2,3-Dichloro-5,6-dicyano-1,4-benzoquinone (DDQ) containing chloro- and cyano- EWGs proved to be the most susceptible to reduction with a reduction potential of 0.887 V, shifted 0.21 V in the positive direction relative to 1,4-benzoquinone. The 2 e$^-$/2 H$^+$ reduction potentials for ring-fused quinones of naphthoquinone and anthraquinone increased when dichlorinated (Figure 3.4).[15] Furthermore, direct correlations have been established between reduction potentials and the cytotoxicity of heterocyclic quinones.[16-19]
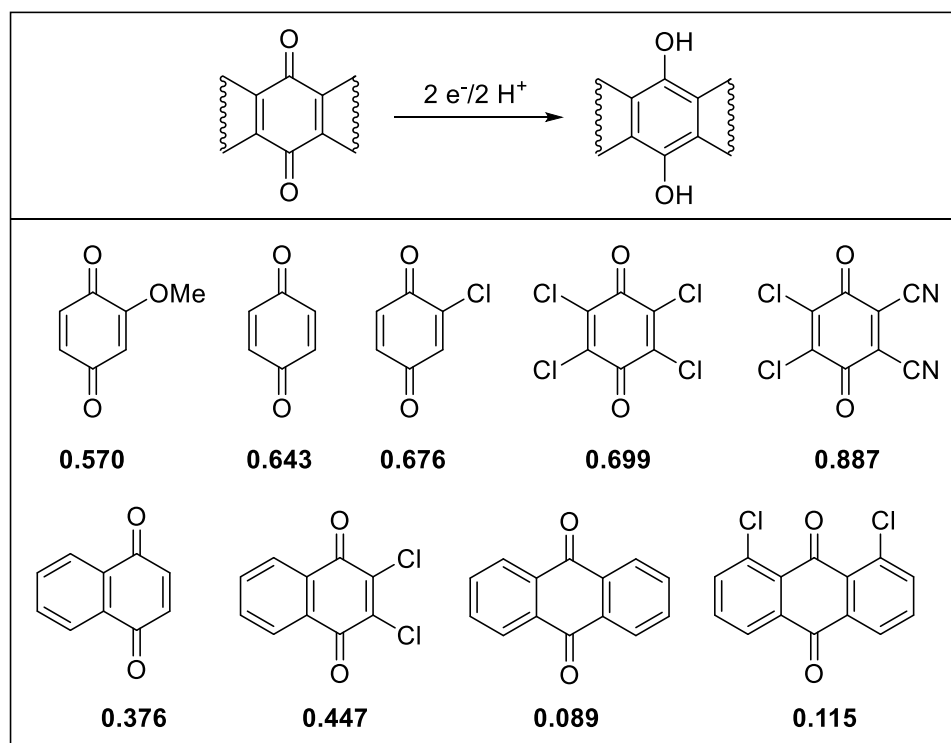
Figure 3.4. 2 e$^-$/2 H$^+$ reduction potentials (V vs. NHE) for 1,4-benzoquinone derivatives.[15]

In addition to tuning electronic structure, halogen substituents serve as points for further functionalization of quinone moieties. For example, nucleophilic substitution[20-23] and transition metal-catalyzed cross-couplings can occur,[24, 25] with the resultant functionalization significantly altering biological activity (Scheme 3.1).[20-24, 26]
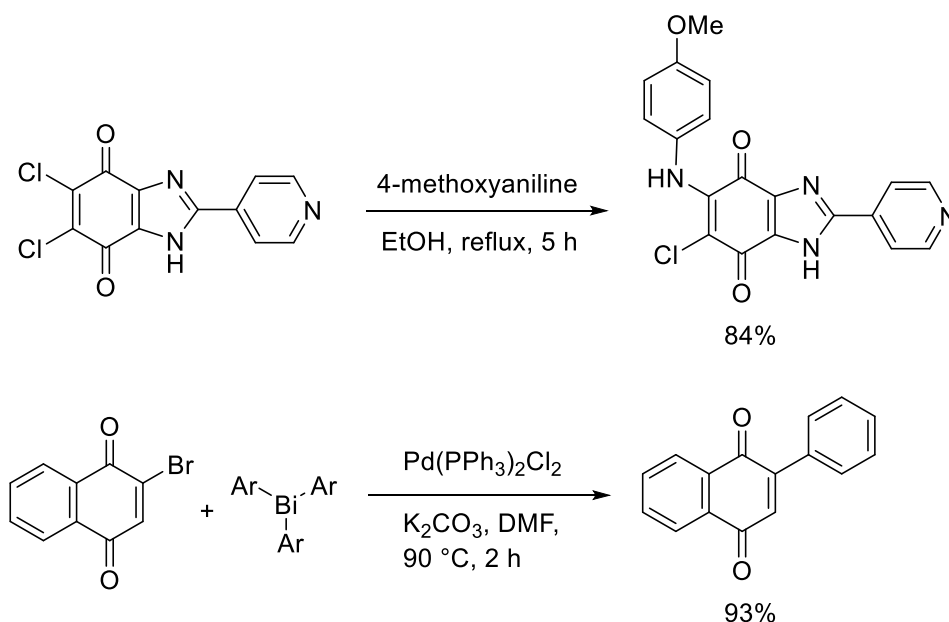
Scheme 3.1. Halogen directed functionalization of quinone moieties.[20, 25]

The cleanest method of generating elemental chlorine and bromine in situ is to mix hydrogen peroxide with excess hydrochloric and hydrobromic acid respectively, since the only by-product is water (Scheme 3.2).[27, 28] The intermediate is hypohalous acid (HOX), which is commonly used to disinfect water. The molecular halogen (X_2) in water equilibrates with an acidic (HX) solution of HOX.[29, 30]

$$H_2O_2 + HX \longrightarrow HOX + H_2O \quad (1)$$

$$HOX + HX \rightleftharpoons X_2 + H_2O \quad (2)$$
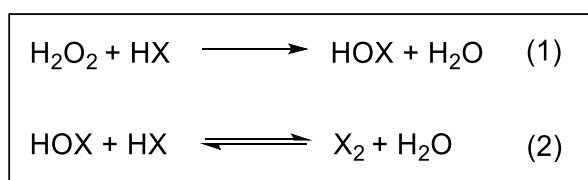
Scheme 3.2. Generation of X_2 (where X = Cl, Br) from H_2O_2/HX.

The H_2O_2/HX system has been employed in the electrophilic halogenation of many activated aromatics,[31] including anilines,[32-34] phenyl ethers,[35] phenols,[33, 36, 37] and amides[38] (Scheme 3.3). The activation of electrophilic halogenation can proceed under microwave

irradiation[33] or sonication[37] and in benign solvents such as water.[38] Fluorinated alcohols were shown to have a catalytic effect on electrophilic chlorination of inactive aromatics such as benzene and toluene.[28] The by-product of oxidative halogenation, HX can be recycled back to X_2 by oxidation with H_2O_2.[39]
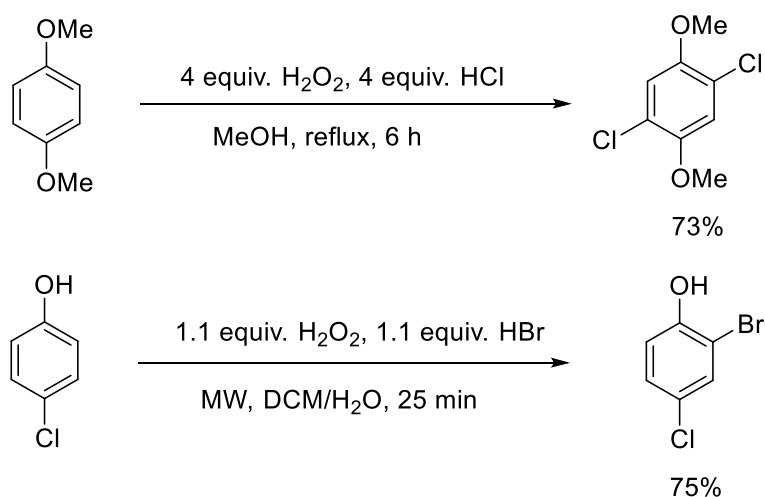
Scheme 3.3. Aromatic halogenation with H_2O_2/HX.[33, 35]

In comparison, the H_2O_2/HX system is relatively underutilized in the synthesis of heterocycles with H_2O_2/HBr used to catalyze the aziridination of alkenes with chloramine-T at room temperature under a nitrogen atmosphere (Scheme 3.4a).[40] The H_2O_2/HCl system was used to carry out the condensation of 1,2-phenylenediamines with aryl aldehydes in acetonitrile at room temperature to furnish 2-substituted benzimidazoles in high yields of 92-99% (Scheme 3.4b)[41]
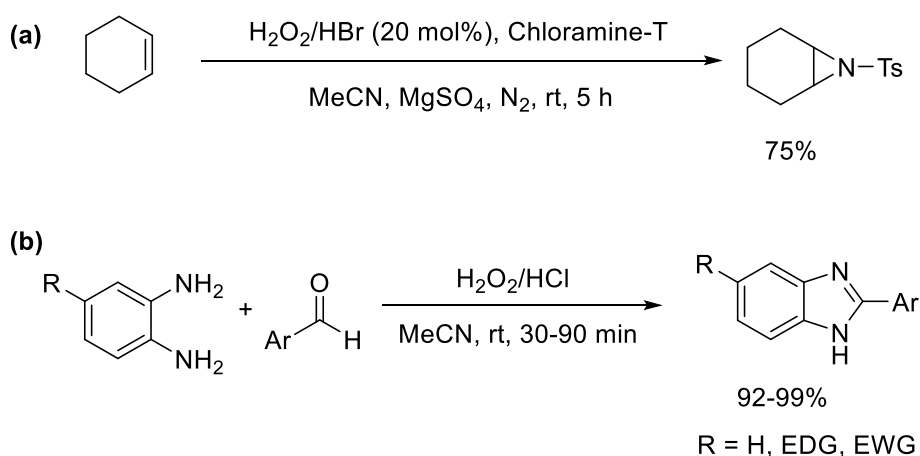
Scheme 3.4. Heterocycle formation using H_2O_2/HX system.[40, 41]

Halogenation onto the benzimidazole scaffold often occurs at a late stage after the benzimidazoles are pre-prepared using methodologies presented in Chapter 1. The difficult to handle reagents of chlorine (Scheme 3.5c) and bromine (Scheme 3.5a) are often employed and issues of regioselectivity can occur (Scheme 3.5c) with the more reactive chlorine.[42, 43] The dibrominated 2-trifluoromethylbenzimidazole was obtained in a good yield of 75% by adding a 5 molar excess of bromine to a suspension of 2-trifluoromethylbenzimidazole in water and then heating to reflux (Scheme 3.5a).[44] The use of H_2O_2 in HCl as solvent at 90 °C facilitated the hydroxyl directed *o*-dichlorination of 5-hydroxy-2-methylbenzimidazole in a moderate yield of 47% (Scheme 3.5b).[45] Chlorine gas was introduced into water at 70-80 °C containing a suspension of 5-chloro-2-trifluoromethylbenzimidazole leading to a mixture of chlorinated isomers that were isolated in 98% yield (Scheme 3.5c).[44] GC analysis showed the major isomer formed was 4,5-chloro-2-trifluoromethylbenzimidazole in 70% while the minor isomer was 5,6-chloro-2-trifluoromethylbenzimidazole in 27%, alongside 3% of unidentified higher chlorinated benzimidazoles (Scheme 3.5c).
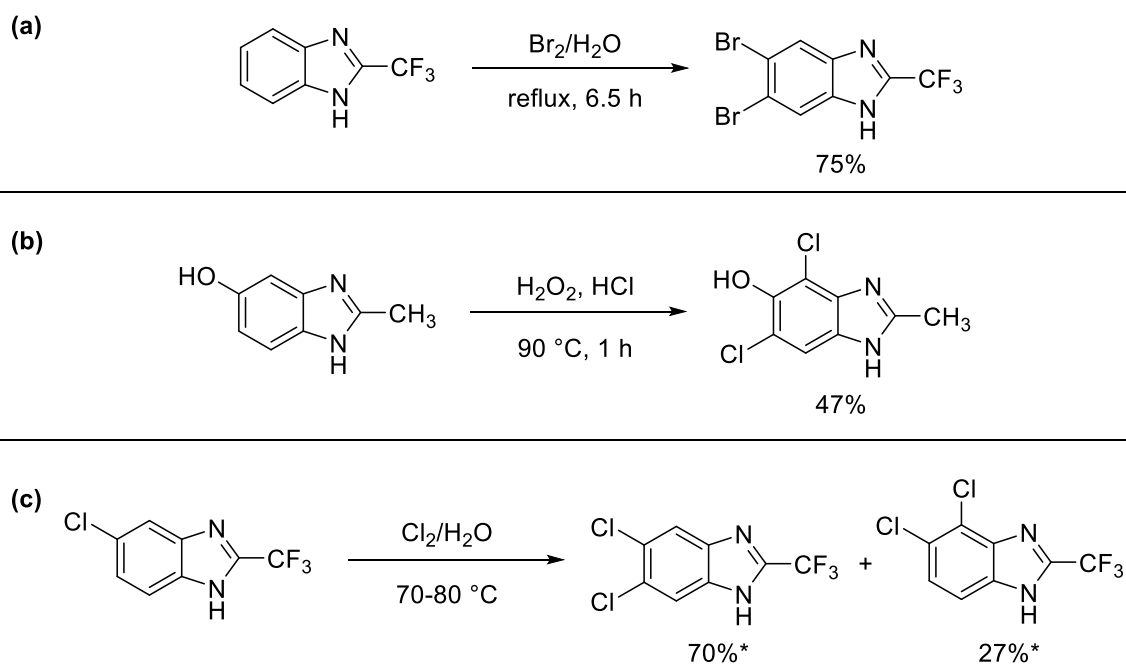
Scheme 3.5. Late-stage halogenation of benzimidazoles.[44, 45] *GC yield.

As part of the thesis of Michael Gurry, late-stage halogenation was avoided by designing a one-pot H_2O_2/HX mediated oxidative cyclization of o-cyclic amine substituted anilines with regioselective dihalogenation that produced a series of ring-fused benzimidazoles (Scheme 3.6).[46] In general, H_2O_2 (10 equiv.) and HX (12 equiv.) were employed to carry out the oxidative transformations in a time of 20 min. The presence of EWGs and EDGs at the R-position were well tolerated in the preparation of dichlorinated ring-fused benzimidazoles. The EWGs and EDGs had no effect on the conversion of anilines or the pattern of halogen substitution when using H_2O_2/HCl (Scheme 3.6, red box).
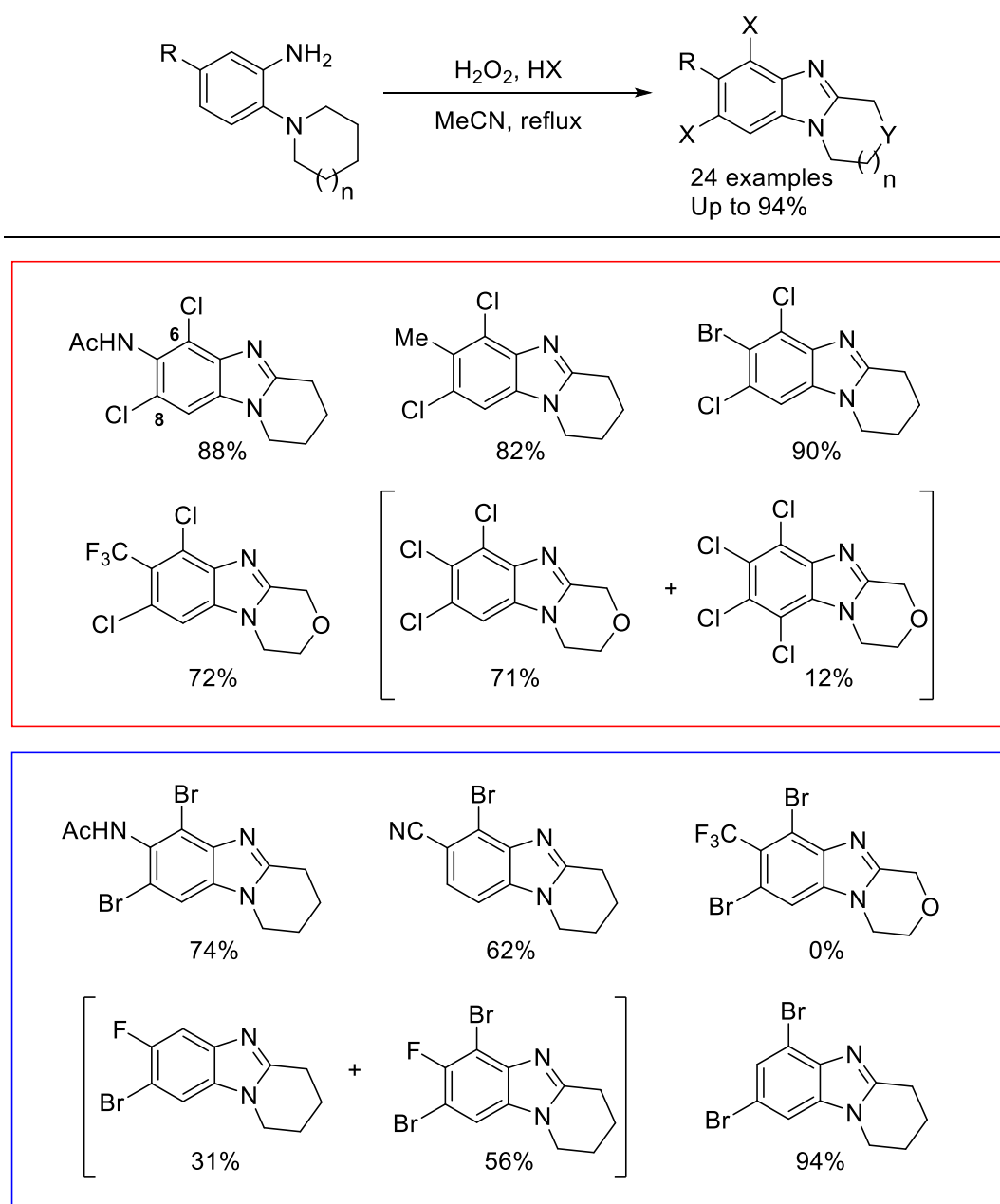
Scheme 3.6. One-pot regioselective formation of halogenated ring-fused benzimidazoles.[46]

The halogenations consistently occurred at the 6,8-position of pyrido[1,2-*a*]benzimidazoles irrespective of substituent present, while in the absence of an EDG or EWG, a mixture of trichlorinated and tetrachlorinated isomers of [1,4]oxazino[4,3-*a*]benzimidazole were formed (Scheme 3.6, red box).

The analogous reactions using HBr/H_2O_2 were affected by varying substituents on the *o*-cyclic amine substituted anilines (Scheme 3.6, blue box). The dibrominated ring-fused benzimidazole containing the resonance activator of NHAc took significantly longer (2 d) to furnish than the counterpart H_2O_2/HCl reaction and required double the amounts of H_2O_2/HBr. As the deactivating nature of the EWG increased, it became more difficult to isolate the regioselective dibrominated ring-fused benzimidazoles. The flouro EWG formed a mixture of mono-brominated isomers, the cyano version was regioselectively mono-brominated while the trifluoromethyl analogue wasn't brominated at all (Scheme 3.6, blue box) Interestingly, 6,8-dibrominated pyrido[1,2-*a*]benzimidazole was regioselectively formed in the absence of a EDG or EWG, indicating the pattern of bromination is dictated by other factors (Scheme 3.6, blue box).

As previously detailed in Chapter 1, ring-fused benzimidazoles serve as synthetic precursors to the bioreducible benzimidazolequinones. Skibo and co-workers popularized aziridinyl-substituted pyrrolo[1,2-*a*]benzimidazolequinones (PBIs) as bioreductive anti-tumour alternatives to the mitomycins.[47] The Aldabbagh group also produced notable benzimidazolequinones with potent cytotoxicity, [18, 20, 21, 26, 48-50, 51, 52] including specificity towards hypoxic tumour cells,[18] NAD(P)H:quinone oxidoreductase 1 (NQO1)[48] and Fanconi anemia cells.[26, 49] Traditionally, *p*-dimethoxybenzenes are precursors to the desired *p*-quinone moiety (Scheme 3.7). The two-step pathway involves a HBr-mediated demethylation to the hydroquinone followed by $FeCl_3$ or CrO_3 mediated oxidation to give benzimidazolequinones (Scheme 3.7). [18, 21, 48, 53, 54] The other route involves a one-step conversion of *p*-dimethoxybenzenes to the desired *p*-quinones and has been effected with nitric acid,[55] AgO-mineral acid,[56] $Ce(NH_4)_2(NO_3)_6$ (CAN),[52, 57-60] CoF_3,[61] NBS with a catalytic amount of H_2SO_4,[49, 62] and $PhIOCOCF_3$ (PIFA) (Scheme 3.7).[63]
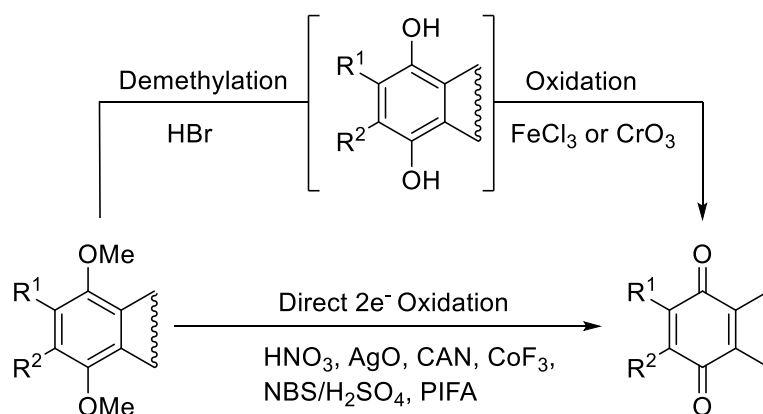
Scheme 3.7. Synthetic routes toward 1,4-benzoquinone derivatives.[18, 21, 48, 49, 52-63]

Both nitric acid and argentic oxide (AgO) use harsh acidic conditions which limits their substrate scope and nitric acid also participates in side reactions such as nitration.[55, 56] The reagent of cobalt(III) fluoride is highly hydroscopic and has to be handled in a glove bag under argon before carrying out oxidative demethylation of aromatic ethers.[61] Cerium(IV) ammonium nitrate (CAN) is the most commonly used reagent for the oxidative cleavage of *p*-dimethoxybenzenes (Scheme 3.8). However, CAN is a high molecular weight reagent (548 g/mol) and radical cationic intermediates facilitate oxidative coupling to form dimeric *p*-quinones (Scheme 3.8).[50, 64]
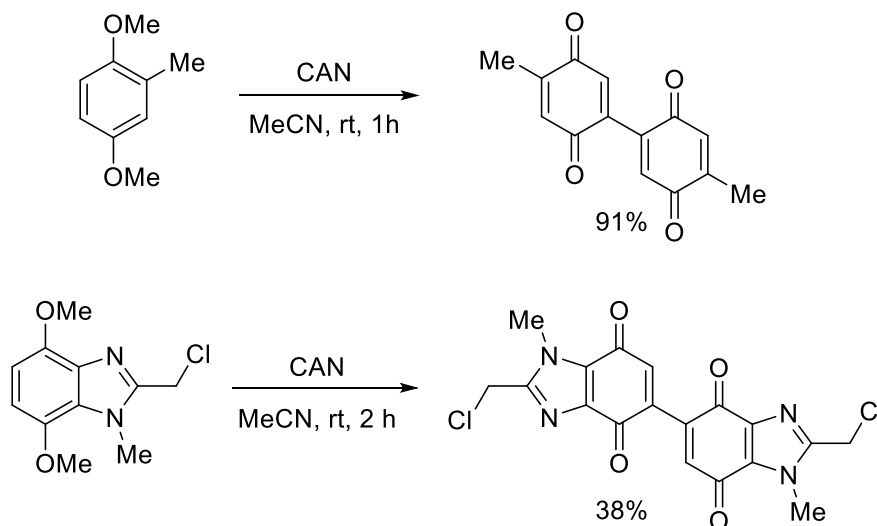
Scheme 3.8. Dimeric *p*-quinone formation as a result of CAN oxidation.[50, 64]

Despite the low atom economy of the hypervalent iodine reagent (PIFA), it offers milder reaction conditions to metal oxidants as it works effectively when immobilized on polymer

supports and uses water as the solvent.[63] PIFA also avoids the formation of dimeric *p*-quinone products.[63] *N*-bromosuccinimide (NBS) with sulfuric acid offers a tunable protocol that can form *p*-quinone products with or without bromination.[62] The acid sensitive substituted aziridine moiety of dimethoxybenzimidazole was well tolerated when NBS and a catalytic amount of sulfuric acid were used to deliver the *N*-[(1-tritylaziridin-2*S*-yl)methyl]benzimidazolequinone in 56% yield (Scheme 3.9).[49]
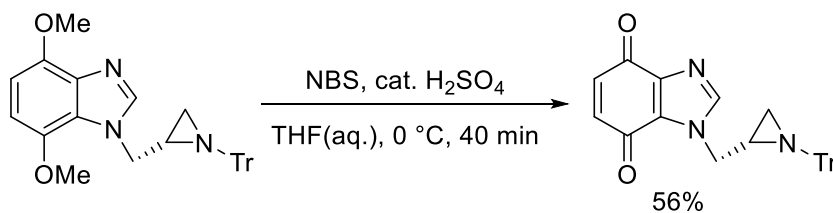
Scheme 3.9. Mild oxidative demethylation conditions using NBS and H_2SO_4.[49]

Both Castagnoli and Rapoport constructed detailed studies to understand the mechanism of oxidative demethylation for their respective oxidants of CAN and argentic oxide.[56, 59] The oxidation process can either involve cleavage of the alkyl-oxygen bond (blue) or the aryl-oxygen bond (red) of the methyl ether. Cleavage via the red bond will result in a loss of methanol and will involve the introduction of an external source of oxygen to form the *p*-quinone. Castagnoli reacted 1,4-dimethoxy-2,3,5,6-tetramethylbenzene with CAN and labeled water in dry acetonitrile to ascertain the mechanism of oxidation (Scheme 3.10). The doubly labeled duroquinone was obtained providing evidence to support aryl bond cleavage, with water providing the external source of oxygen. Rapoport used argentic oxide and $H_2^{18}O$-labeled 85% phosphoric acid to oxidize 2,3-dimethyl-1,4-dimethoxynaphthalene to give the doubly labeled 2,3-dimethyl-l,4-naphthoquinone which again, supported a mechanism of aryl-oxygen bond cleavage.[56]
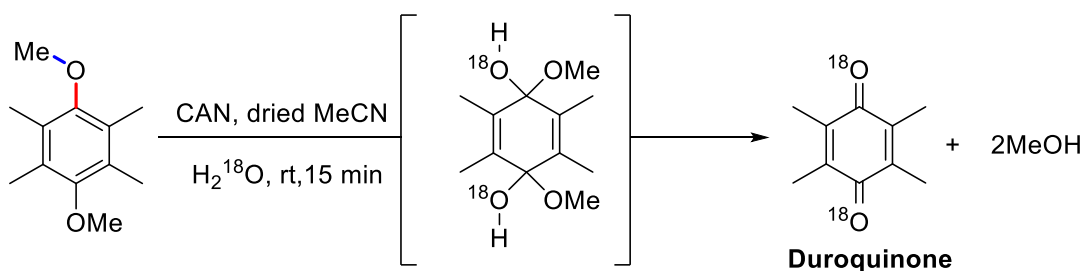
Scheme 3.10. Castagnoli isotopic labeling study of 1,4-dimethoxy-2,3,5,6-tetramethylbenzene with $H_2^{18}O$.[59]

Another route to *p*-quinones involves pre-prepared fused aromatics that undergo a sequence of nitration, reduction and finally an oxidation with the long-lived free radical of potassium nitrosodisulfonate (Fremy's salt) (Scheme 3.11). The disadvantage of this process is the multiple steps required and group tolerance issues as harsh conditions are used. This methodology has been commonly employed in the synthesis route for aziridine substituted benzimidazolequinones.[26, 47, 65-67] Normally direct access to *p*-quinones isn't feasible from a benzene substrate, hence the sequence of nitration, reduction and oxidation. Nonetheless, Takehira and co-workers showed that H_2O_2 in formic acid was capable of oxidizing highly activated methoxy substituted benzenes to *p*-quinones.[68]
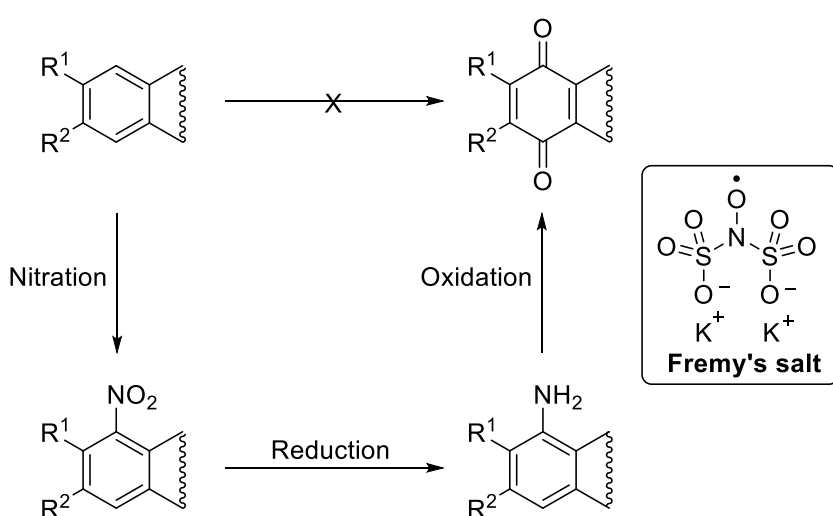
Scheme 3.11. Nitration, reduction, oxidation sequence to access *p*-quinones.

The use of aqua regia (HNO_3/HCl (1:3)) which generates Cl_2 in situ among other NOx substances[69] is reported to perform oxidative demethylation and dichlorination of various substituted 4,7-dimethoxybenzimidazoles to give 5,6-dichlorobenzimidazolequinones in moderate yields (Scheme 3.12).[20, 51] A two-step process is used involving demethylation with HBr followed by HBr/NaBrO_3 oxidation to access the analogous 5,6-dibromobenzimidazolequinone in moderate yield (Scheme 3.12).[51] Molecular bromine effected the oxidative demethylation and dibromination of 4,7-dimethoxy-1-methylbenzimidazole in methanol at room temperature for 1 h with no reported yield (Scheme 3.12).[23]
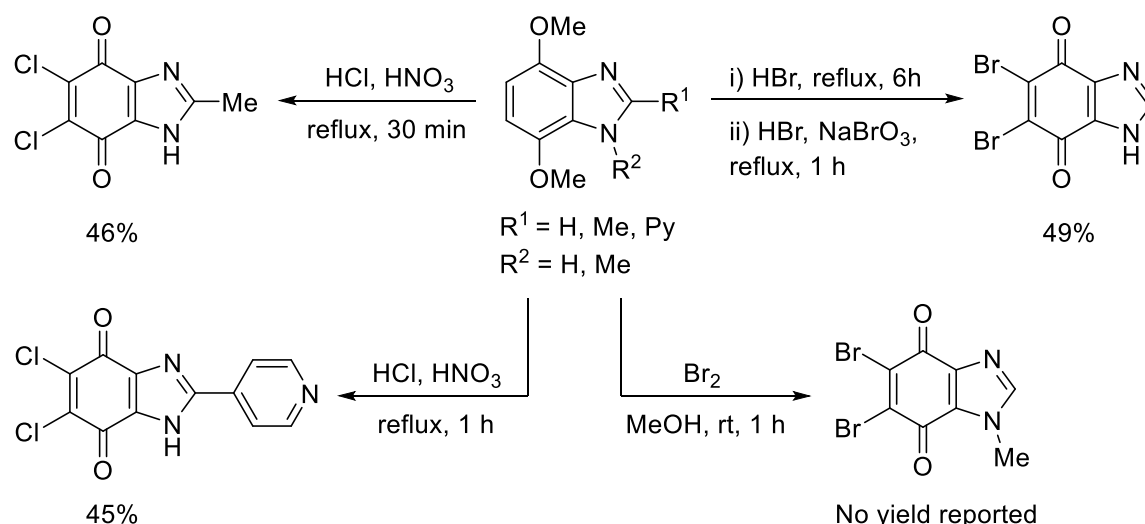
Scheme 3.12. Halogenation and oxidative demethylation of 4,7-dimethoxybenzimidazoles with various halide sources.[20, 23, 51]

Trichloroisocyanuric acid (TCCA) was added to 5,8-dimethoxyisoquinoline in conc. HCl and stirred for 3 h at room temperature to generate 6,7-dichloroisoquinolinedione without a reported yield (Scheme 3.13). [60] However, TCCA is thermally unstable and ultimately the synthesis of TCCA requires the use of molecular chlorine either directly or indirectly.[70] An alternative one-step approach to halogenated *p*-quinones could employ easy to handle H_2O_2/HX, which would have advantages of high atom economy[71] and low cost.
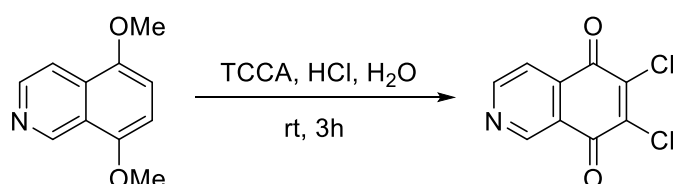
Scheme 3.13. TCCA in HCl enables halogenation and oxidative demethylation of 5,8-dimethoxyisoquinoline.[60]

3.2. Aims and Objectives

- Utilize H_2O_2/HX to carry out a 4-electron oxidative cyclization and regioselective halogenation on a series of ring-expanded and ring-contracted substituted anilines.
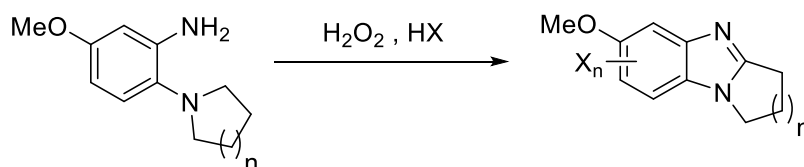
Scheme 3.14. Expected preparation of regioselectively halogenated ring-fused benzimidazoles using H_2O_2/HX.

- Avoid traditional multi-step routes to halogenated benzimidazolequinones, by providing a direct one-pot route which combines 4-electron oxidative cyclization, aromatic halogenation, and 2-electron oxidative demethylation of 3,6-dimethoxy-2-(cycloamino)anilines mediated by H_2O_2/HX.

- Provide a tunable protocol by adjusting the molar ratio of H_2O_2 to HX, thus allowing dihalogenated ring-fused dimethoxybenzimidazoles to be obtained when a higher molar ratio of H_2O_2 is used.
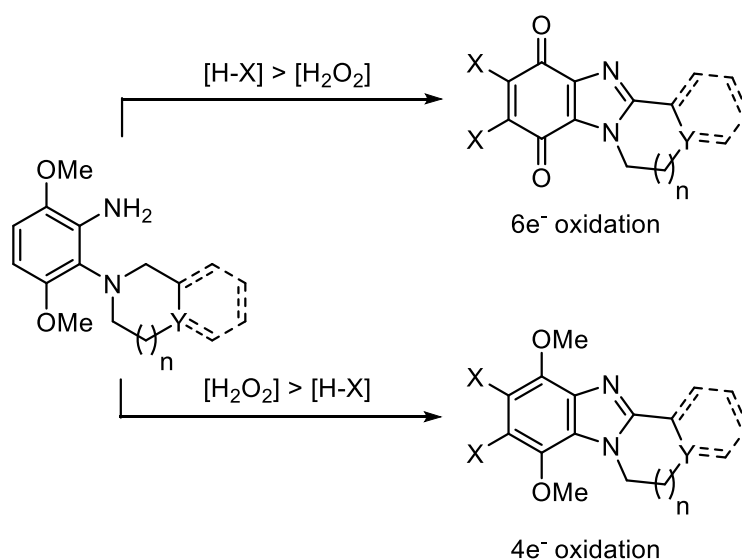
Scheme 3.15. Possible implementation of a tunable protocol to access 4-electron and 6-electron oxidation products with H_2O_2/HX.

- To determine if elemental halogens (X_2) participate in the oxidative transformations of 3,6-dimethoxy-2-(cycloamino)anilines.

- Nitrate the commercially available 2-fluoro-1,4-dimethoxybenzene in nitric acid to give 2-fluoro-1,4-dimethoxy-3-nitrobenzene as a synthetic intermediate.
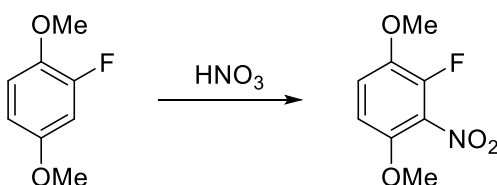
Scheme 3.16. Proposed preparation of 2-fluoro-1,4-dimethoxy-3-nitrobenzene.

3.3. Results and Discussion

3.3.1. One-pot synthesis of selectively dihalogenated ring-fused benzimidazoles

The preparation of *o*-cyclic tertiary amine substituted anilines as substrates for H_2O_2/HX mediated oxidative cyclization and halogenation involves a two-step synthesis. Commercially available 1-chloro-4-methoxy-2-nitrobenzene undergoes nucleophilic aromatic substitution (S_NAr) with an excess of pyrrolidine and azepane secondary amines at 80 °C in DMF for 3 days (Scheme 3.17). The S_NAr involving the eight-membered secondary amine of azocane was performed in ethanol at reflux for 4 days with 1-chloro-4-methoxy-2-nitrobenzene as previously reported by Fahey.[65] The resultant *o*-cyclic tertiary amine substituted nitrobenzenes then undergo reduction in the presence of iron with aqueous ammonium chloride in ethanol at reflux to give the corresponding anilines **1a**, **1c** and **1d** in a two-step yield of 38-70% (Scheme 3.17).[72]
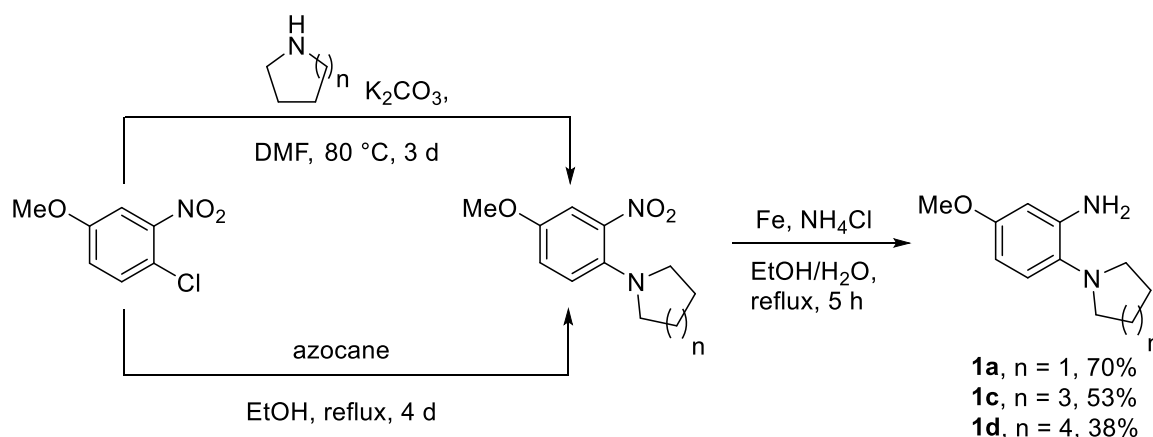
Scheme 3.17. S_NAr and reduction to prepare o-cyclic tertiary amine substituted anilines.

A series of ring-expanded and ring-contracted [1,2-*a*]benzimidazoles were prepared alongside pyrido[1,2-*a*]benzimidazoles to determine if the alicyclic ring-size affected the performance of the H_2O_2/HX system (Scheme 3.18). Selectively dichlorinated five to eight-membered ring-fused [1,2-*a*]benzimidazoles **2-4** were isolated in 78-93% yield after reaction times of 20 minutes using H_2O_2 (10 equiv.) with an excess of HCl (12 equiv.). The brominations were found to be significantly slower than the analogous chlorinations, and double the number of equivalents of H_2O_2/HBr were required to obtain the desired ring-fused [1,2-*a*]benzimidazoles (Scheme 3.18).
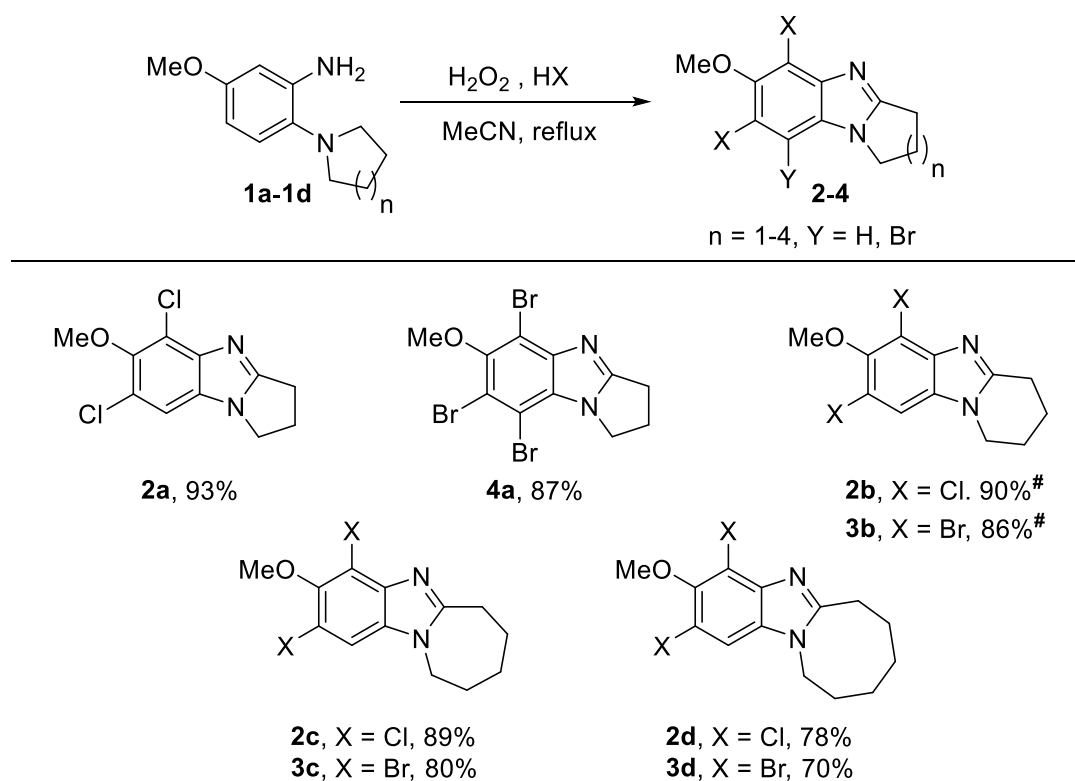
Conditions: For the synthesis of dichlorides **2a-2d**: **1a-1d** (1.0 mmol), H_2O_2 (10 mmol), HCl (12 mmol), MeCN (10 mL), 20 min. For the synthesis of the bromides **3b-3d**, **4a**: **1a-1d** (1.0 mmol), H_2O_2 (20 mmol), HBr (24 mmol), MeCN (10 mL), 4 d for (**3c** & **3d**) and 5 d for (**3b** & **4a**).

Scheme 3.18. Synthesis of five to eight-membered ring-fused benzimidazoles.

Voudrais and co-workers carried out kinetic studies on the electrophilic aromatic halogenation of *p*-xylene using a series of halogenating agents with a pH range of 2.5-7.5 (Scheme 3.19).[42] The rate of halogenation was in the following order: HOCl ≪HOBr < Br_2 < Cl_2 ≈ Cl_2O < BrCl. More importantly, Br_2 was shown to react 230 times slower than Cl_2 (Scheme 3.19) which is in line with our observation of slower bromination (Scheme 3.18).
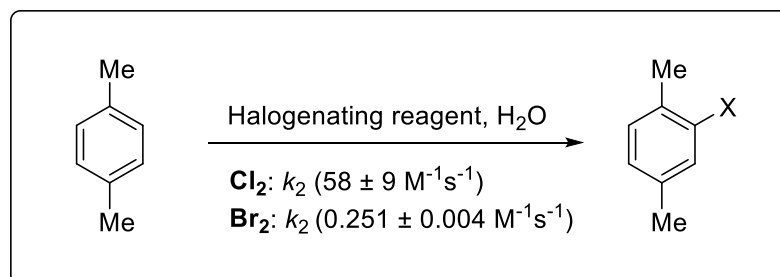
Scheme 3.19. The Cl_2 and Br_2 second order rates for the halogenation of *p*-xylene.[42]

In general, brominating agents have been reported as more reactive towards electrophilic aromatic substitution (EAS) than their chlorinating analogues in water due to their greater polarizability and lower bond energies.[73-75] However, steric factors might be contributing to a slower rate of EAS for the brominations in our work.[74]
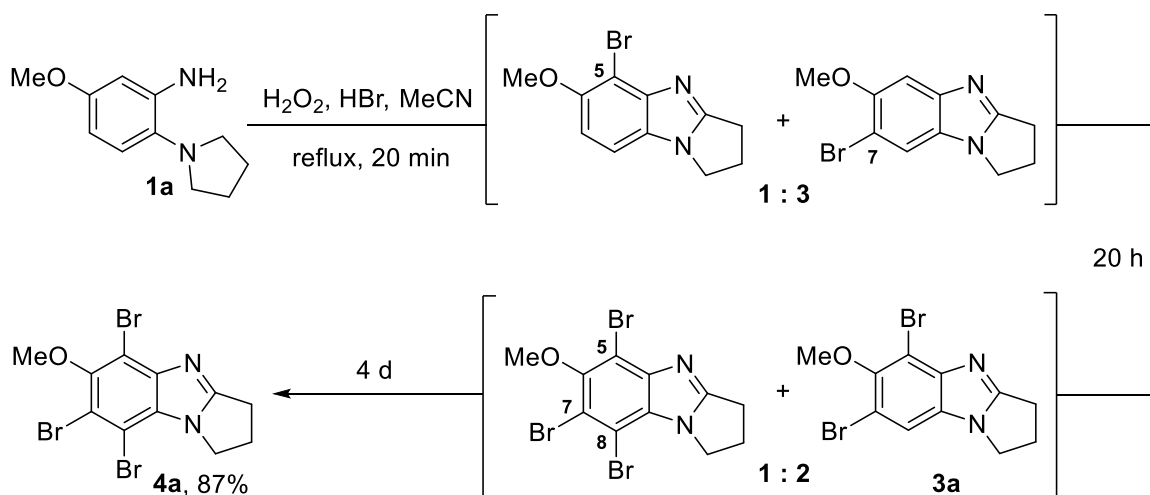
Scheme 3.20. The oxidative cyclization and bromination of **1a** with H_2O_2/HBr, monitored by ^{1}H NMR.

Despite the slower reaction rate with H_2O_2/HBr, regioselective dibrominated pyrido-, azepino- and azocino ring-fused [1,2-*a*]benzimidazoles **3b-3d** & **4a** were isolated in high yields of 70-86%. The progress of **1a** reacting with H_2O_2/HBr was monitored using ^{1}H NMR and after 20 minutes a mixture of monobromides; 5- and 7-bromobenzimidazoles was observed in an approximate 1:3 ratio (Scheme 3.20). The preferential site of mono-bromination is clearly directed towards the 7-position, *para* to the 4-*N* of the imidazole. After 20 hours a mixture of di- and tribromides **3a** and **4a** remained in an approximate 2:1 ratio (Scheme 3.20). Due to a mixture of brominated products, it was not possible to cleanly isolate 5,7-dibromopyrrolo[1,2-*a*]benzimidazole **3a** and therefore the reaction was allowed to proceed to the tribromide **4a** in an excellent yield of 87% (Scheme 3.20).

3.3.2. One-pot synthesis of dihalogenated ring-fused benzimidazolequinones

Access to both halogenated ring-fused benzimidazoles and benzimidazolequinones begins with the dinitration of the commercially available 1,4-dimethoxybenzene in concentrated nitric acid that leads to a mix of isomeric 1,4-dimethoxydinitrobenzenes in a ratio of 5.7 to 1.[76] The major *o*-nitrated isomer 1,4-dimethoxy-2,3-dinitrobenzene was isolated using column chromatography in a yield of 70% (Scheme 3.21).
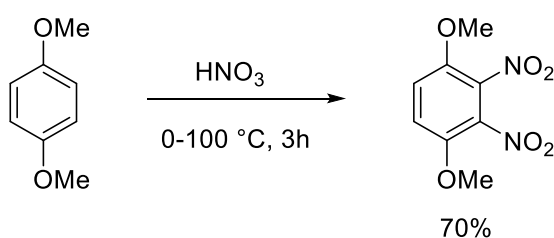
Scheme 3.21. Preparation of 1,4-dimethoxy-2,3-dinitrobenzene.[76]

The novel morpholino and tetrahydroisoquinolino (THIQ) substituted 3,6-dimethoxynitrobenzenes were prepared by nucleophilic aromatic substitution (SNAr) with 1,4-dimethoxy-2,3-dinitrobenzene in the dipolar aprotic solvent of acetonitrile with a base of potassium carbonate for 3 days at reflux (Scheme 3.22). The morpholino analogue was isolated in a poor yield of 39%, presumably attributed to the inductive effect of the electronegative oxygen atom of the [1,4]oxazino heterocycle. The THIQ analogue was isolated in a good yield of 67% , considering that Nguyen and co-workers observed that redox condensation of nitrobenzenes with THIQ can occur under specific conditions to form cyclized products.[77] The morpholino substituted 3,6-dimethoxynitrobenzene was reduced using iron powder with aqueous ammonium chloride in EtOH to give **5c** in an overall two-step yield of 32% (Scheme 3.22).[72] In an analogous manner, the synthesis of 3,6-dimethoxy-2-(cycloamino)anilines **5a**, **5b**, **5d** and **5e**[53] were previously prepared and are detailed in (Chapter 2, Scheme 2.4). The THIQ substituted 3,6-dimethoxynitrobenzene was more effectively reduced with H$_2$ gas under palladium catalysis in EtOAc/MeOH at atmospheric pressure when compared to the iron methodology. The THIQ aniline **5f** was isolated in a two-step yield of 52% (Scheme 3.22).
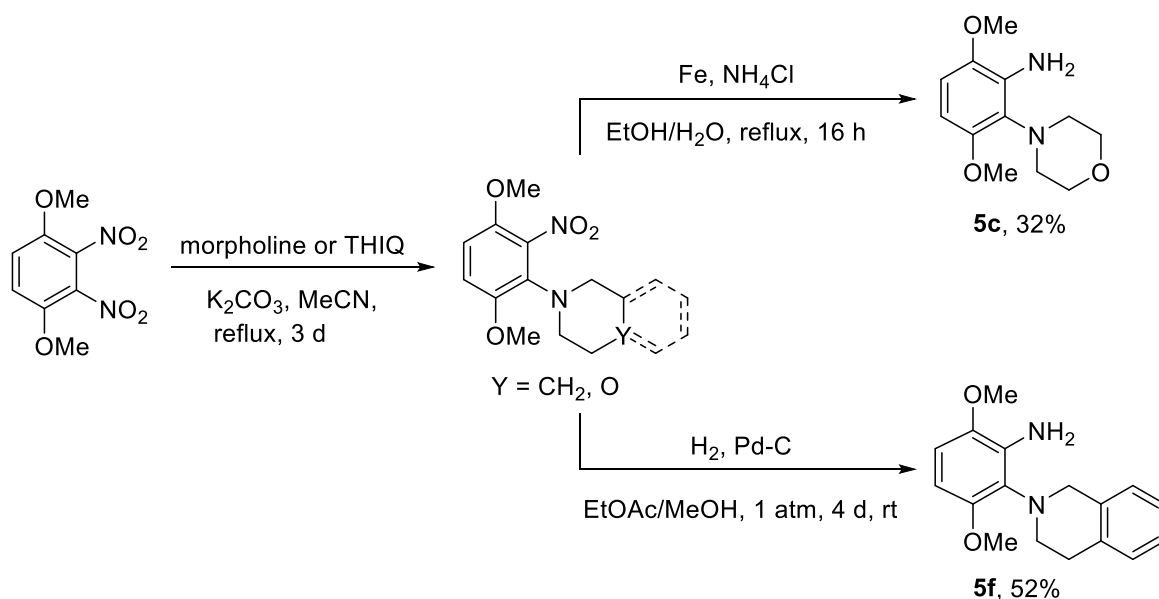
Scheme 3.22. S_NAr and reduction to prepare 3,6-dimethoxy-2-(cycloamino)anilines **5c** and **5f**.

3,6-Dimethoxy-2-(cycloamino)anilines **5a-5e** were treated with higher amounts of H_2O_2 (10 equiv.) relative to HX (5 equiv.) to favour the formation of hypohalous acids (HOX) (Scheme 3.2). The resultant reaction gave novel ring-fused dimethoxy substituted benzimidazoles via a 4-electron oxidative cyclization and dihalogenation in mostly high yields and without the need for chromatography (Scheme 3.23). 2-(Pyrrolidin-1-yl)aniline **5a** and 2-(piperidin-1-yl)aniline **5b** were found to be consumed within 20 min in MeCN under reflux to give dichlorinated and dibrominated pyrrolo[1,2-*a*]benzimidazoles (**6a**, **7a**) and pyrido[1,2-*a*]benzimidazoles (**6b**, **7b**) respectively in yields of 80-92% (Scheme 3.23). For cyclizations of morpholine **5c**, azepane **5d** and azocane **5e** using H_2O_2/HCl, some oxidation to the benzimidazolequinone was detected at reflux. [1,4]Oxazino[4,3-*a*]benzimidazole **6c**, azepino[1,2-*a*]benzimidazole **6d**, and azocino[1,2-*a*]benzimidazole **6e** were selectively formed in good to high yields (67-95%) by lowering the reaction temperature (from reflux to 40 °C or rt) and increasing the reaction time (from 20 min to 2-24 h). Benzimidazolequinone formation was not detected in the HBr-mediated cyclizations of **5c**, **5d** and **5e** at reflux, with **7c** obtained in 89% yield, while a 6 h reaction time afforded complete dibromination to give **7d** and **7e** in excellent yield (92 & 95%, respectively) (Scheme 3.23). X-ray crystal structures for the eight-membered dichlorinated and dibrominated adducts **7e** and **7e** were obtained due to similarities of chemical shifts in respective NMR spectra.
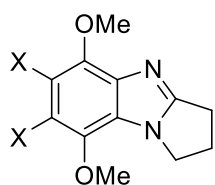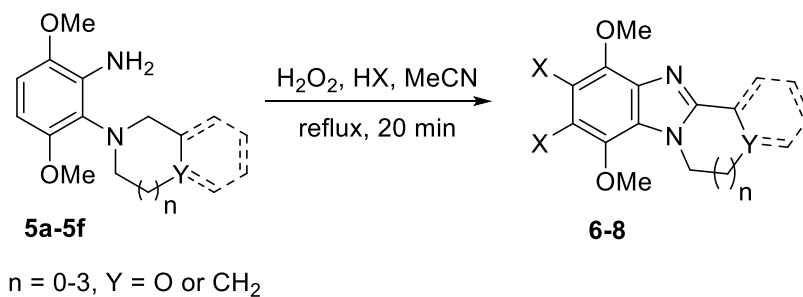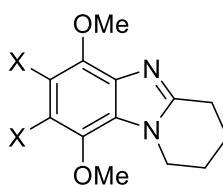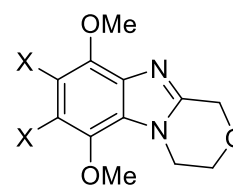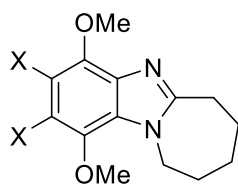
Scheme 3.23. Synthesis of dihalogenated benzimidazoles using H_2O_2/HX.
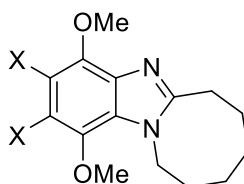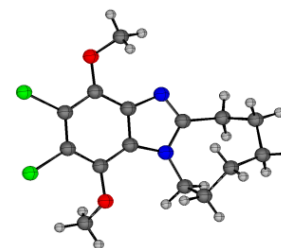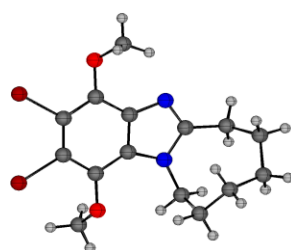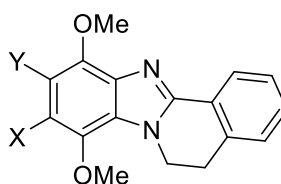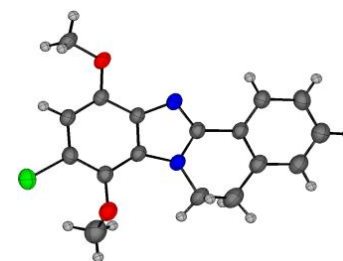
Conditions: **5a**-**5f** (1.0 mmol), H_2O_2 (10 mmol), HX (5 mmol), MeCN (10 mL). [a]2 h, 40 °C. [b]24 h, rt. [c]5 h, 40 °C. [d]6 h. [e]MeCN (15 mL), 24 h, rt. [f]MeCN (15 mL). [g]MeCN (15 mL), 4.5 h, rt. X-ray crystal structures showing one of the two molecules in the asymmetric unit cell for **6e** and **7e** with thermal ellipsoids set at 40% probability, and for **8f** thermal ellipsoids set at 40%. probability.

The utility of the H$_2$O$_2$/HX-mediated system was investigated using the more challenging 2-(3,4-dihydroisoquinolin-2(1H)-yl)-3,6-dimethoxyaniline (THIQ substrate) **5f** with potential for halogenation on the additional aromatic ring (Scheme 3.23). Upon treatment of **5f** in a more dilute solution of MeCN (0.07 M) with H$_2$O$_2$ (10 equiv.) and HBr (5 equiv.) at reflux for 20 min, oxidative cyclization was observed at the benzylic position to afford **7f** in 73% yield.
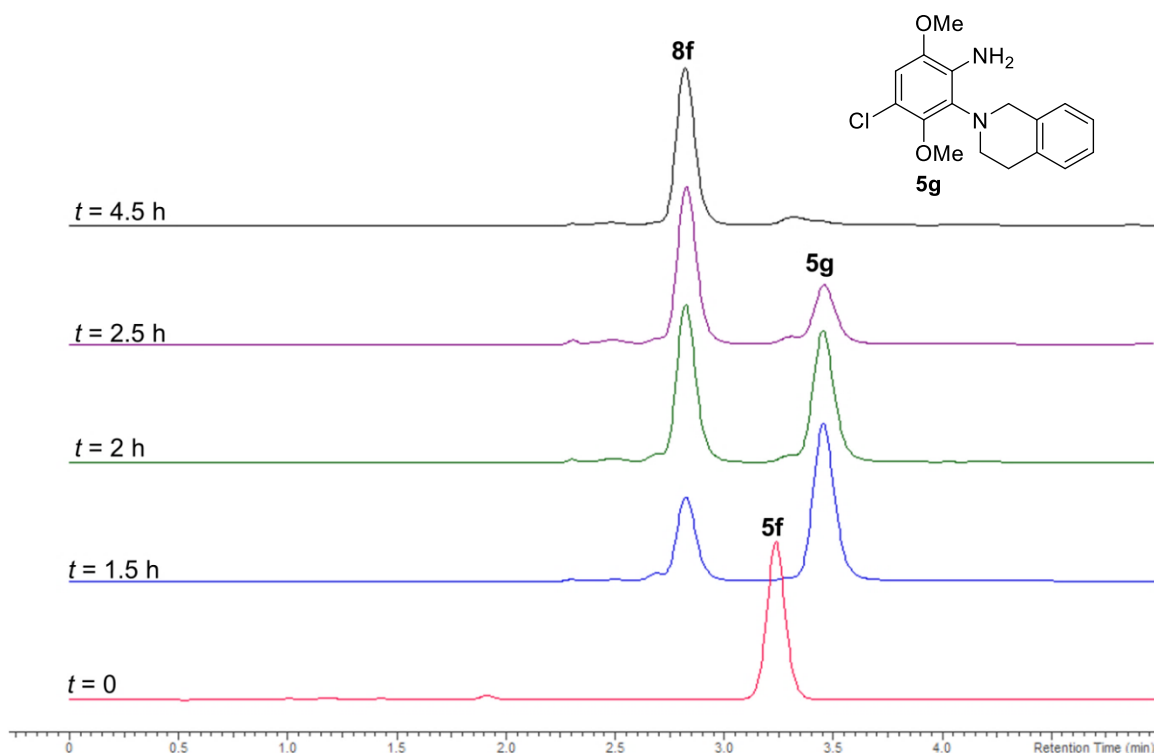
Figure 3.5. HPLC chromatograms as a function of time (t) for the reaction of 2-(3,4-dihydroisoquinolin-2(1H)-yl)-3,6-dimethoxyaniline **5f** with H$_2$O$_2$ (10 mmol) and HCl (5 mmol) in MeCN (15 mL) at rt. ESI HRMS (Figure 3.6) was used to detect 4-chloro-2-(3,4-dihydroisoquinolin-2(1H)-yl)-3,6-dimethoxyaniline **5g**.

The H$_2$O$_2$/HCl system could be tuned to deliver mono- or dichlorinated ring-fused [1,2-*a*]benzimidazoles. At room temperature and a 4.5 h reaction time, only monochlorination was observed, affording **8f** in 60% yield, while a 24 h reaction time afforded the dichlorinated product **6f** in 51% yield. The site of monochlorination was at the 9-position of **8f** and was confirmed by X-ray crystallography (Scheme 3.23). The room temperature reaction allowed reaction profiling by HPLC (Figure 3.5) with mass spectrometry detection of chlorinated aniline intermediate **5g** (Figure 3.6), suggested that chlorination of **5f** occurs prior to oxidative cyclization. This observation may explain the regioselectivity, as the NH$_2$ group of the *o*-cyclic amine substituted aniline directs *para* towards EAS.
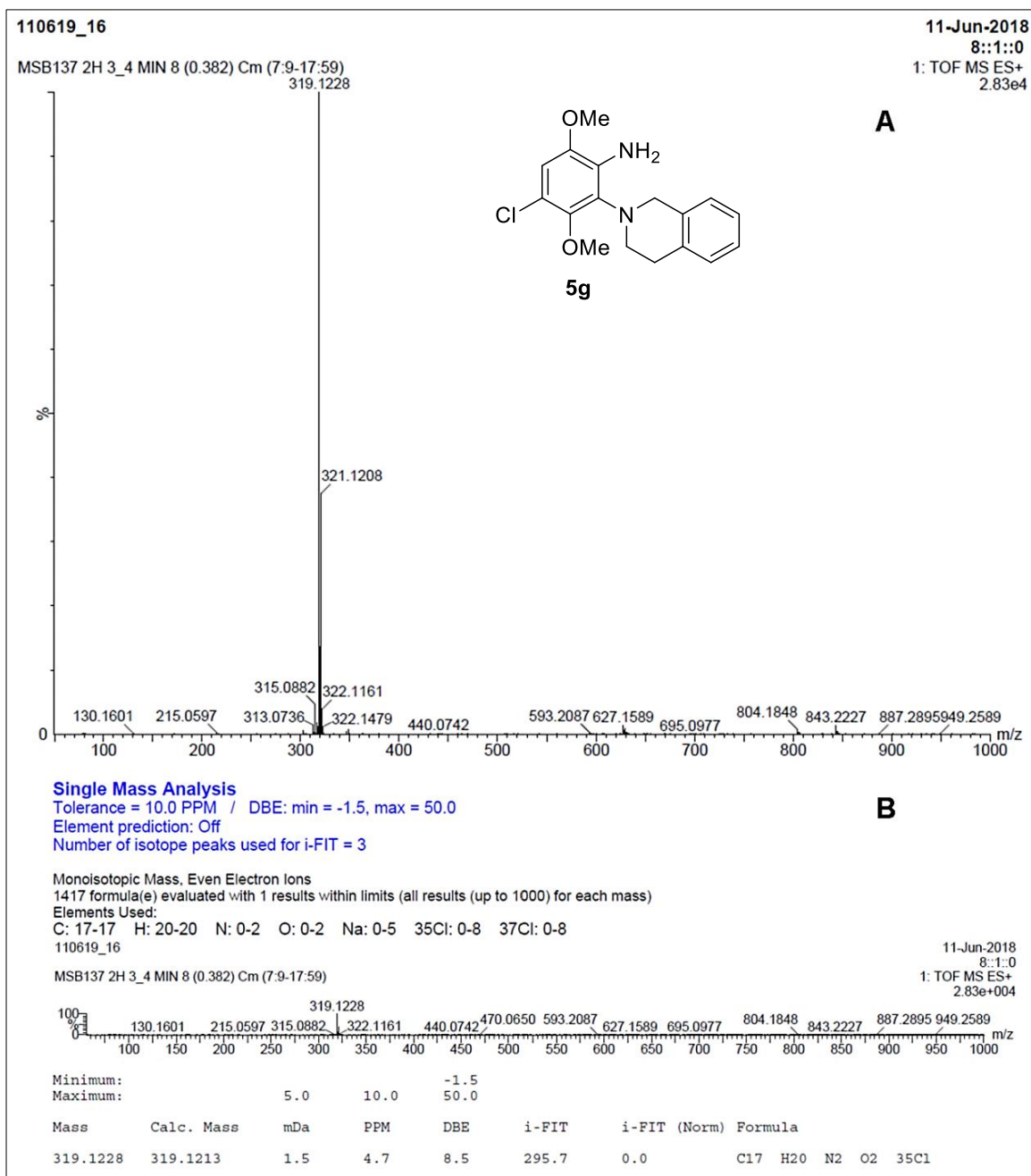
Figure 3.6. ESI HRMS of 4-chloro-2-(3,4-dihydroisoquinolin-2-(1*H*)-yl)-3,6-dimethoxyaniline **5g**: (**A**) The high resolution mass spectrum. (**B**) The single mass analysis indicates the molecular formula of the proposed structure **5g** to be within 5 ppm.

This insight can be retrospectively applied to explain the regioselectivity for the one-pot oxidative cyclizations and halogenation to form ring-fused [1,2-a]benzimidazoles (Scheme 3.6).[46] In the case of H_2O_2/HCl system, selectivity occurred in the majority of cases independently of EWGs or EDGs located at the R-position. The H_2O_2/HBr system even brominated selectively in the absence of EDGs or EWGs where it can be assumed that the NH_2 of o-cyclic amine substituted aniline is strongly o,p-directing the electrophilic substitution (Scheme 3.24).
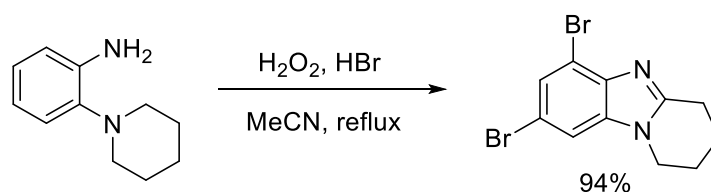
Scheme 3.24. Regioselective bromination possibly due to occurrence of halogenation before oxidative cyclization.[46]

Conboy and Aldabbagh observed the formation of phenazine derivatives when 3,6-dimethoxy o-morpholino substituted aniline **1c** was reacted with a H_2O_2/HI system.[78] The phenazine formation wasn't observed with the H_2O_2/HCl system, instead regioselective chlorination occurred para to the NH_2 directing group of the 3,6-dimethoxy o-morpholino substituted aniline (Scheme 3.25). The chlorination occurred before oxidative cyclization and the regioselectivity was confirmed by X-ray crystallography, with 4-chloro-3,6-dimethoxy-2-(morpholin-4-yl)aniline **5h** isolated in a good yield of 76%.[78] The experimental evidence presented by Conboy and Aldabbagh supports the formation of our HRMS detected intermediate **5g** that forms the mono-chlorinated dimethoxybenzimidazole **8f**, with chlorination occurring before cyclization.
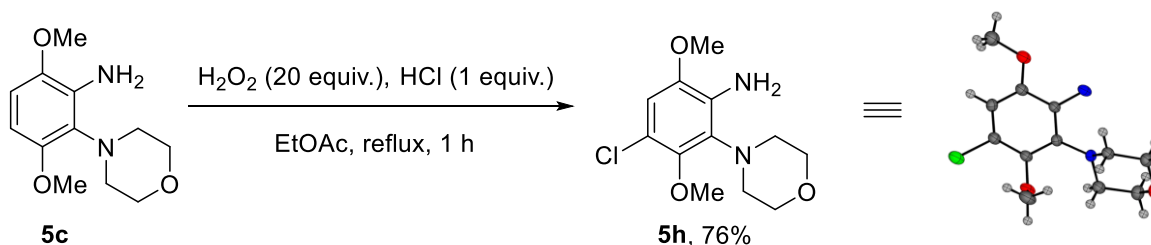
Scheme 3.25. Regioselectively chlorinated 3,6-dimethoxy o-morpholino substituted aniline using H_2O_2/HX.[78]

The molar ratio of HCl was increased relative to that of H_2O_2 to produce conditions which favoured X_2 formation. These conditions facilitated the novel one-pot overall 6-electron oxidation, affording dihalogenated benzimidazolequinones (Scheme 3.2, Scheme 3.26). H_2O_2 (50 equiv.) and HCl (180 equiv.) converted anilines **5a-5d** into dichlorinated ring-fused benzimidazolequinones **9a-9d** in moderate to high yields (62-80%) after 4 h in MeCN at 80 °C, while **9e** was isolated in 54% yield (Scheme 3.26). Due to the greater reactivity of Cl_2 relative to Br_2 towards electrophilic halogenation reactions,[42, 43] the 6-electron oxidation was not performed neat in HCl and instead the reaction was diluted with MeCN to minimize the risk of over-chlorination.

For the H_2O_2/HBr mediated transformations, the high concentrations of HBr required for quinone formation and the less reactive nature of Br_2, made it desirable to perform the brominations neat (Scheme 3.26). However, the 9,10-dibromo-5,6-dihydrobenzimidazo[2,1-*a*]isoquinoline-8,11-dione **10f** was furnished in higher yield by employing an equivolume mixture of MeCN and HBr (Scheme 3.26). Generally, dibrominated analogues **10a-10e** were obtained in high yield (67-92%) using H_2O_2 (60 equiv.) in neat HBr (30 mL) under reflux for 12 h (Scheme 3.26). Ring-fused dihalogenated benzimidazolequinones (Scheme 3.26) were purified by flash column chromatography with the exception of dibrominated pyrrolo[1,2-*a*]benzimidazolequinone **10a**, which was isolated cleanly without purification. X-ray crystal structures of 7,8-dichloro-3,4-dihydro-1*H*-[1,4]oxazino[4,3-*a*]benzimidazole-6,9-dione **9c**, dichlorinated and dibrominated pyrrolo[1,2-*a*]benzimidazolequinones **9a** and **10a**, and azepino[1,2-*a*]benzimidazolequinones **9d** and **10d** were obtained to demonstrate the ease at which these series of quinones can be recrystallized to produce X-ray quality crystals.
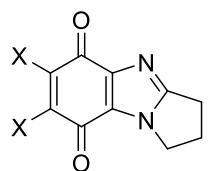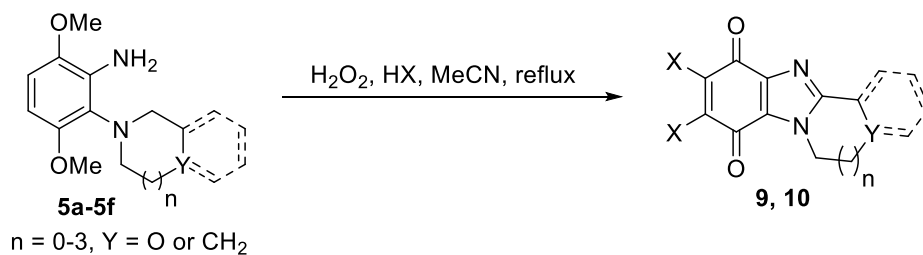
9a, X = Cl, 73%
10a, X = Br, 81%

9a
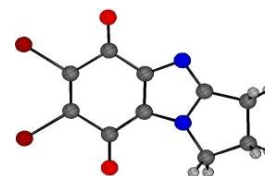
10a
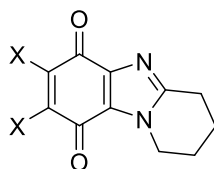
9b, X = Cl, 76%
10b, X = Br, 74%
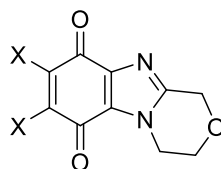
9c, X = Cl, 62%
10c, X = Br, 67%

9c
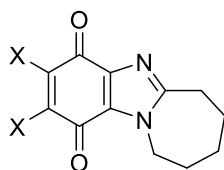
9d, X = Cl, 80%
10d, X = Br, 86%
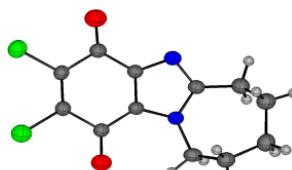
9d
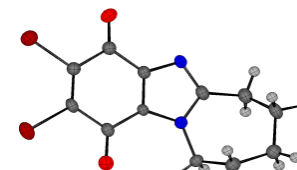
10d
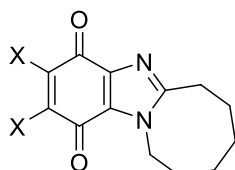
9e, X = Cl, 45%[†]
10e, X = Br, 92%[†]
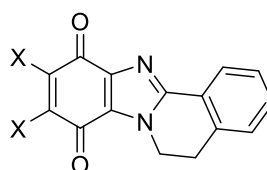
9f, X = Cl, 56%[a]
10f, X = Br, 68%[b]
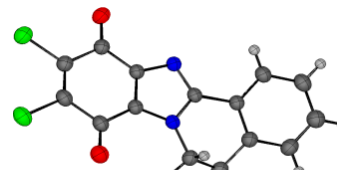
9f

Conditions: For the synthesis of dichlorides **9a**-**9e**: **5a**-**5e** (1.0 mmol), H_2O_2 (50 mmol), HCl (180 mmol), MeCN (10 mL), 4 h, 80 °C. For the synthesis of dibromides **10a**-**10f**: **5a**-**5f** (1.0 mmol), H_2O_2 (60 mmol), HBr (30 mL), 12 h, reflux. [a]H_2O_2 (10 mmol), HCl (5 mmol), MeCN (15 mL), 72 h, rt. [b]HBr (135 mmol), MeCN (15 mL), 7h. X-ray crystal structures shown of **9a**, **9c**, **9d**, **9f**, **10a**, and **10d** have thermal ellipsoids set at 40% probability.

Scheme 3.26. Synthesis of dihalogenated benzimidazolequinones using H_2O_2/HX.

Isolation of significant amounts of 9,10-dichloro-5,6-dihydrobenzimidazo[2,1-*a*]isoquinoline-8,11-dione **9f** was however not possible by treatment of THIQ **5f** with a high molar ratio of HCl relative to H_2O_2 at reflux. Even with reduced equivalents and an equimolar ratio of HCl relative to H_2O_2, THIQ **5f** at room temperature still gave mainly inseparable products with ESI HRMS (m/z 388.9-392.9) indicative of tetrachlorination (Figure 3.7).
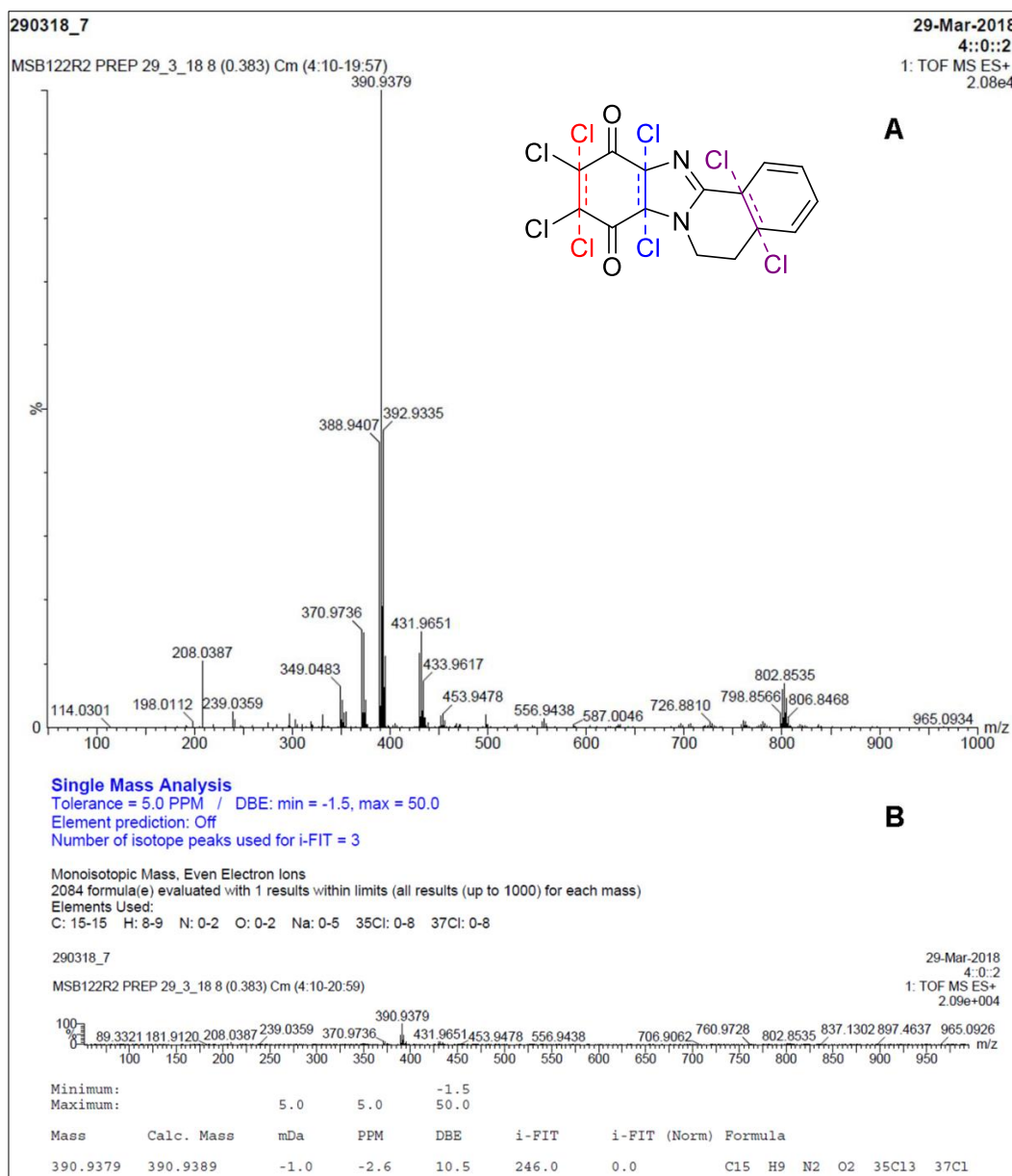
Figure 3.7. ESI HRMS of one HPLC fraction for the reaction of 2-(3,4-dihydroisoquinolin-2-(1*H*)-yl)-3,6-dimethoxyaniline **5f** (1.0 mmol) with H_2O_2 (35 mmol), HCl (35 mmol), MeCN (15 mL), rt, 21 h. (**A**) The high resolution mass spectrum of tetrachlorinated benzimidazolequinone product with three chlorination positions possible shown in red, blue and purple. (**B**) The single mass analysis indicates the molecular formula of the proposed structure to be within 5 ppm.

106

This led us to employ the relatively mild conditions of H_2O_2 (10 equiv.) and HCl (5 equiv.) at room temperature, that allowed aromatic monochloride and dichloride **8f** and **6f** to be isolated in good yields after 4.5 and 24 h respectively (Scheme 3.23, Figure 3.5). The extension of H_2O_2 (10 equiv.) and HCl (5 equiv.) conditions to 72 h gave benzimidazolequinone **9f** in an isolated yield of 56% (Scheme 3.26, Figure 3.8). The structure of **9f** was confirmed by X-ray crystallography (Scheme 3.26). In contrast, the dibrominated analogue **10f** was isolated in 68% yield from a 7 h reflux in the presence of a large excess of HBr with no over-bromination adducts detected.
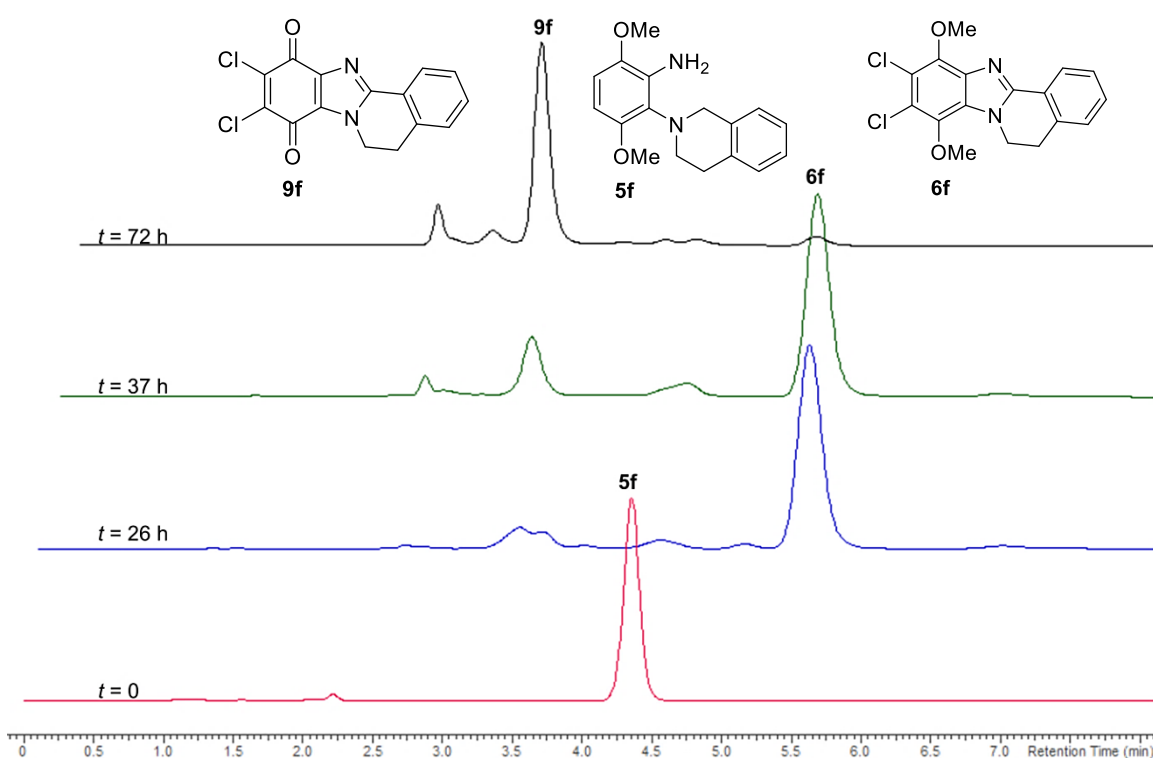
Figure 3.8. HPLC chromatograms as a function of time (*t*) for the reaction of 2-(3,4-dihydroisoquinolin-2-(1*H*)-yl)-3,6-dimethoxyaniline **5f** with H_2O_2 (10 equiv.) and HCl (5 equiv.) in MeCN (15 mL) at rt.

HBr is a well-known demethylating agent of aromatic ethers (Scheme 3.7).[54, 79] HCl to our knowledge is only applicable as a demethylating agent of aromatic ethers under very specific conditions of high temperature, pressure or in combination with other reagents. Weinberger and Day showed that 2-methyl dimethoxybenzimidazole was demethylated by using conc. HCl in a sealed pyrex tube with heating at 100 °C for 20 h (Scheme 3.27a).[54] 4-methoxyphenylbutyric acid was demethylated in 3 h when reacted neat with pyridinium chloride under nitrogen at 180 °C to produce the hydroxyl derivative in an excellent yield of 97% (Scheme 3.27b).[80]
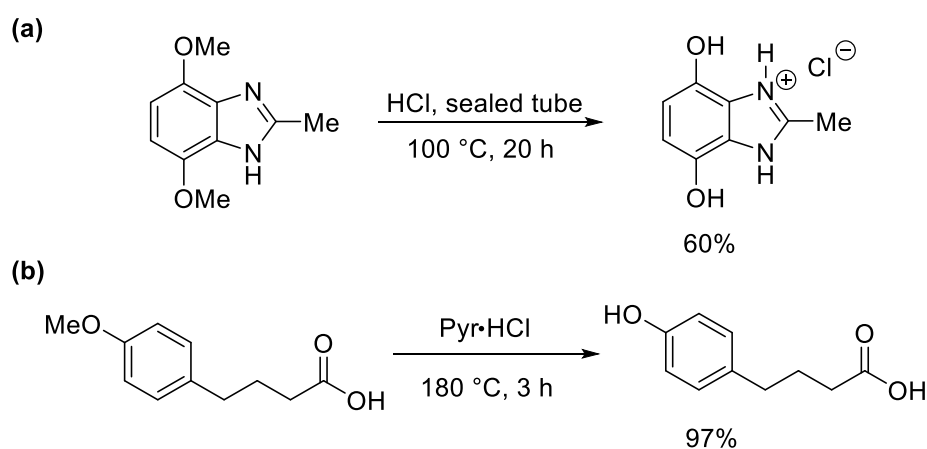
Scheme 3.27. Demethylation of phenyl methyl ethers with HCl reagents.[54, 80]

Following the conditions to form dichlorinated benzimidazolequinones (Scheme 3.26), dichlorinated morpholino[1,2-*a*]benzimidazole **6c** was treated with conc. HCl while stirring for 4 h at 80 °C to investigate if HCl could demethylate our series of aromatic ethers (Scheme 3.28). However, there was no observed reaction for **6c** (Scheme 3.28), presumably due to the milder reaction conditions used in comparison to that of Weinberger and Day.[54]
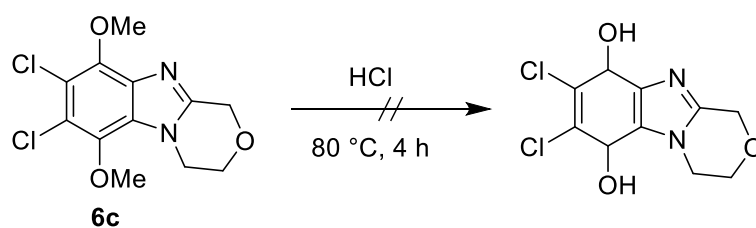
Scheme 3.28. Attempted demethylation of **6c** in concentrated HCl.

Due to the suspected high concentration of Cl_2 in the one-pot 6-electron oxidative cyclizations with dihalogenation, Cl_2 was investigated as the active reagent involved in the demethylation of the aromatic ethers. Commercially available 1,4-dimethoxybenzene was chosen as a test substrate to investigate the ability of Cl_2 gas to oxidize aromatic ethers and the reactions were monitored by GC-MS. The theoretical amount of Cl_2 gas generated from the combination of H_2O_2 and HCl was 50 equivalents relative to the starting aniline as shown in Scheme 3.26. Cl_2 (50 equiv.) was generated by the dropwise addition of concentrated HCl onto $KMnO_4$ as described by Leonard et al.,[81] but only a mix of polychlorinated 1,4-dimethoxybenzenes were formed. At 200 equiv. of Cl_2, a mixture of tetrachlorinated benzoquinone **11** and tetrachlorinated 1,4-dimethoxybenzene **12** was formed (Table 3.1). Despite further doubling the equivalents of chlorine gas (400 equiv.), full conversion to tetrachlorinated benzoquinone **11** was never achieved due to the deactivation of the aromatic ring by the addition of four electron-withdrawing chlorine groups (Table 3.1). This demonstrates the necessitation of an activated substrate such as benzimidazoles to achieve full quinone formation with chlorine gas.

Table 3.1. The chlorination and oxidation of 1,4-dimethoxybenzene with Cl_2.
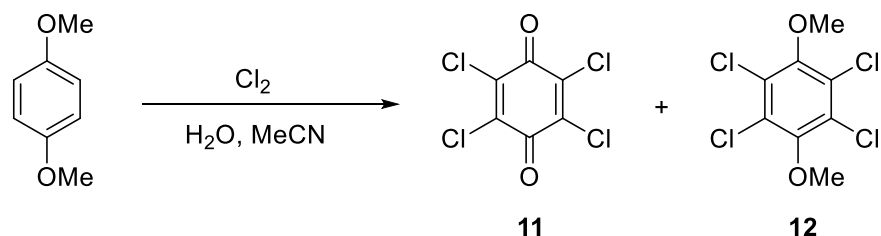
Entry	Cl_2 equiv.	GC-MS Yield (%)	
		11	**12**
1	200	53	47
2	400	64	36

The more activated substrate of dichlorinated [1,4]oxazino[4,3-*a*]benzimidazole **6c** was subjected to Cl_2 gas (50 equiv.) in acetonitrile with added water at 80 °C (Scheme 3.29). The aromatic ether of benzimidazole **6c** underwent a 2-electron oxidation using Cl_2 gas, fully converting **6c** to the desired dihalogenated benzimidazolequinone **9c** in a good yield of 73% (Scheme 3.29).
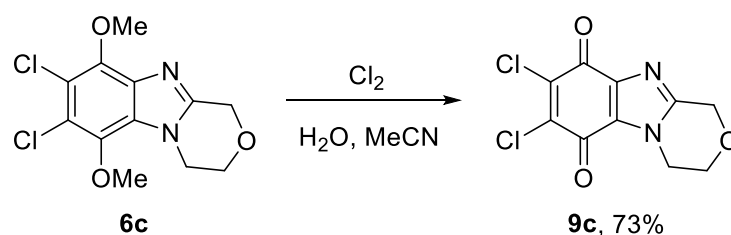
Scheme 3.29. Halogenated dimethoxybenzimidazole 2-electron oxidation produces benzimidazolequinone using Cl_2.

Next, it was decided to investigate if the formation of ring-fused dihalogenated benzimidazolequinones could be effected by elemental X_2, with or without water. Chlorine gas was bubbled into a solution of anilines **5b**-**5e** in MeCN containing added H_2O (Table 3.2).

Table 3.2. Synthesis of dihalogenated benzimidazolequinones using elemental chlorine and bromine.[a]
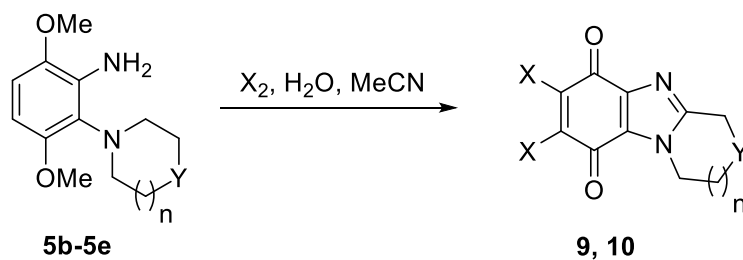
aniline	X	Y	n	yield (%)
5b	Cl	CH_2	1	**9b**, 41
5c	Cl	O	1	**9c**, 54
"	"	"	"	**9c**, 47[b]
5d	Cl	CH_2	2	**9d**, 71
5e	Cl	CH_2	3	**9e**, 58[†]
5b	Br	CH_2	1	**10b**, 71
5d	Br	CH_2	2	**10d**, 90
5e	Br	CH_2	3	**10e**, 90[†]

[a]Conditions: For synthesis of dichlorides: **5b**-**5e** (1.0 mmol), Cl_2 (50.0 mmol), H_2O (1.8 mL), MeCN (10 mL), reflux, 10 min. For synthesis of dibromides: **5b**, **5d**, **5e** (1.0 mmol), Br_2 (50 mmol), H_2O (1.8 mL), MeCN (10 mL), 40 °C, 4 h. [b]H_2O (10.75 mL).

Dichlorinated benzimidazolequinones **9b-9d** were isolated, but in lower yields in comparison to the H$_2$O$_2$/HCl method, although **9e** was given in a comparable yield of 58% in this 10 min reflux reaction (Table 3.2). A comparative study, using **5c** and Cl$_2$ was carried out in an equivalent amount of water (10.75 mL) to the H$_2$O$_2$/HCl protocol but the yield of **9c** was decreased further from 54% to 47% (Table 3.2). Thus, an excess of water is required but not to the extent of the H$_2$O$_2$/HCl method.

Moreover, yields deteriorated when the Cl$_2$ reaction was performed under anhydrous conditions with inseparable over-chlorinated products detected by NMR and mass spectrometry. Presumably, the absence of water leads to the predominant presence of Cl$_2$ (Scheme 3.2) which is a stronger oxidant than HOCl, resulting in a combination of chlorine electrophilic addition and substitution reactions (Figure 3.7) that give over-chlorination. Johnson et al. observed the formation of different isomers of pentachlorinated 1-methylnapthalene when excess Cl$_2$ gas was used under protic or aprotic conditions to chlorinate 1-methyl naphthalene (Scheme 3.30). [82] Johnson proposed that aprotic conditions might promote a radical mechanism. In our case, anhydrous conditions could promote a similar type of mechanism that results in chlorine electrophilic addition reactions.
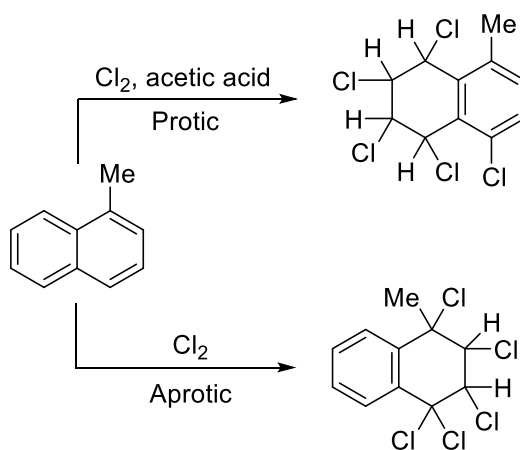
Scheme 3.30. Formation of different pentachlorinated isomers in protic or aprotic conditions with Cl$_2$ gas.[82]

In the optimization reactions for brominated quinone formation, the aniline **5b** was treated with varying equivalents of molecular bromine. The cyclized product **7b** was obtained in 90% yield using 10 equivalents of Br$_2$. The subsequent reactions followed with incremental increases in the amount of Br$_2$ (up to 40 equiv.) but still only produced **7b** with no detection

of the brominated quinone derivative **10b**. Finally, using 50 equivalents of Br₂ led to the desired dibrominated benzimidazolequinone **10b** in 71% yield (Table 3.2). Overall, higher yields (71-90%) were achieved for the one-pot transformation giving dibrominated benzimidazolequinones **10b**, **10d** and **10e** using Br₂ and H_2O at 40 °C for 4 h (Table 3.2), when compared to the analogous Cl_2 reactions. This is indicative of the greater control achieved with less reactive Br₂ that is not susceptible to over-bromination.
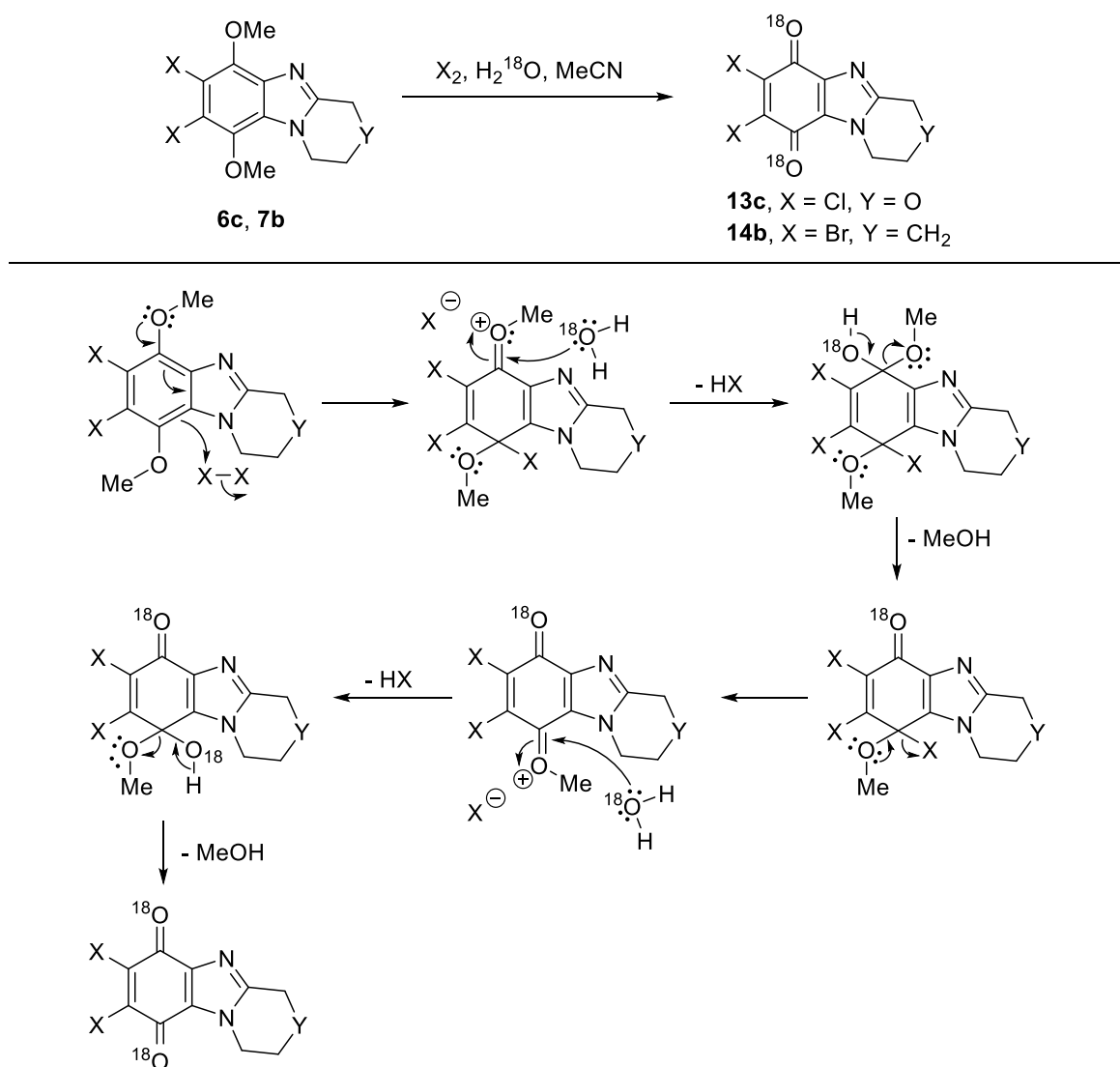
Reaction conditions: For dichloride **13c**: **6c** (0.07 mmol), Cl_2 (3.40 mmol), $H_2^{18}O$ (0.14 mL), dried MeCN (0.73 mL), reflux, 10 min. For dibromide **14b**: **7b** (0.04 mmol), Br₂ (2.05 mmol), $H_2^{18}O$ (0.08 mL), dried MeCN (1 mL), 40 °C, 4 h.

Scheme 3.31. Detecting the role of water in quinone formation with proposed mechanism.

Finally, we investigated whether the quinone formation went through a two-step oxidative demethylation or a direct one-step oxidation via hydroxylation intermediates. We had to determine if cleavage occurred at the alkyl- or aryl-oxygen bond of the methyl ether. The role of water in the quinone formation step is fundamental to understanding the mechanism of action so labeled $H_2^{18}O$ was employed. 7,8-Dihalo-6,9-dimethoxybenzimidazoles **6c** and **7b** were respectively treated with Cl_2 and Br_2 (both 50 equiv.), and $H_2^{18}O$ (100 equiv.) in dried MeCN under inert conditions (Scheme 3.31).

The formation of the doubly ^{18}O-labeled dihalogenated benzimidazolquinones **13c** and **14b** was confirmed by EI-MS (Appendix, Figure A.2.1 and A.2.2). It follows that for both the Cl_2 and Br_2 mediated reactions, MeO-aryl bond cleavage occurred, and quinone formation did not proceed through the hydroquinone (Scheme 3.31). The MeO-aryl bond cleavage mechanism for quinone formation with X_2 is consistent with that described in literature for other reagents such as argentic oxide[56] and CAN.[59] A control experiment treating 7,8-dichloro-3,4-dihydro-1*H*-[1,4]oxazino[4,3-*a*]benzimidazole-6,9-dione **9c** with $H_2^{18}O$ for 4 h indicated no exchange.

113

3.3.2.1. Electrochemical analysis of benzimidazolequinones

In collaboration with the Biomolecular Electronics Research Laboratory at NUI Galway, the redox properties of our potential anti-cancer drugs was studied with the aim to establish structure activity relationships.[83] The redox properties of both halogenated and non-halogenated pyrido[1,2-*a*]benzimidazolequinones were characterised by cyclic voltammetry (CV). CV conditions of pyrido[1,2-*a*]benzimidazolequinones (5 mM) in the aprotic solvent of DMF (vs. Fc/Fc$^+$) with 0.1 M of the electrolyte tetrabutylammonium perchlorate (TBAP) were employed. The CV work presented in Table 3.3 was performed by Claire Elwood as part of her Master's thesis at NUI Galway.[83] The pyrido[1,2-*a*]benzimidazolequinone **15b** which has been previously reported with cytotoxicity in the nanomolar range under hypoxic conditions[18] gave a formal potential of -0.92 V (Table 3.3). As expected, the placement of electron withdrawing chlorine and bromine groups onto pyrido[1,2-*a*]benzimidazolequinone resulted in a more easily reduced quinone core. The reduction potentials of the dihalogenated pyrido[1,2-*a*]benzimidazolequinones **9b** and **10b** are shifted approximately 0.22 V in the positive direction relative to the non-halogenated analogue **15b** (Table 3.3). There is a negligible difference in the formal potentials for the chlorine and bromine pyrido[1,2-*a*]benzimidazolequinone analogues probably due to their similar inductive effects (Table 3.3). The PhD candidate Lee-Ann Keane (Aldabbagh group) carried out cytotoxicity assays to determine if there was any correlation between the reduction potentials and the cytotoxic response of **9b**, **10b**, and **15b**. The results will be discussed in her thesis.

Table 3.3. Formal potentials (E°') (V) (vs. (Fc/Fc$^+$) for halogenated and non-halogenated pyridobenzimidazolequinones in aprotic solvent of DMF.[83]
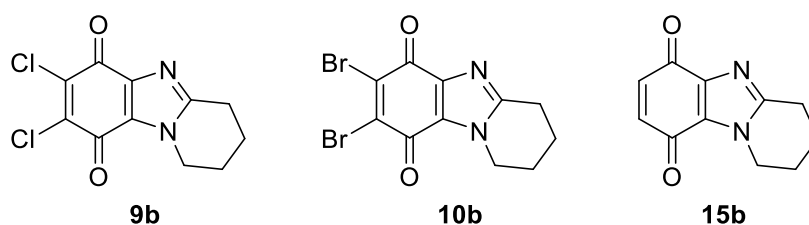
Quinone	E°′ (V)
9b	-0.70
10b	-0.71
15b	-0.92

3.3.3 Synthesis of 1-fluoro-2,5-dimethoxy-4-nitrobenzene

Fagan and Aldabbagh showed that the introduction of acyclic *N*-dibutyl substituents onto [5,4-*f*]imidazobenzimidazolequinones produces a greater cytotoxic response towards both HeLa and DU-145 cancer cell lines when compared to that of alicyclic ring-fused [5,4-*f*]imidazobenzimidazolequinones (Figure 3.9).[84]

HeLa: 1.67 ± 0.05 µM
DU-145: 1.99 ± 0.39 µM

HeLa: 1.28 ± 0.005 µM
DU-145: 1.35 ± 0.11 µM

HeLa: 0.44 ± 0.04 µM
DU-145: 1.34 ± 0.06 µM
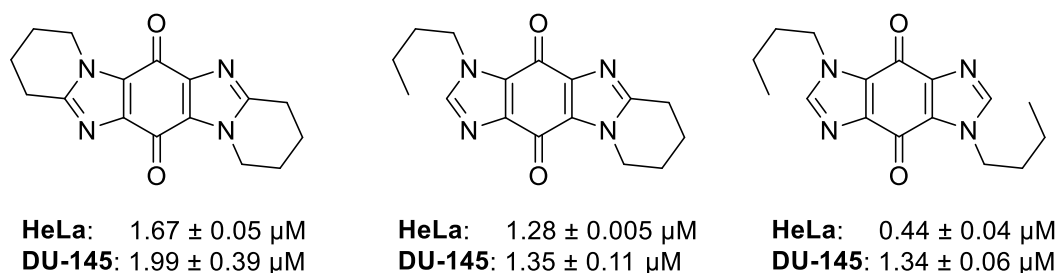
Figure 3.9. The cytotoxicity comparison of acyclic vs cyclic substituted derivatives of [5,4-*f*]imidazobenzimidazolequinones.[84]

Therefore we proposed a synthetic route to prepare 1,2-dibutylamino substituted dihalogenated benzimidazolequinone **16** to assess the cytotoxicity profile relative to the ring-fused analogues (Scheme 3.26), starting from either commercially available materials of 1,4-dimethoxybenzene or 2-fluoro-1,4-dimethoxybenzene (Scheme 3.32).
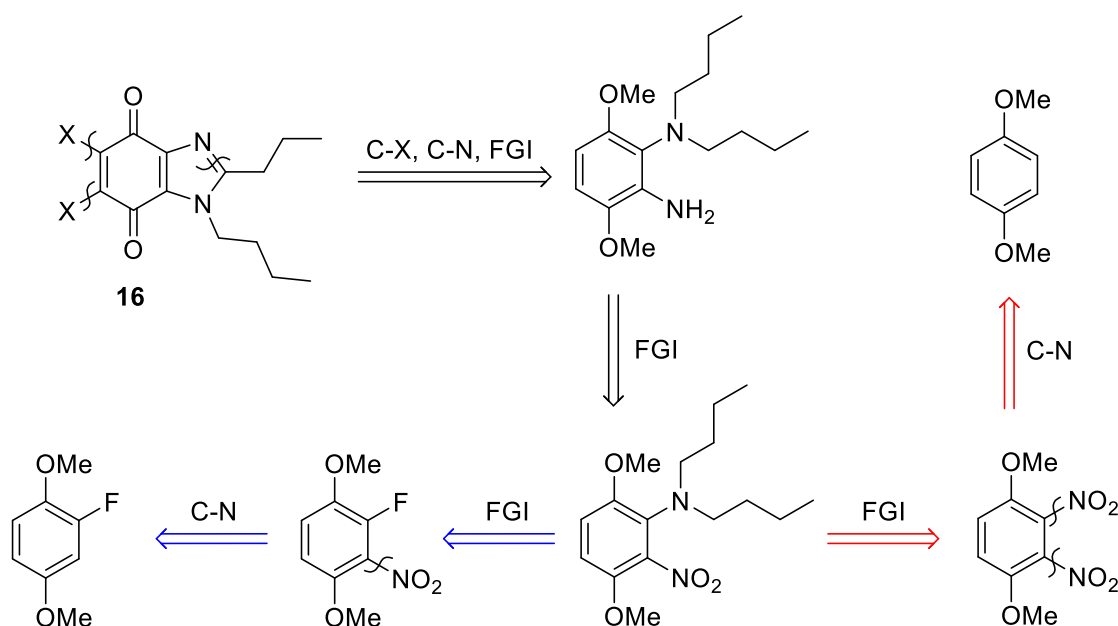
Scheme 3.32. Retrosynthetic analysis of 1,2-dibutylamino substituted halogenated benzimidazolequinone.

The reaction of 1,4-dimethoxybenzene (Flurochem UK, £15 for 100 g) with nitric acid is reported in literature and the major isomer 2,3-dinitro-1,4-dimethoxybenzene predominates in isolated yields of 76-90% (Scheme 3.33a).[76, 85, 86] 2-Fluoro-1,4-dimethoxybenzene is available from Fluorochem in the UK at £60 for 25 g and nitration would give a suitably activated aromatic substrate for nucleophilic aromatic substitution with dibutylamine (Scheme 3.32). Halogens are *o*, *p*-directing towards EAS due to combination of the dual opposing effects of resonance and induction. The nitration of 2-fluoro-1,4-dimethoxybenzene was expected to give the *p*-nitrated product 1-fluoro-2,5-dimethoxy-4-nitrobenzene **18** as the major isomer due to the reduced electron density at the *o*-position from fluorine induction, with 2-fluoro-1,4-dimethoxy-3-nitrobenzene **17** as the minor product (Scheme 3.33b). However, nitration was *p*-selective giving only isomer **18** in high yield. This meant that the intended use of 3-nitro isomer **17** as the substrate for nucleophilic aromatic substitution, could not be pursued due to regioselectivity of the nitration.
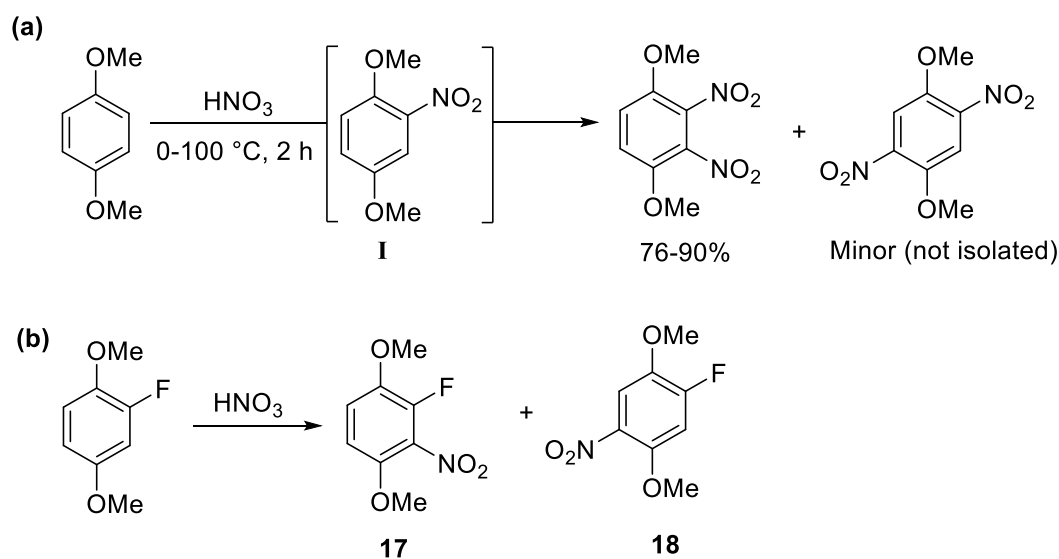
Scheme 3.33. Predicted *o*- and *p*-nitration of 2-fluoro-1,4-dimethoxybenzene based upon similar literature reaction of 1,4-dimethoxybenzene.[76, 85, 86]

Treating 2-fluoro-1,4-dimethoxybenzene with nitric acid (64-66%) over 10 minutes at 0 °C gave 1-fluoro-2,5-dimethoxy-4-nitrobenzene **18** in 90% yield (Scheme 3.34). This is the first reported synthesis and characterisation of **18**, even though alleged commercial sources exist.[87]
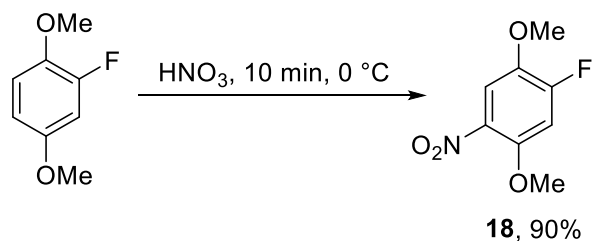
Scheme 3.34. Preparation of 1-fluoro-2,5-dimethoxy-4-nitrobenzene **18**.

X-ray crystallography confirmed the location of the regioselective substitution (Figure 3.10). The fluoro-substituent was found to be exclusively *p*-directing, in contrast to the nitro group of the intermediate 1,4-dimethoxy-2-nitrobenzene **I**, which directs the electrophile to the *o*-position to give 2,3-dinitro-1,4-dimethoxybenzene in the analogous nitration of 1,4-dimethoxybenzene (Scheme 3.33a). Nitro groups are well-known to participate in adjacent group coordination and reactions, especially under strong acidic conditions that also favour their protonation.[88] In addition, the polarity of the solvent plays a major role in determining whether the site of nitration on intermediate **I** is directed *ortho* or *para* to the nitro group, with nitric acid (polar solvent) strongly *o*-directing.[89]
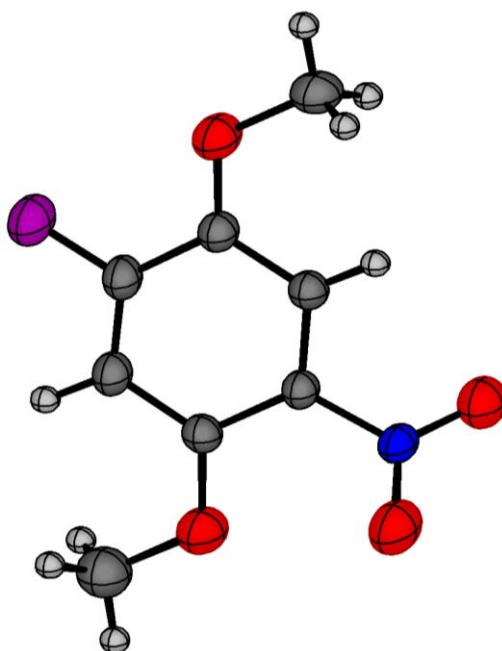
Figure 3.10. The X-ray crystal structure of 1-fluoro-2,5-dimethoxy-4-nitrobenzene **18**.

An alternative route to the 1,2-dibutylamino substituted benzimidazolequinones, could involve the introduction of dibutylamino onto the aromatic system before nitration occurs. Cao and Lin have previously prepared *N,N*-dibutyl-2,5-dimethoxyaniline **19** in a moderate yield of 45% by amination of the commercially available 2-fluoro-1,4-dimethoxybenzene in the presence of *n*-butyllithium at room temperature under inert conditions (Scheme 3.35).[90] The treatment of *N,N*-dibutyl-2,5-dimethoxyaniline with nitric acid could be envisaged to present issues of regioselectivity as evidenced with 1-fluoro-2,5-dimethoxy-4-nitrobenzene **18**. The bulkiness of the dibutylamino could direct regioselectivity but MacLachlan and co-workers have demonstrated that solvent factors are more prominent than steric ones for regioselectivity on the 1,4-dimethoxybenzene system.[89] Therefore, with more emphasis placed on solvent choice for nitration, an isomer *o*-nitrated to the dibutylamine could be isolated in reasonable yields.
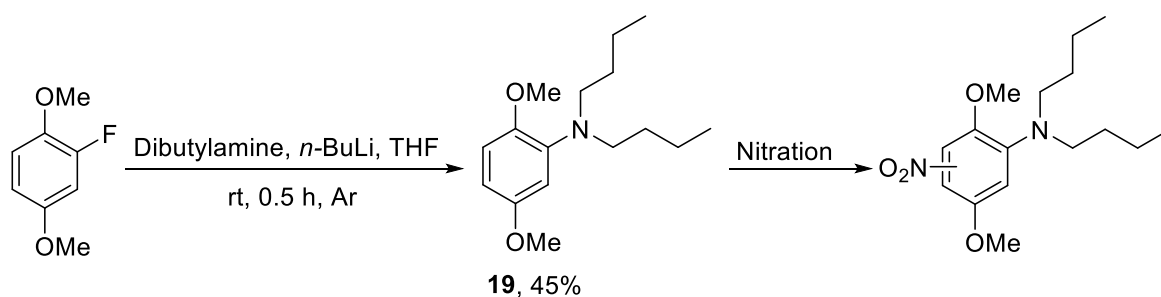
Scheme 3.35. Proposed amination of 2-fluoro-1,4-dimethoxybenzene followed by nitration as a new route towards 1,2-dibutylamino substituted benzimidazolequinones.[89, 90]

3.3.4. Nucleophilic reactions at fluorine site of 1-fluoro-2,5-dimethoxy-4-nitrobenzene

The rate of nucleophilic aromatic substitution onto an arylfluoride is fastest of all in the halogen series due to the high electronegativity of the fluorine atom that stabilises the anionic intermediate at the rate determining step.[91] However, a nitro substituted aromatic has an even faster rate due to a greater anion stabilising ability exerted through resonance. As the synthesis of the isomer **17** was not a viable option, 2,3-dinitro-1,4-dimethoxybenzene was trialled as a substrate for nucleophilic aromatic substitution with dibutylamine (Scheme 3.36a). 2,3-dinitro-1,4-dimethoxybenzene was added to neat dibutylamine and was heated with stirring for three days at 120 °C. Unfortunately only a trace amount of the substituted product was detected on TLC and GC-MS. To determine if substitution at a position *para* to the nitro group is more favoured, 1-fluoro-2,5-dimethoxy-4-nitrobenzene **18** was subjected to the same substitution conditions with dibutylamine as 2,3-dinitro-1,4-dimethoxybenzene (Scheme 3.36a). The reaction was monitored by GC-MS and showed full conversion of **18** after 3 days, producing the regioselectively substituted *N,N*-dibutyl-2,5-dimethoxy-4-nitroaniline **20** in a moderate yield of 60% (Scheme 3.36b).
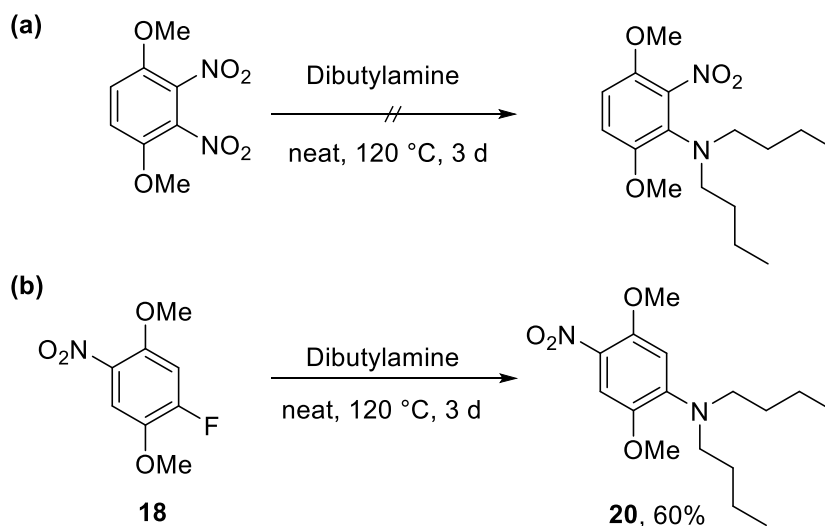
Scheme 3.36. Dibutylamine S_NAr of 1-fluoro-2,5-dimethoxy-4-nitrobenzene **18**.

The aromatic tethered piperazine compound shown in Scheme 3.37a has been reported in literature using pentafluoropyridine in slight excess over piperazine to give a yield of

52%.[92] This methodology was applied towards our phenyl methyl ether system, starting with the substrate of 1-fluoro-2,5-dimethoxy-4-nitrobenzene **18** in three times excess relative to piperazine in acetronitrile at reflux with the base of potassium carbonate to try and produce 1,4-bis(2,5-dimethoxy-4-nitrophenyl)piperazine **21** (Scheme 3.37b).
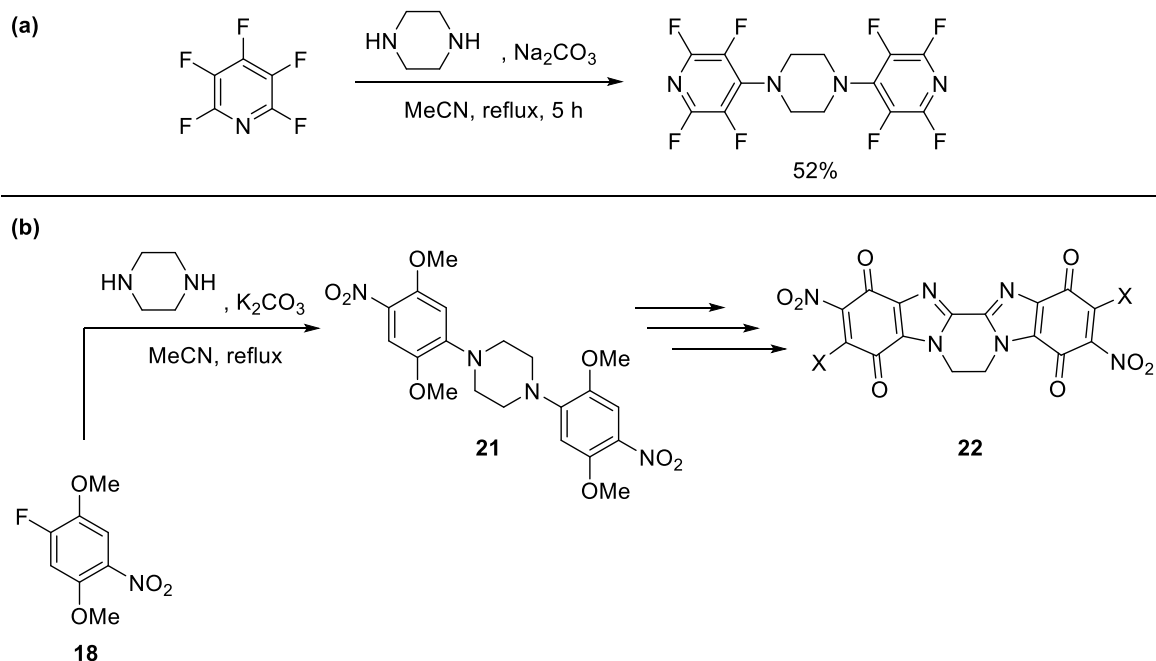
Scheme 3.37. Proposed approach to highly conjugated quinone via aromatic tethered piperazines.[92]

The synthetic intermediate **21** would then be used to access the highly conjugated dihalogenated diquinone (3,11-dinitro-6,7-dihydrobenzimidazo[2',1':3,4]pyrazino[1,2-*a*]benzimidazole-1,4,9,12-tetrone) **22**. This would occur via a sequence of nitration and reduction which would be followed by a one-pot cyclization, halogenation and oxidation similar to that in Scheme 3.26.
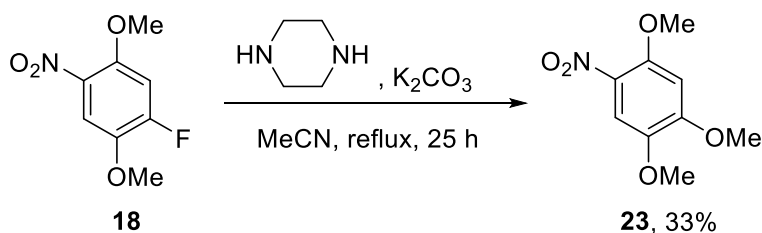
Scheme 3.38. Methoxylation of 1-fluoro-2,5-dimethoxy-4-nitrobenzene **18**.

To our surprise, no nucleophilic aromatic substitution occurred with piperazine but instead nucleophilic displacement of the fluoride atom was carried out with a methoxy group to form 1,2,4-trimethoxy-5-nitrobenzene **23** in a poor yield of 33% (Scheme 3.38). 1-Fluoro-2,5-dimethoxy-4-nitrobenzene **18** was used in three times excess relative to piperazine and presumably this is the source of the methoxide for nucleophilic displacement. X-ray crystallography supported NMR data that the introduction of the methoxy group was regioselectively at the 1-fluorine position and not at the 4-nitro position (Figure 3.11).
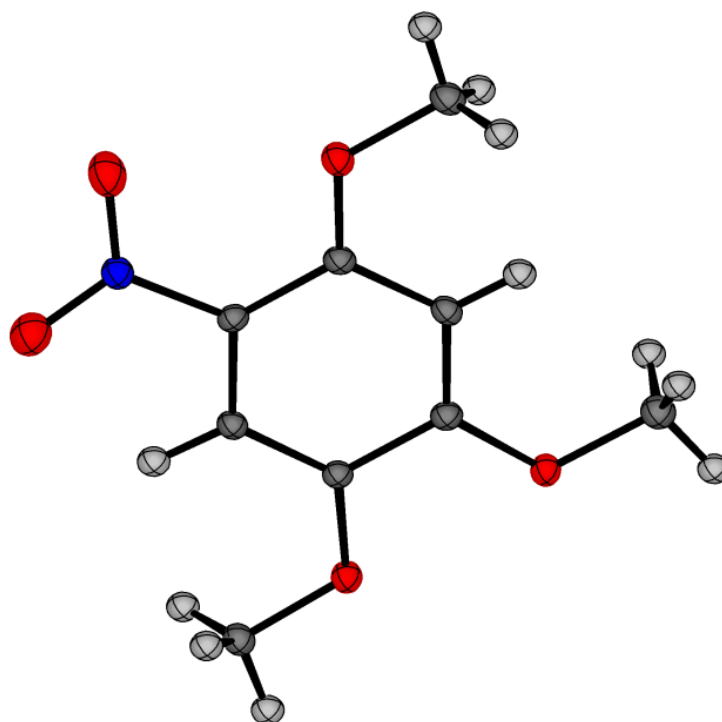
Figure 3.11. The X-ray crystal structure of 1,2,4-trimethoxy-5-nitrobenzene **23**.

The methoxylation of aromatics traditionally involves the use of a methoxide salt in a polar solvent and can be either transition metal-catalysed or metal-free.[93, 94] In one particular case, the pentafluorobenzoyl chloride analogue of DNA base uracil was reacted with methyl iodide in DMF alongside sodium carbonate at room temperature to develop standards for gas chromatography analysis (Scheme 3.39).[95] The expected methylated derivative was formed in 47% but the unexpected 3-(*p*-methoxytetrafluorobenzoyl)-l-methyl derivative was obtained in 20% yield. From isotopic labeling, the oxygen source for the methoxy group was determined to come from DMF and when the reaction solvent was changed to acetonitrile, no *p*-methoxylation was observed.[95]
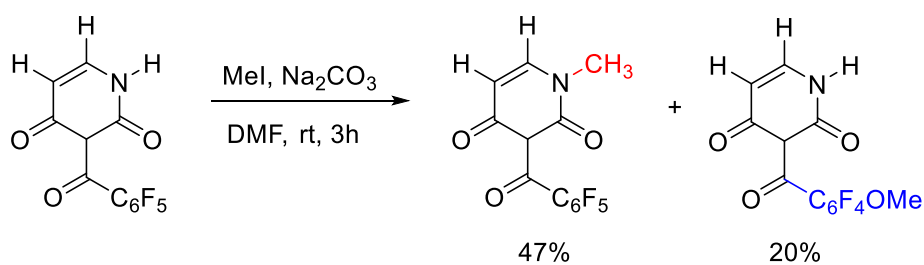
Scheme 3.39. Unexpected methoxylation of pentafluorobenzoyl chloride derivative of uracil owing to solvent of DMF.[95]

An alternative route to synthesize 1,4-bis(2,5-dimethoxy-4-nitrophenyl)piperazine **21** could involve a preparation analogous to that employed by Cao and Lin, which reacted fluorobenzene with 2.5 equivalents of piperazine alongside the base of *n*-BuLi to furnish 1,4-diphenylpiperazine in 65% yield (Scheme 3.40).[90] The utilization of a strong base of *n*-BuLi, combined with a reduced excess of 1-fluoro-2,5-dimethoxy-4-nitrobenzene **18** relative to piperazine could promote piperazine substitution instead of methoxylation.
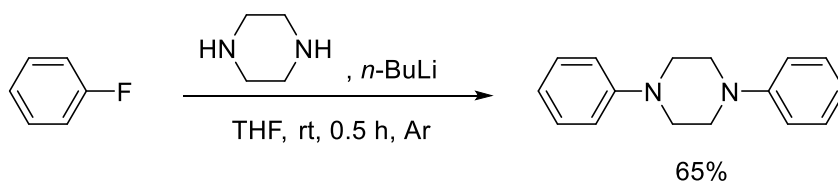
Scheme 3.40. The employment of strong base *n*-BuLi to form aromatic tethered piperazine.[90]

3.4. Experimental

3.4.1. Materials

All chemicals were obtained from commercial sources and were used without purification, except for MeCN (Honeywell CHROMASOLV™ reagent, ≥99.9%), which was distilled over CaH_2 (Acros, ca. 93%, extra pure, 0-2 mm grain size) for the isotopic labeling experiments. 1,4-Dimethoxy-2,3-dinitrobenzene was prepared from 1,4-dimethoxybenzene (Sigma Aldrich 99% (GC)) and nitric acid (Honeywell Fluka, 64-66%).[76, 96] 3,6-dimethoxy-2-(cycloamino)anilines **5a**, **5b**, **5d**, and **5e** were previously reported in Chapter 2 using the respective nucleophilic aromatic substitutions of pyrrolidine (Acros, ≥99%), piperidine (Sigma Aldrich, 99%), azepane (TCI, >98% (GC)) and azocane (TCI, >98% (GC)) onto 1,4-dimethoxy-2,3-dinitrobenzene followed by reduction with iron powder (Sigma Aldrich, ≥99%, reduced, powder (fine)).[53] The *o*-cyclic tertiary amine substituted anilines **1a**, **1c**, and **1d** were prepared in the same manner as above starting with 1-chloro-4-methoxy-2-nitrobenzene (TCI, >98% (GC)). H_2O_2 (Honeywell Fluka, 50% w/v in water, stabilized), HBr (Honeywell Fluka, ≥48% w/v in water), HCl (Sigma Aldrich, ≥37% w/v in water) and Br_2 (Sigma Aldrich, ≥ 99%) were used as received. Cl_2 (50 mmol) was generated by the dropwise addition of concentrated HCl onto $KMnO_4$ (Sigma Aldrich, ≥99%) as described by Leonard et al.[81] Thin layer chromatography (TLC) was carried out on Merck TLC silica gel 60 F_{254} plates using a UV lamp (λ = 254 nm) for visualization. Flash column chromatography was carried out using silica gel (Sigma Aldrich, technical grade, particle size 40-63 μm).

3.4.2. Measurements

Melting point and Infrared spectroscopy: Melting points were measured on a Stuart Scientific melting point apparatus SMP1. Infrared spectra were recorded using a Perkin-Elmer Spec 1 with ATR attached.

High Resolution Mass Spectrometry (HRMS): HRMS was carried out using ESI time-of-flight mass spectrometer (TOF-MS) using a Waters LCT Mass Spectrometry instrument. The precision of all accurate mass measurements was better than 5 ppm.

Gas chromatography: GC-MS was used to monitor the formation of dihalogenated ring-fused benzimidazoles and benzimidazolequinones from their respective anilines. GC-MS analysis was performed on an Agilent 6890 Series GC system equipped with an Agilent 5975 Inert Mass Selective Detector (EI) and a DB-1, 30 m, ID 0.25 mm, FD 0.25 μm column. The carrier gas used was He at a flow rate of 2.4 mL/min. The injector was heated to 160 °C and the oven temperature was increased from 150 to 180 °C at the rate of 22 °C/min and was then further increased to 320 °C at 40 °C/min. This EI detector was also used for the isotopic labeling experiments to detect the incorporation of ^{18}O.

HPLC analysis: A Hewlett Packard series 1100 HPLC was equipped with a UV detector operating at 254 nm and a Phenomenex® BondClone™ 10 μm C18, 250 × 4.6 mm column. The mobile phase was an isocratic MeCN/H_2O system (90/10 eluent ratio was used in Figure 3.5 and 80/20 eluent ratio was used in Figure 3.8) at a flow rate of 1.5 mL min^{-1}. The sample (5 μL) was injected by an automatic injector. The fractions were diluted to 1 mg/L and the components identified by HRMS.

Nuclear Magnetic Resonance (NMR spectroscopy): NMR spectra were recorded using a JEOL ECX 400 MHz instrument equipped with a Dell Precision 360 computer workstation, except for the ^{1}H and ^{13}C NMR spectrum of **8f** and ^{1}H spectrum of **10f**, which were recorded on a Varian VNMRS 500 MHz instrument. The chemical shifts are in ppm relative to tetramethylsilane. ^{13}C NMR data have complete proton decoupling. NMR assignments are supported by Distortionless Enhancement by Polarization Transfer (DEPT) and ^{1}H-^{1}H and ^{1}H-^{13}C correlation.

Single crystal X-ray diffraction: Single crystals of **9a**, **9c**, **9d**, **9f**, **10a**, **10d** and **18** were grown by slow evaporation from CH_2Cl_2, while single crystals of **8f** and **23** were grown by liquid/liquid diffusion from CH_2Cl_2/hexane. Single crystal data was collected using an Oxford Diffraction Xcalibur system operated using the CrysAlisPro software and the data collection temperature was controlled at 298 K using a Cryojet system from Rigaku Oxford Diffraction. The crystal structures were solved using ShelxT version 2014/55,[97] and refined using ShelxL version 2017/1,[98] both of which were operated within the Oscail software package.[99] Crystallographic data for compounds **8f**, **9a**, **9c**, **9d**, **9f**, **10a**, **10d** and **18** were deposited with the Cambridge Crystallographic Data Centre with deposit numbers of CCDC 1863030, CCDC 1863027, CCDC 1863026, CCDC 1863025, CCDC 1863029, CCDC 1863024, CCDC 1863028 and CCDC 1819149 respectively. This data is available free of charge via www.ccdc.cam.ac.uk/data_request/cif (or from the Cambridge Crystallographic Data Centre, 12 Union Road, Cambridge CB2 1EZ, U.K.; fax +44 1223 336033; or e-mail deposit@ccdc.cam.ac.uk).

Elemental Analysis: Elemental analysis was carried out on an Exeter Analytical CE-440 analyzer (Exeter Analytical, Coventry, UK).

3.4.3. Compound data

3.4.3.1. Synthesis of ring-fused dihalogenated benzimidazoles 2a, 2c, 2d, 3c, 3d, and 4a using H_2O_2/HX

Reaction conditions are described in Scheme 3.18. EtOAc (20 mL) was added and the solution was washed with NH_4OH (10%, 2 x 10 mL). The organic extract was dried (Na_2SO_4) and evaporated to dryness. Residues of products **2a**, **2c**, **3c**, and **4a** did not require purification. Compounds **2d** and **3d** are oils, and were purified by column chromatography with isocratic elution of pet. ether and EtOAc.
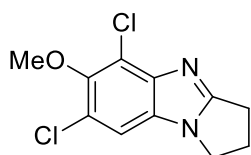
5,7-Dichloro-6-methoxy-2,3-dihydro-1*H*-pyrrolo[1,2-*a*]benzimidazole (**2a**): 0.240 g, 93%; brown solid; mp 112-116 °C; v_{max} (neat, cm^{-1}) 2938, 1611, 1520, 1455, 1397, 1292, 1165, 1026; δ_H (400 MHz, CDCl$_3$) 2.65-2.73 (m, 2H), 3.02 (t, *J* 7.6 Hz, 2H), 3.87 (s, 3H), 4.03 (t, *J* 7.1 Hz, 2H), 7.15 (s, 1H); δ_C (100 MHz, CDCl$_3$) 23.7, 26.2, 43.3 (all CH$_2$), 61.3 (Me), 108.9 (CH), 118.4, 123.1, 129.1, 145.4, 147.5, 163.2 (all C); HRMS (ESI) *m/z* (M + H)$^+$, C$_{11}$H$_{11}$N$_2$O^{35}Cl$_2$ calcd. 257.0248, observed 257.0260.
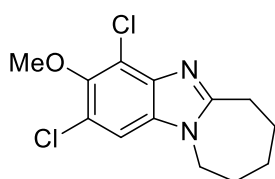
2,4-Dichloro-3-methoxy-7,8,9,10-tetrahydro-6*H*-azepino[1,2-*a*]benzimidazole (**2c**): 0.254 g, 89%; brown solid; mp 158-160 °C; v_{max} (neat, cm^{-1}) 2927, 2848, 1513, 1474, 1437, 1403, 1344, 1198; δ_H (400 MHz, CDCl$_3$) 1.72-1.78 (m, 4H), 1.86-1.89 (m, 2H), 3.08 (t, *J* 5.5 Hz, 2H), 3.86 (s, 3H), 4.03 (t, *J* 4.8 Hz, 2H), 7.15 (s, 1H); δ_C (100 MHz, CDCl$_3$) 25.2, 28.5, 29.9, 30.7, 45.2 (all CH$_2$), 61.3 (Me), 108.4 (CH), 118.2, 123.5, 132.3, 138.8, 147.5, 159.5 (all C); HRMS (ESI) *m/z* (M + H)$^+$, C$_{13}$H$_{15}$N$_2$O^{35}Cl$_2$ calcd. 285.0573, observed 285.0561.
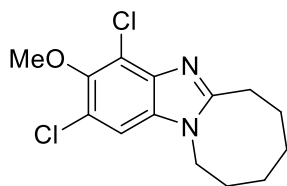
2,4-Dichloro-3-methoxy-6,7,8,9,10,11-hexahydroazocino[1,2-*a*]benzimidazole **(2d)**: 0.232 g, 78%; clear oil; R_f 0.33 (50:50 EtOAc / pet. ether); ν_{max} (neat, cm^{-1}) 2930, 2857, 1508, 1461, 1421, 1404, 1354, 1304, 1201, 1176; δ_H (400 MHz, CDCl$_3$) 1.16-1.22 (m, 2H), 1.42-1.48 (m, 2H), 1.78 (quint, *J* 6.2 Hz, 2H), 1.83-1.89 (m, 2H), 2.98 (t, *J* 6.2 Hz, 2H), 3.88 (s, 3H), 4.14 (t, *J* 6.2 Hz, 2H), 7.17 (s, 1H); δ_C (100 MHz, CDCl$_3$) 23.9, 25.5, 27.1, 29.6, 31.0, 42.0 (all CH$_2$), 61.2 (Me), 108.5 (CH), 118.1, 123.3, 131.3, 140.0, 147.4, 158.7 (all C); HRMS (ESI) *m/z* (M + H)$^+$, C$_{14}$H$_{17}$N$_2$O^{35}Cl$_2$ calcd. 299.0718, observed 299.0731.
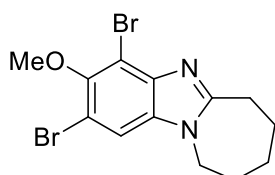
2,4-Dibromo-3-methoxy-7,8,9,10-tetrahydro-6*H*-azepino[1,2-*a*]benzimidazole **(3c)**: 0.298g, 80%; off-white solid; mp 196-198 °C; ν_{max} (neat, cm^{-1}) 2933, 2855, 1507, 1470, 1449, 1428, 1398, 1339, 1193; δ_H (400 MHz, CDCl$_3$) 1.78-1.84 (m, 4H), 1.91-1.93 (m, 2H), 3.12 (t, *J* 5.7 Hz, 2H), 3.90 (s, 3H), 4.07 (t, *J* 5.0 Hz, 2H), 7.41 (s, 1H); δ_C (100MHz, CDCl$_3$) 25.3, 28.6, 30.1, 30.8, 45.2 (all CH$_2$), 61.3 (Me), 107.7, 111.6 (both C), 111.9 (CH), 132.9, 141.6, 149.2, 159.6 (all C); HRMS (ESI) *m/z* (M + H)$^+$, C$_{13}$H$_{15}$N$_2$O^{79}Br$_2$ calcd. 372.9551, observed 372.9561.
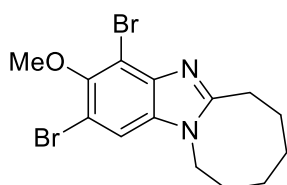
2,4-Dibromo-3-methoxy-6,7,8,9,10,11-hexahydroazocino[1,2-*a*]benzimidazole **(3d)**: 0.271g, 70%; clear oil; R_f 0.30 (50:50 EtOAc / pet. ether); ν_{max} (neat, cm^{-1}) 2929, 2855, 1506, 1456, 1417, 1402, 1245, 1202, 1148; δ_H (400 MHz, CDCl$_3$) 1.18-1.23 (m, 2H), 1.44-1.49 (m, 2H), 1.76-1.82 (m, 2H), 1.84-1.90 (m, 2H), 2.99 (t, *J* 6.2 Hz, 2H), 3.88 (s, 3H), 4.14 (t, *J* 6.0 Hz, 2H), 7.38 (s, 1H); δ_C (100 MHz, CDCl$_3$) 23.9, 25.5, 27.1, 29.6, 31.0, 42.0

(all CH$_2$), 61.2 (Me), 107.7, 111.5 (both C), 112.1 (CH), 131.7, 142.3, 149.2, 158.7 (all C); HRMS (ESI) *m/z* (M + H)$^+$, C$_{14}$H$_{17}$N$_2$O^{79}Br$_2$ calcd. 386.9708, observed 386.9715.
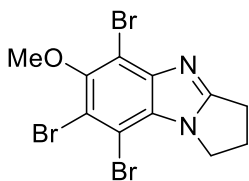
5,7,8-Tribromo-6-methoxy-2,3-dihydro-1*H*-pyrrolo[1,2-*a*]benzimidazole (4a): 0.370 g, 87%; off-white solid; mp 176-180 °C; ν_{max} (neat, cm^{-1}) 2936, 1516, 1449, 1414, 1374, 1275, 1069; δ_H (400 MHz, CDCl$_3$) 2.67-2.75 (m, 2H), 3.07 (t, *J* 7.8 Hz, 2H,), 3.90 (s, 3H), 4.46 (t, *J* 7.1 Hz, 2H); δ_C (100 MHz, CDCl$_3$) 23.7, 26.0, 45.9 (all CH$_2$), 61.2 (Me), 105.1, 107.2, 115.4, 129.5, 147.0, 150.3, 163.7 (all C); HRMS (ESI) *m/z* (M + H)$^+$, C$_{11}$H$_{10}$N$_2$O^{79}Br$_3$ calcd. 422.8343, observed 422.8330.

3.4.3.2. Preparation of 3,6-dimethoxy-2-(cycloamino)anilines 5c and 5f
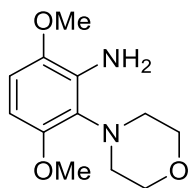
3,6-Dimethoxy-2-(morpholin-4-yl)aniline (5c)

1,4-Dimethoxy-2,3-dinitrobenzene (4.00 g, 17.5 mmol), morpholine (6.09 g, 70.0 mmol) and K_2CO_3 (12.10 g, 87.5 mmol) were stirred in MeCN (60 mL) at reflux for 3 days. EtOAc (100 mL) was added and the organic layer washed with brine (80 mL). The organic extract was dried ($MgSO_4$), evaporated to dryness, and purified by column chromatography with isocratic elution of pet. ether and EtOAc to give 4-(3,6-dimethoxy-2-nitrophenyl)morpholine (1.83 g, 39%) as an orange solid; mp 148-150 °C (lit.[100] mp 148-149 °C); R_f 0.25 (40:60 EtOAc / pet. ether); v_{max} (neat, cm^{-1}) 2938, 2851, 1538 (NO_2), 1493, 1441, 1382 (NO_2), 1259, 1109, 1036; δ_H (400 MHz, CDCl$_3$) 2.71-3.29 (bs, 4H), 3.60 (t, J 4.3 Hz, 4H), 3.73 (s, 3H), 3.76 (s, 3H) 6.76 (d, J 9.2 Hz, 1H), 6.84 (d, J 9.2, 1H); δ_C (100 MHz, CDCl$_3$) 50.5 (CH$_2$), 56.0, 56.7 (both Me), 67.6 (CH$_2$), 110.1, 113.1, (both CH), 132.5, 142.1, 144.2, 152.8 (all C). HRMS (ESI) m/z (M + H)$^+$, $C_{12}H_{17}N_2O_5$ calcd. 269.1137, observed 269.1124.

The above nitrobenzene (1.80 g, 6.7 mmol), Fe powder (1.20 g, 21.4 mmol) and NH$_4$Cl (0.187 g, 3.35 mmol) was stirred at reflux in ethanol (24 mL) and water (8 mL) for 16 h. EtOAc (50 mL) was added to the cooled mixture, the organic layer washed with brine (2 × 20 mL), dried ($MgSO_4$), and evaporated to dryness. The residue was purified by column chromatography with isocratic elution of pet. ether and EtOAc to give **5c** (1.29 g, 81%) as a brown solid; mp 92-94 °C; R_f 0.55 (50:50 EtOAc / pet. ether); v_{max} (neat, cm^{-1}) 3491, 3381, 2950, 2841, 1607, 1548, 1489, 1462, 1253, 1105, 1043; δ_H (400 MHz, CDCl$_3$) 2.61 (d, J 10.7 Hz, 2H), 3.57 (t, J 10.7 Hz, 2H), 3.69 (t, J 10.7 Hz, 2H), 3.75 (s, 3H), 3.79 (s, 3H), 3.89 (d, J 10.7 Hz, 2H), 4.36-4.48 (s, 2H, NH$_2$, D$_2$O exchange), 6.15 (d, J 8.9 Hz, 1H), 6.57 (d, J 8.9 Hz, 1H); δ_C (100 MHz, CDCl$_3$) 50.2 (CH$_2$), 55.3, 56.0 (both Me), 68.6 (CH$_2$), 98.8, 107.8 (both CH), 125.3, 135.7, 142.0, 153.6 (all C). HRMS (ESI) m/z (M + H)$^+$, $C_{12}H_{19}N_2O_3$ calcd. 239.1396, observed 239.1386.
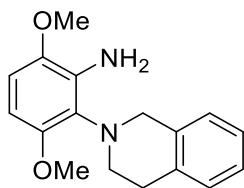
2-(3,4-Dihydroisoquinolin-2(1H)-yl)-3,6-dimethoxyaniline (5f)

1,4-Dimethoxy-2,3-dinitrobenzene (2.00 g, 8.8 mmol), 1,2,3,4-tetrahydroisoquinoline (THIQ, 4.68 g, 35.2 mmol) and K_2CO_3 (6.07 g, 44.0 mmol) were stirred in MeCN (30 mL) at reflux for 3 days. EtOAc (50 mL) was added and the organic layer washed with brine (40 mL). The organic extract was dried ($MgSO_4$), evaporated to dryness, and purified by column chromatography with isocratic elution of pet. ether and EtOAc to give 2-(3,6-dimethoxy-2-nitrophenyl)-1,2,3,4-tetrahydroisoquinoline (1.85 g, 67%) as a yellow solid; mp 180-182 °C; R_f 0.47 (20:80 EtOAc / pet. ether); v_{max} (neat, cm^{-1}) 2939, 2840, 1539 (NO_2), 1494, 1454, 1380 (NO_2), 1264, 1096, 1055; δ_H (400 MHz, CDCl$_3$) 2.88 (t, J 5.4 Hz, 2H), 3.35 (t, J 5.4 Hz, 2H), 3.81 (s, 3H), 3.83 (s, 3H), 4.29 (s, 2H), 6.82 (d, J 9.2 Hz, 1H), 6.92 (d, J 9.2, 1H), 6.97-6.98 (m, 1H), 7.12 (d, J 3.7 Hz, 3H); δ_C (100 MHz, CDCl$_3$) 30.2, 48.6, 52.1 (all CH$_2$), 56.1, 56.8 (both Me), 109.8, 113.0, 125.6, 125.9, 126.2, 129.1 (all CH), 133.5, 134.6, 135.0, 142.2, 144.6, 152.9 (all C); HRMS (ESI) m/z (M + H)$^+$, $C_{17}H_{19}N_2O_4$ calcd. 315.1345, observed 315.1334.

The above nitrobenzene (1.80 g, 5.8 mmol) and Pd-C (10%, 5 mol%, 0.31 g) in EtOAc/MeOH (80/20 mL) was stirred under 1 atm of H_2 at rt for 4 days. The catalyst was removed by filtration and the filtrate was evaporated to dryness. The residue was purified by column chromatography with isocratic elution of pet. ether and EtOAc to give **5f** (1.26 g, 77%) as clear oil; R_f 0.30 (10:90 EtOAc / pet. ether); v_{max} (neat, cm^{-1}) 3477, 3370, 2918, 2834, 1604, 1549, 1489, 1463, 1253, 1101, 1053; δ_H (400 MHz, CDCl$_3$) 2.81-2.85 (m, 1H), 3.13-3.24 (m, 2H), 3.70-3.76 (m, 1H), 3.79 (s, 3H), 3.85 (s, 3H), 3.95 (d, J 15.1 Hz, 1H), 4.43 (s, 2H, NH$_2$, D$_2$O exchange), 4.60 (d, J 15.1 Hz, 1H), 6.24 (d, J 9.0 Hz, 1H), 6.64 (d, J 9.0 Hz, 1H), 7.05-7.07 (m, 1H), 7.16-7.22 (m, 3H); δ_C (100 MHz, CDCl$_3$) 31.3, 48.7, 51.9 (all CH$_2$), 55.5, 56.1 (both Me), 98.9, 107.7, 125.6 (all CH), 125.8 (C), 125.9, 126.5, 129.2 (all CH), 135.1, 135.9, 136.6, 142.1, 153.8 (all C); HRMS (ESI) m/z (M + H)$^+$, $C_{17}H_{21}N_2O_2$ calcd. 285.1603, observed 285.1606.

3.4.3.3. Synthesis of ring-fused dihalogenated dimethoxybenzimidazoles 6a-6f and 7a-7f using H₂O₂/HX

Reaction conditions are described in Scheme 3.23. H_2O_2 was added in one addition to anilines **5a-5f** in MeCN/HX at rt. EtOAc (20 mL) was added and the solution was washed with Na_2CO_3 (sat. sol., 2 × 10 mL). The organic extract was dried ($MgSO_4$) and evaporated to dryness. Residues of products **6c**, **6d**, **7c**, **7d**, and **7e** did not require purification. Products **6a**, **6b**, **7a**, and **7b** were recrystallized from Et_2O. The residues of **6e**, **6f**, **7f**, and **8f** were purified by column chromatography with isocratic elution of pet. ether and EtOAc.
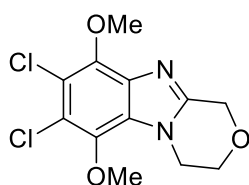
7,8-Dichloro-6,9-dimethoxy-3,4-dihydro-1*H*-[1,4]oxazino[4,3-*a*]benzimidazole **(6c):** 0.203 g, 67%; light brown solid; mp 168-170 °C; ν_{max} (neat, cm⁻¹) 2952, 2841, 1604, 1525, 1491, 1467, 1445, 1421, 1386, 1275, 1097; δ_H (400 MHz, CDCl₃) 3.89 (s, 3H), 4.13 (t, *J* 5.2 Hz, 2H), 4.17 (s, 3H), 4.37 (t, *J* 5.2 Hz, 2H), 4.96 (s, 2H, 1-CH₂); δ_C (100 MHz, CDCl₃) 44.3 (CH₂), 61.6, 62.6 (both Me), 64.0 (CH₂), 65.5 (1-CH₂), 118.1, 120.5, 127.8, 135.2, 138.6, 144.5, 148.2 (all C); HRMS (ESI) *m/z* (M + H)⁺, $C_{12}H_{13}N_2O_3{}^{35}Cl_2$ calcd. 303.0303, observed 303.0294.
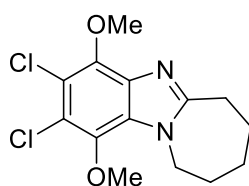
2,3-Dichloro-1,4-dimethoxy-7,8,9,10-tetrahydro-6*H*-azepino[1,2-*a*]benzimidazole **(6d):** 0.281 g, 89%; brown solid; mp 110-112 °C; ν_{max} (neat, cm⁻¹) 2932, 1601, 1516, 1483, 1453, 1417, 1388, 1323, 1238; δ_H (400 MHz, CDCl₃) 1.78-1.93 (m, 6H), 3.10 (t, *J* 5.5 Hz, 2H), 3.89 (s, 3H), 4.20 (s, 3H), 4.46-4.62 (bs, 2H); δ_C (100 MHz, CDCl₃) 25.4, 28.9, 29.7, 30.9, 45.5 (all CH₂), 61.7 (2 × Me), 117.6, 120.7, 128.3, 135.4, 138.2, 144.4, 158.6 (all C); HRMS (ESI) *m/z* (M + H)⁺, $C_{14}H_{17}N_2O_2{}^{35}Cl_2$ calcd. 315.0667, observed 315.0655.
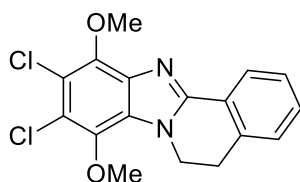
9,10-Dichloro-8,11-dimethoxy-5,6-dihydrobenzimidazo[2,1-*a*]isoquinoline (6f): 0.178 g, 51%; light brown solid; mp 158-160 °C; R_f 0.44 (20:80 EtOAc / pet. ether); v_{max} (neat, cm^{-1}) 2941, 1603, 1532, 1475, 1459, 1422, 1381, 1322, 1265; δ_H (400 MHz, CDCl$_3$) 3.26 (t, *J* 6.8 Hz, 2H), 3.95 (s, 3H), 4.35 (s, 3H), 4.61 (t, *J* 6.8 Hz, 2H), 7.28-7.30 (m, 1H), 7.36-7.41 (m, 2H), 8.25-8.27 (m, 1H); δ_C (100 MHz, CDCl$_3$) 28.5, 42.1 (both CH$_2$), 61.7, 62.3 (both Me), 117.5, 120.9 (both C), 126.1, 127.8, 128.0 (all CH), 128.2 (C), 130.7 (CH), 134.4, 136.7, 138.3, 144.9, 149.5 (all C); HRMS (ESI) *m/z* (M + H)$^+$, C$_{17}$H$_{15}$N$_2$O$_2{}^{35}$Cl$_2$ calcd. 349.0511, observed 349.0524.
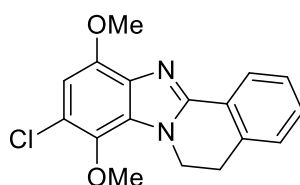
9-Chloro-8,11-dimethoxy-5,6-dihydrobenzimidazo[2,1-*a*]isoquinoline (8f): 0.188 g, 60%; white solid; mp 144-147 °C; R_f 0.30 (20:80 EtOAc / pet. ether); v_{max} (neat, cm^{-1}) 2970, 2936, 1606, 1597, 1508, 1483, 1458, 1392, 1312, 1262, 1216; δ_H (500 MHz, CDCl$_3$) 3.27 (t, *J* 6.8 Hz, 2H), 3.95 (s, 3H), 4.00 (s, 3H), 4.64 (t, *J* 6.8 Hz, 2H), 6.64 (s, 1H), 7.28-7.30 (m, 1H), 7.37-7.39 (m, 2H), 8.36-8.37 (m, 1H); δ_C (125 MHz, CDCl$_3$) 28.6, 42.0 (both CH$_2$), 56.1, 62.2 (both Me), 104.3 (CH), 120.8 (C), 126.0 (CH), 126.4 (C), 127.6, 127.8 (both CH), 128.8 (C), 130.1 (CH), 134.0, 134.7, 136.5, 147.9, 148.7 (all C); HRMS (ESI) *m/z* (M + H)$^+$, C$_{17}$H$_{16}$N$_2$O$_2{}^{35}$Cl calcd. 315.0900, observed 315.0885.
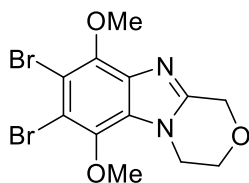
7,8-Dibromo-6,9-dimethoxy-3,4-dihydro-1*H*-[1,4]oxazino[4,3-*a*]benzimidazole (7c): 0.348 g, 89%; brown solid; mp 156-158 °C; v_{max} (neat, cm^{-1}) 2980, 2948, 2836, 1599, 1521, 1485, 1464, 1414, 1385, 1300, 1068; δ_H (400 MHz, CDCl$_3$) 3.91 (s, 3H), 4.16 (t, *J* 5.4 Hz, 2H), 4.20 (s, 3H), 4.42 (t, *J* 5.4 Hz, 2H), 5.00 (s, 2H, 1-CH$_2$); δ_C (100 MHz,

CDCl$_3$) 44.3 (CH$_2$), 61.6, 62.7 (both Me), 64.1 (CH$_2$), 65.6 (1-CH$_2$), 110.9, 113.4, 128.8, 136.2, 139.9, 146.0, 148.1 (all C); HRMS (ESI) m/z (M + H)$^+$, C$_{12}$H$_{13}$N$_2$O$_3$^{79}Br$_2$ calcd. 390.9293, observed 390.9298.
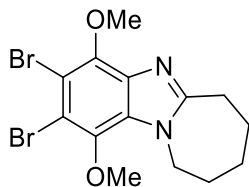
2,3-Dibromo-1,4-dimethoxy-7,8,9,10-tetrahydro-6H-azepino[1,2-a]benzimidazole (7d): 0.372 g, 92%; brown solid; mp 124-126 °C; v_{max} (neat, cm^{-1}) 2930, 1594, 1522, 1478, 1460, 1414, 1382, 1309, 1232; δ_H (400 MHz, CDCl$_3$) 1.75-1.91 (m, 6H), 3.07 (t, J 5.7 Hz, 2H), 3.84 (s, 3H), 4.17 (s, 3H), 4.39-4.61 (bs, 2H); δ_C (100 MHz, CDCl$_3$) 25.4, 28.9, 29.7, 30.9, 45.4 (all CH$_2$), 61.6, 61.7 (both Me), 110.1, 113.5, 129.2, 136.4, 139.4, 145.8, 158.5 (all C); HRMS (ESI) m/z (M + H)$^+$, C$_{14}$H$_{17}$N$_2$O$_2$^{79}Br^{81}Br calcd. 404.9636, observed 404.9643.
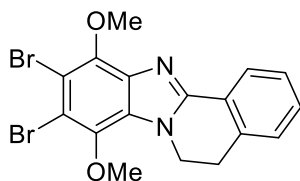
9,10-Dibromo-8,11-dimethoxy-5,6-dihydrobenzimidazo[2,1-a]isoquinoline (7f): 0.320 g, 73%; light brown solid; mp 172-174 °C; R_f 0.39 (20:80 EtOAc / pet. ether); v_{max} (neat, cm^{-1}) 2934, 1597, 1525, 1469, 1455, 1414, 1378, 1307, 1261; δ_H (400 MHz, CDCl$_3$) 3.26 (t, J 6.8 Hz, 2H), 3.93 (s, 3H), 4.34 (s, 3H), 4.61 (t, J 6.8 Hz, 2H), 7.28-7.30 (m, 1H), 7.36-7.42 (m, 2H), 8.26-8.28 (m, 1H); δ_C (100 MHz, CDCl$_3$) 28.6, 42.2 (both CH$_2$), 61.7, 62.4 (both Me), 110.2, 113.7 (both C), 126.1, 127.8, 128.0 (all CH), 129.1 (C), 130.7 (CH), 134.4, 137.5, 139.6, 146.2, 149.4 (all C); HRMS (ESI) m/z (M + H)$^+$, C$_{17}$H$_{15}$N$_2$O$_2$^{79}Br^{81}Br calcd. 438.9480, observed 438.9463.

3.4.3.4. Synthesis of ring-fused dihalogenated benzimidazolequinones 9a-9f and 10a-10f using H$_2$O$_2$/HX

Reaction conditions are described in Scheme 3.26. H$_2$O$_2$ was added in one addition to anilines **5a-5f** in MeCN/HX at rt. The solution was cooled, Na$_2$CO$_3$ (sat. sol. 20 mL) added, and extracted with CH$_2$Cl$_2$ (5 × 20 mL). The combined organic extracts were dried (MgSO$_4$), evaporated to dryness, and purified by column chromatography with isocratic elution of pet. ether and EtOAc or CH$_2$Cl$_2$. Compound **10a** did not require purification.
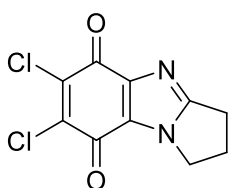
6,7-Dichloro-2,3-dihydro-1*H*-pyrrolo[1,2-*a*]benzimidazole-5,8-dione (9a): 0.187 g, 73%; orange solid; mp (dec. > 224 °C); R_f 0.31 (50:50 EtOAc / CH$_2$Cl$_2$); ν_{max} (neat, cm^{-1}) 2972, 1686 (C=O), 1670 (C=O), 1556, 1507, 1476, 1295, 1247, 1146, 1126, 1069; δ_H (400 MHz, CDCl$_3$) 2.76 (quint, *J* 7.6 Hz, 2H), 3.01 (t, *J* 7.6 Hz, 2H), 4.29 (t, *J* 7.6 Hz, 2H); δ_C (100 MHz, CDCl$_3$) 23.1, 26.4, 45.6 (all CH$_2$), 128.9, 139.5, 141.5, 145.7, 162.3 (all C), 168.1, 171.1 (both C=O); HRMS (ESI) *m/z* (M + H)$^+$, C$_{10}$H$_7$N$_2$O$_2$^{35}Cl$_2$ calcd. 256.9885, observed 256.9889.
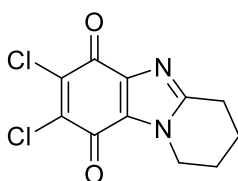
7,8-Dichloro-1,2,3,4-tetrahydropyrido[1,2-*a*]benzimidazole-6,9-dione (9b): 0.205 g, 76%; orange solid; mp 200-202 °C; R_f 0.46 (50:50 EtOAc / CH$_2$Cl$_2$); ν_{max} (neat, cm^{-1}) 2955, 2872, 1676 (C=O), 1528, 1509, 1476, 1243, 1157, 1139, 1085; δ_H (400 MHz, CDCl$_3$) 1.96-2.03 (m, 2H), 2.05-2.11 (m, 2H), 3.02 (t, *J* 6.4 Hz, 2H), 4.33 (t, *J* 6.2 Hz, 2H); δ_C (100 MHz, CDCl$_3$) 19.6, 22.1, 25.0, 45.9 (all CH$_2$), 129.5, 140.2, 140.8, 141.2, 153.6 (all C), 168.3, 171.3 (both C=O); HRMS (ESI) *m/z* (M + H)$^+$, C$_{11}$H$_9$N$_2$O$_2$ ^{35}Cl$_2$ calcd. 271.0041, observed 271.0047.
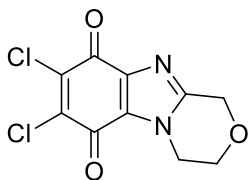
7,8-Dichloro-3,4-dihydro-1*H*-[1,4]oxazino[4,3-*a*]benzimidazole-6,9-dione **(9c):** 0.169 g, 62%; orange solid; mp 246-248 °C; R_f 0.48 (20:80 EtOAc / CH$_2$Cl$_2$); ν_{max} (neat, cm^{-1}) 3354, 2939, 2887, 1694 (C=O), 1674 (C=O), 1552, 1482, 1437, 1313, 1223, 1170, 1148, 1097; δ_H (400 MHz, DMSO-d$_6$) 4.04 (t, *J* 5.1 Hz, 2H), 4.28 (t, *J* 5.1 Hz, 2H), 4.89 (s, 2H, 1-CH$_2$); δ_C (100 MHz, DMSO-d$_6$) 45.3, 63.2 (both CH$_2$), 64.4 (1-CH$_2$), 130.6, 139.7, 140.4, 149.6 (all C), 168.3, 171.5 (both C=O); HRMS (ESI) *m/z* (M + H)$^+$, C$_{10}$H$_7$N$_2$O$_3$^{35}Cl$_2$ calcd. 272.9834, observed 272.9846.
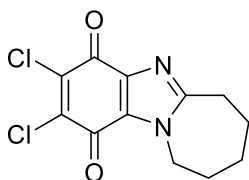
2,3-Dichloro-7,8,9,10-tetrahydro-4*H*-azepino[1,2-*a*]benzimidazole-1,4(6*H*)-dione (9d): 0.228 g, 80%; yellow solid; mp 168-170 °C; R_f 0.32 (50:50 EtOAc / pet. ether); ν_{max} (neat, cm^{-1}) 2929, 2850, 1673 (C=O), 1526, 1472, 1432, 1322, 1263, 1154, 1130; δ_H (400 MHz, CDCl$_3$) 1.73-1.93 (m, 6H), 3.04 (t, *J* 5.5 Hz, 2H), 4.59 (t, *J* 4.4 Hz, 2H); δ_C (100 MHz, CDCl$_3$) 24.7, 28.1, 29.4, 30.7, 46.5 (all CH$_2$), 129.8, 140.4, 140.6, 159.9 (all C), 168.8, 171.3 (both C=O); HRMS (ESI) *m/z* (M + H)$^+$, C$_{12}$H$_{11}$N$_2$O$_2$^{35}Cl$_2$ calcd. 285.0198, observed 285.0187.
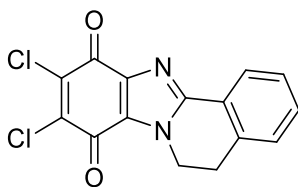
9,10-Dichloro-5,6-dihydrobenzimidazo[2,1-*a*]isoquinoline-8,11-dione **(9f):** 0.179 g, 56%; red solid; mp 296-298 °C; R_f 0.29 (20:80 EtOAc / pet. ether); ν_{max} (neat, cm^{-1}) 3400, 1688 (C=O), 1673 (C=O), 1563, 1522, 1491, 1467, 1427, 1321, 1276, 1217, 1169, 1148; δ_H (400 MHz, CDCl$_3$) 3.25 (t, *J* 7.1 Hz, 2H), 4.66 (t, *J* 7.1 Hz, 2H), 7.31 (d, *J* 7.3 Hz, 1H), 7.39-7.48 (m, 2H), 8.21 (dd, *J* 1.6, 7.6 Hz, 1H); δ_C (100 MHz, CDCl$_3$) 27.6, 42.8 (both CH$_2$), 124.6 (C), 126.2 (CH), 128.2 (2 × CH), 129.5 (C), 131.7 (CH), 133.8, 140.4, 141.2,

142.1, 150.8 (all C), 168.6, 171.3 (both C=O); HRMS (ESI) *m/z* (M + H)$^+$, C$_{15}$H$_9$N$_2$O$_2$^{35}Cl$_2$ calcd. 319.0041, observed 319.0030.
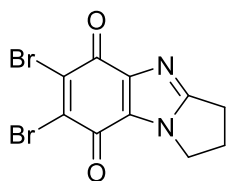
6,7-Dibromo-2,3-dihydro-1*H*-pyrrolo[1,2-*a*]benzimidazole-5,8-dione (10a): 0.280 g, 81%; orange solid; mp (dec. >218 °C); ν_{max} (neat, cm^{-1}) 3125, 3032, 2949, 1684 (C=O), 1657 (C=O), 1500, 1474, 1402, 1294, 1242, 1125; δ_H (400 MHz, CDCl$_3$) 2.76 (quint, *J* 7.5 Hz, 2H), 3.00 (t, *J* 7.5 Hz, 2H), 4.28 (t, *J* 7.5 Hz, 2H); δ_C (100 MHz, CDCl$_3$) 23.1, 26.4, 45.5 (all CH$_2$), 128.6, 138.0, 140.6, 145.4, 162.1 (all C), 168.0, 170.9 (both C=O); HRMS (ESI) *m/z* (M + H)$^+$, C$_{10}$H$_7$N$_2$O$_2$^{79}Br^{81}Br calcd 346.8854, observed 346.8856.
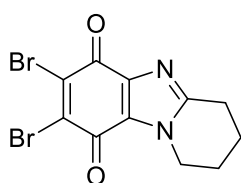
7,8-Dibromo-1,2,3,4-tetrahydropyrido[1,2-*a*]benzimidazole-6,9-dione (10b): 0.266 g, 74%; orange solid; mp 221-223 °C; R_f 0.41 (50:50 EtOAc / CH$_2$Cl$_2$); ν_{max} (neat, cm^{-1}) 2955, 2872, 1676 (C=O), 1528, 1509, 1476, 1243, 1157, 1139, 1085; δ_H (400 MHz, CDCl$_3$) 1.95-2.01 (m, 2H), 2.04-2.10 (m, 2H), 3.01 (t, *J* 6.4 Hz, 2H), 4.32 (t, *J* 6.2 Hz, 2H); δ_C (100 MHz, CDCl$_3$) 19.6, 22.1, 25.0, 45.9 (all CH$_2$), 129.3, 139.0, 139.7, 141.0, 153.4 (all C), 168.2, 171.2 (both C=O); HRMS (ESI) *m/z* (M + H)$^+$, C$_{11}$H$_9$N$_2$O$_2$^{79}Br^{81}Br calcd. 360.9010, observed 360.9009.
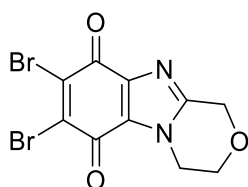
7,8-Dibromo-3,4-dihydro-1*H*-[1,4]oxazino[4,3-*a*]benzimidazole-6,9-dione (10c): 0.242 g, 67%; orange solid; mp (dec. >215 °C); R_f 0.35 (20:80 EtOAc / CH$_2$Cl$_2$); ν_{max} (neat, cm^{-1}) 2931, 2883, 1687 (C=O), 1667 (C=O), 1515, 1480, 1435, 1309, 1219, 1130, 1092; δ_H

(400 MHz, DMSO-d_6) 4.03 (t, J 4.7 Hz, 2H), 4.27 (t, J 4.7 Hz, 2H), 4.88 (s, 2H, 1-CH$_2$); δ_C (100 MHz, DMSO-d_6) 45.2, 63.2 (both CH$_2$), 64.4 (1-CH$_2$), 130.4, 138.9, 139.8, 140.1, 149.4 (all C), 168.5, 171.6 (both C=O); HRMS (ESI) m/z (M + H)$^+$, C$_{10}$H$_7$N$_2$O$_3$^{79}Br^{81}Br calcd. 362.8803, observed 362.8802.
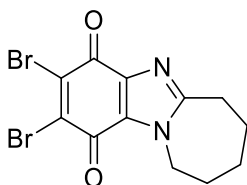
2,3-Dibromo-7,8,9,10-tetrahydro-4H-azepino[1,2-a]benzimidazole-1,4(6H)-dione (10d): 0.322 g, 86%; orange solid; mp 216-218 °C; R_f 0.32 (50:50 EtOAc / pet. ether); ν_{max} (neat, cm^{-1}) 2937, 1686 (C=O), 1666 (C=O), 1512, 1476, 1438, 1315, 1260, 1130, 1105; δ_H (400 MHz, CDCl$_3$) 1.69-1.90 (m, 6H), 2.99 (t, J 5.5 Hz, 2H), 4.54 (t, J 4.4 Hz, 2H); δ_C (100 MHz, CDCl$_3$) 24.7, 28.0, 29.3, 30.6, 46.4 (all CH$_2$), 129.5, 139.2, 139.5, 140.3, 159.7 (all C), 168.6, 171.1 (both C=O); HRMS (ESI) m/z (M + H)$^+$, C$_{12}$H$_{11}$N$_2$O$_2$^{79}Br^{81}Br calcd. 374.9167, observed 374.9156.
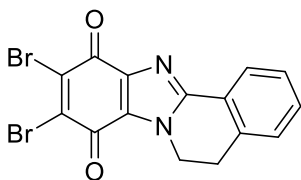
9,10-Dibromo-5,6-dihydrobenzimidazo[2,1-a]isoquinoline-8,11-dione (10f): 0.277 g, 68%; red solid; mp 274-276 °C; R_f 0.48 (CH$_2$Cl$_2$); ν_{max} (neat, cm^{-1}) 1679 (C=O), 1664 (C=O), 1517, 1490, 1491, 1459, 1437, 1424, 1279, 1238, 1126, 1107; δ_H (500 MHz, DMSO-d_6) 3.22 (t, J 7.1 Hz, 2H), 4.56 (t, J 7.1 Hz, 2H), 7.42-7.44 (m, 2H), 7.47-7.50 (m, 1H), 7.99-8.00 (m, 1H); δ_C (100 MHz, DMSO-d_6) 27.2, 42.7 (both CH$_2$), 125.0 (C), 125.4, 128.3, 129.0 (all CH), 130.4 (C), 131.7 (CH), 135.2, 139.3, 139.8, 141.3, 149.6 (all C), 168.8, 171.7 (both C=O); HRMS (ESI) m/z (M + H)$^+$, C$_{15}$H$_9$N$_2$O$_2$^{79}Br^{81}Br calcd. 408.9010, observed 408.8994.

3.4.3.5. Synthesis of ring-fused dihalogenated benzimidazolequinones using Cl_2 and Br_2

Reaction conditions are described in Table 3.2 and the relevant workup is detailed for each molecular halogen below:

For Cl_2: The solution was flushed through with N_2 gas, CH_2Cl_2 (40 mL) was added to the cooled solution and washed with brine (2 × 10 mL). The organic layer was dried ($MgSO_4$), evaporated to dryness, and purified by column chromatography with isocratic elution of pet. ether and EtOAc.

For Br_2: CH_2Cl_2 (40 mL) was added and the solution was washed with Na_2CO_3 (sat. sol., 5 × 20 mL). The organic layer was dried ($MgSO_4$), evaporated to dryness, and purified by column chromatography with isocratic elution of pet. ether and EtOAc.

3.4.3.6. The role of water in quinone formation using isotopic labeling with $H_2^{18}O$

Reaction conditions are described in Scheme 3.31 and the relevant workup is detailed for each molecular halogen below:

For Cl_2: The solution was flushed through with N_2 gas, CH_2Cl_2 (20 mL) was added to the cooled solution and washed with brine (2 mL). The organic layer was dried ($MgSO_4$), evaporated to dryness, and then the sample was evaluated using EI mass spectrometry.

For Br_2: CH_2Cl_2 (10 mL) was added and the solution was washed with Na_2CO_3 (sat. sol., 3 × 2 mL). The organic layer was dried ($MgSO_4$), and then the sample was evaluated using EI mass spectrometry.

3.4.3.7 Synthesis of 1-fluoro-2,5-dimethoxy-4-nitrobenzene 18
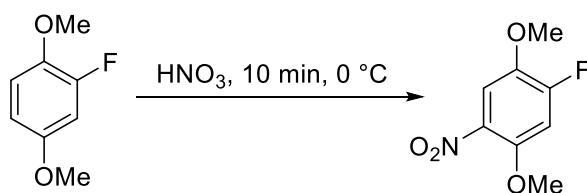
2-Fluoro-1,4-dimethoxybenzene (16.00 g, 0.10 mol) was slowly added to a stirred solution of HNO_3 (64-66%, 143 mL) at 0 °C. The solution was stirred for 10 min, poured onto ice water (600 mL), and stirred for 30 min. The precipitate was collected, washed with water, and dried to give the final product 1-fluoro-2,5-dimethoxy-4-nitrobenzene **18** (18.63 g, 90%), as a yellow solid; mp 116–118 °C; GC-EIMS m/z: 201 [M]$^+$ (100), 154 (48), 141 (39), 125 (65), 97 (68), 95 (48), 69 (34); v_{max} (neat, cm^{-1}) 3073, 2974, 2944, 1640, 1506 (NO_2), 1450, 1351 (NO_2), 1285, 1223, 1194, 1081, 1024; δ_H (400 MHz, $CDCl_3$) 3.90 (s, 3H, Me), 3.92 (s, 3H, Me), 6.88 (d, J 12.2 Hz, 1H, 6-H), 7.62 (d, J 9.2 Hz, 1H, 3-H); δ_C (100 MHz, $CDCl_3$) 57.0, 57.3 (both Me), 103.0 (d, J 24.8 Hz, 6-CH), 111.4 (d, J 3.8 Hz, 3-CH), 134.4 (4-C), 141.1 (d, J 11.4 Hz, C), 149.0 (d, J 9.5 Hz, C), 155.8 (d, J 255.5 Hz, 1-C). Anal. Calcd for $C_8H_8FNO_4$: C, 47.77; H, 4.01; N, 6.96. Found: C, 47.67; H, 3.92; N, 6.79.

3.4.3.8. Synthesis of *N*,*N*-dibutyl-2,5-dimethoxy-4-nitroaniline 20
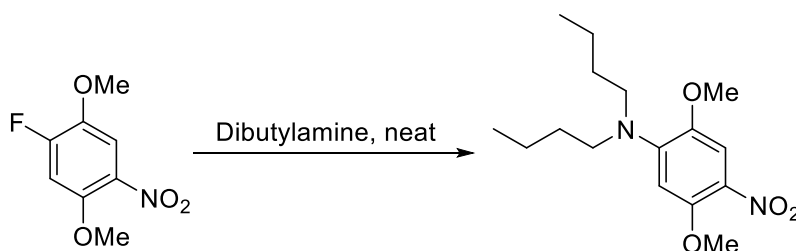
1-Fluoro-2,5-dimethoxy-4-nitrobenzene **18** (3.00 g, 14.9 mmol) was added as a solid to stirred neat dibutylamine (11.55 g, 89.6 mmol) at 120 °C. The mixture was maintained at 120 °C for 3 d with stirring until completion of the reaction. The excess dibutylamine was distilled off, EtOAc (60 mL) was added and the organic layer washed with brine (3 × 10 mL). The organic extract was dried ($MgSO_4$), evaporated to dryness, and purified by

column chromatography with isocratic elution of pet. ether and EtOAc to give *N,N*-dibutyl-2,5-dimethoxy-4-nitroaniline **20** (2.80 g, 60%) as a dark yellow oil; R_f 0.34 (10:90 EtOAc / pet. ether); v_{max} (neat, cm^{-1}); 2956, 2871, 1738, 1608, 1569, 1513, 1448, 1316, 1240, 1211, 1085, 1031; δ_H (400 MHz, CDCl$_3$) 0.92 (t, *J* 7.3 Hz, 6H), 1.26-1.36 (m, 4H), 1.52-1.59 (m, 4H), 3.33 (t, *J* 7.8 Hz, 4H), 3.81 (s, 3H), 3.91 (s, 3H), 6.27 (s, 1H), 7.56 (s, 1H); δ_C (100 MHz, CDCl$_3$) 14.0 (Me), 20.4, 29.9, 52.4 (all CH$_2$), 56.3, 56.8 (both Me), 101.4, 110.2 (both CH), 128.4, 143.7, 147.3, 151.2 (all C). HRMS (ESI) *m/z* (M + H)$^+$, C$_{16}$H$_{27}$N$_2$O$_4$ calcd. 311.1971, observed 311.1971.

3.4.3.9. Synthesis of 1,2,4-trimethoxy-5-nitrobenzene 23
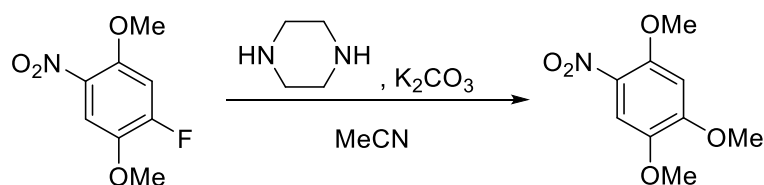
1-Fluoro-2,5-dimethoxy-4-nitrobenzene **18** (1.00 g, 4.98 mmol), piperazine (0.143 g, 1.66 mmol) and K$_2$CO$_3$ (0.920 g, 6.60 mmol) were stirred in MeCN (10 mL) at reflux for 25 h. EtOAc (20 mL) was added and the organic layer washed with brine (2 × 10 mL). The organic extract was dried (MgSO4), evaporated to dryness, and purified by column chromatography with isocratic elution of pet. ether and EtOAc to give 1,2,4-trimethoxy-5-nitrobenzene **23** (0.351 g, 33%) as a yellow solid; mp 130-132 °C (lit.[101] mp 126-127 °C); GC-EIMS m/*z:* 213 [M]$^+$ (100), 198 (29), 166 (16), 137 (37), 125 (19), 109 (34), 94 (13), 77(25), 66 (20), 53 (22); R_f 0.27 (30:70 EtOAc / pet. ether); v_{max} (neat, cm^{-1}); 3010, 2921, 1621, 1585, 1518, 1494, 1436, 1338, 1264, 1213, 1085, 1013; δ_H (400 MHz, CDCl$_3$) 3.84 (s, 3H), 3.93 (s, 3H), 3.94 (s, 3H), 6.52 (s, 1H), 7.51(s, 1H); δ_C (100 MHz, CDCl$_3$), 56.5, 56.6, 57.2 (all Me), 97.5, 108.9 (both CH), 130.8, 142.4, 150.5, 154.9 (all C).

3.5. Conclusions

The one-pot protocol of H_2O_2/HX facilitated dihalogenation and oxidative cyclizations of both ring-expanded and ring-contracted *o*-cycloamino substituted anilines to form the corresponding selectively halogenated benzimidazoles, avoiding the requirement of late-stage halogenation.

H_2O_2/HX has led to an unprecedented one-pot 6-electron oxidative transformation to yield a new series of ring-fused dihalogenated benzimidazolequinones. The reaction follows the order of halogenation, cyclization and oxidative demethylation as shown by reaction profiling of 2-(3,4-dihydroisoquinolin-2(1*H*)-yl)-3,6-dimethoxyaniline **5f** with HPLC and HRMS. Halogenation was regioselective onto the aromatic ethers for the THIQ analogues in the presence of an additional fused aromatic ring. The molecular halogens (X_2) with added water were capable of oxidizing 3,6-dimethoxy-2-(cycloamino)anilines to the corresponding dihalogenated benzimidazolequinones in comparable yields to the H_2O_2/HX methodology. H_2O_2/HCl produces Cl_2 in situ and it is the active species in the oxidative transformation of 3,6-dimethoxy-2-(cycloamino)anilines due to the inability of HCl to demethylate aromatic ethers. On the other hand, Br_2 generated in situ from H_2O_2/HBr, alongside the demethylating agent of HBr are likely to be the active species in the analogous oxidative transformation. Isotopic labeling with $H_2^{18}O$ formed doubly labeled dihalogenated benzimidazolequinones and proved that the oxidation of aromatic ethers with either Cl_2 or Br_2 proceeds through a one-step mechanism involving hydroxylation. The H_2O_2/HX protocol was found to be tunable by adjusting the molar ratio of HX relative to H_2O_2. The selective formation of a new series of ring-fused dihalogenated dimethoxybenzimidazoles was achieved without additional oxidation to the quinone when a higher molar ratio of H_2O_2 relative to HX was employed.

As part of a potential route towards biologically relevant 1,2-acyclic substituted benzimidazolequinones, nitration of 2-fluoro-1,4-dimethoxybenzene unexpectedly formed the *p*-nitrated product 1-fluoro-2,5-dimethoxy-4-nitrobenzene **18** exclusively. The nitrated compound was capable of undergoing nucleophilic substitution with dibutylamine and when **18** was used in excess facilitated the introduction of a methoxy group.

3.6. Future work

The pyrido[1,2-*a*]benzimidazolequinones (Table 3.3) were more easily reduced when substituted with halogen groups relative to the non-halogenated analogue in cyclic voltammetry studies. Fluorine is the most electronegative in the halogen series and therefore its introduction on a benzimidazolequinone motif could produce quinones that are highly activated towards NQO1 due to possible ease of reduction. In addition, fluorine atoms are highly prevalent on pharmaceutical drugs as they improve metabolic stability, enhance physicochemical properties and alter bioavailability.[102] Unfortunately, the electrophilic fluorination of aromatics with hydrofluoric acid (HF) and H_2O_2 is not possible due to the high oxidation potential of HF.[31]

Alternative electrophilic fluorine sources such as 1-(chloromethyl)-4-fluoro-1,4-diazabicyclo[2.2.2]octane-1,4-diium ditetrafluoroborate (Selectfluor) could be used to carry out the oxidative transformation of 3,6-dimethoxy-2-(cycloamino)anilines via a sequence of cyclization, fluorination and oxidative demethylation (Scheme 3.41). Selectfluor is considered a stable and hazard-free source of fluorine in contrast to other hazardous and toxic sources of electrophilic fluorine such as F_2, $FClO_3$, CF_3OF and XeF_2.[103] Selectfluor has dual functionality and apart from fluorination can participate in the oxidations of aromatic ethers,[104] phenols, alcohols, oxidative iodination of aromatics, ring-opening of epoxides and deprotection of functional groups.[105] Selectfluor is the reagent of choice in the pharmaceutical industry with approximately 80% of all steroids fluorinated with it.[106]
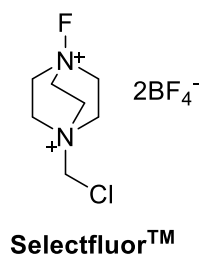
Scheme 3.41. Selectfluor as a proposed electrophilic source of fluorine to form fluorinated benzimidazolequinones.

3.7. References

1. Xu, Z.; Liu, Z.; Chen, T.; Chen, T.; Wang, Z.; Tian, G.; Shi, J.; Wang, X.; Lu, Y.; Yan, X.; Wang, G.; Jiang, H.; Chen, K.; Wang, S.; Xu, Y.; Shen, J.; Zhu, W. *J. Med. Chem.* **2011**, *54*, 5607-5611.

2. Jeschke, P. *Pest Manage. Sci.* **2010**, *66*, 10-27.

3. Herrera-Rodriguez, L. N.; Khan, F.; Robins, K. T.; Meyer, H.-P., Perspectives on biotechnological halogenation Part I: Halogenated products and enzymatic halogenation. *Chim. Oggi – Chem. Today* Jul/Aug, 2011, pp 31-33.

4. Hernandes, M. Z.; Cavalcanti, S. M. T.; Moreira, D. R. M.; de Azevedo, W. F., Jr.; Leite, A. C. L. *Curr. Drug Targets* **2010**, *11*, 303-314.

5. Xu, Z.; Yang, Z.; Liu, Y.; Lu, Y.; Chen, K.; Zhu, W. *J. Chem. Inf. Model.* **2014**, *54*, 69-78.

6. Wilcken, R.; Liu, X.; Zimmermann, M. O.; Rutherford, T. J.; Fersht, A. R.; Joerger, A. C.; Boeckler, F. M. *J. Am. Chem. Soc.* **2012**, *134*, 6810-6818.

7. Wilcken, R.; Zimmermann, M. O.; Lange, A.; Joerger, A. C.; Boeckler, F. M. *J. Med. Chem.* **2013**, *56*, 1363-1388.

8. Cavallo, G.; Metrangolo, P.; Milani, R.; Pilati, T.; Priimagi, A.; Resnati, G.; Terraneo, G. *Chem. Rev.* **2016**, *116*, 2478-2601.

9. Ding, X.; Tuikka, M.; Matti, H., Halogen Bonding in Crystal Engineering, Recent Advances in Crystallography. In *IntechOpen*; Benedict, J. B., Ed. 2012.

10. Koskinen, L.; Hirva, P.; Kalenius, E.; Jääskeläinen, S.; Rissanen, K.; Haukka, M. *CrystEngComm* **2015**, *17*, 1231-1236.

11. Clark, T.; Hennemann, M.; Murray, J. S.; Politzer, P. *J. Mol. Model.* **2007**, *13*, 291-296.

12. Lu, Y.; Wang, Y.; Zhu, W. *Phys. Chem. Chem. Phys.* **2010**, *12*, 4543-4551.

13. Lu, Y.-X.; Zou, J.-W.; Fan, J.-C.; Zhao, W.-N.; Jiang, Y.-J.; Yu, Q.-S. *J. Comput. Chem.* **2009**, *30*, 725-732.

14. Sirimulla, S.; Bailey, J. B.; Vegesna, R.; Narayan, M. *J. Chem. Inf. Model.* **2013**, *53*, 2781-2791.

15. Huynh, M. T.; Anson, C. W.; Cavell, A. C.; Stahl, S. S.; Hammes-Schiffer, S. *J. Am. Chem. Soc.* **2016**, *138*, 15903-15910.

16. Kunz, K. R.; Iyengar, B. S.; Dorr, R. T.; Alberts, D. S.; Remers, W. A. *J. Med. Chem.* **1991**, *34*, 2281-2286.

17. Koyama, J.; Morita, I.; Yamori, T. *Molecules* **2010**, *15*, 6559-6569.

18. Lynch, M.; Hehir, S.; Kavanagh, P.; Leech, D.; O'Shaughnessy, J.; Carty, M. P.; Aldabbagh, F. *Chem. Eur. J.* **2007**, *13*, 3218-3226.

19. Cotterill, A. S.; Moody, C. J.; Mortimer, R. J.; Norton, C. L.; O'Sullivan, N.; Stephens, M. A.; Stradiotto, N. R.; Swann, E.; Stratford, I. J. *J. Med. Chem.* **1994**, *37*, 3834-3843.

20. Ryu, C.-K.; Song, E.-H.; Shim, J.-Y.; You, H.-J.; Choi, K. U.; Choi, I. H.; Lee, E. Y.; Chae, M. J. *Bioorg. Med. Chem. Lett.* **2003**, *13*, 17-20.

21. Garuti, L.; Roberti, M.; Malagoli, M.; Rossi, T.; Castelli, M. *Bioorg. Med. Chem. Lett.* **2000**, *10*, 2193-2195.

22. Ibis, C.; Tuyun, A. F.; Bahar, H.; Ayla, S. S.; Stasevych, M. V.; Musyanovych, R. Y.; Komarovska-Porokhnyavets, O.; Novikov, V. *Med. Chem. Res.* **2014**, *23*, 2140-2149.

23. Entwistle, I. D.; Williams, P. J.; Devlin, B. R. J. Certain Benzotriazole-4,7-dione Derivatives. U.S. Patent 3952003A, April 20, 1976.

24. Louvis, A. d. R.; Silva, N. A. A.; Semaan, F. S.; da Silva, F. d. C.; Saramago, G.; de Souza, L. C. S. V.; Ferreira, B. L. A.; Castro, H. C.; Salles, J. P.; Souza, A. L. A.; Faria, R. X.; Ferreira, V. F.; Martins, D. d. L. *New J. Chem.* **2016**, *40*, 7643-7656.

25. Rao, M. L. N.; Giri, S. *RSC Adv.* **2012**, *2*, 12739-12750.

26. Fahey, K.; O'Donovan, L.; Carr, M.; Carty, M. P.; Aldabbagh, F. *Eur. J. Med. Chem.* **2010**, *45*, 1873-1879.

27. Sivey, J. D.; McCullough, C. E.; Roberts, A. L. *Environ. Sci. Technol.* **2010**, *44*, 3357-3362.

28. Ben-Daniel, R.; de Visser, S. P.; Shaik, S.; Neumann, R. *J. Am. Chem. Soc.* **2003**, *125*, 12116-12117.

29. Eigen, M.; Kustin, K. *J. Am. Chem. Soc.* **1962**, *84*, 1355-1361.

30. Beckwith, R. C.; Wang, T. X.; Margerum, D. W. *Inorg. Chem.* **1996**, *35*, 995-1000.

31. Podgoršek, A.; Zupan, M.; Iskra, J. *Angew. Chem., Int. Ed.* **2009**, *48*, 8424-8450.

32. Vyas, P. V.; Bhatt, A. K.; Ramachandraiah, G.; Bedekar, A. V. *Tetrahedron Lett.* **2003**, *44*, 4085-4088.

33. Bogdal, D.; Lukasiewicz, M.; Pielichowski, J. *Green Chem.* **2004**, *6*, 110-113.

34. Koini, E. N.; Avlonitis, N.; Calogeropoulou, T. *Synlett* **2011**, *2011*, 1537-1542.

35. Barhate, N. B.; Gajare, A. S.; Wakharkar, R. D.; Bedekar, A. V. *Tetrahedron* **1999**, *55*, 11127-11142.

36. Mukhopadhyay, S.; Ananthakrishnan, S.; Chandalia, S. B. *Org. Process Res. Dev.* **1999**, *3*, 451-454.

37. Bhatkhande, B. S.; Adhikari, M. V.; Samant, S. D. *Ultrason. Sonochem.* **2002**, *9*, 31-35.

38. Podgoršek, A.; Stavber, S.; Zupan, M.; Iskra, J. *Tetrahedron* **2009**, *65*, 4429-4439.

39. Jones, C. W.; Clark, J. H., Activation of hydrogen peroxide using inorganic and organic species. In *Applications of Hydrogen Peroxide and Derivatives*, The Royal Society of Chemistry 1999; pp 37-78.

40. Jain, S. L.; Sharma, V. B.; Sain, B. *Tetrahedron Lett.* **2004**, *45*, 8731-8732.

41. Bahrami, K.; Khodaei, M. M.; Kavianinia, I. *Synthesis* **2007**, *2007*, 547-550.

42. Voudrias, E. A.; Reinhard, M. *Environ. Sci. Technol.* **1988**, *22*, 1049-1056.

43. Parr, R. G.; Szentpály, L. v.; Liu, S. *J. Am. Chem. Soc.* **1999**, *121*, 1922-1924.

44. Büchel, K. H., Herbizide Trifluormethyl-benzimidazole. In *Zeitschrift für Naturforschung B*. 1970; Vol. 25b, p 934.

45. Kuznetsov, Y. V.; Stolyarova, L. G.; Lezina, V. P.; Smirnov, L. D. *Bull. Acad. Sci. USSR, Div. Chem. Sci.* **1989**, *38*, 1494-1500.

46. Gurry, M.; Sweeney, M.; McArdle, P.; Aldabbagh, F. *Org. Lett.* **2015**, *17*, 2856-2859.

47. Skibo, E. B.; Jamil, A.; Austin, B.; Hansen, D.; Ghodousi, A. *Org. Biomol. Chem.* **2010**, *8*, 1577-1587.

48. Moriarty, E.; Carr, M.; Bonham, S.; Carty, M. P.; Aldabbagh, F. *Eur. J. Med. Chem.* **2010**, *45*, 3762-3769.

49. O'Donovan, L.; Carty, M. P.; Aldabbagh, F. *Chem. Commun.* **2008**, 5592-5594.

50. Gellis, A.; Kovacic, H.; Boufatah, N.; Vanelle, P. *Eur. J. Med. Chem.* **2008**, *43*, 1858-1864.

51. Chung, K.-H.; Hong, S.-Y.; You, H.-J.; Park, R.-E.; Ryu, C.-K. *Bioorg. Med. Chem.* **2006**, *14*, 5795-5801.

52. Antonini, I.; Claudi, F.; Cristalli, G.; Franchetti, P.; Grifantini, M.; Martelli, S. *J. Med. Chem.* **1988**, *31*, 260-264.

53. Sweeney, M.; Gurry, M.; Keane, L.-A. J.; Aldabbagh, F. *Tetrahedron Lett.* **2017**, *58*, 3565-3567.

54. Weinberger, L.; Day, A. R. *J. Org. Chem.* **1959**, *24*, 1451-1455.

55. Musgrave, O. C. *Chem. Rev.* **1969**, *69*, 499-531.

56. Snyder, C. D.; Rapoport, H. *J. Am. Chem. Soc.* **1972**, *94*, 227-231.

57. Dao, P. D. Q.; Ho, S. L.; Cho, C. S. *ACS Omega* **2018**, *3*, 5643-5653.

58. Joyce, E.; McArdle, P.; Aldabbagh, F. *Synlett* **2011**, *2011*, 1097-1100.

59. Jacob, P.; Callery, P. S.; Shulgin, A. T.; Castagnoli, N. *J. Org. Chem.* **1976**, *41*, 3627-3629.

60. Naciuk, F. F.; Castro, J. A. M.; Serikava, B. K.; Miranda, P. C. M. L. *ChemistrySelect* **2018**, *3*, 436-439.

61. Tomatsu, A.; Takemura, S.; Hashimoto, K.; Nakata, M. *Synlett* **1999**, *1999*, 1474-1476.

62. Kim, D. W.; Choi, H. Y.; Lee, K.-J.; Chi, D. Y. *Org. Lett.* **2001**, *3*, 445-447.

63. Tohma, H.; Morioka, H.; Harayama, Y.; Hashizume, M.; Kita, Y. *Tetrahedron Lett.* **2001**, *42*, 6899-6902.

64. Love, B. E.; Bonner-Stewart, J.; Forrest, L. A. *Synlett* **2009**, *2009*, 813-817.

65. Fahey, K.; Aldabbagh, F. *Tetrahedron Lett.* **2008**, *49*, 5235-5237.

66. Skibo, E. B.; Islam, I.; Schulz, W. G.; Zhou, R.; Bess, L.; Boruah, R. *Synlett* **1996**, 297-309.

67. Zhou, R.; Skibo, E. B. *J. Med. Chem.* **1996**, *39*, 4321-4331.

68. Orita, H.; Shimizu, M.; Hayakawa, T.; Takehira, K. *Bull. Chem. Soc. Jpn.* **1989**, *62*, 1652-1657.

69. Conte, M.; Davies, C. J.; Morgan, D. J.; Davies, T. E.; Elias, D. J.; Carley, A. F.; Johnston, P.; Hutchings, G. J. *J. Catal.* **2013**, *297*, 128-136.

70. Tilstam, U.; Weinmann, H. *Org. Process Res. Dev.* **2002**, *6*, 384-393.

71. Trost, B. M. *Acc. Chem. Res.* **2002**, *35*, 695-705.

72. Zhang, M.-R.; Kumata, K.; Maeda, J.; Haradahira, T.; Noguchi, J.; Suhara, T.; Halldin, C.; Suzuki, K. *J. Med. Chem.* **2007**, *50*, 848-855.

73. Westerhoff, P.; Chao, P.; Mash, H. *Water Res.* **2004**, *38*, 1502-1513.

74. Sivey, J. D.; Arey, J. S.; Tentscher, P. R.; Roberts, A. L. *Environ. Sci. Technol.* **2013**, *47*, 1330-1338.

75. Criquet, J.; Rodriguez, E. M.; Allard, S.; Wellauer, S.; Salhi, E.; Joll, C. A.; von Gunten, U. *Water Res.* **2015**, *85*, 476-486.

76. Hammershøj, P.; Reenberg, T. K.; Pittelkow, M.; Nielsen, C. B.; Hammerich, O.; Christensen, J. B. *Eur. J. Org. Chem.* **2006**, *2006*, 2786-2794.

77.   Nguyen, T. B.; Ermolenko, L.; Al-Mourabit, A. *Chem. Commun.* **2016**, *52*, 4914-4917.

78.   Conboy, D.; Mirallai, S. I.; Craig, A.; McArdle, P.; Al-Kinani, A. A.; Barton, S.; Aldabbagh, F. *J. Org. Chem.* **2019**, *84*, 9811-9818.

79.   Boovanahalli, S. K.; Kim, D. W.; Chi, D. Y. *J. Org. Chem.* **2004**, *69*, 3340-3344.

80.   Schmid, C. R.; Beck, C. A.; Cronin, J. S.; Staszak, M. A. *Org. Process Res. Dev.* **2004**, *8*, 670-673.

81.   Leonard, J.; Lygo, B.; Procter, G., *Advanced Practical Organic Chemistry*. CRC Press: Boca Raton, FL, 2013.

82.   Cum, G.; de la Mare, P. B. D.; Johnson, M. D. *J. Chem. Soc. C* **1967**, 1590-1598.

83.   Elwood, C. Evaluation of the redox properties of novel anti-cancer drugs - towards structure activity relationships. M.Sc. Thesis, National University of Ireland, Galway, Galway, Ireland, 2017.

84.   Fagan, V.; Bonham, S.; Carty, M. P.; Saenz-Méndez, P.; Eriksson, L. A.; Aldabbagh, F. *Bioorg. Med. Chem.* **2012**, *20*, 3223-3232.

85.   Taleb, A.; Alvarez, F.; Nebois, P.; Walchshofer, N. *Heterocycl. Commun.* **2006**, *12*, 111-114.

86.   Gurry, M. The benign synthesis of bioactive heterocycles using photochemistry and hydrogen peroxide with hydrohalic acids. NUI Galway, Galway, Ireland, 2016.

87.   ChemSpace Products. https://chem-space.com/ (accessed Jul 17, 2019).

88.   Laali, K. K. *Coord. Chem. Rev.* **2000**, *210*, 47-71.

89.   Shopsowitz, K.; Lelj, F.; MacLachlan, M. J. *J. Org. Chem.* **2011**, *76*, 1285-1294.

90.   Lin, Y.; Li, M.; Ji, X.; Wu, J.; Cao, S. *Tetrahedron* **2017**, *73*, 1466-1472.

91.   Clayden, J.; Greeves, N.; Warren, S.; Wothers, P., Organic Chemistry. 1st ed.; Oxford University Press: Oxford, 2001; pp 593-594.

92.   Beyki, K.; Haydari, R.; Maghsoodlou, M. T. *SpringerPlus* **2015**, *4*, 757.

93.   Keegstra, M. A.; Peters, T. H. A.; Brandsma, L. *Synth. Commun.* **1990**, *20*, 213-216.

94.   Kawakami, T.; Suzuki, H. *J. Chem. Soc., Perkin Trans. 1* **2000**, 1259-1264.

95.   Chou, T.-Y.; Vouros, P.; David, M.; Saha, M.; Giese, R. W. *Biomed. Environ. Mass Spectrom.* **1987**, *14*, 23-27.

96.   Sweeney, M.; McArdle, P.; Aldabbagh, F. *Molbank* **2018**, *2018*, M984.

97.   Sheldrick, G. *Acta Crystallogr., Sect. A: Found. Adv.* **2015**, *71*, 3-8.

98.   Sheldrick, G. *Acta Crystallogr., Sect. C: Struct. Chem.* **2015**, *71*, 3-8.

99.   McArdle, P. *J. Appl. Crystallogr.* **2017**, *50*, 320-326.

100.   Mustroph, H.; Haessner, R. *J. prakt. Chem.* **1989**, *331*, 319-323.

101.   Blatchly, J. M.; Green, R. J. S.; McOmie, J. F. W.; Searle, J. B. *J. Chem. Soc. C* **1969**, 1353-1358.

102.   Purser, S.; Moore, P. R.; Swallow, S.; Gouverneur, V. *Chem. Soc. Rev.* **2008,** *37*, 320-330.

103.   Nyffeler, P. T.; Durón, S. G.; Burkart, M. D.; Vincent, S. P.; Wong, C.-H. *Angew. Chem., Int. Ed.* **2005**, *44*, 192-212.

104.   Stavber, G.; Zupan, M.; Jereb, M.; Stavber, S. *Org. Lett.* **2004**, *6*, 4973-4976.

105.   Stavber, S. *Molecules* **2011**, *16*, 6432-6464.

106.   Banks, E. Safer, cheaper fluorination – a boon for pharmaceutical manufacturing. https://www.chemistry.manchester.ac.uk/research/impact/safer-cheaper-fluorination/ (accessed Jul 31, 2019).

Chapter 4

Evaluation of Benzo[1,2,4]triazin-7-ones as Thioredoxin Reductase (TrxR) Inhibitors and their Anti-cancer Activity

The material in this Chapter has been published as part of:

Discovery of anti-cancer activity for benzo[1,2,4]triazin-7-ones: Very strong correlation to pleurotin and thioredoxin reductase inhibition

CrossMark

Martin Sweeney [a,†], Robert Coyle [a,†], Paul Kavanagh [a], Andrey A. Berezin [b], Daniele Lo Re [b], Georgia A. Zissimou [b], Panayiotis A. Koutentis [b], Michael P. Carty [c,*], Fawaz Aldabbagh [a,*]

[a] School of Chemistry, National University of Ireland Galway, University Road, Galway, Ireland
[b] Department of Chemistry, University of Cyprus, PO Box 20537, 1678 Nicosia, Cyprus
[c] Centre of Chromosome Biology, Biochemistry, School of Natural Sciences, National University of Ireland Galway, University Road, Galway, Ireland

ARTICLE INFO

ABSTRACT

The thioredoxin (Trx)–thioredoxin reductase (TrxR) system plays a key role in maintaining the cellular redox balance with Trx being over-expressed in a number of cancers. Inhibition of TrxR is an important strategy for anti-cancer drug discovery. The natural product pleurotin is a well-known irreversible inhibitor of TrxR. The cytotoxicity data for benzo[1,2,4]triazin-7-ones showed very strong correlation (Pearson correlation coefficients ~0.8) to pleurotin using National Cancer Institute COMPARE analysis. A new 3-CF$_3$ substituted benzo[1,2,4]triazin-7-one gave submicromolar inhibition of TrxR, although the parent compound 1,3-diphenylbenzo[1,2,4]triazin-7-one was more cytotoxic against cancer cell lines. Benzo-[1,2,4]triazin-7-ones exhibited different types of reversible inhibition of TrxR, and cyclic voltammetry showed characteristic quasi-reversible redox processes. Cell viability studies indicated strong dependence of cytotoxicity on substitution at the 6-position of the 1,3-diphenylbenzo[1,2,4]triazin-7-one ring.

The TrxR inhibition study assays were solely carried out by the author of this thesis. The cytotoxicity assays performed by the author of this thesis are denoted by the symbol: † and the remaining cytotoxicity assays were performed as part of the thesis of Robert Coyle (PhD, NUI Galway 2014).

molecules **MDPI**

Article

Anti-Cancer Activity of Phenyl and Pyrid-2-yl 1,3-Substituted Benzo[1,2,4]triazin-7-ones and Stable Free Radical Precursors

Lee-Ann J. Keane [1], Styliana I. Mirallai [1], Martin Sweeney [1], Michael P. Carty [2], Georgia A. Zissimou [3], Andrey A. Berezin [3], Panayiotis A. Koutentis [3] and Fawaz Aldabbagh [1,4,*]

[1] School of Chemistry, National University of Ireland Galway, University Road, H91 TK3 Galway, Ireland; l.keane19@nuigalway.ie (L-A.J.K.); styliana.mirallai@nuigalway.ie (S.I.M.); m.sweeney5@nuigalway.ie (M.S.)
[2] Biochemistry, School of Natural Sciences, National University of Ireland Galway, University Road, H91 TK33 Galway, Ireland; michael.carty@nuigalway.ie
[3] Department of Chemistry, University of Cyprus, P.O. Box 20537, Nicosia 1678, Cyprus; zissimou.georgia@ucy.ac.cy (G.A.Z.); berezin@ucy.ac.cy (A.A.B.); koutenti@ucy.ac.cy (P.A.K.)
[4] Department of Pharmacy, School of Life Sciences, Pharmacy and Chemistry, Kingston University, Penrhyn Road, Kingston upon Thames, KT1 2EE, UK
[*] Correspondence: f.aldabbagh@kingston.ac.uk; Tel.: +44-20-8417-2528

Abstract: Cell viability studies for benzo[1,2,4]triazin-7-ones and 1,2,4-benzotriazinyl (Blatter-type) radical precursors are described with comparisons made with 2,2,6,6-tetramethyl-1-piperidinyloxy (TEMPO). All of the stable free radicals were several orders of magnitude less cytotoxic than the benzo[1,2,4] triazin-7-ones. The synthesis and evaluation of two new pyrid-2-yl benzo[1,2,4] triazin-7-ones are described, where altering the 1,3-substitution from phenyl to pyrid-2-yl increased cytotoxicity against most cancer cell lines, as indicated using National Cancer Institute (NCI) one-dose testing. COMPARE analysis of five-dose testing data from the NCI showed very strong correlations to the naturally occurring anti-cancer compound pleurotin. COMPARE is program, which analyzes similarities in cytotoxicity data of compounds, and enables quantitative expression as Pearson correlation coefficients. Compounds were also evaluated using the independent MTT assay, which was compared with SRB assay data generated at the NCI.

The author of this thesis analyzed the data of **3a** & **3b** generated from the COMPARE program and DTP-NCI 60 cell line screen with findings presented in Section 4.3.6 of this Chapter.

4.1. Introduction

4.1.1. Synthesis of 1,3-diphenylbenzo[1,2,4]triazin-7-ones

1,3-Diphenylbenzo[1,2,4]triazin-7-one **1a** was first identified in the late 1960s, as a minor product when chloranil was used as a hydrogen acceptor to improve the yield of 4-dihydro-7-methoxy-1,3-diphenyl-1,2,4-benzotriazin-4-yl radical, starting from 4-methoxyphenyliminotriphenylphosphorane (Scheme 4.1).[1]
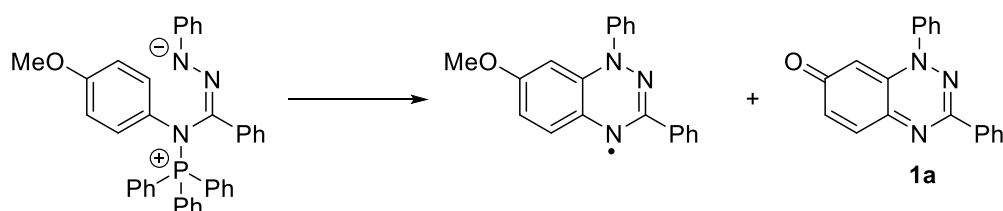
Scheme 4.1. The first isolation of 1,3-diphenylbenzo[1,2,4]triazin-7-one **1a**.[1]

In 1980, Neugebauer isolated **1a** in low yields by the treatment of Blatter's radical with an excess of toxic mercury(II) oxide[2] and other preparations involved expensive oxidants such as silver(II) oxide.[3] More recently, our collaborator from the University of Cyprus, prepared Blatter's radical in a yield of 87% starting from *N*-phenylamidrazone that underwent oxidative cyclization using palladium-on-carbon and 1,8-diazabicyclo[5.4.0]undec-7-ene (DBU) in air (Scheme 4.2).[4] The Blatter radical is air, moisture, and thermally stable with known redox behaviour.[5]
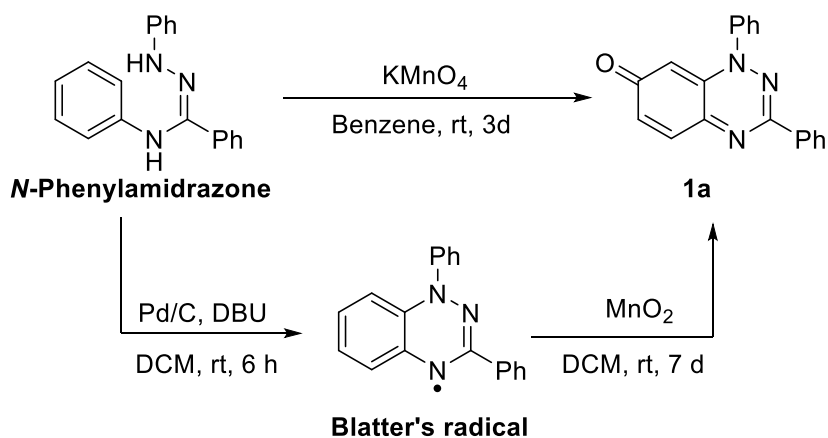
Scheme 4.2. Synthesis of 1,3-diphenylbenzo[1,2,4]triazin-7-one **1a**.[4-6]

The benzotriazinone **1a** was prepared in a high yield of 82% by oxidation of Blatter's radical with MnO_2 in DCM over 7 d (Scheme 4.2).[6] Alternatively, the benzotriazinone **1a** can be formed in 82% yield directly from the *N*-phenylamidrazone precursor using the oxidant of $KMnO_4$ albeit in the carcinogenic solvent, benzene (Scheme 4.2).[4] The Koutentis group have for the first time prepared benzotriazinone derivatives on a multi-gram scale allowing the rich chemistry of these heterocyclic iminoquinones to be explored.[4, 6-10] The 1-phenyl-3-(trifluoromethyl)benzo[1,2,4]triazin-7-one **2** is similarly accessible by mild MnO_2 oxidation of the analogous trifluoromethyl substituted radical **I** (Scheme 4.3).[7]
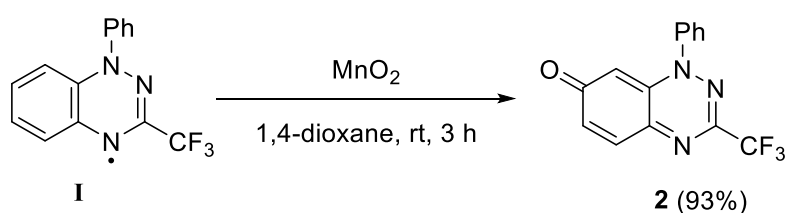
Scheme 4.3. Synthesis of 1-phenyl-3-(trifluoromethyl)benzo[1,2,4]triazin-7-one **2**.

A library of benzotriazinones (**1b-1l**) was formed through the regioselective nucleophilic addition of oxygen and nitrogen based nucleophiles onto the C-6 position of **1a** (Scheme 4.4).[6, 11, 12] Selectivity at C-6 was supported by computational studies and the anionic resonance stabilization across the triazine nitrogens of N-2 and N-4 (Scheme 4.4).[6]
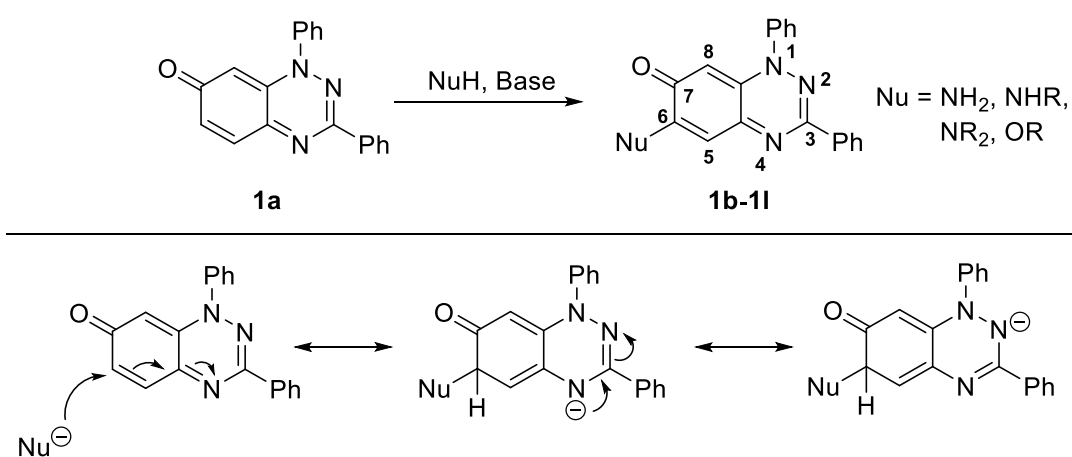
Scheme 4.4. Regioselective nucleophilic addition at C-6 position of benzotriazinone **1a**.[6]

The Benzotriazinone **1a** and its derivatives have been identified as multi-target inhibitors in Alzheimer's disease of beta-amyloid (Aβ) aggregation and acetyl-(AChE)/butyryl-

(BChE) cholinesterase.[11] The planar benzotriazinones act as β-sheet disrupting agents and protonatable amine derivatives interact with the catalytic site of cholinesterases to produce inhibitory effects.[11] The Alddabagh group produced derivatives of imidazo[5,4-*f*]benzimidazolequinones containing the iminoquinone moiety. As previously discussed (Chapter 1, Figure 1.5), dipyridoiminoquinone (DPIQ) displayed high specificity towards the prostate cancer cell line (DU-145) over normal cell lines (GM00367) and was shown to have good specificity towards NAD(P)H:quinone oxidoreductase 1 (NQO1) using National Cancer Institute (NCI) COMPARE analysis.[13, 14]

4.1.2. National Cancer Institute (NCI) -60 DTP human tumour cell line screen

In 1985, the NCI decided to develop a new anti-cancer screening program based on human solid tumours instead of the previously murine based system that only led to drug candidates through clincal trial and error.[15] The aim of the NCI high-throughput screen was to identify tumour specific drug candidates and became operational in 1990 under the Development Therapeutics program (DTP).[15-17] The NCI employs a panel of 60 human tumour cell lines that represent nine major diseases of leukemia, melanoma, lung, colon, CNS, ovarian, renal, prostate, and breast cancers.[16] The NCI-60 uses the Sulforhodamine B (SRB) assay to screen the in vitro cytotoxicity (Figure 4.1).[18, 19] SRB determines the cellular protein content after 48 h of incubation with the drug candidate.
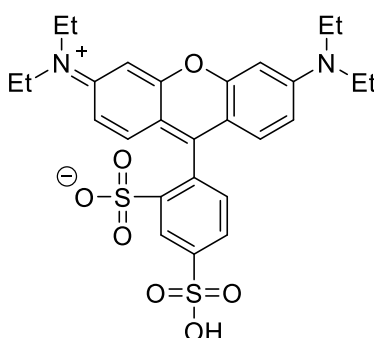
Figure 4.1. The aminoxanthene Sulforhodamine B (SRB) dye.

There are two stages involved for a potential drug candidate at the NCI-60 in vitro screening. Initially, 10 μM of the drug candidate is tested at the one-dose stage against all 60 cell lines. The one-dose graph represents growth relative to the untreated cells, and relative to time zero number of cells when the drug candidate is first added. The graph ranges from 100% growth (uninhibited) to -100% growth (lethality, all cells present at time zero are killed). If the drug candidate meets the selection criteria of approximately 60%[20] mean growth against all 60 cell lines, the candidate is forwarded for testing at the five-dose stage.

Five-dose testing involves treating the 60 cell line panel with the drug candidate at a range of concentrations (0.01 μM to 100 μM) from which a dose-response curve is generated (Figure 4.2). The end point values of Growth Inhibition (GI_{50}), Total Growth Inhibition (TGI), and Lethal Concentration (LC_{50}) are then determined from the dose-response curve.

154

The three end-points are defined and graphically represented on the five-dose response curve in Figure 4.2. If the percentage growth of the three reference levels (+50%, 0%, -50%) for a particular cell line is not met or exceeded, then the given end point (i.e. GI_{50}) is assigned either the lowest or highest concentration tested.[21] The NCI replaced the IC_{50} value with GI_{50} in order to account for the cell count at time zero when the drug is first added.[22] IC_{50} and GI_{50} both represent the drug concentration required to inhibit cell growth by 50% but are described by different parameters and results in similar but distinct values.

- **GI_{50}**: concentration at which growth is inhibited by 50% relative to untreated cells.

- **TGI**: concentration at which growth is completely inhibited i.e. cytostatic effect.

- **LC_{50}**: concentration required to reduce the cell population by 50% relative to time zero.
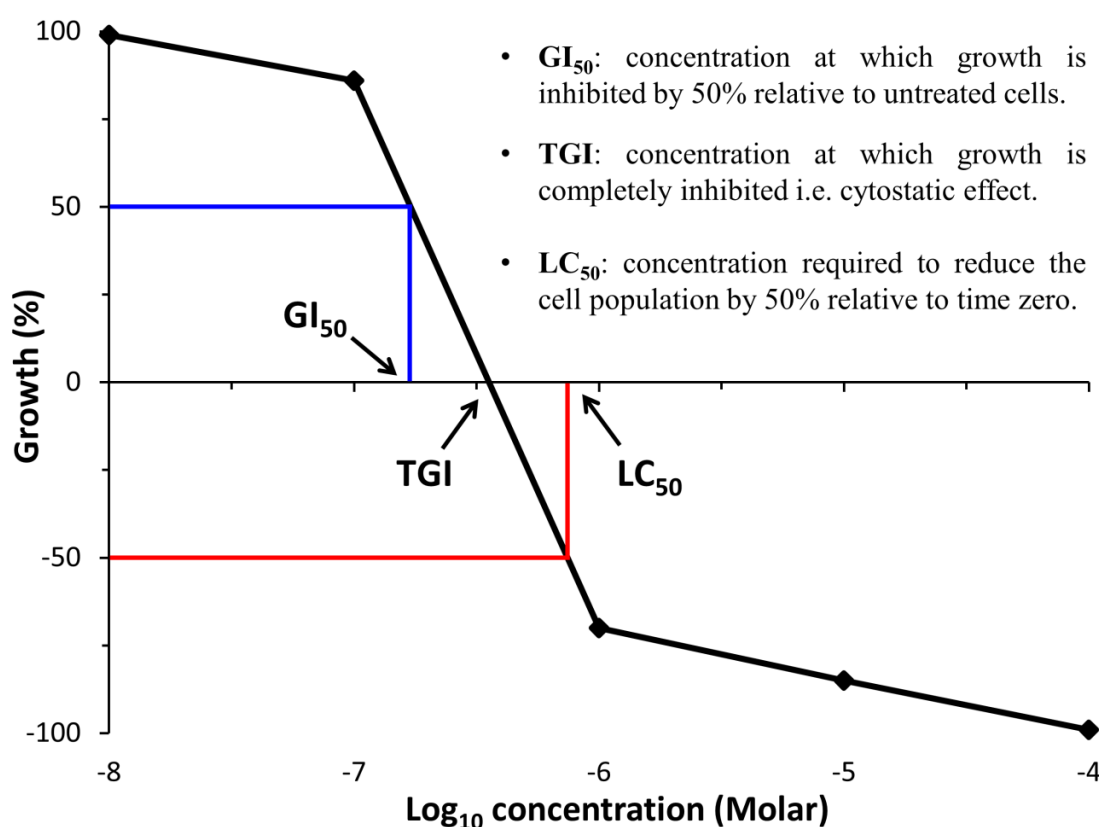
Figure 4.2. Graphical representation and definition of endpoint GC_{50}, TGI, and LC_{50} values from NCI dose-response curves.

The five-dose mean graph is constructed from the dose-response curve end point values to give a unique growth inhibition pattern. The end-point values are converted to the logarithmic scale and the mean $\log_{10}(GI_{50})$, (TGI), and (LC_{50}) values of all 60 cell lines (mean graph-midpoint (MG-MID)) are represented as a vertical line.[21] The response of individual cell lines are then plotted to the left and right of the vertical mean. Cell lines that are more sensitive than the calculated mean, project to the right of the vertical mean. Cell lines that are less sensitive than the calculated mean, project to the left of the vertical mean.[21]

Paull et al observed in NCI screening, that similar growth inhibition patterns of the 60 cell lines was representative for compounds of similar modes of action.[23, 24] This observation was formalised into the COMPARE algorithm that ranks the growth inhibition pattern similarities of any probe compound (or "seed") to compounds in the NCI screening database.[17, 23] The database contains 88,000 pure synthetic compounds and 34,000 natural product crude extracts.[25] The similarities are quantified using Pearson Correlation Coefficients (PCC) that range from -1 to +1 and are calculated with the commercially available SAS statistical package. A value of -1 represents a perfect inverse correlation, 0 represents no correlation and +1 represents a perfect direct correlation.[21] Coefficients that range from (± 0.3 to ± 0.5) are considered weak to moderate strength, (± 0.5 to ± 0.7) are considered moderate to strong and those above (± 0.7) are considered very strong.[26] The mode of action for new compounds can be determined if they correlate very strongly to a compound of known mechanism in the database.
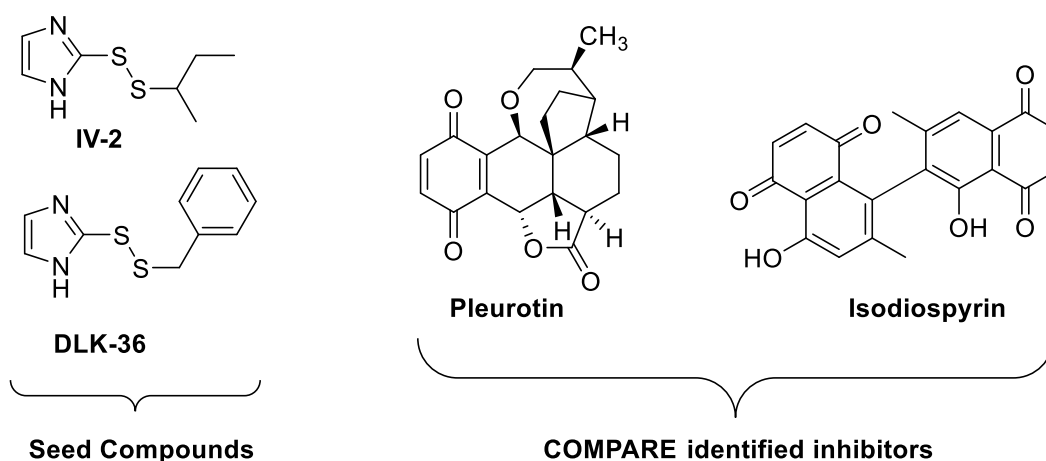
Figure 4.3. Novel TrxR inhibitors discovered through COMPARE analysis.[27]

The mode of action can also be determined if the unique growth inhibition pattern is correlated with molecular target expression.[17, 25] For example, 2-[(butan-2-yl)disulfanyl]-1*H*-imidazole (IV-2) and 2-(benzyldisulfanyl)-1*H*-imidazole (DLK-36) are known inhibitors of the thioredoxin reductase (TrxR) molecular target (Figure 4.3).[27] Both compounds are "seeds" in COMPARE analysis and the quinone containing pleurotin and isodiospyrin were identified as potential inhibitors of TrxR, showing the strongest correlations to IV-2 and DL-36 respectively. Subsequent thioredoxin reductase(TrxR)/thioredoxin(Trx) dependent insulin assays revealed pleurotin and isodiospryin as potent inhibitors of thioredoxin reductase.[27]
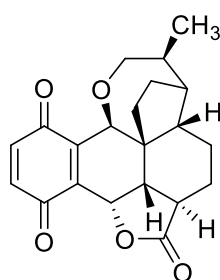
4.1.3. Pleurotin

Figure 4.4. The naturally occuring antibiotic pleurotin.

Fungi especially basidiomycota are well-known producers of terpenoid natural products, including antibiotics.[28] Currently, the diterpene pleuromutilins are the only marketed antibiotics derived from basidiomycete.[29] The antibiotic pleurotin (Figure 4.4) is another metabolite derived from basidiomycete and was first isolated in the 1947 from *Pleurotus griseus*, which is now classified as *Hohenbuehelia grisea*.[30] The first total synthesis of pleurotin was performed by Hart et al. and was isolated in an overall yield of 0.3% across 26 synthetic steps starting from benzoic acid.[31, 32] However, fermentation from the fungus *Hohenbuehelia atrocaerulea* has allowed the formation of pleurotin on a multi-gram scale.[33]

Pleurotin is active against pathogenic fungi,[34] gram-positive bacteria,[30, 35] and displays anti-cancer activity.[35-37]. The interest in pleurotin as a possible anti-cancer drug and treatment for mercury intoxication[38, 39] has increased due to the strong inhibiton of the Trx/TrxR system (IC_{50} 0.17 µM).[27, 40] Pleurotin is reported as an irreversible inhibitor of TrxR with a Ki of 0.28 µM.[27, 37] Pleurotin has undergone NCI-60 five-dose screening with mean graph-midpoint (MG-MID) GI_{50}, TGI, LC_{50} values displayed in Table 4.1.

Table 4.1. NCI five-dose MG-MID GI_{50}, TGI, LC_{50} values of pleurotin over two independent experiments.

	GI_{50} (µM)	TGI (µM)	LC_{50} (µM)
Pleurotin	12.82	29.31	61.66

4.1.4. Thioredoxin Reductase (TrxR)

Two enzyme based systems of thioredoxin and glutathione predominantly maintain intracellular redox homeostasis.[41] Normal cell function is maintained by balancing the generation of reactive oxygen species (ROS) with their elimination by antioxidant systems such as thioredoxin. ROS molecules are derived from oxygen and the main ROS molecules are superoxide ($O_2^{\bullet-}$), H_2O_2, hydroxyl radical ($^{\bullet}OH$), and nitric oxide (NO).[42] The thioredoxin system consists of NADPH, thioredoxin (Trx), and TrxR. TrxR is a homodimer with each monomer containing a FAD prosthetic group, NADPH binding domain, and a redox active selenolthiol site (Figure 4.5b).[43, 44]
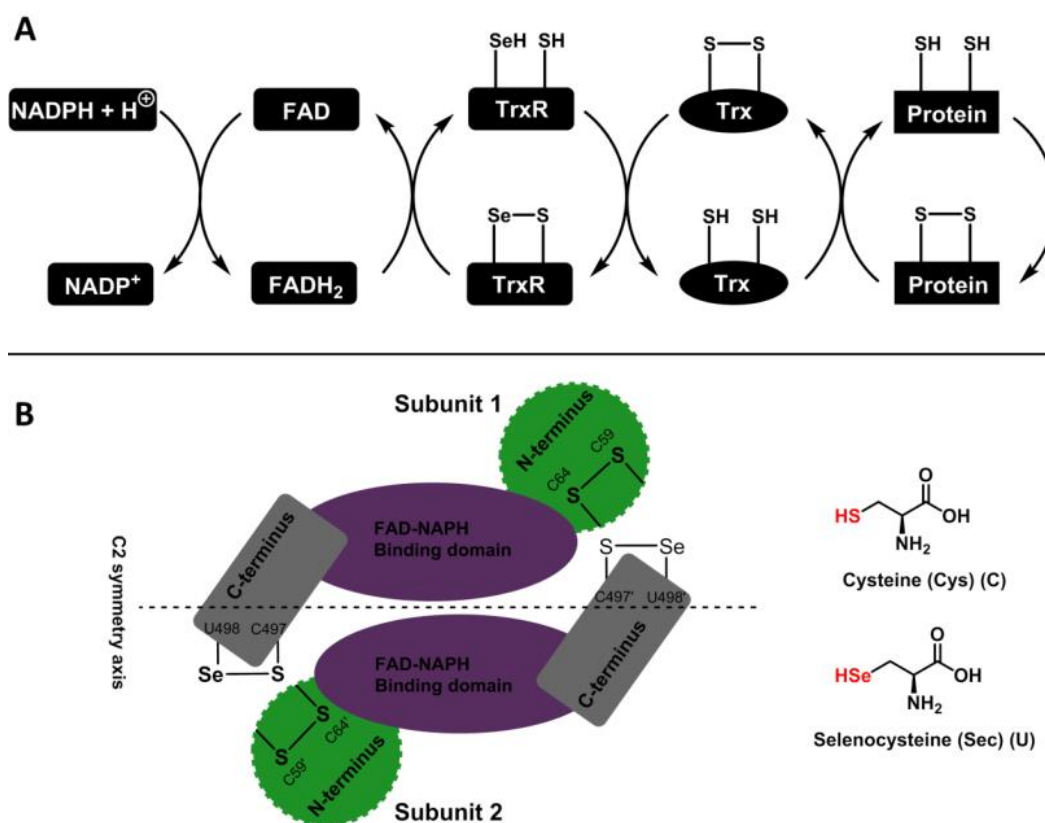
Figure 4.5. (**A**) The redox catalytic cycle of the Trx system. (**B**) Head-to-tail cartoon model of oxidized rat TrxR with N-terminal (C59/C64) and C-terminal (C497/U498) redox pairs explicitly shown.[44-46]

The two subunits of the TrxR homodimer are arranged in a head-to-tail fashion with a two-fold symmetry axis lying along the dimerization interface of the two monomers (Figure 4.5b).[45, 46] The oxidised TrxR accepts electrons from NADPH via reduction of enzyme-bound FAD group to give $FADH_2$ (Figure 4.5a). These electrons reduce the N-terminal

disulfide redox active site (C59/C64) buried in the FAD domain of the same monomer (Figure 4.5b). The dithiol pair of the N-terminal then provide reducing equivalents to the neighbouring C-terminal selenenylsulfide redox active site (C497'/U498') of another monomer to produce the active TrxR enzyme. The reduced selenolthiol redox pair (Figure 4.5a) then provide reducing equivalents to Trx, which maintains intracellular redox regulatory functions and antioxidant defences through interaction with downstream protein disulfides (Figure 4.5a).

Trx acts a hydrogen donor to ribonucleotide reductase (RNR) that reduces ribonucleotides involved in DNA synthesis.[47] Trx provides reducing equivalents to Trx peroxidase (peroxiredoxins) and methionine sulfoxide reductase (Msr) that in turn reduce peroxides and methionine sulfoxides respectively to scavenge ROS and protect against oxidative damage.[48] Trx interacts with redox sensitive molecules such as apoptosis signal-regulating kinase 1 (ASK1) and protein tyrosine phosphatase and tensin homolog (PTEN), which are involved in regulating cell death (apoptosis).[43, 47, 49] Trx has been shown to control gene expression through reduction of Cys residues in certain transcription factors such as hypoxia inducible factor-1α (HIF-1α), p53, nuclear factor kB (NF-kB), activating protein 1 (AP-1), and nuclear factor erythroid 2-related factor 2 (Nrf-2).[47, 48, 50] Overall, a pool of reduced Trx is used to control DNA synthesis, ROS scavenging, cell proliferation, apoptosis and cell signaling.

However, once a tumour phenotype develops, Trx protein is over-expressed facilitating tumour progression through cellular signaling pathways that promote cell proliferation, anti-apoptosis and angiogenesis.[46, 51] For example, Trx upregulates HIF-1α expression to maintain angiogenesis of the tumour in hypoxic conditions[47, 51] and inhibits the tumour suppressor protein PTEN.[49] Trx is over-expressed in a number of cancers such as lung, pancreatic, prostate, breast, and colorectal.[47, 52] The over-expression of Trx leads to resistance of chemotherapy drugs (docetaxel and cisplatin) and affects the treatment of B-cell lymphoma and ovarian cancer.[47] A study showed that in the absence of Trx activity, the tumour progression of MCF-7 breast cancer was severely diminished.[53] Thus targeting of TrxR seems an effective anti-cancer strategy, as it is the only known enzyme to reduce Trx which sustains tumour progression.

The C-terminal of TrxR is surface exposed, and is flexible with a long chain of 16 amino acids containing the Sec residue offering broad substrate scope for reduction outside of oxidised Trx.[45, 54] The disulfide containing 5,5'-dithiobis(2-nitrobenzoic acid) (DTNB) can be used as a mimic for Trx. DTNB is catalytically reduced to the yellow 5-thio-2-nitro-benzoicacid (TNB) with TrxR and NADPH is used as the electron source (Scheme 4.5). The DTNB assay can be used to determine small molecule inhibitors of TrxR as a decrease in TrxR activity is directly proportional to the intensity of the yellow colour produced, which is measured spectrophotometrically at 405 nm.[40, 55]
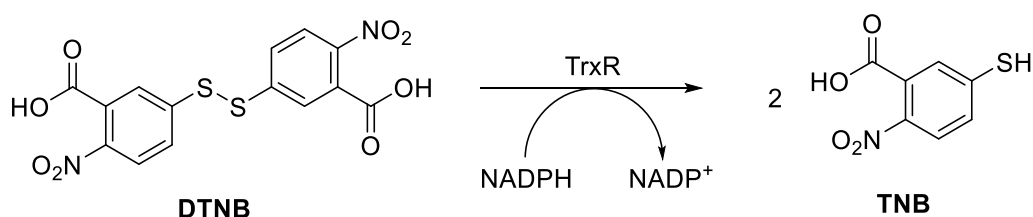
Scheme 4.5. The DTNB colorimetric assay produces two mole of TNB.

The Sec residue has a lower pKa (5.8) than the Cys residue (8.30), meaning selenol ionises as the senolate ion (R-Se$^-$) more readily than the equivalent thiol to thiolate.[45, 46, 54] The selenol group is more nucleophilic by roughly one order of magnitude than the thiolate and therefore very reactive towards electrophiles forming covalent bonds.[46, 56] The soft atoms of metals act as good electrophiles and there are several gold-, platinum- and ruthenium-based inhibitors.[56] The gold complex Auranofin (Ki 4 nM)[57] is under NIH clinical trials as a thioredoxin reductase inhibitor,[58, 59] and has toxicity towards cisplatin-sensitive and -resistant ovarian cancer cells.[56, 60] Natural electrophilic compounds such as flavonoids, polyphenols, and curcumin derivatives are irreversible inhibitors of TrxR.[61-63] Other classes of compounds such as disulfides/diselenides,[44, 64, 65] arsenic trioxide,[65] and nitroaromatics (1-Chloro-2,4-dinitrobenzene (DNCB)) have been shown to inhibit TrxR too.[65]

Quinones are electrophilic compounds that interact with TrxR by forming covalent bonds through alkylation, and/or transfer electrons in biological redox reactions producing reactive semiquinones and oxygen radicals (ROS) (Chapter 1, Scheme 1.1).[66] It must be noted that indolequinones require reduction to become activated. The archetypal redox prodrug and naturally occurring mitomycin C (MMC) is a strong inhibitor of TrxR.[67] Upon reduction, MMC alkylates and irreversibly inhibits TrxR at the Sec residue of the C-

terminal (Figure 4.6a). Other indolequinones such as 5-methoxy-1,2-dimethyl-3-[(4-nitrophenoxy)methyl]-1*H*-Indole-4,7-dione (ES396) are potent towards pancreatic cancer cells with mode of action through the inhibition of TrxR (Figure 4.6b).[68, 69] Upon reduction, the electrophilic intermediate was shown to form an irreversible covalent bond with C-terminal Sec of TrxR as identified by LC-MS/MS fragmentation patterns.[69] Apoptosis towards the pancreatic cancer cells proceeded through MAPK signaling pathways.[69]
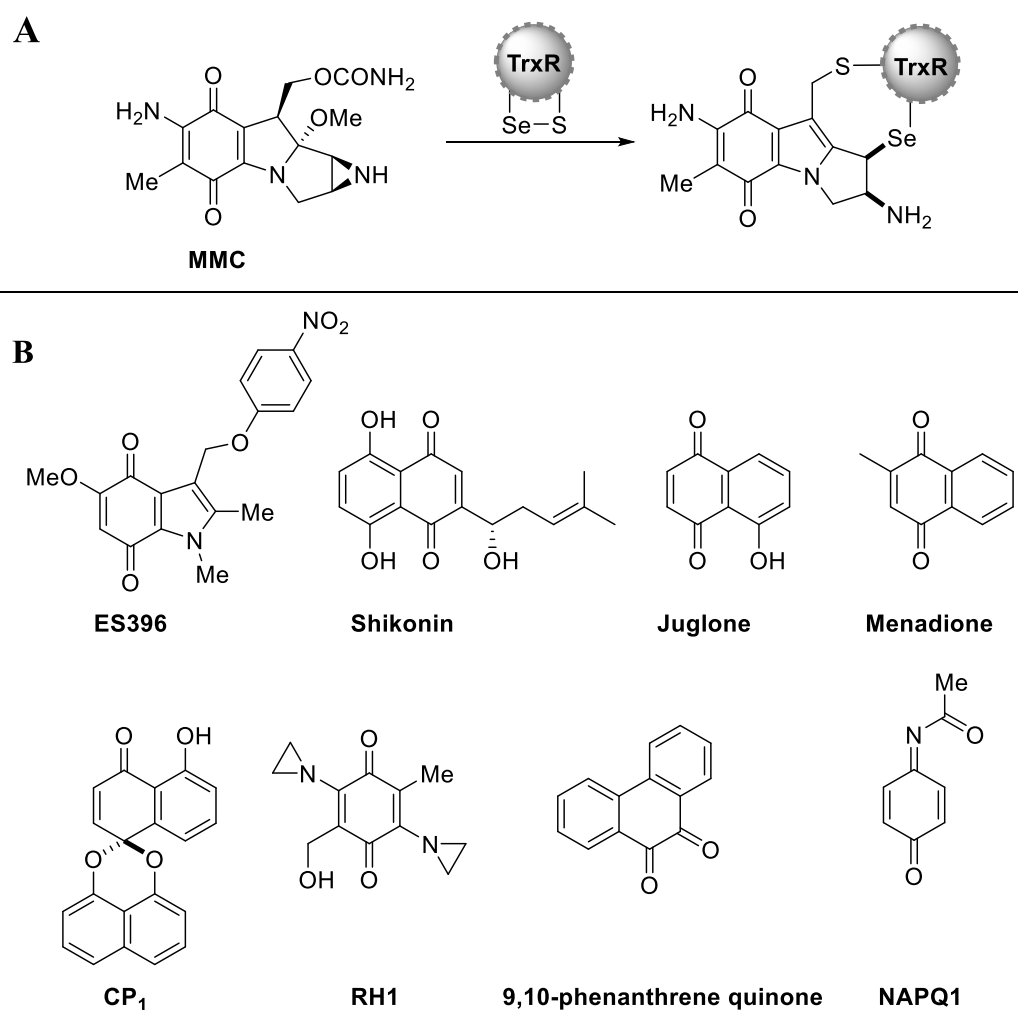
Figure 4.6. The quinone inhibitors and substrates of TrxR.[40, 51, 67-70, 73-77]

A series of aziridinyl-, naphtho- and *o*-quinones were tested by Arnér et al to elucidate their interactions with TrxR.[70] The 9,10-phenanthrene quinone (*o*-quinone) was shown to be a reversible inhibitor of TrxR with a Ki of 6.3 µM (Figure 4.6b). The naphthoquinone juglone (found in walnuts), and the pro-drug aziridinylquinone RH1 were substrates for TrxR rather than inhibitors (Figure 4.6b).[70]

The use of redox modulating compounds (quinones) to alter ROS levels is a therapeutic approach to target cancer cells without causing significant harm to normal cells.[71, 72] In normal cells the ROS levels are tightly regulated due to redox homeostasis and can tolerate a certain amount of external ROS. However, in cancer cells redox disrupted homeostasis results in elevated ROS levels and a decreased toxic threshold induces cell death.[72, 73] Later work by Arnér et al showed the TrxR substrate juglone, actually could be arylated at the Cys residue (C497) of the C-terminal and then undergo one-electron reduction at the FAD-containing N-terminal to produce superoxides (Figure 4.6b).[74] The naphthoquinone menadione produces high level levels of ROS via one-electron reduction by TrxR (Figure 4.6b).[75] Menadione used in combination with ascorbate showed potent anti-cancer activity through enhanced production of ROS.[73]

The naphthoquinone shikonin, found in Chinese herbal medicine, was an irreversible inhibitor of TrxR targeting the Sec residue of the C-terminal (Figure 4.6b).[76] Like Juglone, Shikonin is reduced once bound covalently to TrxR producing superoxides that leads to ROS cell induced death of leukemia HL-60 cells.[76] The spirocyclic naphthoquinone of CP_1 was a potent inhibitor of the Trx/TrxR system with toxicity in the micromolar range (Figure 4.6b).[40, 51] N-acetyl-p-benzoquinone imine (NAPQ1), a metabolite of paracetamol, was shown by LC-MS/MS to inhibit both the N- and C-terminal redox centres of TrxR (Figure 4.6b).[77]

Apoptosis mediated cell death through oxidative stress (ROS) is a common mode of action for all classes of compounds inhibiting TrxR.[62, 69, 76, 78-81] Mitogen-activated protein kinases (MAPKs) mediate signaling in response to environmental stresses such as ROS and inflammatory cytokines to regulate cellular processes.[82] Trx in reduced form controls cell death by directly inhibiting the MAPK of apoptosis signal-regulating kinase 1 (ASK1).[39, 83] The inhibition of TrxR leads to only oxidised Trx, which cannot bind to ASK1. This activates downstream JNK and p38 MAPK signaling pathways that activate transcription factor p53 that ultimately leads to cell death.[62, 78] Traditionally, MAPKs have been seen as tumour suppressors but p38α (MAPK14) a member of the p38 MAPK family can act as both a tumour suppressor and activator.[82] MAPK14 facilitates tumour progression of breast, liver, and colon cancers and helps tumour cells survive chemotherapeutic treatments.[82]

4.1.5. Types of reversible enzyme inhibition

The three types of reversible enzyme inhibition are competitive, uncompetitive and mixed.[84] In competitive inhibition, the inhibitor competes directly with the substrate to bind exclusively to the active site of free enzyme (E).[85, 86] The inhibitor resembles the shape of the substrate and forms an enzyme-inhibitor (EI) complex, which prevents formation of products (Figure 4.7). However, competitive inhibition can be reversed when [S] is much larger than [I]. The inhibition constant K_i, which is a dissociation constant of the EI complex, measures how tightly an inhibitor binds to free enzyme (Figure 4.7b).[85, 86] The lower the K_i value, the more potent that inhibitor is.
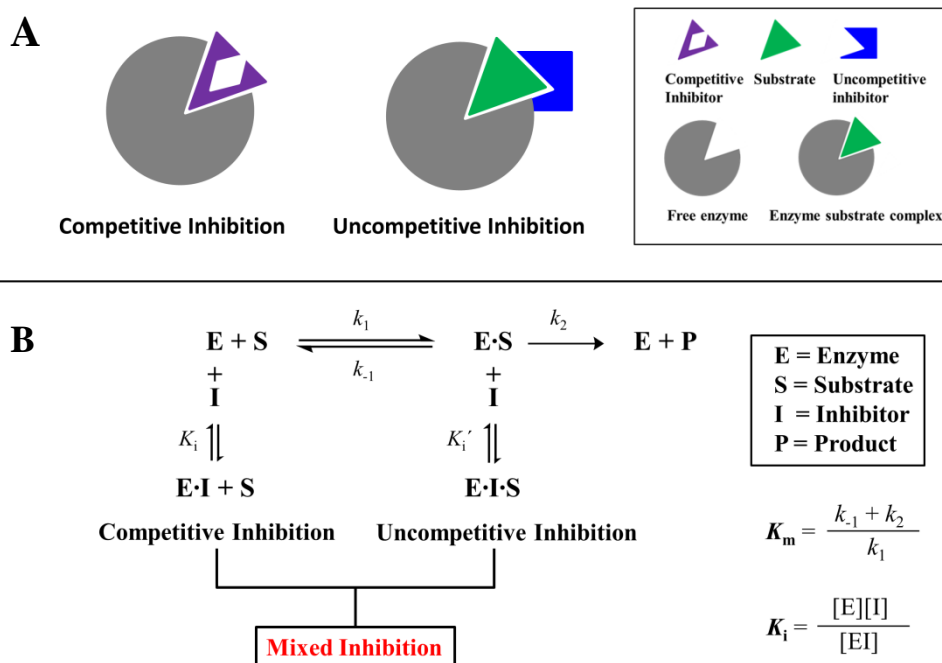
Figure 4.7. (**A**) Cartoon representation of both competitive and uncompetitive types of reversible enzyme inhibition. (**B**) A general scheme of reversible enzyme inhibition with associated kinetic rate constants.

Uncompetitive inhibition involves the inhibitor exclusively binding to the enzyme-substrate (ES) complex (Figure 4.7a). An inactive ESI complex is formed and the inhibition constant K_i' describes the affinity of the inhibitor for the ES complex (Figure 4.7b). Uncompetitive inhibition can't be reversed by increasing [S]. Mixed inhibition involves the inhibitor binding to both the free enzyme and the ES complex with different affinities described by the dissociation constants of K_i and K_i'. Mixed inhibition can be reduced by increasing [S], but not reversed as in competitive inhibition.[85, 86]

163

These observations were formalized into the Michaelis-Menten equation (Figure 4.8), which describes the relationship between substrate concentration and the effect it has on the rate of an enzyme reaction.[85] Enzyme kinetics that follow Michaelis-Menten behaviour produce a hyperbolic shaped curve (Figure 4.8). The Michaelis-Menten constant (K_m) is the [S] required to produce a rate one-half of max velocity (V_{max}) (Figure 4.8). In other words, it is the [S] when half of the enzyme active site is occupied with substrate molecules. The K_m value is dependent on the substrate and environmental conditions of temperature, pH, ionic strength, and polarity.[86] K_m is also described by the rate constants k_1, k_{-1}, and k_2 in Figure 4.7b. K_m is not equal to the dissociation constant of the ES complex except in the case where the binding and release of substrate is much more rapid than the breakdown of the ES complex($k_{-1}>>>k_2$).[87] Any variation in K_m often indicates the presence of an activator or inhibitor.
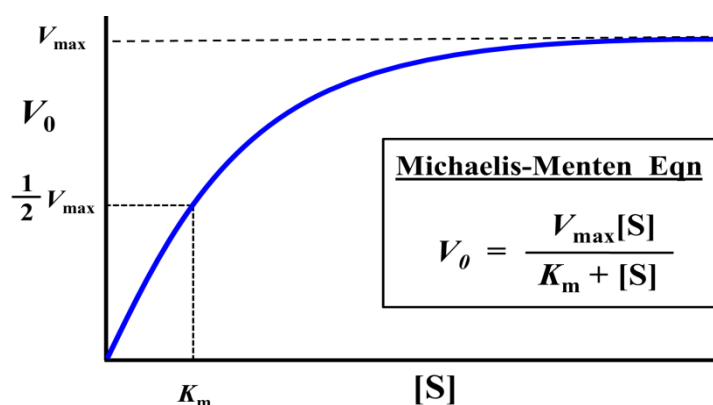
Figure 4.8. Michaelis-Menten kinetics describes the relationship between substrate concentration and the velocity of an enzyme reaction.

During any enzyme catalysed reaction, the enzyme exists in various proportions of the free enzyme and ES complex. At low [S], free enzyme predominates and the reaction of the enzyme with the substrate is directly proportional i.e. doubling the substrate concentration will double the enzyme velocity. As the [S] increases, the enzyme velocity becomes non-linear and continues until all of the enzyme active site becomes occupied with substrate i.e. saturated. The addition of further substrate will not make the rate of reaction any faster. At high [S], the theoretical maximum (V_{max}) is asymptotically approached and the ES complex predominates with the reaction independent of velocity resulting in the plateau observed in the hyperbolic curve (Figure 4.8). [84, 85]

The Michaelis-Menten hyperbolic curve is converted into a double-reciprocal plot which is called the Lineweaver-Burk plot to facilitate linear regression analysis.[88] $1/V_0$ is plotted against $1/[S]$ to give a family of straight lines that pass through the y-intercept and cross the negative x-axis (Figure 4.9). The V_{max} and K_m values are determined from these intercept points on the y- and x-axes respectively.[86] Characteristic patterns displayed on the Lineweaver-Burk plots are indicative of the different types of reversible inhibition.
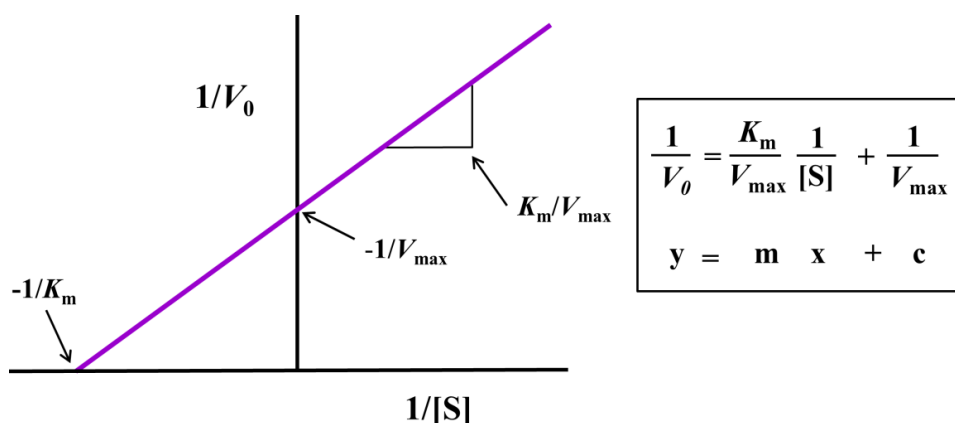
Figure 4.9. The double reciprocal, Lineweaver-Burk plot.

Competitive inhibition as seen in Figure 4.7 involves direct competition between substrate and inhibitor for the free enzyme. In competitive inhibition, at saturating levels of the substrate, there is no free enzyme for inhibitor to bind with and therefore V_{max} is independent of the inhibitor concentration. The y-intercept ($1/V_{max}$) value remains constant and as a result V_{max} remains unchanged in presence of varied inhibitor concentrations (Figure 4.10a). At lower $[S]$, the inhibitor can compete to bind with free enzyme. The slope (K_m/V_{max}) represents the rate of the reaction at lower $[S]$. As the $[I]$ increases, the slope values increase too representing a decrease in the rate of the reaction as the inhibitor occupies more of the free enzyme than substrate does (Figure 4.10a).[85]

Uncompetitive inhibition as seen in Figure 4.7 represents the binding of an inhibitor to an ES complex. The rate of reaction is unaffected by varying $[I]$ at low $[S]$, as the inhibitor only binds to the ES complex. This gives a series of parallel lines with an unchanged slope (K_m/V_{max}) (Figure 4.10b). At saturated levels of the substrate, the inhibitor binds to the ES complex. As the $[I]$ increases, the y-intercept ($1/V_{max}$) values increase (Figure 4.10b), representing a decrease in V_{max}. The reduction in amount of ES complex also leads to a reduced K_m value.[85]

165

Mixed inhibition as seen in Figure 4.7 refers to the ability of the inhibitor to bind either free enzyme or the ES complex. Increasing [I] gives a reduced V_{max} as shown by the increasing y-intercept ($1/V_{max}$) values, and this is due to the fact that the inhibitor can affect the rate of the reaction even when the ES complex is present (Figure 4.10c). In most cases, the inhibitors affinity for the ES complex or free enzyme is different and that will determine whether K_m is increasing or decreasing. The example shown in Figure 4.10c has K_m increasing due to greater affinity for free enzyme. When the affinity for both the ES complex and free enzyme are equal, there is no change in K_m. This special case is called non-competitive inhibition.[85]
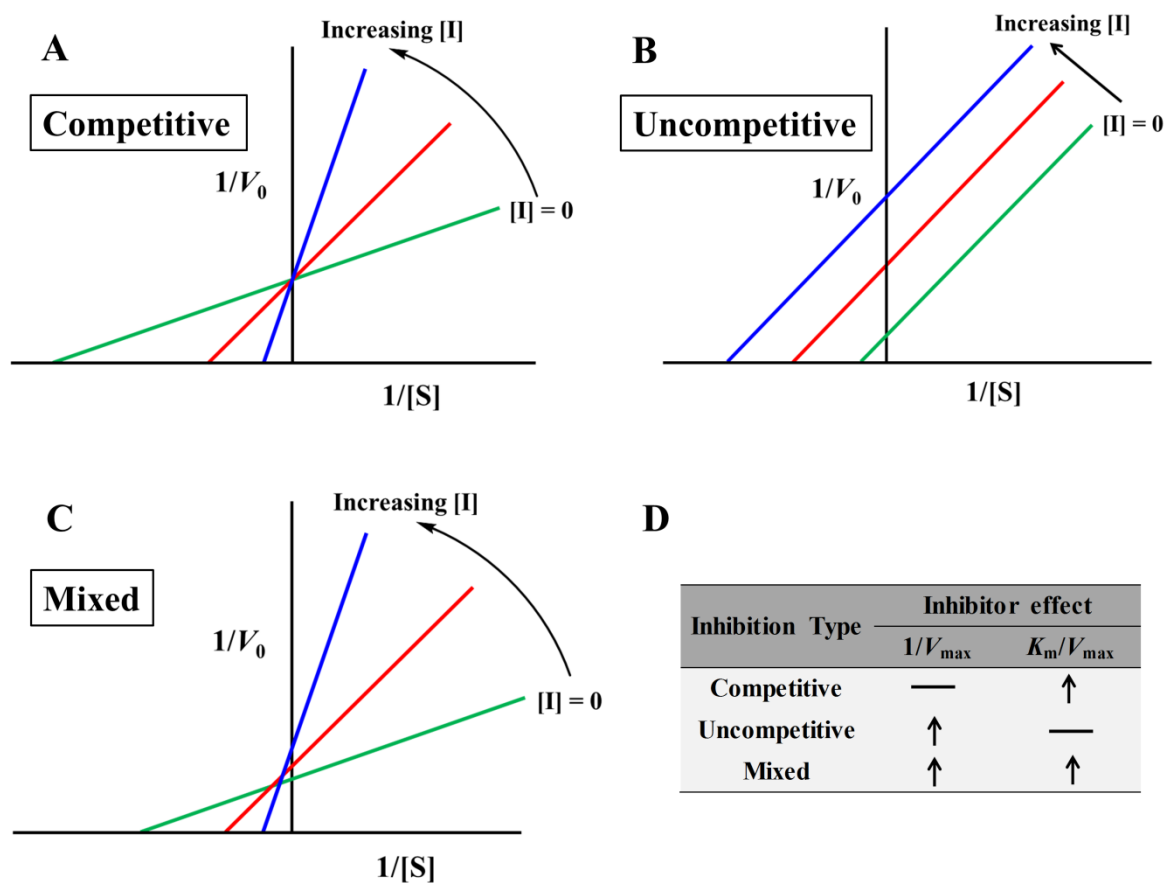
Figure 4.10. Characteristic competitive (**A**), uncompetitive (**B**) and mixed inhibition (**C**) kinetics represented by Lineweaver-Burk plots. (**D**) Characteristic changes to y-intercept and slope values in presence of increasing [I].

The inhibition constant K_i can be determined from secondary plots. The plots are graphed using either the slopes or intercepts from the Lineweaver-Burk plot against the inhibitor concentrations. The family of straight lines produced cross the negative x-axis and the reciprocal of the intercept is equal to the K_i value for that specific inhibitor.[89]

4.2. Aims and Objectives

- To investigate substituent effects at the 6-position of the 1,3-diphenylbenzo[1,2,4]triazin-7-one scaffold (**1a-1l**) on cytotoxicity against cancer cell lines using the MTT assay.

- To determine if the highly electronegative trifluoromethyl (CF_3) substituent **2** will increase the potency of the benzotriazinone scaffold through MTT and NCI-60 screening.

- To identify possible common mechanisms of action for anti-cancer activity with other agents in the NCI database by using NCI COMPARE analysis.

- To determine if the benzo[1,2,4]triazin-7-ones **1a** and **2** inhibit TrxR using the DTNB assay and use Lineweaver-Burk plots to assess the mode of TrxR inhibition.

1b-1l (Table 4.2)
1a: R = H (NSC: S768093)

2
(NSC: 780813)
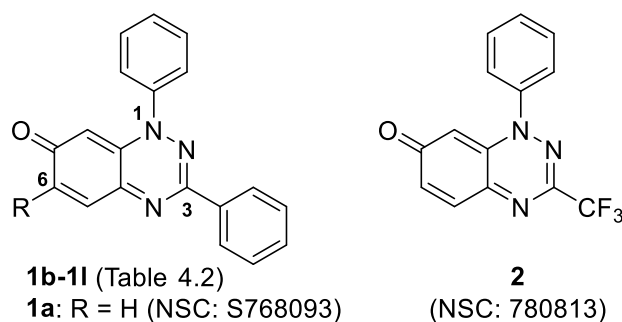
Figure 4.11. Benzo[1,2,4]triazin-7-ones **1a-1l** and **2**.

- To assess the biological effect of introducing pyridine rings onto the benzotriazinone scaffold at the 1- and 3- positions with NCI-60 cell line screening data and COMPARE analysis.

3a
(NSC: 780815)

3b
(NSC: 780816)
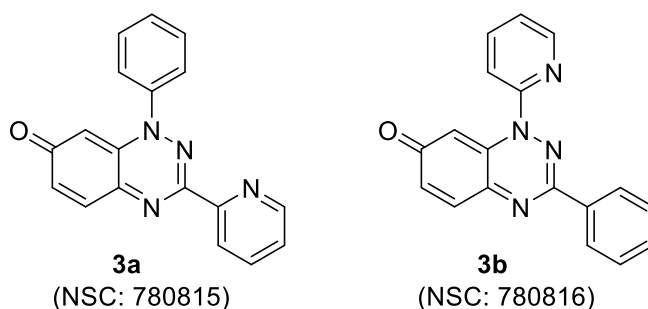
Figure 4.12. Benzo[1,2,4]triazin-7-ones **3a** and **3b**.

4.3. Results and Discussion

4.3.1. Cytotoxicity evaluation of 1,3-diphenylbenzo[1,2,4]triazin-7-ones 1a-1l using the MTT assay

A way to determine cytotoxicity or cellular viability from in vitro testing is to employ an end-point colorimetric assay that detects changes in a biochemical marker producing a colour that is detected by a spectrophotometer. One of the most popular colorimetric assays is the MTT (3-(4,5-dimethylthiazol-2-yl)-2,5-diphenyltetrazolium bromide) assay (Scheme 4.6). First introduced by Mosmann for cell proliferation and cell viability measurements,[90] the yellow coloured tetrazolium salt (MTT) is reduced by mitochondrial or cell plasma enyzmes in viable cells to produce purple water insoluble formazan crystals. Therefore DMSO or acidic isopropanol are required to solubilize the crystals before absorbance can be measured with a spectrophotometer.[90, 91] The intensity of the purple colour produced is directly proportional to the metabolic activity of living cells.

The assay is fast, cheap, reproducible, quantitative and can be used on a wide range of human cancer cell lines. However, measurements cannot be taken in real-time due to formation of insoluble formazan crystals. The extent of MTT reduction can be altered by non-enzymatic reductions (ascorbic acid, gluthathione),[91] variable metabolic activity of cell lines,[92] and concentration of glucose in the cell media.[93] This can lead to inaccurate measurements of viable cells if specific assay conditions aren't implemented for each cell line/test compound assayed.[92]
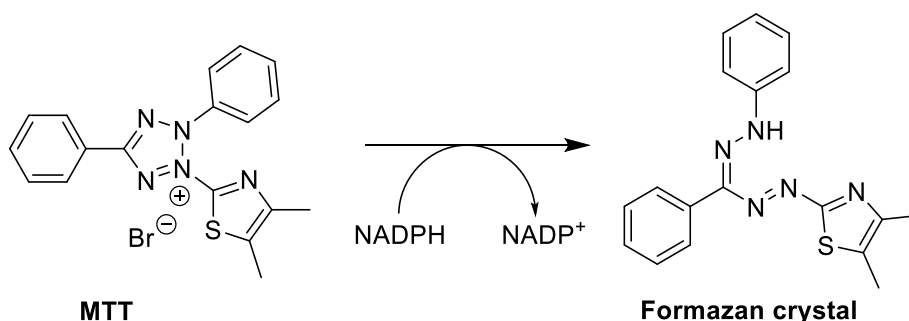
Scheme 4.6. The formation of purple formazan crystals from the reduction of MTT by mitochondrial or cell plasma reductases.

To determine the specificity and overall cytotoxicity towards selected cancer cell lines, the effect of substitution at the 6-position of the 1,3-diphenylbenzo[1,2,4]triazin-7-one scaffold with amine, amide and alkoxy substituents was investigated (compounds **1a**-**1l** in Table 4.2). Cytotoxicity was determined against the NQO1 over-expressing prostate cancer cell line DU-145[94] and breast cancer cell line MCF-7[95] using the MTT assay (Table 4.2). These cell lines form part of the NCI-60 human tumour cell line screen. As a control, the response of a normal human-skin fibroblast cell line GM00637 was determined.
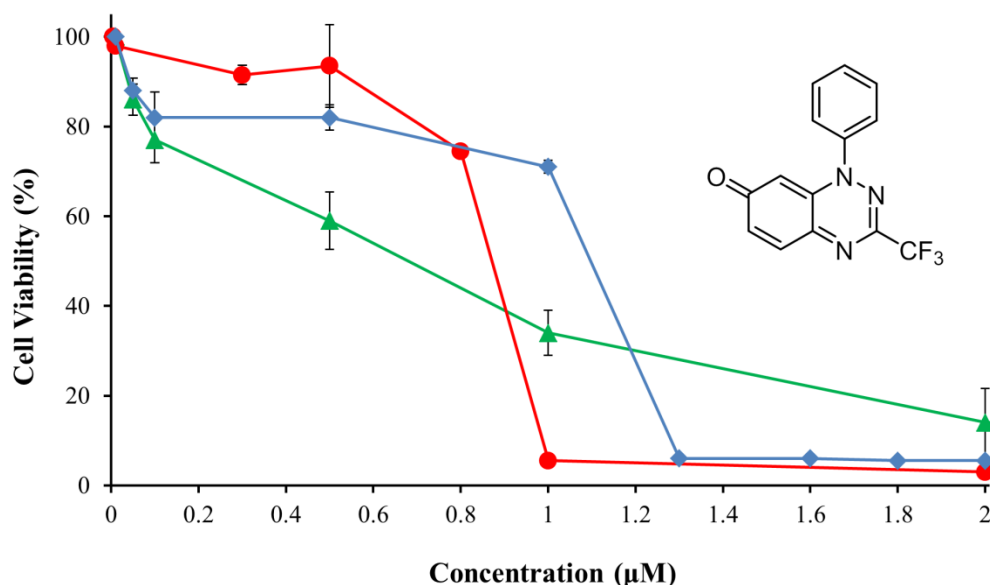
Figure 4.13. Dose-response curve of **2** showing cell-viability of GM00637 (♦)[†], MCF-7 (▲)[†] and DU145 (●) cell lines determined using the MTT assay under aerobic conditions for 72 h at 37 °C. Each data point is the mean of at least three independent experiments. The lines shown are trend lines.

A typical dose-response curve (Figure 4.13) is generated by treating the cancer cell lines and GM00367 cell line with compound **2** under a concentration range of 0.01 to 2 μM. From this dose-response curve, the compound concentration required for the reduction of the mean cell viability to 50% is interpolated and representative of the IC$_{50}$ value.

Pleurotin exerted a mean cytotoxicity of 0.36 μM towards the prostate and breast cancer cell lines, the most potent response of all 14 compounds evaluated at NUI Galway (Table 4.2). The parent benzo[1,2,4]triazin-7-one **1a** displayed a similar mean toxicity of 0.52 μM towards both cancer cell lines. 1-Phenyl-3-(trifluoromethyl)-benzo[1,2,4]triazin-7-one **2** is

structurally distinct from benzotriazinone **1a** since the 3-phenyl is replaced by a strong inductively electron-withdrawing trifluoromethyl (CF$_3$) group. Compound **2** showed mean toxicity of 0.73 μM to DU-145 and MCF-7 cancer cell lines, which was reduced from the response of **1a** and half the activity of pleurotin. Out of these three most potent compounds, **2** was the most selective towards the cancer cell lines giving a 2-3 times greater cytotoxic effect when compared to that of the normal fibroblast cell line (GM00637). The strong electron-withdrawing substituent at the 3-position of **2** was evaluated due to the fact that the 6-position is an electrophilic site and can't be substituted with electrophilic moieties (Scheme 4.4).[6]
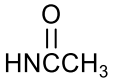
The average toxicity of the acyclic amines **1b**-**1e** was 1.95 μM towards both cancer cell lines (Table 4.2). However, the activity diminished as the bulk of the alkyl group increased, with the diethylamine **1e** showing a 7-fold decrease in cytotoxicity towards MCF-7 when compared to parent compound **1a**. The NH$_2$ analogue **1b** exhibited a two-folded specificity towards MCF-7 over the normal human cell line.

The cyclic amines **1f**-**1i** exerted an average cytotoxicity of 1.65 μM towards both cancer cell lines (Table 4.2). The pryrrolo- analogue **1f** was five times more specific toward the MCF-7 cancer cell line and displayed similar toxicity to that of pleurotin. The pyrido- substituent **1g** offered greater toxicity when compared to **1f**. The soft sulfur nucleophile of **1i** enhanced the toxicity relative to the morpholino analogue **1h**, especially towards the MCF-7 cancer cell line.

The cytotoxicity of alkoxy substituted compounds **1k** and **1l** and acetamide **1j** were reduced to negligible values relative to **1a**. For example, the ethoxy substituent **1l** was approximately 25 times less potent towards the MCF-7 cancer line when compared to the response of **1a**. Heterocyclic quinones substituted with electron donating alkoxy groups proved more difficult to reduce when compared to aziridinyl substituents [96, 97] The impact on reductive potentials leads to significant reductions in toxicity towards cell lines.[96, 97]

As none of the substituted analogues at the 6-position **1b**-**1l** offered a discernible improvement in cytotoxicity, the rest of this Chapter will be focused on the biological evaluation of **1a** and **2**.

Table 4.2. Cytotoxicity evaluation using the MTT assay: IC_{50} values (μM)[a]

Compound	R	Cell Lines		
		GM00637	DU-145	MCF-7
Pleurotin	—	0.51 ± 0.12[†]	0.43 ± 0.06	0.28 ± 0.03[†]
1a	H	0.23 ± 0.01	0.23 ± 0.03	0.81 ± 0.08
1b	NH_2	2.04 ± 0.21	1.83 ± 0.08	0.95 ± 0.03[†]
1c	NHMe	0.93 ± 0.03	0.98 ± 0.06	0.69 ± 0.12[†]
1d	NHEt	0.24 ± 0.01	0.22 ± 0.01	1.62 ± 0.24
1e	NEt_2	2.73 ± 0.36	3.11 ± 0.08	>5.0
1f	(N-pyrrolidinyl)	1.79 ± 0.12	2.46 ± 0.19	0.36 ± 0.08[†]
1g	(N-piperidinyl)	1.19 ± 0.02	0.61 ± 0.05	1.98 ± 0.06
1h	(N,O-morpholinyl)	2.29 ± 0.06	3.21 ± 0.37	2.37 ± 0.07
1i	(N,S-thiomorpholinyl)	1.63 ± 0.31	1.22 ± 0.06	0.97 ± 0.16[†]
1j	$HNCCH_3$ (C=O)	>5.0	>5.0	>5.0
1k	OMe	>5.0	>5.0	>5.0
1l	OEt	>5.0	>5.0	>5.0[†]
2	—	1.61 ± 0.21[†]	0.85 ± 0.04	0.60 ± 0.13[†]

[a]IC_{50} represents the compound concentration required for the reduction of the mean cell viability to 50% of the control value after incubation for 72 h at 37 $^{\circ}$C. Results represent the mean $\pm$ SD of three independent experiments. [†]Work carried out by Martin Sweeney

4.3.2. Development Therapeutic Program (DTP) National Cancer Institute (NCI) - 60 human tumour cell line screen

As previously described in Section 4.1.2, the NCI screening begins with initial one-dose testing (10 µM) that gives a mean growth percent plot across the 60 cell lines. The two prostate cancer cell lines (DU-145, PC-3) are represented separately in Figure 4.14 to exemplify the potential disparity in cytotoxic response towards quinones, as NQO1 enzyme activity in DU-145 is substantially greater than that of PC-3.[94] MCF-7 is also displayed separately as it expresses elevated levels of NQO1, which is associated with breast cancer progression.[95] Previous research of imidazobenzimidazolequinones in the Aldabbagh group has also shown specificity towards the MCF-7 cancer cell line.[98]

The parent 1,3-diphenylbenzo[1,2,4]triazin-7-one **1a** had excellent overall activity with a mean growth of 2.46% across the 60 cell lines and lethality towards numerous cancers including leukemia, colon, and renal cancers (Figure 4.14). Highest activity was observed against the OVCAR-3 cell line (ovarian) at -98.15% mean growth after 48 h (Appendix, Table A.4.1). In fact, **1a** was cytotoxic to 28 out of the 60 cancer cell lines at 10 µM dosage (Appendix, Table A.4.1).
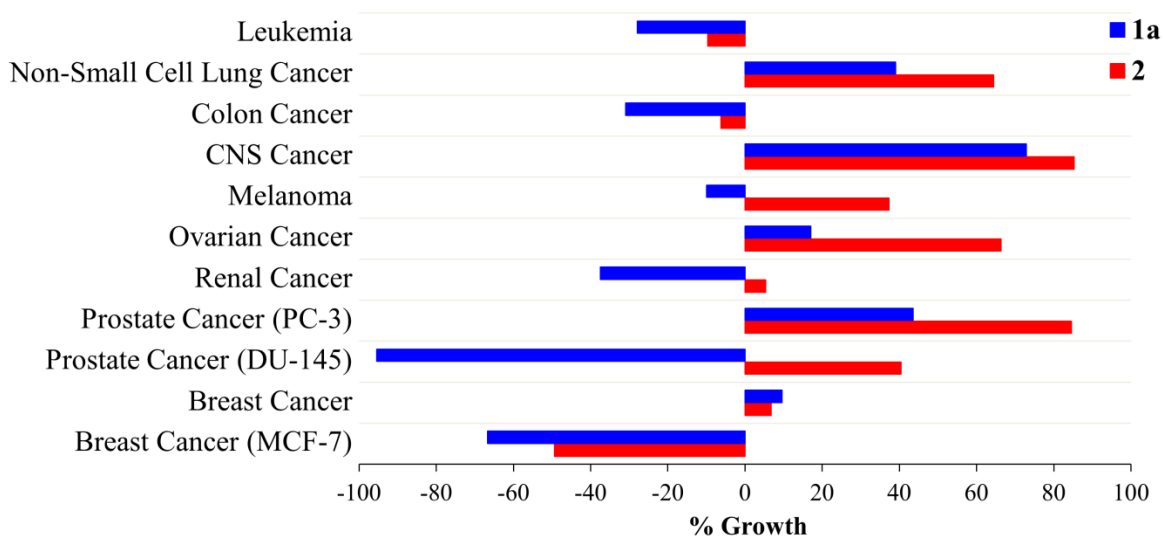
Figure 4.14. Summary of DTP NCI-60 one-dose (10 µM) screening results for benzotriazinones **1a** (blue) and **2** (red) expressed as mean percent growth of each cancer cell type relative to untreated cells.

Significant activity was apparent towards the prostate cancer line DU-145 (-95.45%) and breast cancer cell line MCF-7 (-66.74%) correlating well to our MTT assay in NUI Galway (Figure 4.14). CF_3-substituted compound **2** had good activity with a mean growth of 33.29% from one-dose testing and the highest activity was against the TK-10 cell line (renal cancer) with -98.03% mean growth (Appendix, Table A.4.3). Similarly to **1a**, **2** displayed lethality towards 21 individual cell lines out of the 60 and as a whole towards leukemia and colon cancers. Other than that, **2** only had moderate growth inhibition towards the other main cancer types (Figure 4.14). However, **2** demonstrated selectivity towards breast cancer with 93% growth inhibition and lethality towards MCF-7 (-49.33% mean growth) (Appendix, Table A.4.3). In contrast to **1a**, **2** didn't exert any lethality towards DU-145 but still inhibited the cell growth by 60% (Figure 4.14).

Both of the benzotriazinones **1a** and **2** met the pre-determined thresholds of less than 60%[20] mean growth at the one-dose testing stage, and were forwarded for evaluation at the five-dose stage. Representative dose-response curves of **2** are shown in Figure 4.15 that use a benzotriazinone concentration range of 0.01 µM to 100 µM, from which the GI_{50}, TGI, and LC_{50} values are interpolated.
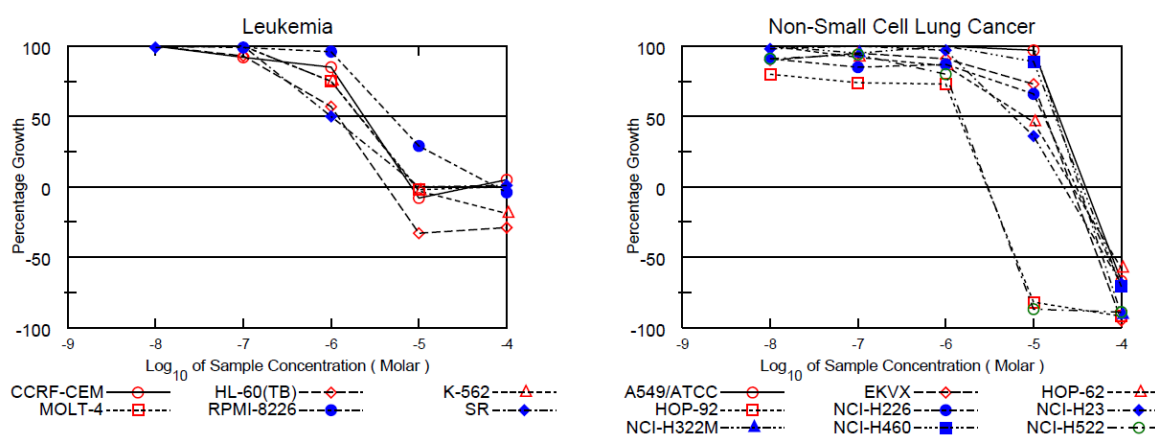
Figure 4.15. Selected dose-response curves for five-dose testing of 1-phenyl-3-(trifluoromethyl)benzo[1,2,4]triazin-7-one **2**.

The parent compound **1a** displayed greater activity with all MG-MID GI_{50}, TGI, and LC_{50} values lower than that of **2** which is in agreement with that observed in one-dose testing (Table 4.3, Figure 4.14). The MG-MID GI_{50} values for **1a** and **2** were 2.51 and 4.27 µM respectively (Table 4.3), which is approximately three to five times less than the pleurotin

value of 12.82 µM (Table 4.1). As shown in Figure 4.16, **1a** was more active across all cancer types when compared to **2** (melanoma cancer omitted for illustrative purposes).

Table 4.3. Mean graph-midpoint (MG-MID) GI_{50}, TGI, LC_{50} values of **1a** and **2** against all 60 cell lines in the NCI panel.

Compound	GI_{50} (µM)	TGI (µM)	LC_{50} (µM)
1a	2.51	6.31	21.38
2	4.27	12.39	33.11

If the test compound has a GI_{50} value lower than the MG-MID towards a particular cancer type, it is considered selective. Both of the benzotriazinones were most selective towards leukemia (Figure 4.16). Compound **1a** was selective to leukemia and breast cancers (Appendix, Table A.4.2) and particularly active against SR, ACHN, NCI-H522 and MCF-7 cell lines.
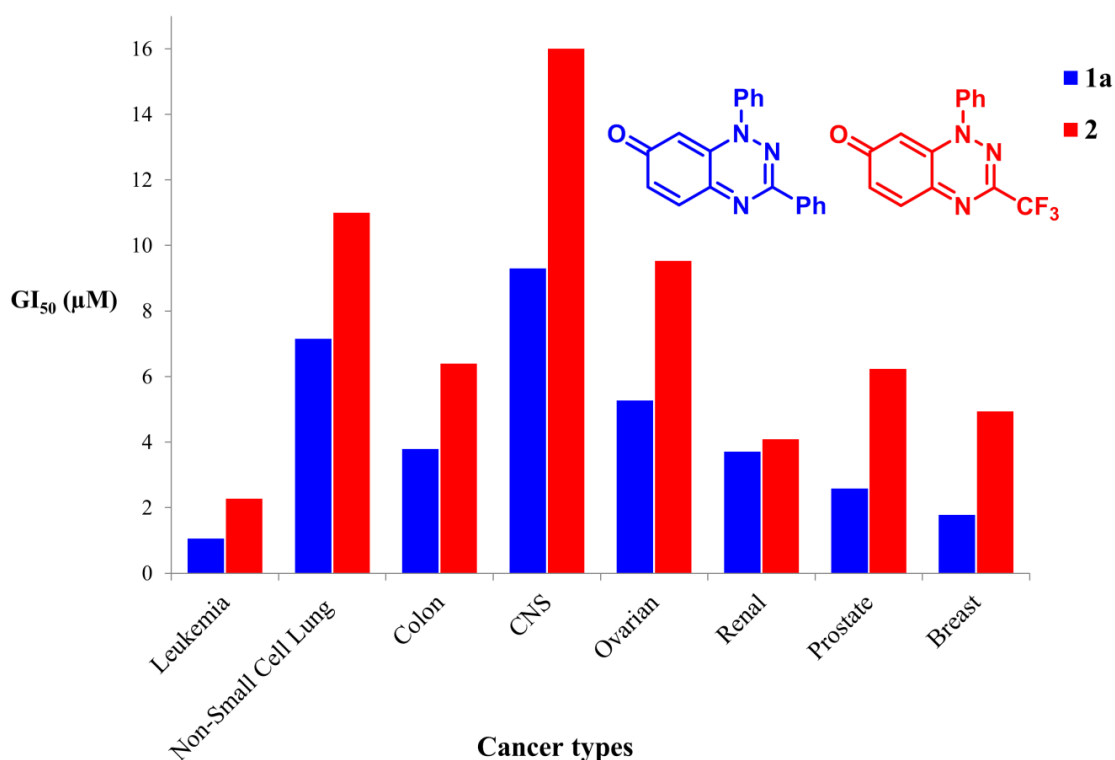
Figure 4.16. Summary of Benzotriazinones **1a** (blue) and **2** (red) NCI-60 activites, given as mean GI_{50} values against each cancer cell type relative to untreated cells.

Benzotriazinone **2** was selective against leukemia and renal cancers but most active against the MCF-7 cell line with a GI_{50} of 0.49 μM (Appendix, Table A.4.4). Other cell lines with notable activity against **2** were DU-145, OVCAR-3, HCI-15 and NCI-H522.

The five-dose screen is used to differentiate if a cytostatic (slows or stops the growth of tumour cells without killing them) or cytotoxic (kills tumour cells) effect is produced for a given compound against a particular cancer type or cancer cell line. For example, the dose-response curve for leukemia (Figure 4.15) levelled off after 10 μM dosage of **2** and didn't cross the reference level for LC_{50} interpolation. Thus, a LC_{50} default value of (>100 μM) was assigned meaning that **2** exerted a cytostatic effect towards leukemia rather than a cytotoxic one. This cytostatic response was observed also with the benzotriazinone **1a** against leukemia (Appendix, Table A.4.2). Targeted cancer therapies are often cytostatic while chemotherapy is cytotoxic and does not differentiate between rapidly dividing normal and cancerous cells.[99]

The NCI one- and five-dose testing data contradict each other concerning the biological effect of compound **2** towards DU-145 and MCF-7 cell lines. An LC_{50} value of 5.62 μM was recorded towards the DU-145 cell line, which is in contrast to only growth inhibition recorded in one-dose screening (Appendix, Table A.4.3 and Table A.4.4). On the other hand, lethality was expressed against the MCF-7 cell line in one-dose screening while five-dose screening reported a cytostatic effect. However, five-dose testing operates over a larger concentration range and should be more representative of the actual activity for the compound of interest.

The NCI reported mean IC_{50} values for compounds **1a** and **2** against DU-145 and MCF-7 cell lines as 1.84 μM and 1.97 μM respectively. This follows the trend of **1a** being more active than **2** towards DU-145 and MCF-7 cell lines in the MTT assay. The IC_{50} absolute values are different though and this difference can presumably be attributed to the employment of the different SRB assay at the NCI (Figure 4.1).

4.3.3 COMPARE analysis

The NCI COMPARE program employs an algorithm to determine closely matching cytotoxicity profiles across the NCI-60 from the endpoint values generated in five-dose testing.[16] GI_{50} values of **1a** and **2** were used in COMPARE and correlated with those of synthetic compound and molecular target data subsets within the NCI database. Out of ~88,000 pure synthetic compounds in the NCI database, pleurotin had one of the highest correlation coefficients to benzotriazinone **1a** at 0.84, which represents a very strong correlation (Table 4.4). Compound **2** was overall less active against the main cancer types in comparison to **1a** (Figure 4.14, Figure 4.16), but still had a very strong correlation to compound **1a** and pleurotin using COMPARE analysis (Table 4.4). The correlation of GI_{50} values for **1a** and **2** against pleurotin are reported in the Appendix (Table A.5.1 and Table A.5.2). The large Pearson correlation coefficients of approximately 0.8 indicated possible common pathways for anti-cancer activity.

Table 4.4. Pearson correlation coefficients obtained by COMPARE analysis.

Compound	2	Pleurotin	MAPK14
1a	0.803	0.840	0.450
2	—	0.793	0.470

Both Benzotriazinones **1a** and **2** have a moderate correlation coefficient of approximately 0.46 towards the biological marker of MAPK14. As discussed in Section 4.1.4, apoptotic cell death is controlled by the MAP kinase (ASK1) and MAP kinases direct cell signaling pathways that can also promote the survival of certain types of cancer such as breast,[100] colon and liver.[82] The targeting of MAPK14 by indirect TrxR inhibition could be one possible mode of action for the benzotriazinones.

4.3.4. Cyclic Voltammetry

Cyclic voltammetry on compounds **1a** and **2** was carried out in anticipation that bioreductive activation may be implicated in cytotoxicity (Figure 4.17). Redox response experiments were carried out in dichloromethane, which showed that both **1a** and **2**

undergo two characteristic quasi-reversible one-electron redox processes corresponding to the 0/-1 redox transition (I and I′) and -1/-2 redox transition (II and II′).

Table 4.5. Formal Potentials ($E°′$) (±0.010 V) calculated as (Epc + Epa)/2 from cyclic voltammograms recorded at 100 mVs^{-1}.

Compound	$E°′$ [V] versus Fc/Fc$^+$	
	$E°′$ (I)	$E°′$ (II)
1a	-1.12	-1.75
2	-0.86	-1.55

Benzotriazinone **1a** displayed a redox potential ($E°′$) of -1.12 V vs. Fc/Fc$^+$ for the 0/-1 redox transition (I) and -1.75 V vs. Fc/Fc$^+$ for the -1/-2 redox transition (II) (Table 4.5). Benzotriazinone **2** produced a similar redox response to **1a**, although $E°′$ values for equivalent redox couples (I′ and II′) were shifted approximately +0.23 V in the positive direction (Table 4.5). This can be attributed to the strong inductive withdrawal by the 3-CF$_3$ of **2** relative to the 3-phenyl substituent present in **1a** resulting in an enhanced susceptibility of **2** to undergo reduction.
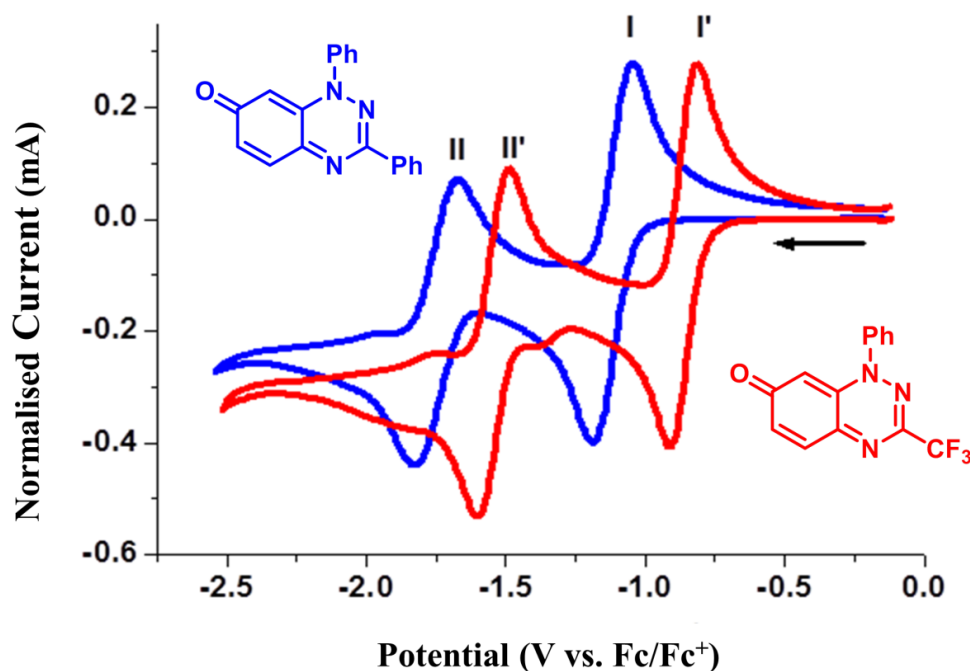
Figure 4.17. Cyclic voltammograms of **1a** (blue line) and **2** (red line) recorded in dichloromethane (0.1 M TBAP) at a glassy carbon electrode (scan rate: 0.1 V s^{-1}). Arrow indicates direction of scan.

4.3.5. Thioredoxin Reductase (TrxR) inhibition assays

To determine whether **1a** and **2** inhibited TrxR, the DTNB assay (Scheme 4.5) was used to estimate enzyme activity in the absence and presence of varying concentrations of inhibitor. The DTNB assay was performed in a 96-well microplate with the experimental set-up adapted from the Sigma-Aldrich technical bulletin (CS0170 Assay kit). A representative set-up using 40 µM DTNB as the substrate is shown in Table 4.6. A range of additional concentrations of 56, 80, 160, and 400 µM DTNB were used to follow enzyme activity. The positive control (Table 4.6) represents full uninhibited activity of TrxR. In contrast, positive control inhibition (Table 4.6) uses a known TrxR inhibitor that gives a baseline activity representing the total inhibition of TrxR. The inhibitors tested (Table 4.6) should display activity against TrxR between the baseline and full activity parameters. The assay was carried out in aqueous phosphate buffered solutions containing EDTA (metal ion sequestrant) and NADPH as an electron source for the DTNB reduction.

Table 4.6. Experimental setup for 96 well microplate assay.

Sample	Enzyme (TrxR)	Inhibitor	1× Assay Buffer	Diluted Inhibitor Solution	Working Buffer	DTNB (40 µM)
Positive Control DMSO	5 µL	2 µL (DMSO)	7 µL	—	180 µL	6 µL
Positive Control Inhibition	5 µL	—	5 µL	4 µL	180 µL	6 µL
1a (X µM)	5 µL	2 µL	7 µL	—	180 µL	6 µL

The reduction of DTNB by TrxR with NADPH to produce TNB (Scheme 4.5) gave a linear increase in absorbance at 405 nm with absorbance measured at intervals of 5 minutes for a period of 50 minutes. The change in absorbances with varied inhibitor concentrations was converted into TrxR activity using Equation 4.1.

$$Unit\ mL^{-1} = \frac{\Delta A_{405} min^{-1}(thioredoxin\ reductase) \times dil\ \times vol}{enzvol}$$

Equation 4.1. A unit of mammalian TrxR is defined as the amount of enzyme that will cause an increase in A_{405} of 1.0 min^{-1}mL^{-1} at pH 7.0 and 25 °C. ΔA_{405} min^{-1}(TrxR) = [ΔA_{405} min^{-1} (sample) - ΔA_{405} min^{-1} (sample + inhibitor)]; dil = sample dilution factor; vol = total reaction volume; enzvol = enzyme volume.

Taking the ΔA_{405} from the linear portion of the absorbance plot, TrxR activity was quantified at each [S] in presence and absence of different [I]. The enzyme specific activity (Units/µg protein) or initial velocity (V_0) was calculated by dividing the Unit mL^{-1} value by TrxR concentration (2.5×10^{-3} µg/mL) in the well. The reciprocal of V_0 data was plotted against the reciprocal of [S] and analysed on Lineweaver-Burk plots (Figure 4.18).
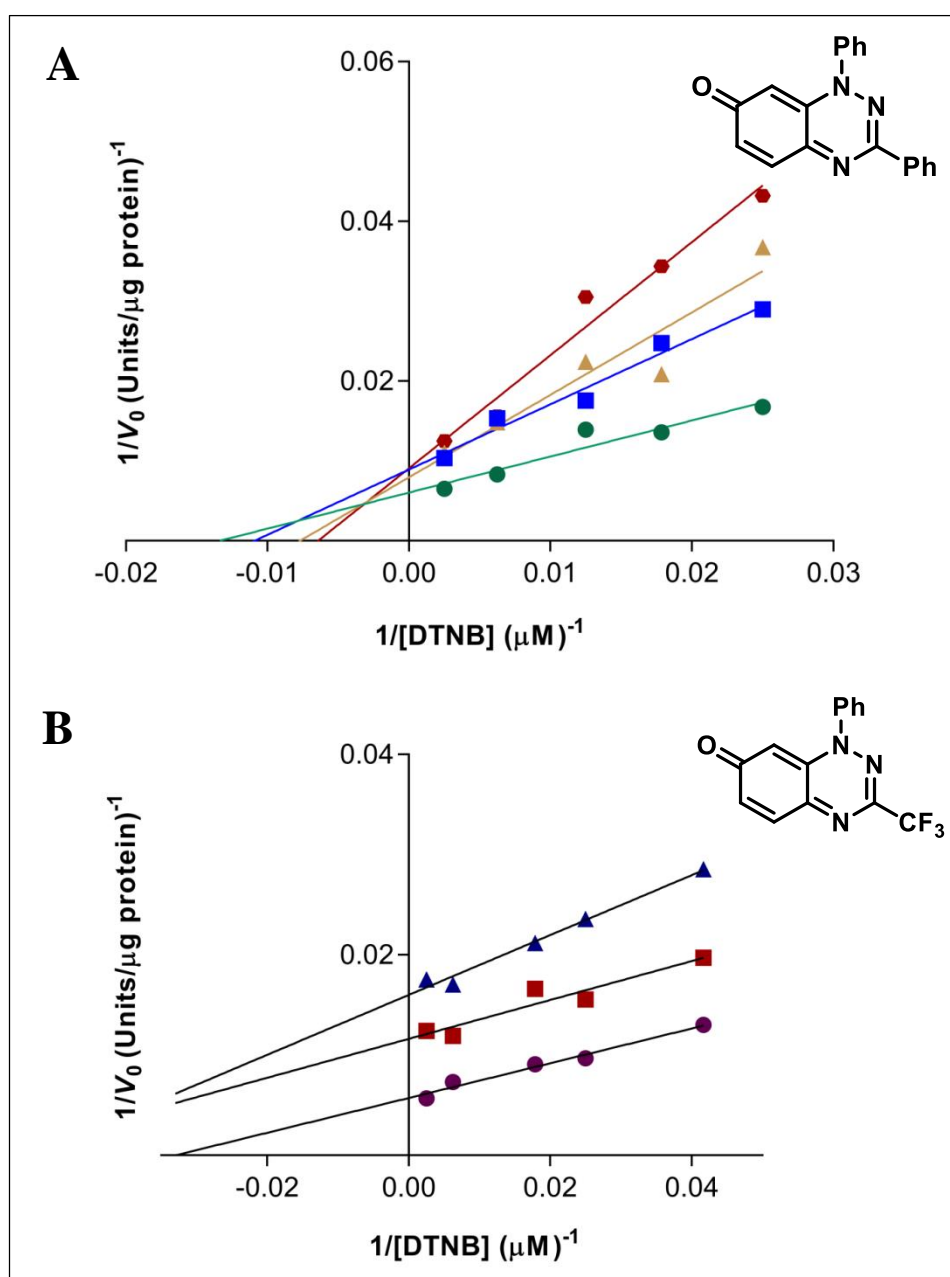
Figure 4.18. Kinetics of thioredoxin reductase (TrxR) inhibition by **1a** and **2** using DTNB as the substrate: (**A**) Lineweaver-Burk plot with inhibitor **1a** concentrations of 0 (●), 0.15 (■), 0.30 (▲) and 0.50 (●) µM. (**B**) Lineweaver-Burk plot with inhibitor **2** concentrations of 0 (●), 0.30 (■) and 1 (▲) µM. Each assay point represents an average from three independent experiments carried out in duplicate.

In the case of **1a**, V_{max} decreased and K_m increased with increasing inhibitor, characteristic of mixed inhibition. However, **2** is more characteristic of uncompetitive inhibition where V_{max} decreased with increasing inhibitor and K_m was lower in the presence of inhibitor, than in the uninhibited condition (Figure 4.18). To estimate the K_i value, a secondary plot (Figure 4.19) of the slopes of the Lineweaver-Burk plot against inhibitor concentrations was generated. K_i values were found to be 3.90 and 0.78 μM for compounds **1a** and **2** respectively. The lower K_i for **2** towards the reductase enzyme may be attributed to the greater ease of reduction as determined by cyclic voltammetry (Figure 4.17, Table 4.5). Therefore benzotriazinones **1a** and **2** clearly inhibit TrxR, but unlike pleurotin the mode of inhibition is reversible rather than irreversible. The K_i value for the electron-deficient iminoquinone **2** is closer in magnitude to that of pleurotin (K_i 0.28 μM).[37, 27]
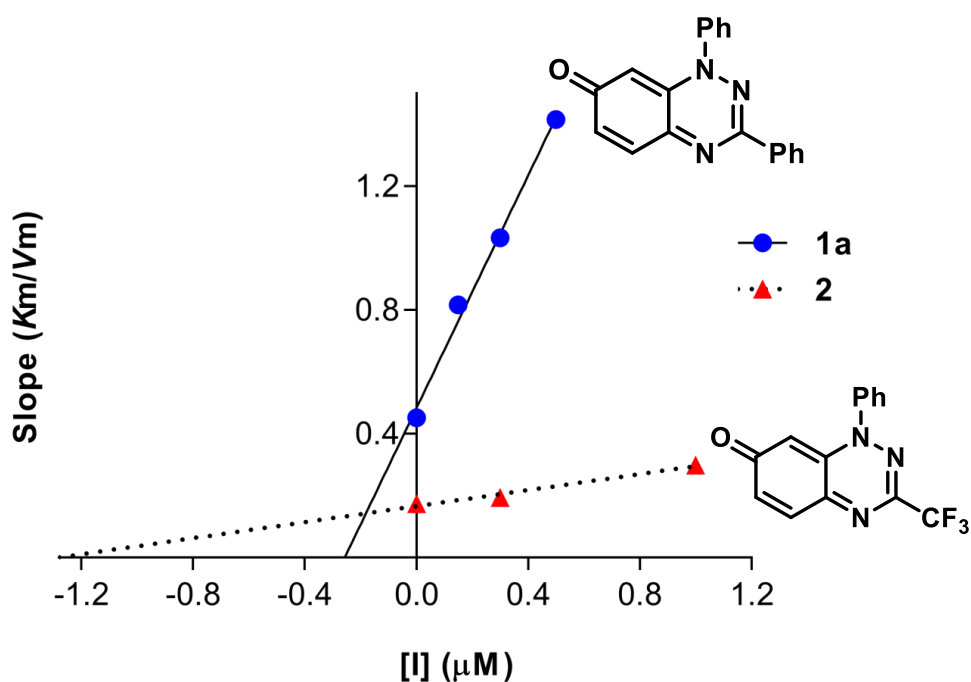
Figure 4.19. Graphical determination of K_i for **1a** and **2** using the slopes of the Lineweaver-Burk plots in Figure 4.18 plotted against inhibitor concentrations.

4.3.6. NCI-60 human tumour cell line screen and COMPARE anaylsis of pyridinyl substituted benzo[1,2,4]-triazine-7-ones

Our collaborators prepared pyridinyl substituted benzotriazinones **3a** and **3b** (Figure 4.20),[101] as incorporation of pyridine rings and varying the position of its *N*-heteroatom on the pyridine substituent, has been reported to alter the toxicity of benzimidazolequinones.[102]

3a

NSC: 780815

3b

NSC: 780816
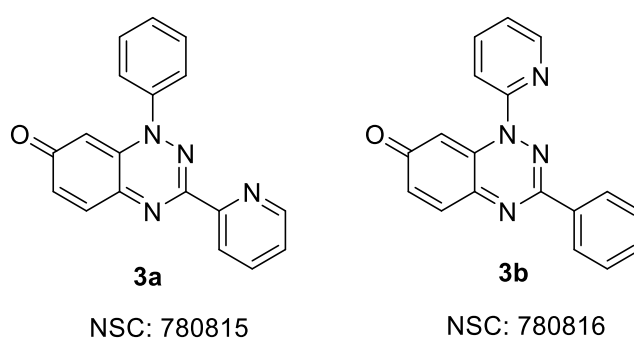
Figure 4.20. Pyridinyl substituted benzo[1,2,4]-triazine-7-ones **3a** and **3b** evaluated by NCI-60 screening and COMPARE analysis.

The isomeric compounds were evaluated at the NCI against the 60 cell line panel and exhibited similar cytotoxicity profiles with one-dose screening indicating little variability with changes in the location of the pyridine nitrogen (Figure 4.21).
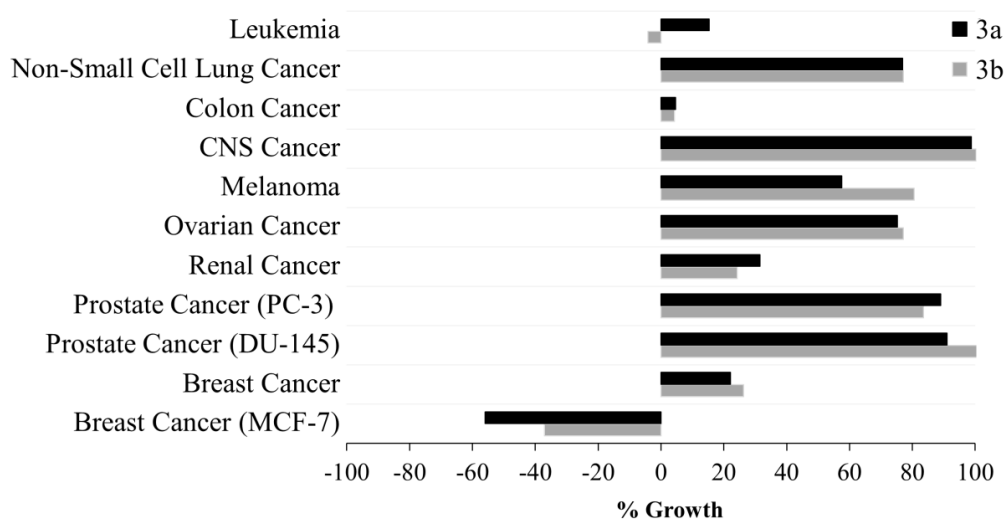
Figure 4.21. Summary of DTP NCI-60 one-dose (10 μM) screening results for compounds **3a** and **3b** expressed as average percent growth of each cancer type relative to untreated cells.

Similarly to the parent compound **1a**, pyridine substituted benzotriazinones **3a** and **3b** showed exceptional specificity towards the breast cancer MCF-7 cell line despite a lack of lethality towards the other cell lines. Compound **3a** had a mean growth of 50.31% and was most active against the ACHN cell line with a mean growth of -84.7% (Figure 4.21, Appendix (Table A.4.5)). Similarly compound **3b** had a mean growth of 53.32% and again displayed the greatest lethality towards the ACHN cell line with mean growth of -91.85% (Appendix, Table A.4.7). The DU-145 cell line was resistant to treatment with both **3a** and **3b** (Figure 4.21), in sharp contrast to high activity observed against **1a** and **2** (Figure 4.14). A slight difference in activity towards leukemia was observed, with **3b** expressing lethality by having a mean growth of -4.13% while **3a** expressed cell growth inhibition (Figure 4.21).

Table 4.7. Mean graph-midpoint (MG-MID) GI_{50}, TGI, LC_{50} values of **3a** and **3b** against all 60 cell lines in NCI panel.

Compound	GI_{50} (µM)	TGI (µM)	LC_{50} (µM)
3a	2.88	8.91	28.18
3b	6.92	19.50	53.70

The NCI selected **3a** and **3b** for further five-dose testing. The 3-substitued pyridinyl **3a** is two times more active than **3b** across the GI50, TGI, and LC_{50} endpoint values (Table 4.7) despite both of them exhibiting similar mean percent growths in one-dose testing. In fact, **3a** is more active than pleurotin and compound **2** (Table 4.1, Table 4.3) but the parent compound **1a** remains the most active of the benzotriazinones tested. Both compounds **3a** and **3b** were most selective towards renal cancer. The pryridinyl isomers were cytostatic towards leukemia (Appendix, Table A.4.6 and Table A.4.8), an effect that was also observed for **1a** and **2**. In addition, both **3a** and **3b** were cytostatic toward the MCF-7 breast cancer cell line. Pyridine **3a** altered activity towards prostate cancer with selectivity flipped towards the PC-3 prostate cancer cell line, which is opposite to that reported for **1a** and **2** which were selective towards the DU-145 prostate cancer cell line (Appendix, Table A.4.2 and Table A.4.4). Pyridine **3b** displayed no selectivity at all to either prostate cancer cell line and had an insignificant GI_{50} value of approximately 14 µM against prostate cancer (Appendix, Table A.4.8).

COMPARE analysis correlated the GI$_{50}$ values of **3a** and **3b** with synthetic compounds and molecular targets in the NCI database (Table 4.8). The derived Pearson coefficients produced a similar response to that of **1a** with very strong correlations to the naturally occurring antibiotic of pleurotin (0.73-0.84), implicating them as possible TrxR inhibitors. Interestingly, **3b** had poorer activity against the NCI-60 cell lines, but correlates better to pleurotin. Correlation to the biological marker MAPK14 also showed a preference for the isomer **3b** with a coefficient of 0.527. The PCCs for **3b** towards pleurotin and MAPK14 are the highest of all the benzotriazinones screened, which could implicate **3b** as a potent TrxR inhibitor (Table 4.8).

Table 4.8. Pearson correlation coefficients obtained by COMPARE analysis.

Compound	Pleurotin	MAPK14
1a	0.841	0.450
3a	0.730	0.391
3b	0.842	0.527

4.4. Experimental

4.4.1 Cell culture and cytotoxicity evaluation

4.4.1.1. Cell culture

An SV40-transformed normal human fibroblast cell line (repository number GM00637) was obtained from the National Institute for General Medical Sciences (NIGMS) Human Genetic Cell Repository (Coriell Institute for Medical Research, New Jersey, USA). The DU-145 prostate cancer cell line (ATCC repository number HTB-81) was obtained from Professor R.W.G. Watson, School of Medicine & Medical Sciences, University College Dublin, Ireland. The MCF-7 cell line, a human breast cancer cell line was obtained from Dr. Adrienne Gorman, Biochemistry, School of Natural Sciences, National University of Ireland Galway.

The SV40-transformed normal human skin fibroblast cell line (GM00637) was grown in minimum essential media (MEM) Eagle-Earle BSS supplemented with 15% heat-inactivated fetal bovine serum (FBS), penicillin-streptomycin, 2 mM L-glutamine, 2X essential and non-essential amino acids and vitamins. DU-145 prostate cancer cells were grown in RPMI-1640 medium supplemented with 10% heat-inactivated fetal bovine serum, penicillin-streptomycin and 2 mM L-glutamine. MCF-7 cells were cultured in Dulbecco's modified Eagle medium (DMEM) containing high glucose (4.5 mg/mL) and supplemented with 10% heat-inactivated FBS and 1% penicillin-streptomycin.

4.4.1.2. Cytotoxicity measurement

Cell viability was determined using the MTT colorimetric assay.[90] Normal cells were plated into 96-well plates at a density of 10,000 cells per well (200 µL per well) and allowed to adhere over a period of 24 h. DU-145 cells were plated into 96-well plates at a density of 2,000 cells per well (200 µL per well) and allowed to adhere over a period of 24 h. MCF-7 cells were plated into 96-well plates at a density of 1,000 cells per well (200 µL per well) and allowed to adhere over a period of 24 h. Compound solutions were applied in DMSO (1% v/v final concentration in well). Cells were then incubated at 37 °C under a humified atmosphere containing 5% CO_2 for 72 h. Control cells were exposed to an equivalent concentration of DMSO alone. MTT (20 µL, 5 mg/mL solution) was added, and

the cells were incubated for another 4 h. The supernatant was removed carefully by pipette. The resultant MTT formazan crystals were dissolved in 100 μL of DMSO and absorbance was determined on a plate reader at 550 nm with a reference at 690 nm. Cell viability is expressed as a percentage of the DMSO-only treated value. Dose-response curves were analyzed by non-linear regression analysis and IC_{50} values were estimated using GraphPad Prism software, v 6.03 (GraphPad Inc., San Diego, CA, USA).

4.4.2 Electrochemistry

Cyclic voltammograms were recorded using a PalmsSens EmStat3+ potentiostat. Samples (~2 mmol) were dissolved in dichloromethane containing 0.1 M tetrabutylammonium perchlorate (TBAP) as supporting electrolyte and 1 mM ferrocene (Fc) as an internal reference. Voltammograms were recorded in a single compartment electrochemical cell (0.5 mL volume) containing a glassy carbon disk working electrode (3 mm diameter), an Ag/AgCl reference electrode and a Pt wire counter electrode. All measurements were recorded under nitrogen at room temperature.

4.4.3 Thioredoxin Reductase (TrxR) inhibition studies

4.4.3.1. Materials

The thioredoxin reductase assay kit (Sigma Aldrich CS0170) contained all reagents and enzyme required for the thioredoxin reductase assay and was used as received. Rat liver thioredoxin reductase was in 50 mM Tris-HCl, pH 7.4, containing 1 mM EDTA, 300 mM NaCl, and 10% glycerol. The working buffer contained 100 mM potassium phosphate with 10 mM EDTA, 0.24 mM NADPH and the assay buffer 5× contained 500 mM potassium phosphate, pH 7.0 and 50 mM EDTA.

4.5. Conclusions

In summary, MTT studies showed that varying the substituent at the 6-position of the 1,3-diphenylbenzo[1,2,4]triazin-7-ones decreases toxicity against cancer cell lines. Parent **1a** is generally more cytotoxic towards cancer cell lines, although the 3-CF$_3$ substituted variant **2** shows greater specificity towards solid tumour cell lines in comparison to a normal fibroblast cell line. NCI-60 one- and five-dose testing reported the same trend of **1a** being more active than **2** with both compounds particularly selective towards leukemia and the MCF-7 breast cancer cell line.

Using NCI COMPARE, parent compound **1a** and 3-CF$_3$ substituted analogue **2** were found to have very strong correlations to a naturally occurring anti-cancer agent pleurotin. Benzotriazinones **1a** and **2** are TrxR inhibitors, although the mechanism for inhibition is reversible rather than irreversible as for pleurotin. Specifically, **1a** and **2** display mixed-type and uncompetitive inhibition respectively. The latter CF$_3$-substituted compound is more easily reducible and shows a more than five-fold greater inhibition of TrxR.

Compound **3a** has demonstrated activity two times greater than **3b** across the NCI-60 five-dose screen. Pyridinyl substitution at the 3-position (**3a**) has given unique selectivity towards the PC-3 prostate cancer cell line, which is usually inactive against heterocyclic quinones. Pyridines **3a** and **3b** correlated strongly to pleurotin implicating them also as potential TrxR inhibitors.

4.6.   Future work

The alkoxy and amine substitutents at the 6-position of benzotriazinones gave diminished activity against cancer cell lines when compared to the parent compound **1a**. The introduction of a DNA damaging aziridine moiety at the 6-position could give specificity to different cancer molecular targets (Figure 4.22). Benzimidazolequinones substituted and tethered with aziridinyl moieties have previously induced hypersensitivity of FA cells lacking FANCD2 protein with cytotoxicity in the nanomolar range.[97, 103]
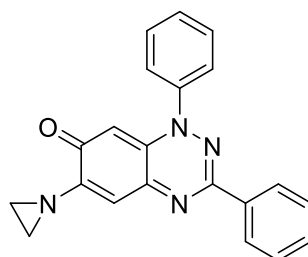
Figure 4.22. Proposed aziridnyl substituted 1,3-diphenylbenzo[1,2,4]triazin-7-one to target Fanconi anaemia.

The fusion of the parent benzotriazinone at N-1 and C-8 positions produces a highly conjugated triazafluoranthenone with four coplanar rings (Figure 4.23). From literature, it is observed that optimal DNA intercalation with quinones involves three or four coplanar rings and a *p*-conjugated quinone containing a nitrogen atom that facilitates hydrogen bonding with DNA.[104, 105] Triazafluoranthenone could serve as a potential topoisomerase inhibitor as numerous heterocyclic quinones exert this inhibition through DNA intercalation.[104]

Triazafluoranthenone
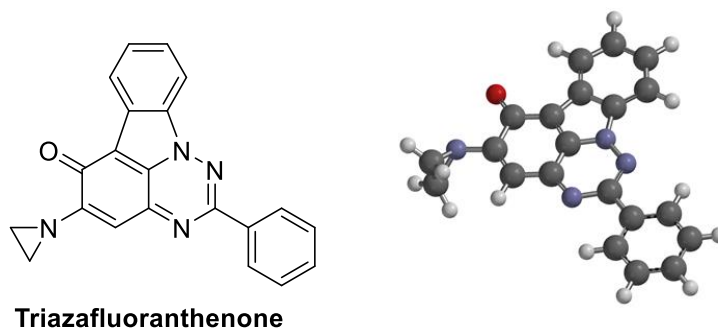
Figure 4.23. Triazafluoranthenone as a potential DNA-intercalator. Model image was rendered using semi-empirical geometry optimization (PM3) in the gas phase at 298 K with Spartan® software.

4.7.   References

1.   Huisgen, R.; Wulff, J. *Chem. Ber.* **1969**, *102*, 1848-1858.

2.   Neugebauer, F. A.; Umminger, I. *Chem. Ber.* **1980**, *113*, 1205-1225.

3.   Kadirov, M. K.; Buzykin, B. I.; Gazetdinova, N. G. *Russ. Chem. Bull.* **2002**, *51*, 1796-1799.

4.   Koutentis, P. A.; Lo Re, D. *Synthesis* **2010**, *2010*, 2075-2079.

5.   Constantinides, C. P.; Koutentis, P. A., Chapter Seven - Stable N- and N/S-Rich Heterocyclic Radicals: Synthesis and Applications. In *Adv. Heterocycl. Chem.*, Scriven, E. F. V.; Ramsden, C. A., Eds. Academic Press 2016; Vol. 119, pp 173-207.

6.   Koutentis, P. A.; Krassos, H.; Lo Re, D. *Org. Biomol. Chem.* **2011**, *9*, 5228-5237.

7.   Constantinides, C. P.; Berezin, A. A.; Zissimou, G. A.; Manoli, M.; Leitus, G. M.; Bendikov, M.; Probert, M. R.; Rawson, J. M.; Koutentis, P. A. *J. Am. Chem. Soc.* **2014**, *136*, 11906-11909.

8.   Berezin, A. A.; Constantinides, C. P.; Drouza, C.; Manoli, M.; Koutentis, P. A. *Org. Lett.* **2012**, *14*, 5586-5589.

9.   Ioannou, T. A.; Koutentis, P. A.; Krassos, H.; Loizou, G.; Lo Re, D. *Org. Biomol. Chem.* **2012**, *10*, 1339-1348.

10.   Berezin, A. A.; Zissimou, G.; Constantinides, C. P.; Beldjoudi, Y.; Rawson, J. M.; Koutentis, P. A. *J. Org. Chem.* **2014**, *79*, 314-327.

11.   Catto, M.; Berezin, A. A.; Lo Re, D.; Loizou, G.; Demetriades, M.; De Stradis, A.; Campagna, F.; Koutentis, P. A.; Carotti, A. *Eur. J. Med. Chem.* **2012**, *58*, 84-97.

12.   Koutentis, P. A.; Loizou, G.; Lo Re, D. *J. Org. Chem.* **2011**, *76*, 5793-5802.

13.   Fagan, V.; Bonham, S.; Carty, M. P.; Saenz-Méndez, P.; Eriksson, L. A.; Aldabbagh, F. *Bioorg. Med. Chem.* **2012**, *20*, 3223-3232.

14.   Fagan, V.; Bonham, S.; McArdle, P.; Carty, M. P.; Aldabbagh, F. *Eur. J. Org. Chem.* **2012**, *2012*, 1967-1975.

15.   Chabner, B. A. *J. Natl. Cancer Inst.* **2016**, *108*, djv388.

16.   Shoemaker, R. H. *Nat. Rev. Cancer* **2006**, *6*, 813-823.

17.   Paull, K. D.; Lin, C. M.; Malspeis, L.; Hamel, E. *Cancer Res.* **1992**, *52*, 3892-3900.

18.   Skehan, P.; Storeng, R.; Scudiero, D.; Monks, A.; McMahon, J.; Vistica, D.; Warren, J. T.; Bokesch, H.; Kenney, S.; Boyd, M. R. *J. Natl. Cancer Inst.* **1990**, *82*, 1107-1112.

19. Vichai, V.; Kirtikara, K. *Nat. Protoc.* **2006**, *1*, 1112-1116.

20. Beck, D. E.; Abdelmalak, M.; Lv, W.; Reddy, P. V. N.; Tender, G. S.; O'Neill, E.; Agama, K.; Marchand, C.; Pommier, Y.; Cushman, M. *J. Med. Chem.* **2015**, *58*, 3997-4015.

21. Boyd, M. R.; Paull, K. D. *Drug Dev. Res.* **1995**, *34*, 91-109.

22. COMPARE Analysis Methodology. https://dtp.cancer.gov/databases_tools/docs/compare/compare_methodology.htm (accessed Sep 12, 2019).

23. Paull, K. D.; Shoemaker, R. H.; Hodes, L.; Monks, A.; Scudiero, D. A.; Rubinstein, L.; Plowman, J.; Boyd, M. R. *J. Natl. Cancer Inst.* **1989**, *81*, 1088-1092.

24. Holbeck, S. L.; Collins, J. M.; Doroshow, J. H. *Mol. Cancer Ther.* **2010**, *9*, 1451-1460.

25. COMPARE Analysis. https://dtp.cancer.gov/databases_tools/compare.htm (accessed Sep 12, 2019).

26. Akoglu, H. *Turk. J. Emerg. Med.* **2018**, *18*, 91-93.

27. Kunkel, M. W.; Kirkpatrick, D. L.; Johnson, J. I.; Powis, G. *Anti-Cancer Drug Des.* **1997**, *12*, 659-670.

28. Schmidt-Dannert, C., Biosynthesis of Terpenoid Natural Products in Fungi. In *Biotechnology of Isoprenoids*, Schrader, J.; Bohlmann, J., Eds. Springer International Publishing: Cham, 2015; pp 19-61.

29. Novak, R. *Ann. N. Y. Acad. Sci.* **2011**, *1241*, 71-81.

30. Robbins, W. J.; Kavanagh, F.; Hervey, A. *Proc. Natl. Acad. Sci. U.S.A.* **1947**, *33*, 171-176.

31. Hart, D. J.; Huang, H. C. *J. Am. Chem. Soc.* **1988**, *110*, 1634-1635.

32. Hart, D. J.; Huang, H. C.; Krishnamurthy, R.; Schwartz, T. *J. Am. Chem. Soc.* **1989**, *111*, 7507-7519.

33. Shipley, S. M.; Barr, A. L.; Graf, S. J.; Collins, R. P.; McCloud, T. G.; Newman, D. J. *J. Ind. Microbiol. Biotechnol.* **2006**, *33*, 463-468.

34. Berdicevsky, I.; Kaufman, G.; Newman, D. J.; Horwitz, B. A. *Mycoses* **2009**, *52*, 313-317.

35. Stadler, M.; Sheldrick, W. S.; Dasen-brock, J.; Steglich, W.; Anke, H. *Nat. Prod. Lett.* **1994**, *4*, 209-216.

36. Riondel, J.; Beriel, H.; Dardas, A.; Carraz, G.; Oddoux, L. *Arzneim. Forsch.* **1981**, *31*, 293−299.

37. Welsh, S. J.; Williams, R. R.; Birmingham, A.; Newman, D. J.; Kirkpatrick, D. L.; Powis, G. *Mol. Cancer Ther.* **2003**, *2*, 235-243.

38. Carvalho, C. M. L.; Chew, E.-H.; Hashemy, S. I.; Lu, J.; Holmgren, A. *J. Biol. Chem.* **2008**, *283*, 11913-11923.

39. Holmgren, A.; Lu, J. *Biochem. Biophys. Res. Commun.* **2010**, *396*, 120-124.

40. Wipf, P.; Hopkins, T. D.; Jung, J.-K.; Rodriguez, S.; Birmingham, A.; Southwick, E. C.; Lazo, J. S.; Powis, G. *Bioorg. Med. Chem. Lett.* **2001**, *11*, 2637-2641.

41. Gromer, S.; Urig, S.; Becker, K. *Med. Res. Rev.* **2004**, *24*, 40-89.

42. Nordberg, J.; Arnér, E. S. J. *Free Radical Biol. Med.* **2001**, *31*, 1287-1312.

43. Mustacich, D.; Powis, G. *Biochem. J.* **2000**, *346*, 1-8.

44. Cai, W.; Zhang, L.; Song, Y.; Wang, B.; Zhang, B.; Cui, X.; Hu, G.; Liu, Y.; Wu, J.; Fang, J. *Free Radical Biol. Med.* **2012**, *52*, 257-265.

45. Zhang, B.; Zhang, J.; Peng, S.; Liu, R.; Li, X.; Hou, Y.; Han, X.; Fang, J. *Expert Opin. Ther. Pat.* **2017**, *27*, 547-556.

46. Zhang, J.; Li, X.; Han, X.; Liu, R.; Fang, J. *Trends Pharmacol. Sci.* **2017**, *38*, 794-808.

47. Jia, J.-J.; Geng, W.-S.; Wang, Z.-Q.; Chen, L.; Zeng, X.-S. *Cancer Chemother. Pharmacol.* **2019**, *84*, 453-470.

48. Lee, S.; Kim, S. M.; Lee, R. T. *Antioxid. Redox Signaling* **2012**, *18*, 1165-1207.

49. Meuillet, E. J.; Mahadevan, D.; Berggren, M.; Coon, A.; Powis, G. *Arch. Biochem. Biophys.* **2004**, *429*, 123-133.

50. Arnér, E. S. J.; Holmgren, A. *Eur. J. Biochem.* **2000**, *267*, 6102-6109.

51. Wipf, P.; Lynch, S. M.; Birmingham, A.; Tamayo, G.; Jiménez, A.; Campos, N.; Powis, G. *Org. Biomol. Chem.* **2004**, *2*, 1651-1658.

52. Karlenius, T. C.; Tonissen, K. F. *Cancers* **2010**, *2*, 209-232.

53. Gallegos, A.; Gasdaska, J. R.; Taylor, C. W.; Paine-Murrieta, G. D.; Goodman, D.; Gasdaska, P. Y.; Berggren, M.; Briehl, M. M.; Powis, G. *Cancer Res.* **1996**, *56*, 5765-5770.

54. Anestål, K.; Prast-Nielsen, S.; Cenas, N.; Arnér, E. S. J. *PLoS One* **2008**, *3*, e1846.

55. Arnér, E. S. J.; Holmgren, A., Measurement of Thioredoxin and Thioredoxin Reductase. In *Current Protocols in Toxicology*, John Wiley & Sons, New York, 2005; Vol. 24, pp 7.4.1-7.4.14.

56. Gandin, V.; Fernandes, A. P. *Molecules* **2015**, *20*, 12732-12756.

57. Becker, K.; Gromer, S.; Schirmer, R. H.; Müller, S. *Eur. J. Biochem.* **2000**, *267*, 6118-6125.

58. Kirkpatrick, D. L.; Powis, G. *Antioxid. Redox Signaling* **2016**, *26*, 262-273.

59. Zhang, X.; Selvaraju, K.; Saei, A. A.; D'Arcy, P.; Zubarev, R. A.; Arnér, E. S. J.; Linder, S. *Biochimie* **2019**, *162*, 46-54.

60. Marzano, C.; Gandin, V.; Folda, A.; Scutari, G.; Bindoli, A.; Rigobello, M. P. *Free Radical Biol. Med.* **2007**, *42*, 872-881.

61. Liu, Y.; Li, Y.; Yu, S.; Zhao, G. *Curr. Drug Targets* **2012**, *13*, 1432-1444.

62. Bian, M.; Fan, R.; Zhao, S.; Liu, W. *J. Med. Chem.* **2019**, *62*, 7309-7321.

63. Fang, J.; Lu, J.; Holmgren, A. *J. Biol. Chem.* **2005**, *280*, 25284-25290.

64. Zhang, B.; Liu, Y.; Li, X.; Xu, J.; Fang, J. *Chem. –Asian J.* **2018**, *13*, 3593-3600.

65. Mohammadi, F.; Soltani, A.; Ghahremanloo, A.; Javid, H.; Hashemy, S. I. *Cancer Chemother. Pharmacol.* **2019**, *84*, 925-935.

66. O'Brien, P. J. *Chem.-Biol. Interact.* **1991**, *80*, 1-41.

67. Paz, M. M.; Zhang, X.; Lu, J.; Holmgren, A. *Chem. Res. Toxicol.* **2012**, *25*, 1502-1511.

68. Yan, C.; Shieh, B.; Reigan, P.; Zhang, Z.; Colucci, M. A.; Chilloux, A.; Newsome, J. J.; Siegel, D.; Chan, D.; Moody, C. J.; Ross, D. *Mol. Pharmacol.* **2009**, *76*, 163-172.

69. Yan, C.; Siegel, D.; Newsome, J.; Chilloux, A.; Moody, C. J.; Ross, D. *Mol. Pharmacol.* **2012**, *81*, 401-410.

70. Cenas, N.; Nivinskas, H.; Anusevicius, Z.; Sarlauskas, J.; Lederer, F.; Arnér, E. S. J. *J. Biol. Chem.* **2004**, *279*, 2583-2592.

71. Schumacker, P. T. *Cancer Cell* **2006**, *10*, 175-176.

72. Trachootham, D.; Alexandre, J.; Huang, P. *Nat. Rev. Drug Discovery* **2009**, *8*, 579-591.

73. Verrax, J.; Beck, R.; Dejeans, N.; Glorieux, C.; Sid, B.; Pedrosa, R. C.; Benites, J.; Vasquez, D.; Valderrama, J. A.; Calderon, P. B. *Anti-Cancer Agents Med. Chem.* **2011**, *11*, 213-221.

74. Xu, J.; Cheng, Q.; Arnér, E. S. J. *Free Radical Biol. Med.* **2016**, *94*, 110-120.

75. Li, J.; Zuo, X.; Cheng, P.; Ren, X.; Sun, S.; Xu, J.; Holmgren, A.; Lu, J. *Metallomics* **2019**, *11*, 1490-1497.

76. Duan, D.; Zhang, B.; Yao, J.; Liu, Y.; Fang, J. *Free Radical Biol. Med.* **2014**, *70*, 182-193.

77. Jan, Y.-H.; Heck, D. E.; Dragomir, A.-C.; Gardner, C. R.; Laskin, D. L.; Laskin, J. D. *Chem. Res. Toxicol.* **2014**, *27*, 882-894.

78. Tonissen, K. F.; Di Trapani, G. *Mol. Nutr. Food Res.* **2009**, *53*, 87-103.

79. Cox, A. G.; Brown, K. K.; Arner, E. S. J.; Hampton, M. B. *Biochem. Pharmacol.* **2008**, *76*, 1097-1109.

80. Cheng, X.; Holenya, P.; Can, S.; Alborzinia, H.; Rubbiani, R.; Ott, I.; Wölfl, S. *Mol. Cancer* **2014**, *13*, 221.

81. Xie, W.; Ma, W.; Liu, P.; Zhou, F. *Mitochondrion* **2019**, *47*, 38-46.

82. Igea, A.; Nebreda, A. R. *Cancer Res.* **2015**, *75*, 3997-4002.

83. Saitoh, M.; Nishitoh, H.; Fujii, M.; Takeda, K.; Tobiume, K.; Sawada, Y.; Kawabata, M.; Miyazono, K.; Ichijo, H. *EMBO J.* **1998**, *17*, 2596-2606.

84. Ochs, R. S. *J. Chem. Educ.* **2000**, *77*, 1453-1456.

85. Gilbert, H. F., Enzyme Kinetics. In *Basic concepts in biochemistry: a student's survival guide*, 2001 International ed.; McGraw-Hill: Boston, 2001; pp 95-119.

86. Mohan, C.; Long, K. D.; Mutneja, M. An Introduction to Inhibitors and their Biological Applications. https://www.researchgate.net/publication/280494256_Introduction_to_Inhibitors (accessed Sep 12, 2019).

87. Cohlberg, J. A. *J. Chem. Educ.* **1979**, *56*, 512-514.

88. Lineweaver, H.; Burk, D. *J. Am. Chem. Soc.* **1934**, *56*, 658-666.

89. Cornish-Bowden, A., *Fundamentals of enzyme kinetics* Rev. ed.; Portland Press: London, 1995; pp 30-37, 56-57.

90. Mosmann, T. *J. Immunol. Methods* **1983**, *65*, 55-63.

91. Präbst, K.; Engelhardt, H.; Ringgeler, S.; Hübner, H., Basic Colorimetric Proliferation Assays: MTT, WST, and Resazurin. In *Cell Viability Assays: Methods and Protocols*, Gilbert, D. F.; Friedrich, O., Eds. Springer New York: New York, NY, 2017; pp 1-17.

92. Sylvester, P. W., Optimization of the Tetrazolium Dye (MTT) Colorimetric Assay for Cellular Growth and Viability. In *Drug Design and Discovery: Methods and Protocols*, Satyanarayanajois, S. D., Ed. Humana Press: Totowa, NJ, 2011; pp 157-168.

93. Vistica, D. T.; Skehan, P.; Scudiero, D.; Monks, A.; Pittman, A.; Boyd, M. R. *Cancer Res.* **1991**, *51*, 2515-2520.

94. Fitzsimmons, S. A.; Workman, P.; Grever, M.; Paull, K.; Camalier, R.; Lewis, A. D. *J. Natl. Cancer Inst.* **1996**, *88*, 259-269.

95. Yang, Y.; Zhang, Y.; Wu, Q.; Cui, X.; Lin, Z.; Liu, S.; Chen, L. *J. Exp. Clin. Cancer Res.* **2014**, *33*, 14.

96. Naylor, M. A.; Jaffar, M.; Nolan, J.; Stephens, M. A.; Butler, S.; Patel, K. B.; Everett, S. A.; Adams, G. E.; Stratford, I. J. *J. Med. Chem.* **1997**, *40*, 2335-2346.

97. Fahey, K.; O'Donovan, L.; Carr, M.; Carty, M. P.; Aldabbagh, F. *Eur. J. Med. Chem.* **2010**, *45*, 1873-1879.

98. Fagan, V. Synthesis and anti-cancer activity of novel imidazo[5, 4-*f*]benzimidazolequinones. Ph.D. Thesis, NUI Galway, Galway, Ireland 2011.

99. Targeted Cancer Therapies. https://www.cancer.gov/about-cancer/treatment/types/targeted-therapies/targeted-therapies-fact-sheet (accessed Sep 8, 2019).

100. Limoge, M.; Safina, A.; Truskinovsky, A. M.; Aljahdali, I.; Zonneville, J.; Gruevski, A.; Arteaga, C. L.; Bakin, A. V. *Oncotarget* **2017**, *8*, 61969-61981.

101. Keane, L.-A.; Mirallai, S.; Sweeney, M.; Carty, M.; Zissimou, G.; Berezin, A.; Koutentis, P.; Aldabbagh, F. *Molecules* **2018**, *23*, 574.

102. Garuti, L.; Roberti, M.; Pizzirani, D.; Pession, A.; Leoncini, E.; Cenci, V.; Hrelia, S. *Il Farmaco* **2004**, *59*, 663-668.

103. O'Donovan, L.; Carty, M. P.; Aldabbagh, F. *Chem. Commun.* **2008**, 5592-5594.

104. Garuti, L.; Roberti, M.; Pizzirani, D. *Mini-Rev. Med. Chem.* **2007**, *7*, 481-489.

105. Pindur, U.; Haber, M.; Sattler, K. *J. Chem. Educ.* **1993**, *70*, 263-269.

Appendix

A.1 NMR data of unpublished compounds

^{1}H NMR (400 MHz) of *N,N*-dibutyl-2,5-dimethoxy-4-nitroaniline (20) in CDCl₃

20
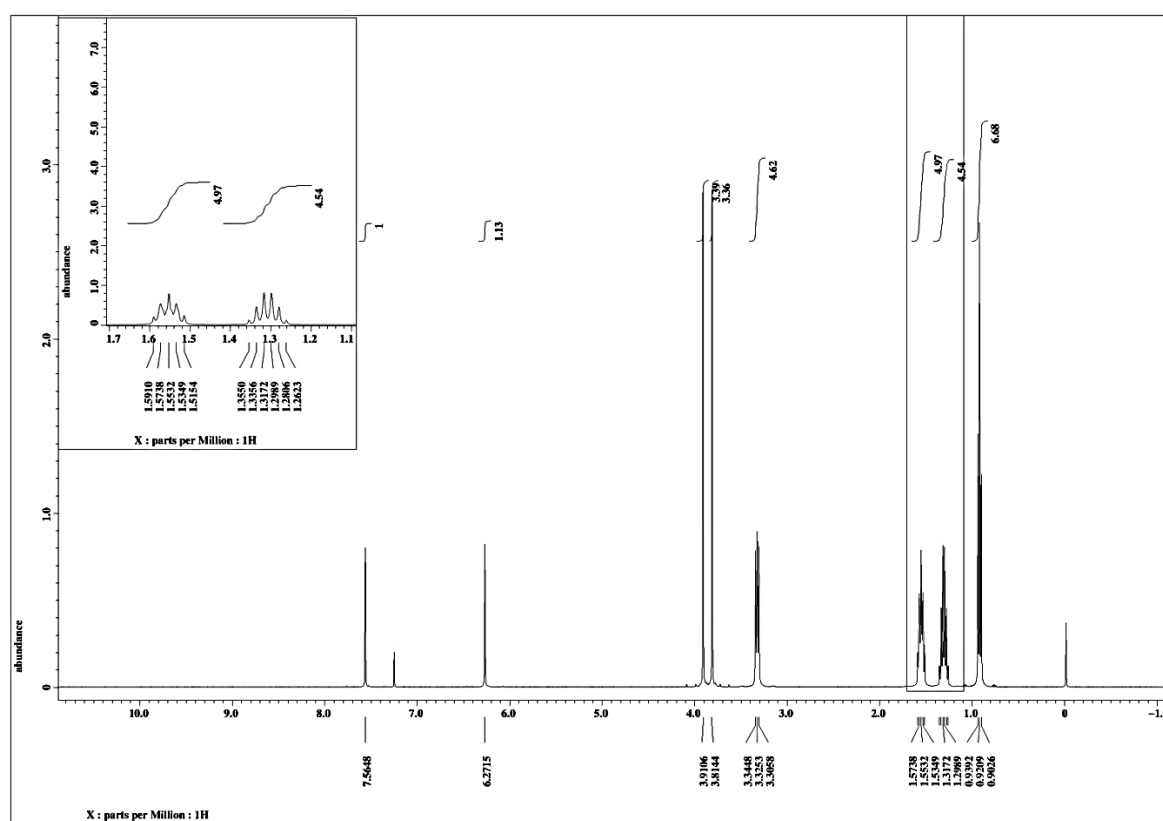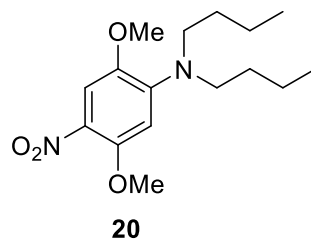
^{13}C NMR (100 MHz) of *N,N*-dibutyl-2,5-dimethoxy-4-nitroaniline (20) in CDCl$_3$

20

X : parts per Million : 13C

151.1816
147.2534
143.7065
128.3940
110.2211
101.4111
56.8274
56.3125
52.4224
29.9208
20.3862
14.0362

X : parts per Million : 13C
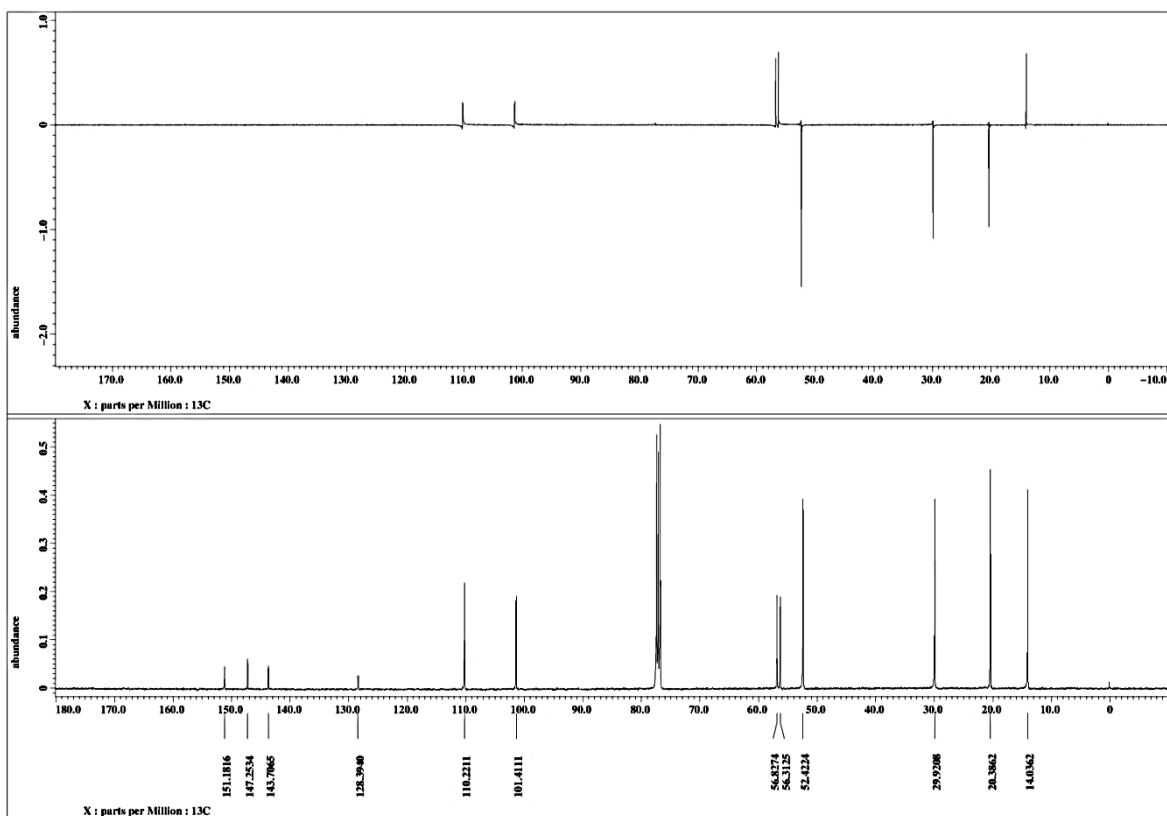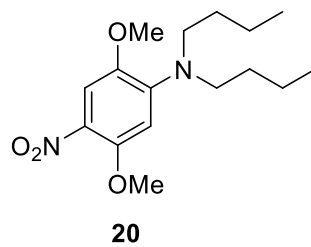
^{1}H NMR (400 MHz) of 1,2,4-trimethoxy-5-nitrobenzene (23) in CDCl$_3$

23
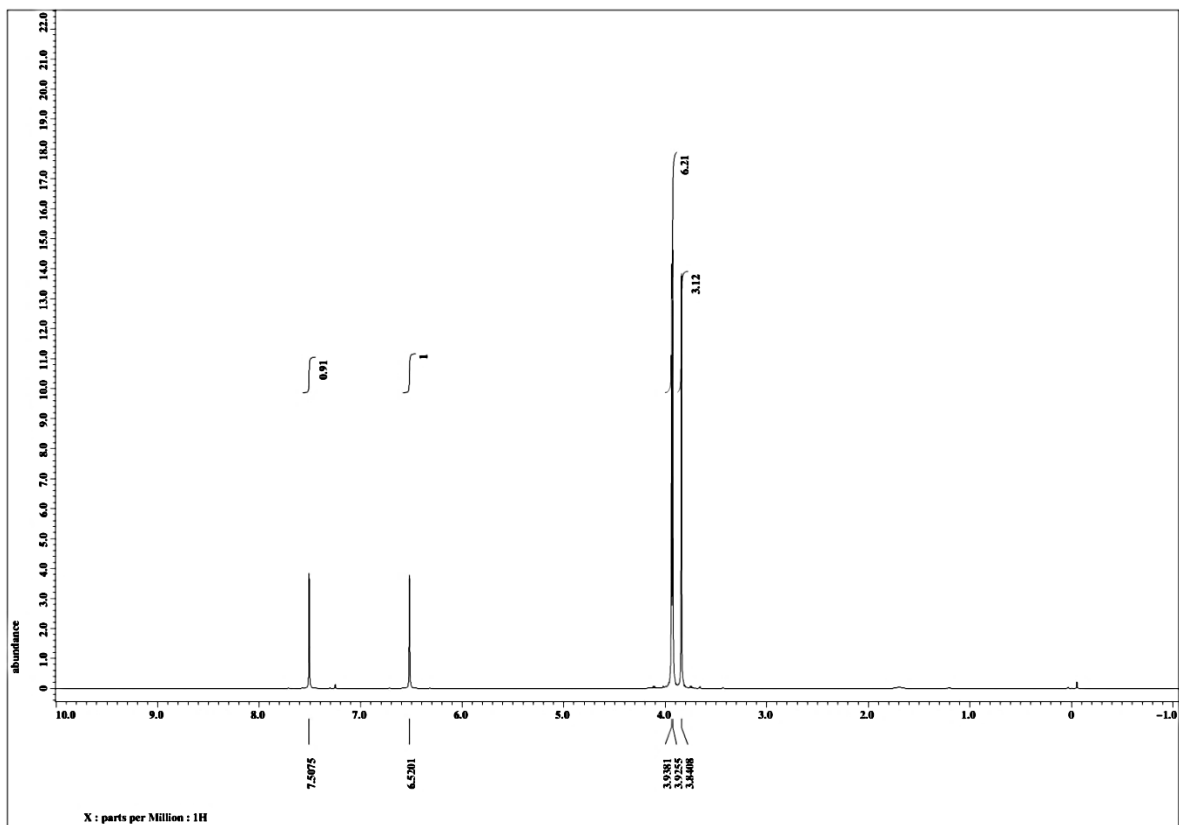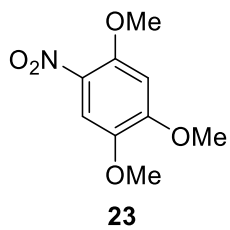
¹³C NMR (100 MHz) of 1,2,4-trimethoxy-5-nitrobenzene (23) in CDCl₃

23

X : parts per Million : 13C

X : parts per Million : 13C

154.8810
150.4761
142.7717
130.7967
108.9434
97.5210
57.2279
56.5604
56.5223
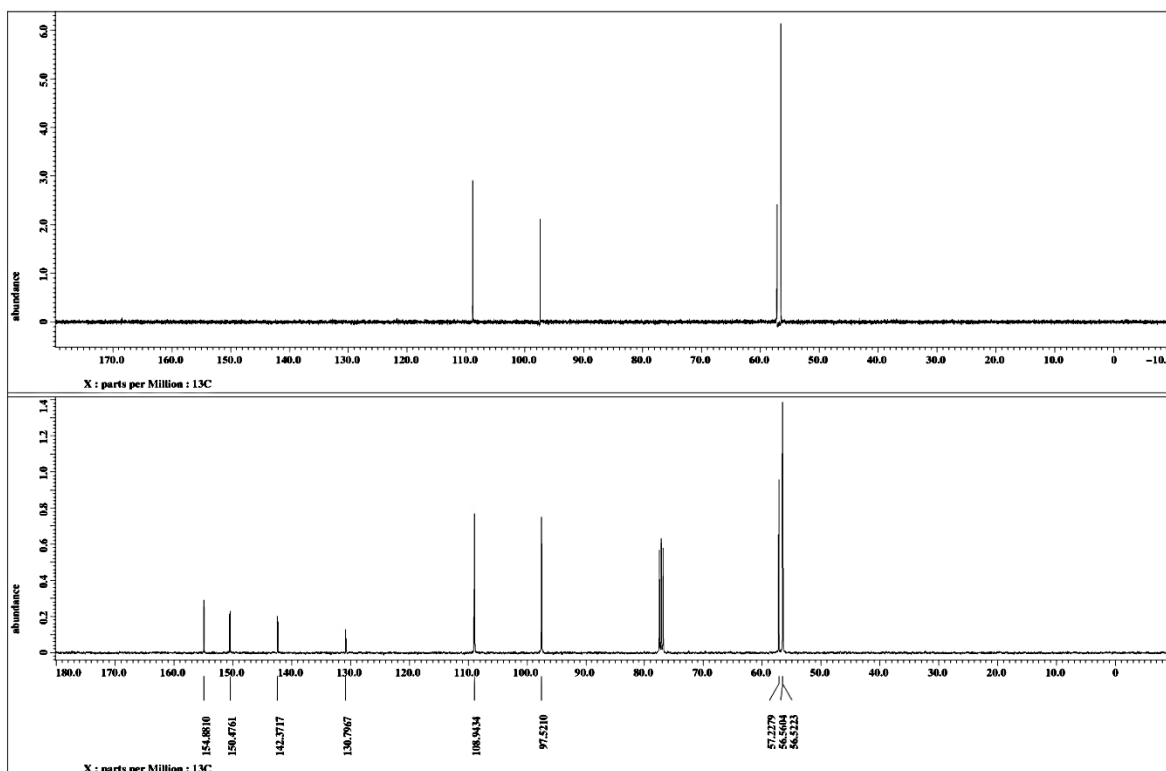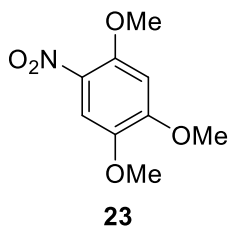
A.2 EI-MS spectra for ^{18}O-labeling experiments
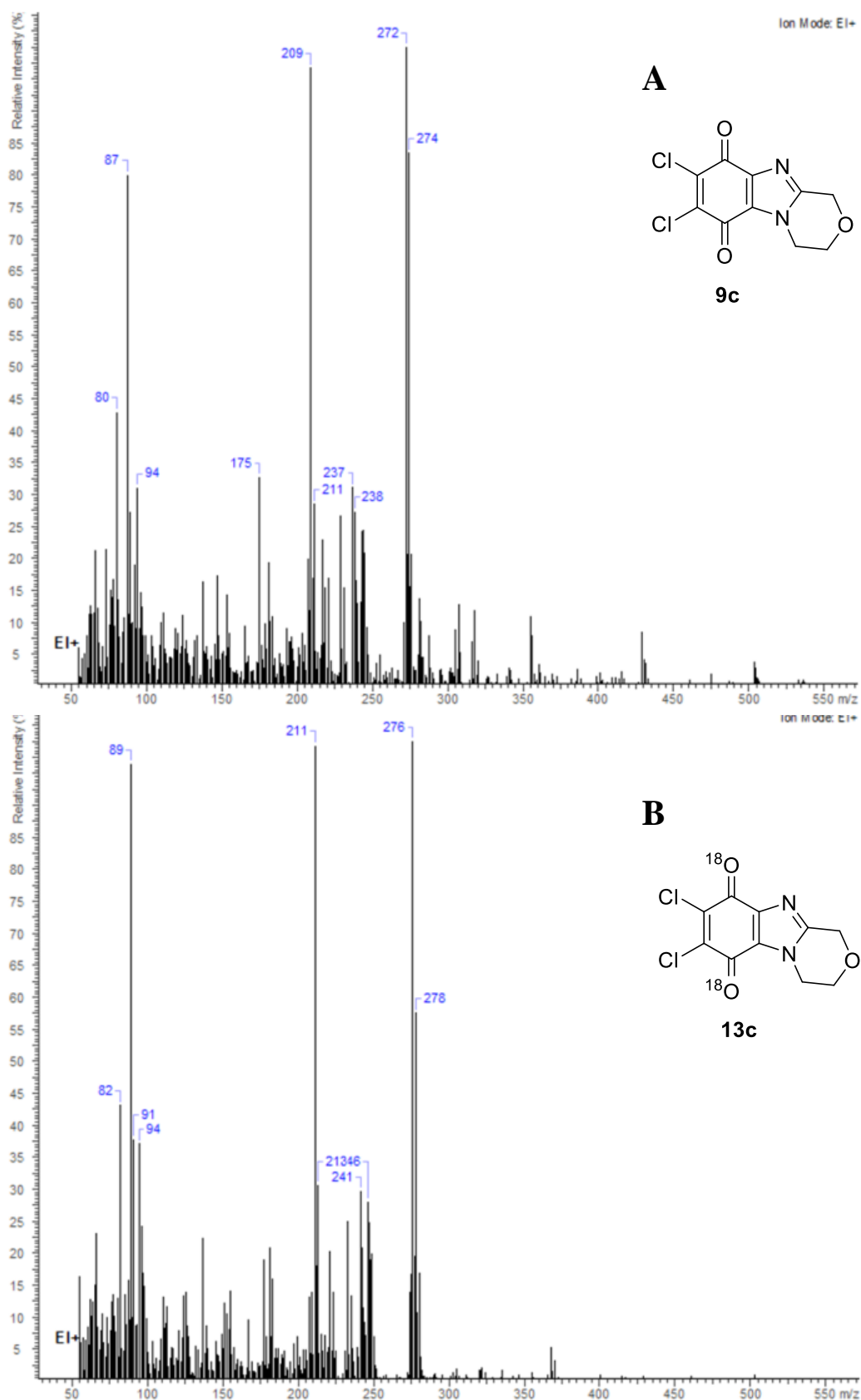
Figure A.2.1. (A) EI mass spectrum of 7,8-dichloro-3,4-dihydro-1*H*-[1,4]oxazino[4,3-*a*]benzimidazole-6,9-dione (**9c**). **(B)** EI mass spectrum, detecting doubly ^{18}O-labeled **13c**, indicating the role of water in quinone formation.
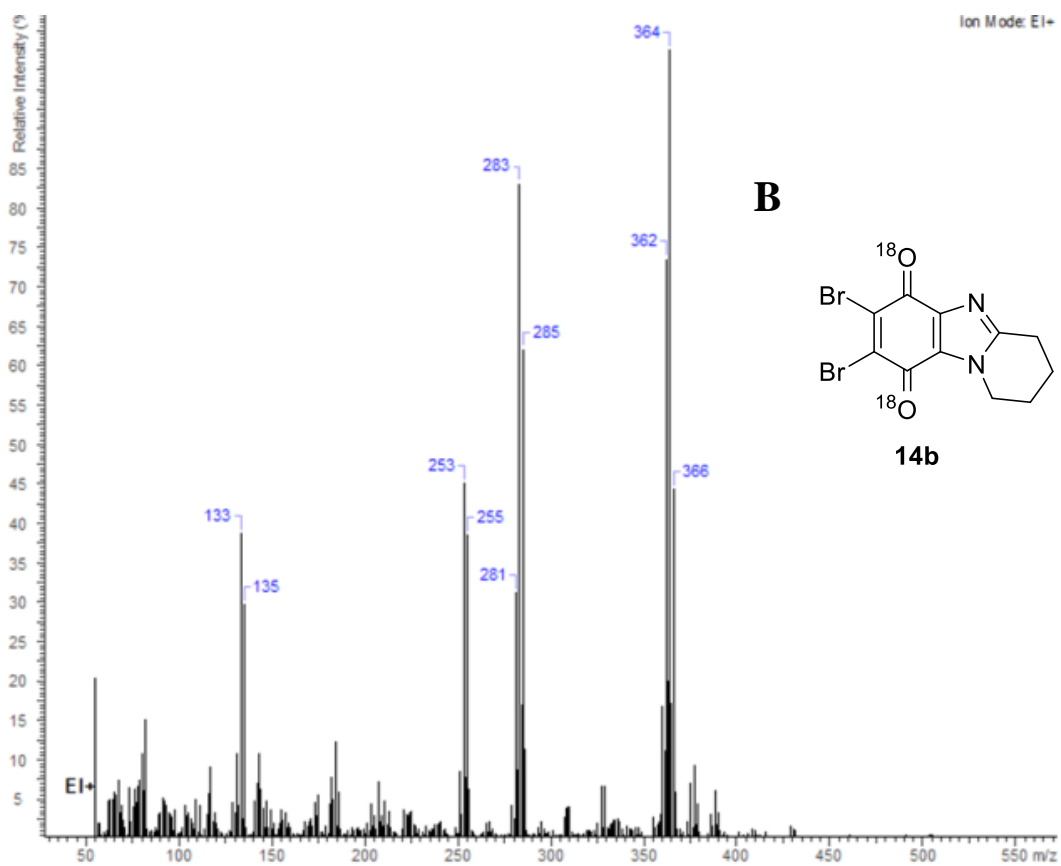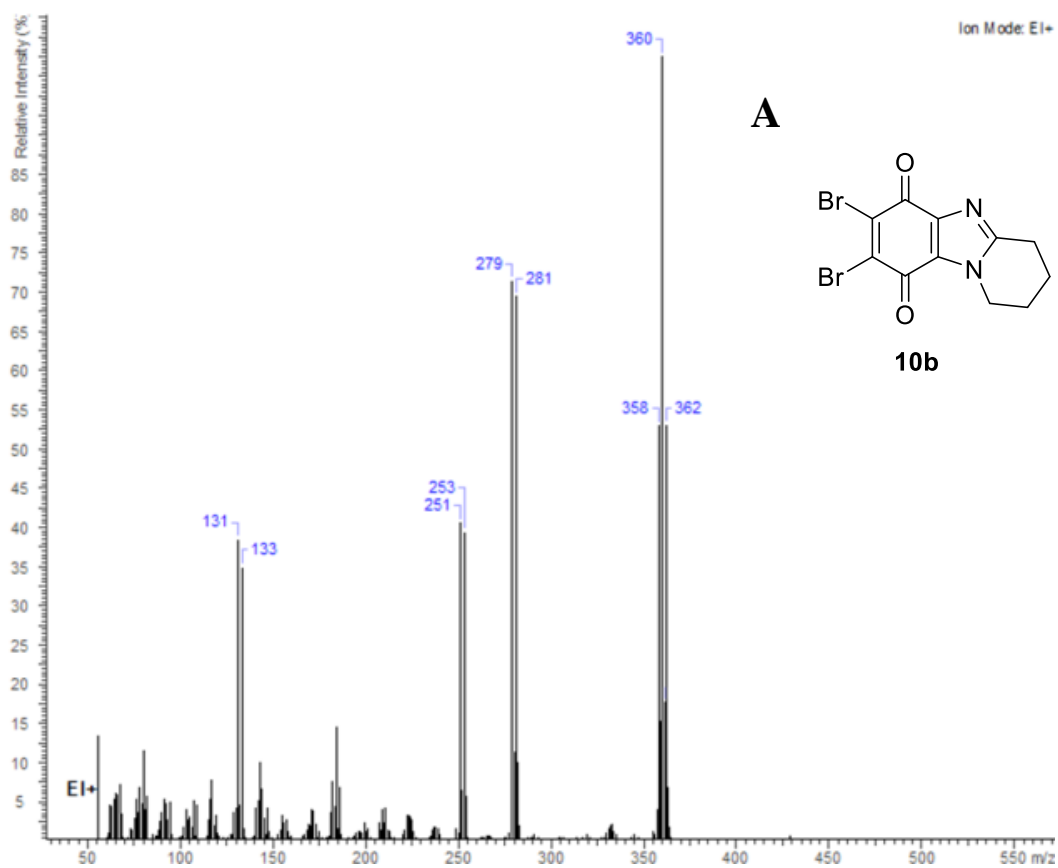
Figure A.2.2. **(A)** EI mass spectrum of 7,8-dibromo-1,2,3,4-tetrahydropyrido[1,2-*a*]benzimidazole-6,9-dione (**10b**). **(B)** EI mass spectrum, detecting doubly ^{18}O-labeled **14b**, indicating the role of water in quinone formation.

A.3 X-ray crystallography data

Table A.3.1. Single crystal X-ray data and structure refinement for **8f**.
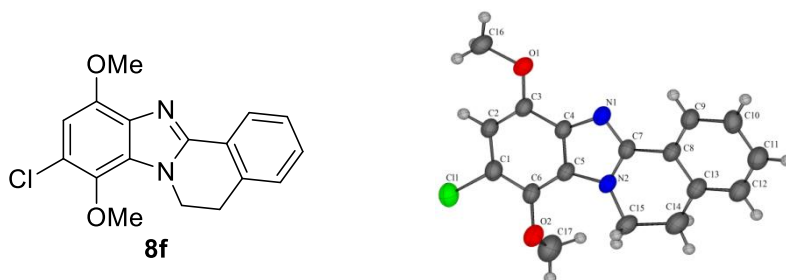
Empirical formula	$C_{17}H_{15}ClN_2O_2$
Formula weight	314.76
Temperature	300.1(7) K
Wavelength	0.71073 Å
Crystal system	Triclinic
Space group	P-1
Unit cell dimensions	a = 7.8992(15) Å $\quad$ α = 104.343(14)°.
	b = 8.6907(14) Å $\quad$ β = 92.934(15)°.
	c = 11.316(2) Å $\quad$ γ = 97.644(15)°.
Volume	743.0(2) Å^3
Z	2
Density (calculated)	1.407 Mg/m^3
Absorption coefficient	0.266 mm^{-1}
F(000)	328
Crystal size	0.50 x 0.40 x 0.20 mm^3
Theta range for data collection	3.588 to 29.272°.
Index ranges	-10<=h<=7, -10<=k<=11, -14<=l<=15
Reflections collected	5420
Independent reflections	3381 [R(int) = 0.0502]
Completeness to theta = 25.242°	99.6 %
Absorption correction	Semi-empirical from equivalents
Max. and min. transmission	1.00000 and 0.67518
Refinement method	Full-matrix least-squares on F^2
Data / restraints / parameters	3381 / 0 / 201
Goodness-of-fit on F^2	1.017
Final R indices [I>2sigma(I)]	R1 = 0.0769, wR2 = 0.2008
R indices (all data)	R1 = 0.1204, wR2 = 0.2526
Extinction coefficient	n/a
Largest diff. peak and hole	0.398 and -0.439 e.Å^{-3}

Table A.3.2. Single crystal X-ray data and structure refinement for **9a**.
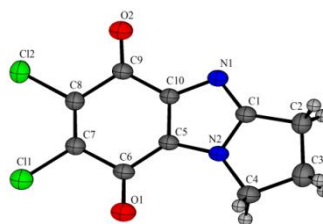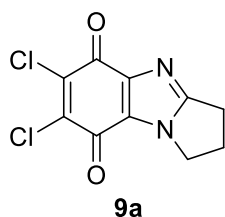
Empirical formula	$C_{10}H_6Cl_2N_2O_2$
Formula weight	257.07
Temperature	298.7(7) K
Wavelength	0.71073 Å
Crystal system	Orthorhombic
Space group	Pna2$_1$
Unit cell dimensions	a = 7.4153(4) Å $\alpha = 90°$
	b = 11.4252(5) Å $\beta = 90°$
	c = 11.8761(7) Å $\gamma = 90°$
Volume	1006.16(9) Å^3
Z	4
Density (calculated)	1.697 Mg/m^3
Absorption coefficient	0.628 mm^{-1}
F(000)	520
Crystal size	0.50 x 0.40 x 0.20 mm^3
Theta range for data collection	3.567 to 29.434°.
Index ranges	-10<=h<=9, -15<=k<=15, -10<=l<=15
Reflections collected	7637
Independent reflections	2069 [R(int) = 0.0246]
Completeness to theta = 25.242°	99.7 %
Absorption correction	Semi-empirical from equivalents
Max. and min. transmission	1.00000 and 0.77868
Refinement method	Full-matrix least-squares on F^2
Data / restraints / parameters	2069 / 1 / 146
Goodness-of-fit on F^2	1.109
Final R indices [I>2sigma(I)]	R1 = 0.0318, wR2 = 0.0738
R indices (all data)	R1 = 0.0398, wR2 = 0.0803
Absolute structure parameter	-0.02(3)
Extinction coefficient	0.0154(19)
Largest diff. peak and hole	0.225 and -0.207 e.Å^{-3}

Table A.3.3. Single crystal X-ray data and structure refinement for **9c**.
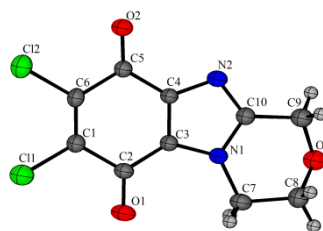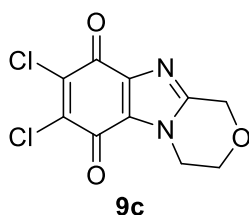
Empirical formula	$C_{10}H_6Cl_2N_2O_3$
Formula weight	273.07
Temperature	297.2(4) K
Wavelength	0.71073 Å
Crystal system	Orthorhombic
Space group	Pna2$_1$
Unit cell dimensions	a = 19.859(2) Å $\alpha = 90°$.
	b = 4.1152(6) Å $\beta = 90°$.
	c = 12.5806(15) Å $\gamma = 90°$.
Volume	1028.2(2) Å^3
Z	2
Density (calculated)	1.764 Mg/m^3
Absorption coefficient	0.627 mm^{-1}
F(000)	552
Crystal size	0.50 x 0.40 x 0.10 mm^3
Theta range for data collection	3.835 to 28.991°.
Index ranges	-25<=h<=20, -3<=k<=5, -16<=l<=16
Reflections collected	2766
Independent reflections	1865 [R(int) = 0.0239]
Completeness to theta = 25.242°	99.7 %
Absorption correction	Semi-empirical from equivalents
Max. and min. transmission	1.00000 and 0.76867
Refinement method	Full-matrix least-squares on F^2
Data / restraints / parameters	1865 / 1 / 154
Goodness-of-fit on F^2	0.940
Final R indices [I>2sigma(I)]	R1 = 0.0350, wR2 = 0.0680
R indices (all data)	R1 = 0.0458, wR2 = 0.0756
Absolute structure parameter	0.40(5)
Extinction coefficient	n/a
Largest diff. peak and hole	0.205 and -0.248 e.Å^{-3}

Table A.3.4. Single crystal X-ray data and structure refinement for **9d**.
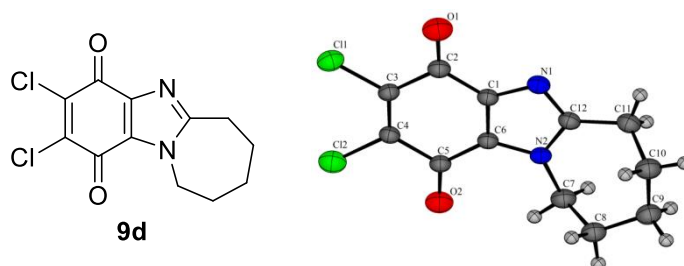
Empirical formula	$C_{12}H_{10}Cl_2N_2O_2$
Formula weight	285.12
Temperature	299.9(7) K
Wavelength	0.71073 Å
Crystal system	Monoclinic
Space group	P2$_1$/c
Unit cell dimensions	a = 9.4420(7) Å $\quad$ $\alpha = 90°$
	b = 5.7599(4) Å $\quad$ $\beta = 99.280(8)°$
	c = 22.2284(18) Å $\quad$ $\gamma = 90°$
Volume	1193.07(16) Å^3
Z	4
Density (calculated)	1.587 Mg/m^3
Absorption coefficient	0.538 mm^{-1}
F(000)	584
Crystal size	0.50 x 0.40 x 0.20 mm^3
Theta range for data collection	3.657 to 28.940°.
Index ranges	-12<=h<=11, -4<=k<=7, -30<=l<=18
Reflections collected	5273
Independent reflections	2739 [R(int) = 0.0213]
Completeness to theta = 25.242°	99.8 %
Absorption correction	Semi-empirical from equivalents
Max. and min. transmission	1.00000 and 0.94200
Refinement method	Full-matrix least-squares on F^2
Data / restraints / parameters	2739 / 0 / 163
Goodness-of-fit on F^2	1.020
Final R indices [I>2sigma(I)]	R1 = 0.0405, wR2 = 0.0934
R indices (all data)	R1 = 0.0616, wR2 = 0.1074
Extinction coefficient	n/a
Largest diff. peak and hole	0.221 and -0.260 e.Å^{-3}

Table A.3.5. Single crystal X-ray data and structure refinement for **9f**.
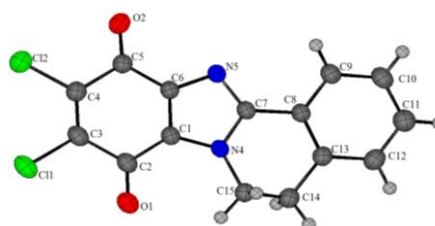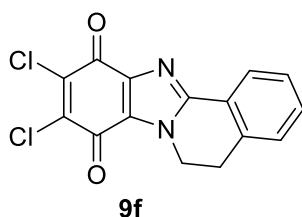
Empirical formula	$C_{15}H_8Cl_2N_2O_2$	
Formula weight	319.13	
Temperature	299.6(3) K	
Wavelength	0.71073 Å	
Crystal system	Monoclinic	
Space group	P2$_1$/c	
Unit cell dimensions	a = 10.2787(5) Å	$\alpha = 90°$.
	b = 6.8864(4) Å	$\beta = 93.647(4)°$.
	c = 18.8958(8) Å	$\gamma = 90°$.
Volume	1334.80(12) Å^3	
Z	4	
Density (calculated)	1.588 Mg/m^3	
Absorption coefficient	0.491 mm^{-1}	
F(000)	648	
Crystal size	0.50 x 0.18 x 0.15 mm^3	
Theta range for data collection	3.563 to 29.336°.	
Index ranges	-13<=h<=13, -9<=k<=7, -25<=l<=19	
Reflections collected	10092	
Independent reflections	3214 [R(int) = 0.0274]	
Completeness to theta = 25.242°	99.8 %	
Absorption correction	Semi-empirical from equivalents	
Max. and min. transmission	1.00000 and 0.82819	
Refinement method	Full-matrix least-squares on F^2	
Data / restraints / parameters	3214 / 0 / 190	
Goodness-of-fit on F^2	1.057	
Final R indices [I>2sigma(I)]	R1 = 0.0469, wR2 = 0.1085	
R indices (all data)	R1 = 0.0733, wR2 = 0.1234	
Extinction coefficient	n/a	
Largest diff. peak and hole	0.315 and -0.436 e.Å^{-3}	

Table A.3.6. Single crystal X-ray data and structure refinement for **10a**.
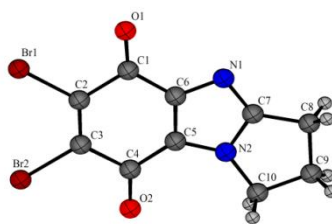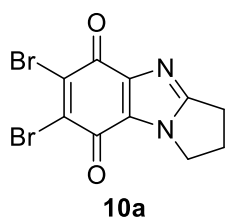
Empirical formula	$C_{10}H_6Br_2N_2O_2$	
Formula weight	345.99	
Temperature	299.0(1) K	
Wavelength	0.71073 Å	
Crystal system	Triclinic	
Space group	P-1	
Unit cell dimensions	a = 8.9723(6) Å	α = 85.557(4)°.
	b = 17.1128(9) Å	β = 86.407(5)°.
	c = 20.5895(12) Å	γ = 88.947(5)°.
Volume	3145.4(3) Å^3	
Z	12	
Density (calculated)	2.192 Mg/m^3	
Absorption coefficient	7.715 mm^{-1}	
F(000)	1992	
Crystal size	0.50 x 0.15 x 0.10 mm^3	
Theta range for data collection	3.454 to 25.350°.	
Index ranges	-10<=h<=10, -17<=k<=20, -24<=l<=24	
Reflections collected	22502	
Independent reflections	11482 [R(int) = 0.0641]	
Completeness to theta = 25.242°	99.7 %	
Absorption correction	Semi-empirical from equivalents	
Max. and min. transmission	1.00000 and 0.24026	
Refinement method	Full-matrix least-squares on F^2	
Data / restraints / parameters	11482 / 840 / 865	
Goodness-of-fit on F^2	0.863	
Final R indices [I>2sigma(I)]	R1 = 0.0539, wR2 = 0.0725	
R indices (all data)	R1 = 0.1422, wR2 = 0.0977	
Extinction coefficient	n/a	
Largest diff. peak and hole	0.758 and -0.651 e.Å^{-3}	

Table A.3.7. Single crystal X-ray data and structure refinement for **10d**.
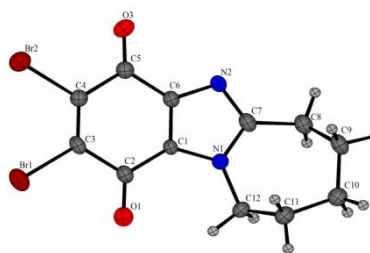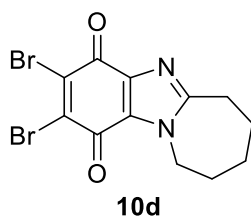
Empirical formula	$C_{12}H_{10}Br_2N_2O_2$
Formula weight	374.04
Temperature	299.9(9) K
Wavelength	0.71073 Å
Crystal system	Monoclinic
Space group	$P2_1/c$
Unit cell dimensions	a = 9.3124(7) Å $\alpha = 90°$
	b = 7.6450(6) Å $\beta = 92.959(7)°$
	c = 17.1919(11) Å $\gamma = 90°$
Volume	1222.32(15) Å^3
Z	4
Density (calculated)	2.033 Mg/m^3
Absorption coefficient	6.626 mm^{-1}
F(000)	728
Crystal size	0.50 x 0.40 x 0.20 mm^3
Theta range for data collection	3.569 to 29.008°.
Index ranges	-6<=h<=12, -5<=k<=9, -22<=l<=22
Reflections collected	5294
Independent reflections	2812 [R(int) = 0.0463]
Completeness to theta = 25.242°	99.7 %
Absorption correction	Semi-empirical from equivalents
Max. and min. transmission	1.00000 and 0.40238
Refinement method	Full-matrix least-squares on F^2
Data / restraints / parameters	2812 / 0 / 164
Goodness-of-fit on F^2	0.925
Final R indices [I>2sigma(I)]	R1 = 0.0583, wR2 = 0.1317
R indices (all data)	R1 = 0.1176, wR2 = 0.1704
Extinction coefficient	0.0191(15)
Largest diff. peak and hole	0.914 and -0.829 e.Å^{-3}

Table A.3.8. Single crystal X-ray data and structure refinement for **18**.
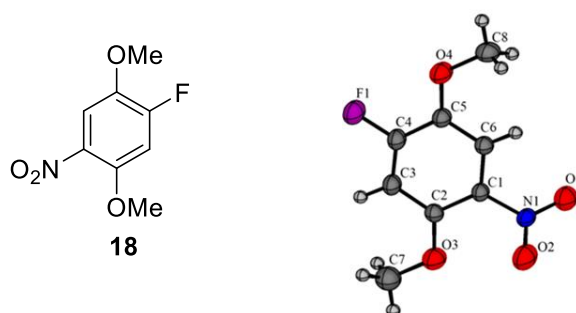
Identification code	ms_6_1
Empirical formula	$C_8H_8F NO_4$
Formula weight	201.15
Temperature	298.4(4) K
Wavelength	0.71073 Å
Crystal system	Monoclinic
Space group	Cc
Unit cell dimensions	a = 7.9538(6) Å $\alpha = 90°$.
	b = 13.5379(11) Å $\beta = 89.983(6)°$.
	c = 16.0790(13) Å $\gamma = 90°$.
Volume	1731.4(2) $Å^3$
Z	8
Density (calculated)	1.543 Mg/m^3
Absorption coefficient	0.138 mm^{-1}
F(000)	832
Crystal size	0.50 x 0.40 x 0.20 mm^3
Theta range for data collection	3.905 to 29.220°.
Index ranges	-10<=h<=9, -18<=k<=17, -20<=l<=20
Reflections collected	6792
Independent reflections	3164 [R(int) = 0.0214]
Completeness to theta = 25.242°	99.6 %
Absorption correction	Semi-empirical from equivalents
Max. and min. transmission	1.00000 and 0.92979
Refinement method	Full-matrix least-squares on F^2
Data / restraints / parameters	3164 / 2 / 258
Goodness-of-fit on F^2	1.059
Final R indices [I>2sigma(I)]	R1 = 0.0755, wR2 = 0.1838
R indices (all data)	R1 = 0.0903, wR2 = 0.2067
Absolute structure parameter	1(2)
Extinction coefficient	n/a
Largest diff. peak and hole	0.725 and -0.227 e.$Å^{-3}$

Table A.3.9. Single crystal X-ray data and structure refinement for **23**.
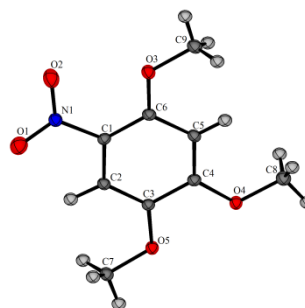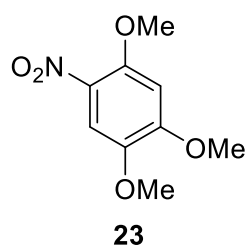
Empirical formula	$C_9H_{11}NO_5$
Formula weight	213.19
Temperature	118.0(5) K
Wavelength	0.71073 Å
Crystal system	Tetragonal
Space group	P4$_2$
Unit cell dimensions	a = 15.6031(7) Å α= 90°.
	b = 15.6031(7) Å β= 90°.
	c = 3.8114(3) Å γ = 90°.
Volume	927.90(12) Å^3
Z	4
Density (calculated)	1.526 Mg/m^3
Absorption coefficient	0.126 mm^{-1}
F(000)	448
Crystal size	0.50 x 0.40 x 0.20 mm^3
Theta range for data collection	3.693 to 29.277°.
Index ranges	-20<=h<=17, -11<=k<=21, -4<=l<=5
Reflections collected	4082
Independent reflections	2078 [R(int) = 0.0209]
Completeness to theta = 25.242°	99.5 %
Absorption correction	Semi-empirical from equivalents
Max. and min. transmission	1.00000 and 0.97581
Refinement method	Full-matrix least-squares on F^2
Data / restraints / parameters	2078 / 1 / 180
Goodness-of-fit on F^2	1.041
Final R indices [I>2sigma(I)]	R1 = 0.0359, wR2 = 0.0757
R indices (all data)	R1 = 0.0431, wR2 = 0.0800
Absolute structure parameter	-0.3(6)
Extinction coefficient	n/a
Largest diff. peak and hole	0.189 and -0.200 e.Å^{-3}

A.4 DTP NCI-60 mean growth percent graphs

Table A.4.1. One-dose mean graph for 1,3-diphenylbenzo[1,2,4]triazin-7-one (**1a**).

| Developmental Therapeutics Program | NSC: 768093 / 1 | Conc: 1.00E-5 Molar | Test Date: Nov 05, 2012 |
| One Dose Mean Graph | Experiment ID: 1211OS74 | | Report Date: Aug 02, 2019 |

Panel/Cell Line	Growth Percent	Mean Growth Percent - Growth Percent
Leukemia		
CCRF-CEM	-16.30	
HL-60(TB)	-45.48	
K-562	-39.00	
MOLT-4	-37.89	
RPMI-8226	-8.63	
SR	-20.23	
Non-Small Cell Lung Cancer		
A549/ATCC	73.67	
HOP-62	69.49	
HOP-92	-33.03	
NCI-H226	68.07	
NCI-H23	54.42	
NCI-H322M	88.21	
NCI-H460	81.45	
NCI-H522	-90.51	
Colon Cancer		
COLO 205	-78.78	
HCC-2998	99.95	
HCT-116	-90.71	
HCT-15	-75.93	
HT29	-53.48	
KM12	63.06	
SW-620	-80.55	
CNS Cancer		
SF-268	70.49	
SF-295	23.90	
SF-539	105.34	
SNB-19	78.05	
SNB-75	93.28	
U251	66.23	
Melanoma		
LOX IMVI	-51.89	
MALME-3M	-92.51	
M14	51.19	
MDA-MB-435	24.65	
SK-MEL-2	44.86	
SK-MEL-28	26.39	
SK-MEL-5	19.82	
UACC-257	-97.33	
UACC-62	30.15	
Ovarian Cancer		
IGROV1	2.66	
OVCAR-3	-98.15	
OVCAR-4	-40.65	
OVCAR-5	102.41	
OVCAR-8	-2.36	
NCI/ADR-RES	96.18	
SK-OV-3	59.15	
Renal Cancer		
786-0	48.58	
A498	84.39	
ACHN	-96.01	
CAKI-1	-90.90	
RXF 393	-92.82	
SN12C	40.17	
TK-10	-95.94	
UO-31	-97.49	
Prostate Cancer		
PC-3	43.53	
DU-145	-95.45	
Breast Cancer		
MCF7	-66.74	
MDA-MB-231/ATCC	76.31	
HS 578T	75.94	
BT-549	90.19	
T-47D	-36.53	
MDA-MB-468	-81.64	
Mean	2.46	
Delta	100.61	
Range	203.49	

150   100   50   0   -50   -100   -150

Table A.4.2. Mean graph response for five-dose testing of 1,3-diphenylbenzo[1,2,4]triazin-7-one (**1a**).

National Cancer Institute Developmental Therapeutics Program — Mean Graphs

NSC :768093/1 | Report Date :August 02, 2019 | Units :Molar | SSPL :0Y1U | Test Date :July 29, 2013 | EXP. ID :1307RS19

Panel/Cell Line	Log₁₀ GI50	Log₁₀ TGI	Log₁₀ LC50
Leukemia			
CCRF-CEM			
HL-60(TB)			
K-562			
MOLT-4			
RPMI-8226			
SR			
Non-Small Cell Lung Cancer			
A549/ATCC			
HOP-62			
HOP-92			
NCI-H226			
NCI-H23			
NCI-H322M			
NCI-H460			
NCI-H522			
Colon Cancer			
COLO 205			
HCC-2998			
HCT-116			
HCT-15			
HT29			
KM12			
SW-620			
CNS Cancer			
SF-268			
SF-295			
SF-539			
SNB-19			
SNB-75			
U251			
Melanoma			
LOX IMVI			
M14			
MDA-MB-435			
SK-MEL-2			
SK-MEL-28			
SK-MEL-5			
UACC-257			
UACC-62			
Ovarian Cancer			
IGROV1			
OVCAR-3			
OVCAR-4			
OVCAR-5			
OVCAR-8			
NCI/ADR-RES			
SK-OV-3			
Renal Cancer			
786-0			
A498			
ACHN			
CAKI-1			
RXF 393			
SN12C			
TK-10			
UO-31			
Prostate Cancer			
PC-3			
DU-145			
Breast Cancer			
MCF7			
MDA-MB-231/ATCC			
HS 578T			
BT-549			
T-47D			
MDA-MB-468			

	Log₁₀ GI50	Log₁₀ TGI	Log₁₀ LC50
MID	-5.6	-5.2	-4.67
Delta	0.87	0.69	0.68
Range	1.74	1.74	1.35

Table A.4.3. One-dose mean graph for 1-phenyl-3-(trifluoromethyl)benzo[1,2,4]triazin-7-one (**2**).

Developmental Therapeutics Program	NSC: D-780813 / 1	Conc: 1.00E-5 Molar	Test Date: May 27, 2014
One Dose Mean Graph	Experiment ID: 1405OS93		Report Date: Aug 02, 2019

Panel/Cell Line	Growth Percent
Leukemia	
CCRF-CEM	-0.27
HL-60(TB)	-36.64
K-562	-35.08
MOLT-4	-20.54
RPMI-8226	45.81
SR	-11.31
Non-Small Cell Lung Cancer	
A549/ATCC	93.02
EKVX	95.78
HOP-62	68.96
HOP-92	35.24
NCI-H226	77.72
NCI-H23	67.74
NCI-H322M	99.79
NCI-H460	97.33
NCI-H522	-55.98
Colon Cancer	
COLO 205	-70.72
HCC-2998	102.13
HCT-116	35.21
HCT-15	-79.74
HT29	-64.31
KM12	96.77
SW-620	-63.31
CNS Cancer	
SF-268	77.42
SF-295	91.94
SF-539	92.81
SNB-19	93.47
SNB-75	86.47
U251	69.69
Melanoma	
LOX IMVI	4.30
MALME-3M	-41.74
M14	62.07
MDA-MB-435	62.29
SK-MEL-2	78.30
SK-MEL-28	35.73
SK-MEL-5	32.74
UACC-257	35.58
UACC-62	66.36
Ovarian Cancer	
IGROV1	71.65
OVCAR-3	-26.13
OVCAR-4	79.85
OVCAR-5	102.42
OVCAR-8	73.06
NCI/ADR-RES	84.03
SK-OV-3	79.30
Renal Cancer	
786-0	22.22
A498	79.99
ACHN	-89.04
CAKI-1	56.03
RXF 393	-20.46
SN12C	67.93
TK-10	-98.03
UO-31	24.04
Prostate Cancer	
PC-3	84.59
DU-145	40.46
Breast Cancer	
MCF7	-49.33
MDA-MB-231/ATCC	61.04
HS 578T	74.03
BT-549	69.23
T-47D	-40.82
MDA-MB-468	-73.48
Mean	33.29
Delta	131.32
Range	200.45

Mean Growth Percent - Growth Percent

Axis: 150 100 50 0 -50 -100 -150

Table A.4.4. Mean graph response for five-dose testing of 1-phenyl-3-(trifluoromethyl)benzo[1,2,4]triazin-7-one (**2**).

National Cancer Institute Developmental Therapeutics Program — Mean Graphs

NSC : D - 78081311 Report Date : August 02, 2019 Units : Molar SSPL : 0Y1U Test Date : June 30, 2014 EXP. ID : 1406NS10

Panel / Cell Line	Log$_{10}$ GI50	Log$_{10}$ TGI	Log$_{10}$ LC50
Leukemia			
CCRF-CEM	-5.93	-5.53	-4.10
HL-60(TB)	-5.92	-5.18	-4.27
K-562	-5.68	-4.61	-4.24
MOLT-4	-5.67	-4.09	-4.15
RPMI-8226	-5.32	-4.08	-4.13
SR	-6.00	-5.39	-5.22
Non-Small Cell Lung Cancer			
A549/ATCC	-4.71	-4.41	> -4.19
EKVX	-4.87	-4.57	-4.27
HOP-62	-5.10	-4.56	-4.28
HOP-92	-5.85	-5.53	-5.18
NCI-H226	-4.88	-4.52	-4.25
NCI-H23	-4.73	-4.45	-4.26
NCI-H322M	-4.75	-4.44	-4.19
NCI-H460	-5.58	-5.24	> -5.00
NCI-H522	-5.82	-5.52	-5.22
Colon Cancer			
COLO 205	-5.64	-5.24	-5.18
HCC-2998	-4.81	-4.53	-4.26
HCT-116	-5.84	-5.59	-5.28
HCT-15	-5.58	-5.47	-5.27
HT29	-5.79	-5.43	-5.07
KM12	-4.71	-4.43	-4.36
SW-620	-5.76		
CNS Cancer			
SF-268	-4.82	-4.54	-4.28
SF-295	-4.84	-4.57	-4.34
SF-539	-4.80	-4.53	-4.29
SNB-75	-4.88	-4.54	-4.20
U251	-4.87	-4.54	-4.32
Melanoma			
LOX IMVI	-5.80	-5.49	-5.22
MALME-3M	-5.24	-4.48	-4.00
M14	-5.34	-4.72	-4.34
MDA-MB-435	-5.44	-4.81	-4.23
SK-MEL-2	-5.77	-5.49	-5.20
SK-MEL-28	-5.11	-4.68	-4.32
SK-MEL-5	-5.72	-5.39	-5.07
UACC-257	-5.29	-4.75	-4.36
UACC-62			
Ovarian Cancer			
IGROV1	-4.92	-4.59	> -4.00
OVCAR-3	-5.80	-5.53	-5.27
OVCAR-4	-5.83	-5.55	-5.29
OVCAR-5	-4.81	-4.54	-4.26
OVCAR-8	-5.38	-4.47	> -4.00
NCI/ADR-RES	-4.7?	-4.19	> -4.00
SK-OV-3	-4.82	> -4.00	> -4.00
Renal Cancer			
786-0	-4.85	-4.57	-4.28
A498	-5.93	-5.61	-5.25
ACHN	-5.84	-5.55	-5.27
CAKI-1	-5.83	-5.55	-5.00
RXF 393	-5.44	-5.24	> -4.00
SN12C	-5.83	-5.54	-5.23
TK-10	-5.14	-4.63	-4.28
UO-31	-5.83	-5.50	> -4.28
Prostate Cancer			
PC-3	-4.97	> -4.63	> -4.25
DU-145	-5.75		
Breast Cancer			
MCF7	-5.31	-5.39	-5.25
MDA-MB-231/ATCC	-4.91	-4.08	> -4.00
HS 578T	-4.91	-4.61	> -4.57
BT-549	-5.26		> -4.50
T-47D	-5.77	-5.18	-4.30
MDA-MB-468	-5.97	-5.53	-5.08
MID	-5.37	-4.9	-4.48
Delta	0.94	0.71	0.81
Range	1.67	1.61	1.29

(Graph axis scale: +3, +2, +1, 0, -1, -2, -3 for each of the GI50, TGI and LC50 mean-graph panels.)

Table A.4.5. One-dose mean graph for 1-phenyl-3-(pyridin-2-yl)[1,2,4]benzotriazin-7-one (**3a**).

| Developmental Therapeutics Program One Dose Mean Graph | NSC: D-780815 / 1 | Conc: 1.00E-5 Molar | Test Date: May 27, 2014 |
| | Experiment ID: 1405OS93 | | Report Date: Aug 15, 2019 |

Panel/Cell Line	Growth Percent	Mean Growth Percent - Growth Percent
Leukemia		
CCRF-CEM	8.49	
HL-60(TB)	31.09	
K-562	-8.79	
MOLT-4	5.56	
RPMI-8226	50.30	
SR	5.21	
Non-Small Cell Lung Cancer		
A549/ATCC	101.41	
EKVX	115.24	
HOP-62	93.40	
HOP-92	36.76	
NCI-H226	90.08	
NCI-H23	89.48	
NCI-H322M	102.00	
NCI-H460	109.06	
NCI-H522	-44.97	
Colon Cancer		
COLO 205	-59.36	
HCC-2998	98.83	
HCT-116	48.73	
HCT-15	-47.98	
HT29	-44.20	
KM12	98.41	
SW-620	-61.79	
CNS Cancer		
SF-268	97.99	
SF-295	96.28	
SF-539	102.73	
SNB-19	98.93	
SNB-75	98.37	
U251	98.29	
Melanoma		
LOX IMVI	11.67	
MALME-3M	-20.61	
M14	90.30	
MDA-MB-435	90.68	
SK-MEL-2	106.14	
SK-MEL-28	70.67	
SK-MEL-5	36.01	
UACC-257	60.25	
UACC-62	72.67	
Ovarian Cancer		
IGROV1	87.90	
OVCAR-3	-21.89	
OVCAR-4	81.82	
OVCAR-5	108.96	
OVCAR-8	87.10	
NCI/ADR-RES	98.00	
SK-OV-3	84.86	
Renal Cancer		
786-0	53.60	
A498	91.86	
ACHN	-84.72	
CAKI-1	72.54	
RXF 393	65.04	
SN12C	84.60	
TK-10	-70.85	
UO-31	40.14	
Prostate Cancer		
PC-3	89.04	
DU-145	91.04	
Breast Cancer		
MCF7	-55.97	
MDA-MB-231/ATCC	68.38	
HS 578T	93.86	
BT-549	86.58	
T-47D	-28.41	
MDA-MB-468	-32.06	
Mean	50.31	
Delta	135.03	
Range	199.96	

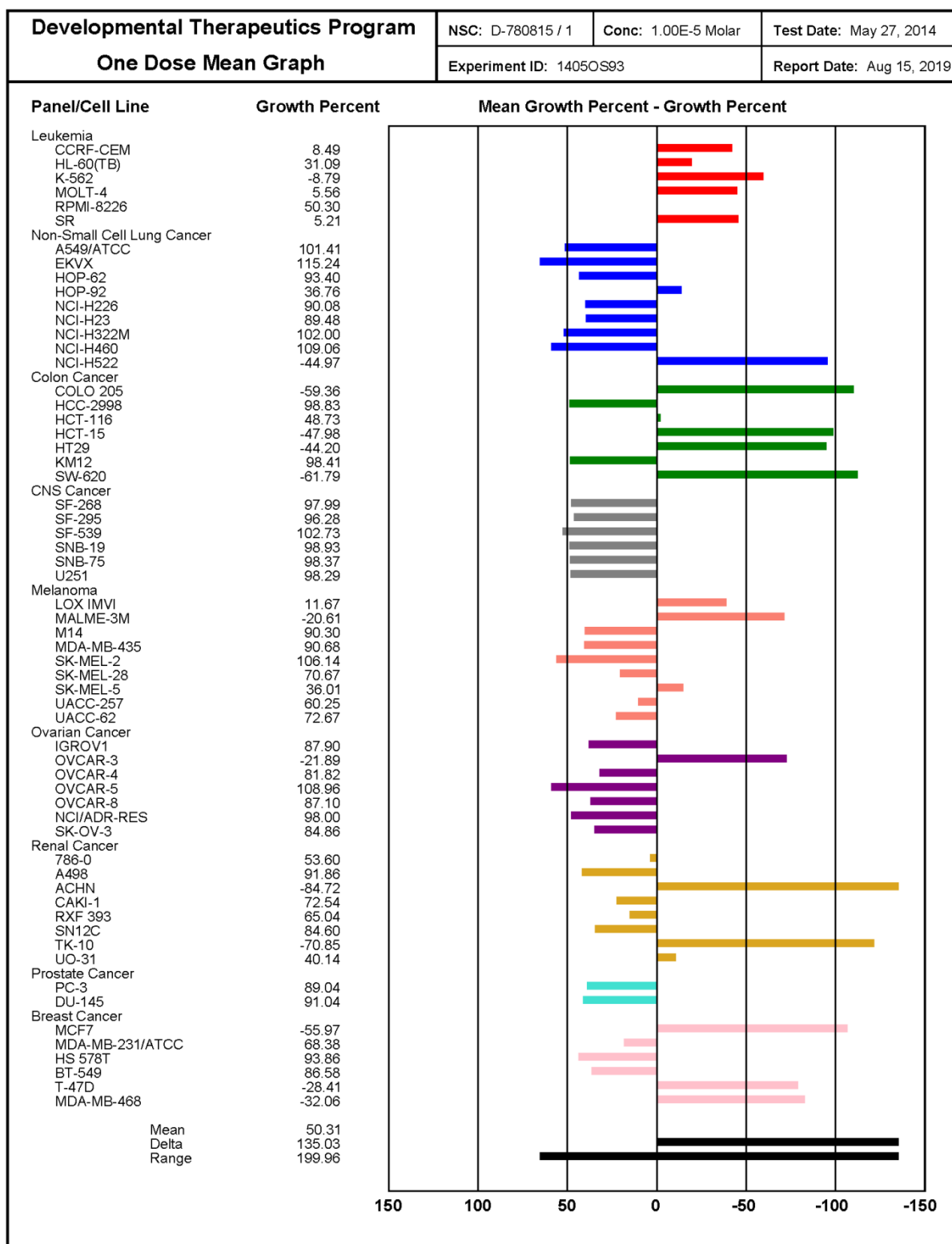150   100   50   0   -50   -100   -150

214

Table A.4.6. Mean graph response for five-dose testing of 1-phenyl-3-(pyridin-2-yl)[1,2,4]benzotriazin-7-one (**3a**).

Table A.4.7. One-dose mean graph for 3-phenyl-1-(pyridin-2-yl)benzo[1,2,4]triazin-7-one (**3b**).

Developmental Therapeutics Program One Dose Mean Graph	NSC: D-780816 / 1	Conc: 1.00E-5 Molar	Test Date: May 27, 2014
	Experiment ID: 1405OS93		Report Date: Aug 15, 2019

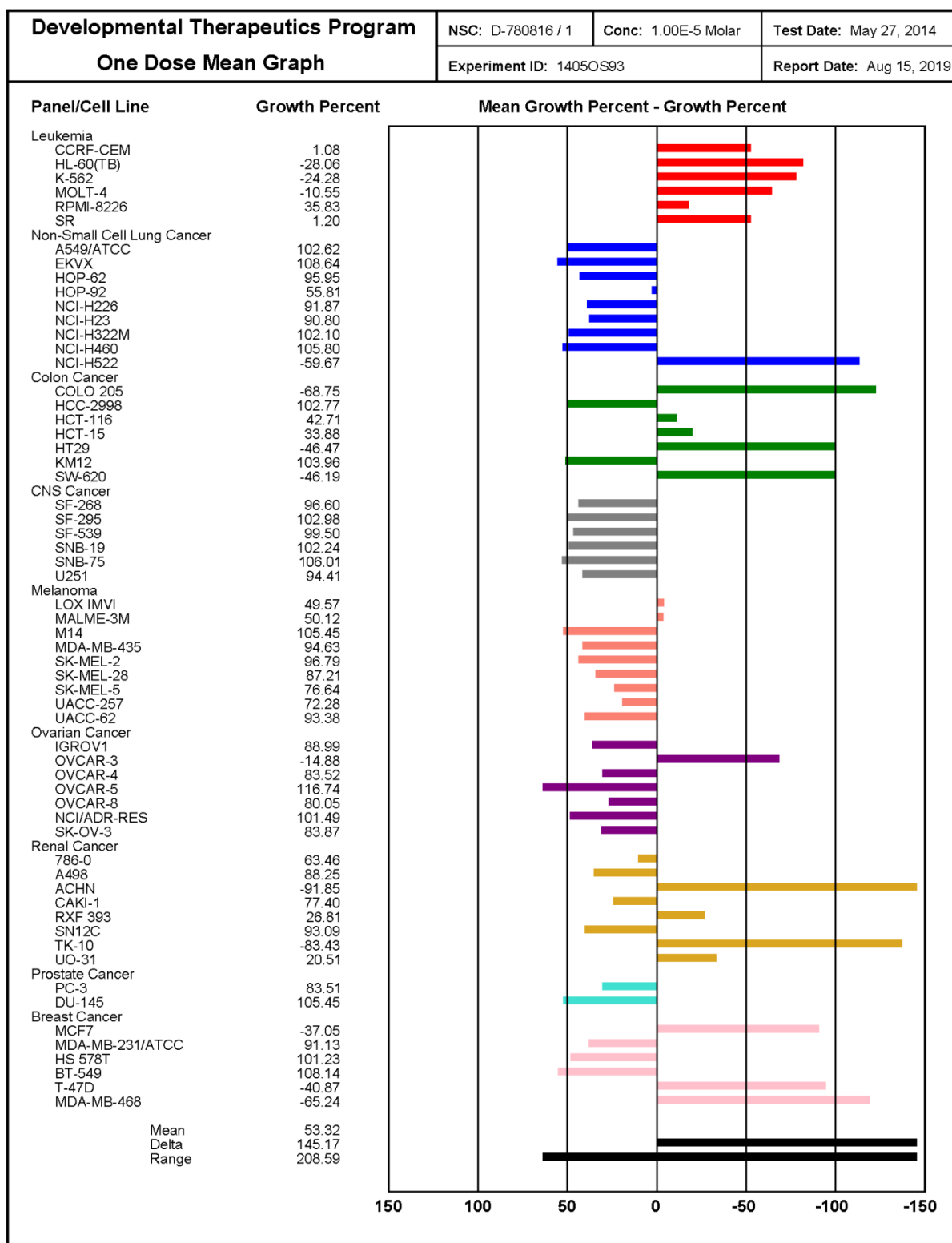| Panel/Cell Line	Growth Percent	Mean Growth Percent - Growth Percent
Leukemia		
CCRF-CEM	1.08	
HL-60(TB)	-28.06	
K-562	-24.28	
MOLT-4	-10.55	
RPMI-8226	35.83	
SR	1.20	
Non-Small Cell Lung Cancer		
A549/ATCC	102.62	
EKVX	108.64	
HOP-62	95.95	
HOP-92	55.81	
NCI-H226	91.87	
NCI-H23	90.80	
NCI-H322M	102.10	
NCI-H460	105.80	
NCI-H522	-59.67	
Colon Cancer		
COLO 205	-68.75	
HCC-2998	102.77	
HCT-116	42.71	
HCT-15	33.88	
HT29	-46.47	
KM12	103.96	
SW-620	-46.19	
CNS Cancer		
SF-268	96.60	
SF-295	102.98	
SF-539	99.50	
SNB-19	102.24	
SNB-75	106.01	
U251	94.41	
Melanoma		
LOX IMVI	49.57	
MALME-3M	50.12	
M14	105.45	
MDA-MB-435	94.63	
SK-MEL-2	96.79	
SK-MEL-28	87.21	
SK-MEL-5	76.64	
UACC-257	72.28	
UACC-62	93.38	
Ovarian Cancer		
IGROV1	88.99	
OVCAR-3	-14.88	
OVCAR-4	83.52	
OVCAR-5	116.74	
OVCAR-8	80.05	
NCI/ADR-RES	101.49	
SK-OV-3	83.87	
Renal Cancer		
786-0	63.46	
A498	88.25	
ACHN	-91.85	
CAKI-1	77.40	
RXF 393	26.81	
SN12C	93.09	
TK-10	-83.43	
UO-31	20.51	
Prostate Cancer		
PC-3	83.51	
DU-145	105.45	
Breast Cancer		
MCF7	-37.05	
MDA-MB-231/ATCC	91.13	
HS 578T	101.23	
BT-549	108.14	
T-47D	-40.87	
MDA-MB-468	-65.24	
Mean	53.32	
Delta	145.17	
Range	208.59	

Axis: 150 100 50 0 -50 -100 -150

Table A.4.8. Mean graph response for five-dose testing of 3-phenyl-1-(pyridin-2-yl)benzo[1,2,4]triazin-7-one (**3b**).

A.5 COMPARE analysis

Table A.5.1. Correlation of seed compound **1a** to pleurotin (red).
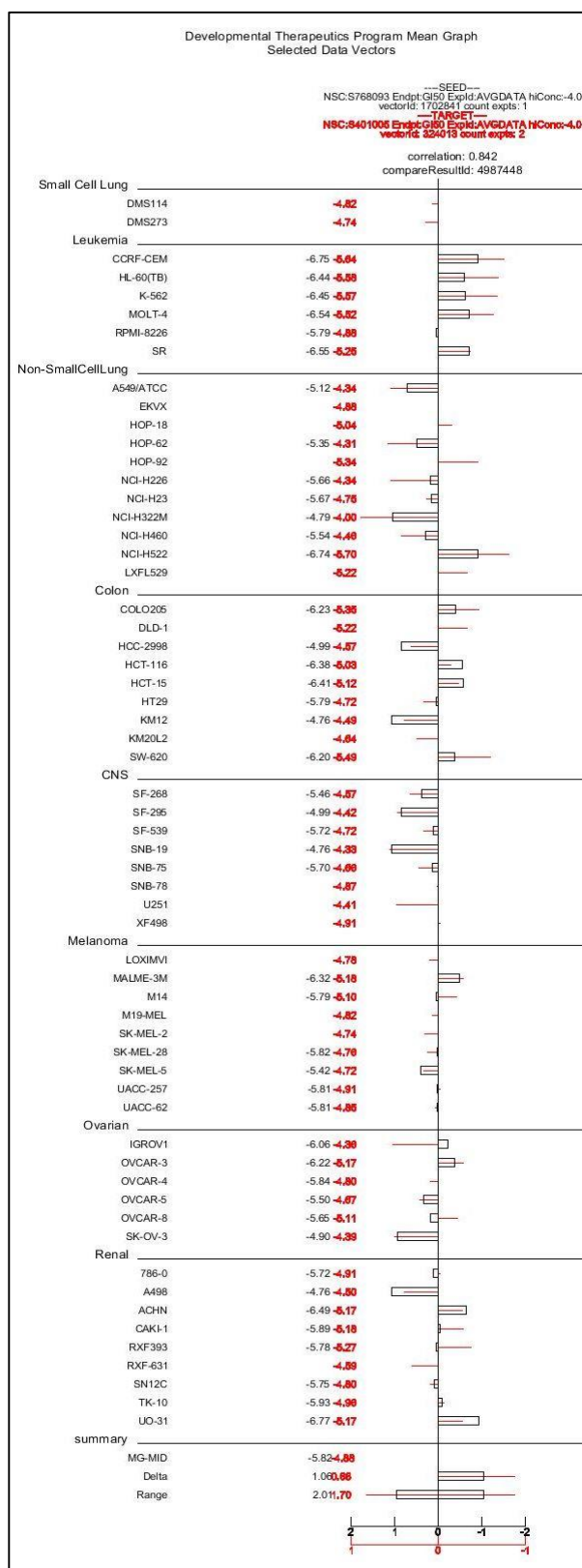
Table A.5.2. Correlation of seed compound **2** to pleurotin (red).

Developmental Therapeutics Program Mean Graph
Selected Data Vectors

----SEED----
NSC:S780813 Endpt:GI50 Expld:1406NS10 hiConc:-4.0
vectorId: 9849940 count expts: 1
----TARGET----
NSC:S401005 Endpt:GI50 Expld:AVGDATA hiConc:-4.0
vectorId: 334363 count expts: 2

correlation: 0.793
compareResultId: 6544059

Panel / Cell Line	Seed	Target
Small Cell Lung		
DMS114		-4.82
DMS273		-4.74
Leukemia		
CCRF-CEM	-5.63	-5.84
HL-60(TB)	-5.92	-5.58
K-562	-5.68	-5.57
MOLT-4	-5.67	-5.52
RPMI-8226	-5.32	-4.88
SR	-6.00	-5.25
Non-Small Cell Lung		
A549/ATCC	-4.71	-4.34
EKVX	-4.87	-4.88
HOP-18		-5.04
HOP-62	-5.10	-4.31
HOP-92	-5.85	-5.34
NCI-H226	-4.88	-4.34
NCI-H23	-5.22	-4.75
NCI-H322M	-4.73	-4.00
NCI-H460	-4.75	-4.46
NCI-H522	-5.82	-5.70
LXFL529		-5.22
Colon		
COLO205	-5.64	-5.35
DLD-1		-5.22
HCC-2998	-4.81	-4.57
HCT-116	-5.79	-5.03
HCT-15	-5.84	-5.12
HT29	-5.58	-4.72
KM12	-4.71	-4.49
KM20L2		-4.84
SW-620	-5.76	-5.49
CNS		
SF-268	-4.82	-4.57
SF-295	-4.64	-4.42
SF-539	-4.80	-4.72
SNB-19		-4.33
SNB-75	-4.88	-4.96
SNB-78		-4.57
U251	-4.87	-4.41
XF498		-4.91
Melanoma		
LOXIMVI	-5.80	-4.76
MALME-3M	-5.74	-5.18
M14	-5.24	-5.10
M19-MEL		-4.82
SK-MEL-2	-5.44	-4.74
SK-MEL-28	-5.77	-4.76
SK-MEL-5	-5.11	-4.72
UACC-257	-5.72	-4.91
UACC-62	-5.29	-4.85
Ovarian		
IGROV1	-4.92	-4.36
OVCAR-3	-5.80	-5.17
OVCAR-4	-5.83	-4.80
OVCAR-5	-4.81	-4.87
OVCAR-8	-5.38	-5.11
SK-OV-3	-4.82	-4.39
Renal		
786-0		-4.91
A498	-4.85	-4.50
ACHN	-5.93	-5.17
CAKI-1	-5.83	-5.18
RXF393	-5.84	-5.27
RXF-631		-4.59
SN12C	-5.14	-4.80
TK-10	-5.79	-4.96
UO-31	-5.83	-5.17
summary		
MG-MID	-5.37	-4.88
Delta	0.73	0.86
Range	1.66	1.70

A.6 Peer-reviewed publications

- **Sweeney**, **Martin**; Keane, Lee-Ann J.; Gurry, Michael; McArdle, Patrick and Aldabbagh, Fawaz. One-pot synthesis of dihalogenated ring-fused benzimidazolequinones from 3,6-dimethoxy-2-(cycloamino)anilines using hydrogen peroxide and hydrohalic acid. *Organic Letters* **2018**, *20*, 6970-6974.

- Keane, Lee-Ann J.; Mirallai, Styliana; **Sweeney**, **Martin**; Carty, Michael P.; Zissimou, Georgia A.; Berezin, Andrey A.; Koutentis, Panayiotis A. and Aldabbagh, Fawaz. Anti-cancer activity of phenyl and pyrid-2-yl 1,3-substituted benzo[1,2,4]triazin-7-ones and stable free radical precursors. *Molecules* **2018**, *23*, 574.

- **Sweeney**, **Martin**; McArdle, Patrick and Aldabbagh, Fawaz. 1-Fluoro-2,5-dimethoxy-4-nitrobenzene. *Molbank* **2018**, *1*, M984.

- **Sweeney**, **Martin**; Gurry, Michael; Keane, Lee-Ann J. and Aldabbagh, Fawaz. Greener synthesis using hydrogen peroxide in ethyl acetate of alicyclic ring-fused benzimidazoles and anti-tumour benzimidazolequinones. *Tetrahedron Letters* **2017**, *58*, 3565-3567.

- **Sweeney**, **Martin**; Coyle, Robert; Kavanagh, Paul; Berezin, Andrey A.; Lo Re, Daniele; Zissimou, Georgia A.; Koutentis, Panayiotis A.; Carty, Michael P. and Aldabbagh, Fawaz. Discovery of anti-cancer activity for benzo[1,2,4]triazin-7-ones: very strong correlation to pleurotin and thioredoxin reductase inhibition. *Bioorganic and Medicinal Chemistry* **2016**, *24*, 3565-3570.

- Gurry, Michael; **Sweeney**, **Martin**; McArdle, Patrick and Aldabbagh, Fawaz. One-pot hydrogen peroxide and hydrohalic acid induced ring closure and selective aromatic halogenation to give new ring-fused benzimidazoles. *Organic Lettters* **2015**, *17*, 2856-2859.

A.7 Conference proceedings

- "H$_2$O$_2$-HX mediated synthesis of halogenated ring-fused benzimidazolequinone anti-cancer agents" M. Sweeney, Bioheterocycles 2017: 17th International Conference on Heterocycles in Bioorganic Chemistry, Galway, Ireland, 28th to 31st of May 2017. *Oral Presentation*, *First Prize*.

- "Anti-cancer activity for benzo[1,2,4]triazin-7-ones: Very strong correlation to pleurotin and thioredoxin reductase inhibition" M. Sweeney, R. Coyle, P. Kavanagh, A. A. Berezin, D. L. Re, G. A. Zissimou, P. A. Koutentis, M. P. Carty, and F. Aldabbagh. Bioheterocycles 2017: 17th International Conference on Heterocycles in Bioorganic Chemistry, Galway, Ireland, 28th to 31st of May 2017. *Poster Presentation*.

- "Synthesis and Evaluation of New Heterocyclic Drug Candidates" M. Sweeney, BOC Postgraduate Award, NUI Galway, 5th of April, 2017. *Oral Presentation*, *First Prize*.

- "Anti-cancer activity for benzo[1,2,4]triazin-7-ones: Very strong correlation to pleurotin and thioredoxin reductase inhibition" M. Sweeney, R. Coyle, P. Kavanagh, A. A. Berezin, D. L. Re, G. A. Zissimou, P. A. Koutentis, M. P. Carty, and F. Aldabbagh. 1st Medicinal Chemistry Ireland Conference, Trinity College Dublin, Dublin, Ireland, 1st of July, 2016. *Poster Presentation*.

Anti-Cancer Activity for Benzo[1,2,4]triazin-7-ones: Very Strong Correlation to Pleurotin and Thioredoxin Reductase Inhibition

Martin Sweeney,[a] **Robert Coyle,**[a] **Paul Kavanagh,**[a] **Daniele Lo Re,**[b] **Andrey A. Berezin,**[b] **Georgia A. Zissimou,**[b] **Panayiotis A. Koutentis,**[b] **Michael P. Carty**[c] **and Fawaz Aldabbagh**[a]

[a] *School of Chemistry, National University of Ireland Galway, Ireland*
[b]*Department of Chemistry, University of Cyprus, Cyprus*
[c]*School of Natural Sciences, National University of Ireland Galway, Ireland*

OÉ Gaillimh
NUI Galway

Πανεπιστήμιο Κύπρου
University of Cyprus

Introduction

The thioredoxin (Trx)-thioredoxin reductase (TrxR) system plays a key role in maintaining cellular redox balance with Trx being over-expressed in a number of cancers. Inhibition of TrxR is an important strategy for anti-cancer drug discovery. The naturally occurring antibiotic product pleurotin is a well-known irreversible inhibitor of TrxR with K_i of 0.28 µM.

Pleurotin   **Benzo[1,2,4]triazin-7-ones**

National Cancer Institute (NCI) Compare Analysis & Tumour Cell Line Screen

The NCI COMPARE analysis quantifies the degree of similarity between different cytotoxicity profiles as a Pearson correlation coefficient. Out of ~250,000 compounds in the NCI database, both compounds **1** and **2** gave very strong Pearson correlation coefficients (~0.8) to pleurotin. This suggests similar structure-activity relationships for anti-cancer activity.

Cyclic Voltammetry
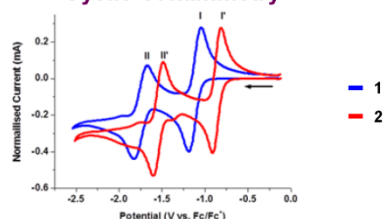
Cyclic voltammetry showed both **1** and **2** undergo characteristic quasi-reversible one-electron redox processes. Benzotriazinone **2** was more easily reduced due to the electron withdrawing CF_3 group. This suggests that bioreductive activation is implicated in cytotoxicity.
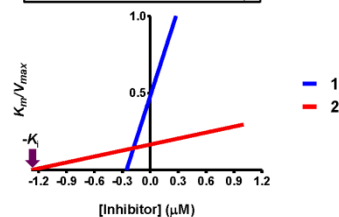
TrxR Inhibition Studies

The TrxR assay involves the reduction of 5,5'-dithiobis(2-nitrobenzoic) acid (DTNB) with NADPH to 5-thio-2-nitro-benzoic acid (TNB) producing a yellow colour at 405 nm. Inhibition of TrxR prevents the formation of coloured TNB. To determine whether **1** and **2** inhibited TrxR, enzyme activity of TrxR was estimated in the absence or presence of varying concentrations of inhibitor.
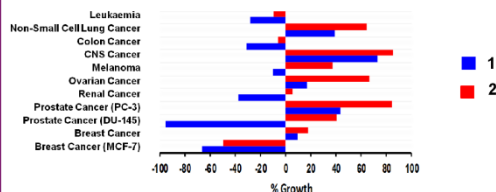

A secondary plot was used to estimate the K_i value by plotting the slopes of the Lineweaver-Burk graph against inhibitor concentrations. K_i values were found to be 3.90 and 0.78 µM for benzotriazinones **1** and **2** respectively.

Conclusions

- Benzo[1,2,4]triazin-7-ones **1** and **2** displayed very strong correlation to naturally occurring antibiotic pleurotin.

- Benzo[1,2,4]triazin-7-ones **1** and **2** are reversible TrxR inhibitors whereas pleurotin is irreversible.

- The 3-CF_3 substituted analogue gave sub-micromolar inhibition of TrxR.

222